

DISSERTATION

submitted to the

Combined Faculties of the Natural Sciences and Mathematics
of the Ruperto-Carola University of Heidelberg, Germany

for the degree of

DOCTOR OF NATURAL SCIENCES

Put forward by

MSc. Naseemuddin Khan

born in Aachen, Germany

Oral examination: 03.11.2015

Interplay of Mesonic and Baryonic Degrees of Freedom in Quark Matter

Referees:

Prof. Dr. Jan M. Pawłowski

Prof. Dr. Jürgen Berges

Kurzfassung

In dieser Arbeit untersuchen wir den Einfluss von mesonischen und baryonischen Fluktuationen auf das Phasendiagramm von Quarkmaterie mit zwei Flavoren. Durch das Betrachten des Hadronisierungsprozesses und der damit verbundenen Techniken, werden wir effektive Niederenergiemodelle herleiten, in denen die Gluonen ausintegriert sind. Um unsere Modellrechnungen bei endlichem chemischen Potential mit Gitterrechnungen vergleichen zu können, erproben wir eine QCD-ähnliche Theorie mit zwei Farben, worin das Vorzeichenproblem nicht vorhanden ist. Zu diesem Zweck führen wir ein Quark-Meson-Diquark Modell ein, wo die bosonischen Diquarks die Rolle der farblosen, baryonischen Freiheitsgrade spielen und mit den Mesonen konkurrieren. Um Zugang zum Phasendiagramm zu erlangen und die Phasen der chiralen und Diquark-Kondensation zu bestimmen, bedienen wir uns der Funktionalen Renormierungsgruppe, welche uns ein systematisches, nichtperturbatives Trunkierungsschema ermöglicht. Interessante Phänomene, die aus der Festkörperphysik bekannt sind, treten auf, wie der BEC-BSC Übergang und eine Phase der bezirksweisen Kondensation. Zusätzlich zur Skalenabhängigkeit des effektiven Potentials erkunden wir die Wirkung von laufenden Wellenfunktionsrenormierungen und Yukawa Kopplungen der Quarks und Boson Felder. Währenddessen werden wir die Silver Blaze Eigenschaft und ihre Realisierung innerhalb eines funktionalen Zugangs diskutieren.

Parallel dazu werden wir ein Quark-Meson-Diquark-Baryon Modell für die physikalische QCD formulieren, als eine effektive Niederenergiethorie für baryonische Materie bei großen Dichten, und die Relevanz der Diquark- und Baryon-Freiheitsgrade diskutieren. Im diesen Sinne werden wir ein Phasendiagramm für die QCD durch funktionale Methoden berechnen, einschließlich einer farbsupraleitenden Phase.

Abstract

In this work we study the influence of mesonic and baryonic fluctuations on the phase diagram of quark matter with two flavors. By examining the hadronization process and related techniques, we will derive effective low-energy models, where the gluons are integrated out. To be able to compare our model calculations with lattice results at finite chemical potential, we investigate a QCD-like theory with two colors, where the sign-problem is absent. To this end we introduce a quark-meson-diquark model, where the bosonic diquarks play the role of colorless, baryonic degrees of freedom competing with the mesons. To access the phase diagram and determine the phases of chiral and diquark condensation, we employ a functional renormalization group approach allowing for a systematic non-perturbative truncation scheme. Interesting phenomena arise that are known from condensed matter physics, as the BEC-BSC crossover and a phase of condensation within domains. We explore the impact of running wave function renormalizations and Yukawa couplings for the quarks and the boson fields on top of the scale dependence of the effective potential. In the course of this we will discuss the Silver Blaze property and its realization within a functional approach.

In parallel, we will formulate a quark-meson-diquark-baryon model for physical QCD as a low-energy effective theory for baryonic matter at high density, and discuss the relevance of the diquark and baryon degrees of freedom. In this sense, we will compute a phase diagram for QCD from functional methods, including a color superconducting phase.

Contents

1	Introduction	9
2	From Quarks and Gluons to Mesons, Diquarks and Baryons	19
2.1	Classical QCD	19
2.2	Symmetries and Related Phase Transitions	22
2.2.1	Center Symmetry and Confinement	22
2.2.2	Flavor Symmetries and the Chiral Phase Transition	24
2.2.3	Color Superconductivity	27
2.2.4	Extended Flavor Symmetries for $N_c = 2$	32
2.3	Low Energy Degrees of Freedom	36
2.3.1	Hadronization	36
2.3.2	The Quark-Meson-Diquark Model for QC_2D	41
2.3.3	The Quark-Meson-Diquark-Baryon Model for QCD	43
2.4	Successive Onsets of Densities	45
2.5	Phase Transitions with the Effective Potential	47
2.5.1	The Ground State and Symmetry Breaking	47
2.5.2	Ansatz for the Effective Potential	49
3	Renormalization Group Equations at Finite Temperature and Density	53
3.1	The Functional Renormalization Group	54
3.1.1	The Concept	54
3.1.2	The Flow Equation	55
3.1.3	Solution Methods	57
3.2	Propagators and Masses	60
3.2.1	Bosons	65
3.2.2	Fermions	72
3.3	The Silver Blaze Property	76
3.3.1	Derivation of the Property	76
3.3.2	Silver Blaze & FRG	78
3.3.3	Pole Mass & μ_c	80
3.4	Flow of the Effective Potential	81
3.4.1	Flow Equation for the QMD-Model and a General Discussion	82
3.4.2	Extension for QMDB-Model	88
3.4.3	Flow of the Bosonic Parameters	89
3.5	Vertices	93
3.5.1	Three-Boson Vertex	94

3.5.2	Three-Point Vertices with Fermions	95
3.6	Flow of the Two-Point Function	97
3.6.1	Bosonic Anomalous Dimensions	99
3.6.2	Fermionic Anomalous Dimensions	101
3.6.3	Baryon UV Mass Gap	104
3.6.4	Yukawa Couplings	104
4	Chiral & Diquark Condensation	107
4.1	Boundary Conditions	107
4.2	Pre-condensation	109
4.3	The QC ₂ D Phase Diagram	110
4.4	Truncation Effects	115
4.5	The QCD Phase Diagram	118
5	Summary, Conclusions & Outlook	121
	Appendix	124
A	Conventions and Notations	127
A.1	Units	127
A.2	Euclidean Space-Time	127
A.3	Abbreviations	128
A.4	Dirac Algebra	129
B	Propagators	131
B.1	Boson Propagators	131
B.2	The Nambu-Gorkov Propagator	134
C	Flow Equations	141
C.1	Bosonic Anomalous Dimension	141
C.2	Fermionic Anomalous Dimension	146
C.3	Baryon UV Mass Gap	150
C.4	Yukawa Couplings	151
C.5	Loop Integrals	154
	Bibliography	165

Introduction

The *Standard Model* of particle physics is in principle able to explain much of the physical world and various phenomena therein, in terms of *quantum field theories*. It describes the attributes of fundamental matter, called *leptons* and *quarks* which are *fermions*, and their interaction by the exchange of *gauge bosons*. In addition, a scalar boson was introduced for the generation of the masses without violating a fundamental principle, the *gauge symmetry*. This is called the *Higgs mechanism* and was proven recently by the discovery of the Higgs particle at the LHC. The fundamental forces are: The *weak interaction*, responsible for the radioactive beta decay processes, the *strong interaction*, responsible for the nuclear binding, and the well known *electromagnetic interaction*. Of course there are many important open question, like the generation of neutrino masses, the theoretical description of quantum gravity, the nature of the dark energy and dark matter, which seems to make up most of the universe, and the unification of all forces at high energies with the possibility of an even more elementary nature of the fundamental objects.

The earliest attempt to explain nuclear interaction was made in 1934 by Yukawa [1], saying that the force between the protons and neutrons is mediated trough massive bosons, which he named *mesons*. The famous Yukawa potential has the diverging properties of a Coulomb potential at short range, and an exponential damping factor in terms of the meson mass, for the suppression of long-range interactions. The theory was later approved by the discovery of the pions. Soon after in 1950s, the discovery of numerous particles had begun. If the decay products contained a proton or a neutron, the a particle was classified as a baryon, otherwise it was grouped to the mesons. The “particle zoo” started to become vast, but Gell-Mann and Ne’eman [2–4] noticed that groups of particles were related to each other in a way that matched the representation of $SU(3)$, by the *Eightfold Way*, and thereby predicted the existence of the Ω^- baryon. Then in 1964 it was Zweig [5, 6] and Gell-Mann [7] who proposed the *quark-model* with the *up*, *down* and *strange* quark as the *flavors* in the fundamental representation of $SU(3)$. The model suggested that a baryon is a combination of three quarks (or antiquarks), while the mesons are quark-antiquark pairs. A heavier strange quark was the explanation for the mass difference of the bound states. With the discovery of the Δ^{++} baryon came the next puzzle: This particle was readily interpreted as a bound state of three up quarks with zero orbital angular momentum and all three spins parallel. Seemingly a contradiction to Pauli’s exclusion principle, stating that one quantum state can only be assumed by a single fermion. To reconcile this principle with the baryon spectrum, Han, Nambu [8] and Greenberg [9] proposed that quarks carry an additional quantum number called *color*. The simplest way was to assign quarks to the fundamental representation of a new, internal $SU(3)$ symmetry. Meanwhile Yang and Mills extended the concept of *gauge theory* to non-Abelian groups [10]. Since the color symmetry had no other obvious role, it was natural for

Gell-Mann, Fritzsche and Leutwyler in 1972 [11] to identify the symmetry with a gauge group, in analogy to quantum electrodynamics. This resulted in the model for the strong interactions as it still is today, namely as system of quarks with various flavors coupled to an $SU(3)$ gauge theory, whose excitations are called *gluons*. The theory is known as *Quantum Chromodynamics* (QCD). Around the same time, deep inelastic scattering experiments at SLAC and MIT [12] confirmed the existence of point-like constituents in the protons, and later the three-jet events at DESY posed the evidence for the gluons [13]. In further experiments the heavy flavors *charm* (SLAC and BNL), *bottom* and *top* (both at Fermilab) were discovered. All theory parameters are summarized in Tab. 1.1, where α_s represents the interaction strength or *coupling constant* of the theory.

Flavor	up	down	strange	charm	bottom	top	α_s	N_c
Mass [MeV]	$2.5^{+.6}_{-.8}$	$5.0^{+.7}_{-.9}$	100^{+30}_{-20}	1250^{+50}_{-110}	4190^{+180}_{-60}	$172.9^{+.6}_{-.8} \cdot 10^3$	0.1184 ± 0.0007	3

Table 1.1: Quark masses [14], world average of the strong coupling constant [15] and the number of colors. These microscopic parameters in principle determine the entire world of QCD.

Naturally, the question arose that why quarks or colored object are never directly observed in an isolated form. When Callan and Symanzik formulated the *renormalization group equations* (RGE) [16, 17], which govern the dependence of the theory parameters on the energy scales, it was possible for Gross, Politzer and Wilczek in 1973 [18, 19] to find that non-Abelian gauge theories exhibit *asymptotic freedom*. In this sense, the values given in the above table are only valid at the microscopic scale. The RGE of the strong coupling constant is negative, entailing that the coupling goes asymptotically to zero at high energies, where then the particles become free of interaction. This allows for a perturbative expansion of the theory in the coupling parameter. The predictions made in this way, are in a satisfying agreement with experiments. Of course there is the opposite limit of small energies, or equivalently large distances, where coupling runs into a *Landau pole*. The diverging behavior signals the breakdown of perturbation theory, happening at a scale of $\Lambda_{\text{QCD}} \simeq 200$ MeV, that is identified as the infrared (IR) cutoff of classical QCD. The absence of color charged objects in nature, known as *confinement*, is explained by the increasing coupling at large distances. The energy that is needed to separate colored objects from each other at some point exceeds the threshold for the creation of particles in the middle, which then pair with the initial objects back into color neutral states. The behavior of the coupling is rooted in the non-Abelian nature of the gauge theory, where the gauge field are subject to self-interactions. Hence it is believed that confinement is triggered purely by the gluon dynamics, though a rigorous mathematical proof has yet to be delivered.

Due to confinement the first feeling for the quark masses can only be obtained by dividing the mass of a *hadron* (bound states in QCD) by the number of its constituents. But then one finds a discrepancy between mesons and baryons. The former are far too light to have agreeable constituent masses. The correct understanding requires an approach to contain a well-defined limit of massless quarks in the high energy regime. Then the QCD action possesses a global flavor symmetry known as *chiral symmetry*, that can break *spontaneously* in the ground state through quantum fluctuations. Along with that, according to Goldstone's theorem [20], massless bosons must occur. When there is an initial, small explicit breaking, the Goldstone bosons have small but nonvanishing masses. The masses that are given in the table are the *current masses*, which are obtained from the Higgs mechanisms [21–23] at the electroweak scale ~ 246 MeV. However, the nucleons, which are made of three up and down quarks, have a mass of about 1 GeV. This is understood as the dynamical breaking of chiral symmetry in addition to the explicit breaking

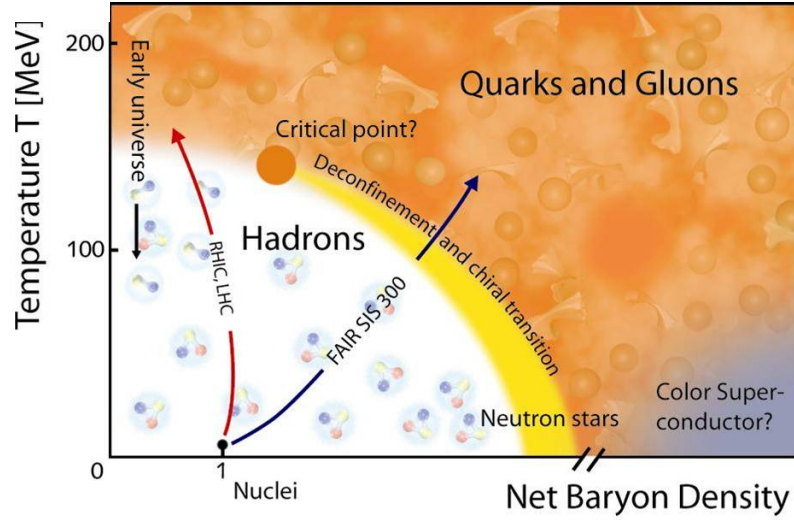


Figure 1.1: Sketch of the phase diagram of QCD [24]. For reviews see [25–29].

by the current masses, and the pions occur as the associated *pseudo* Goldstone bosons with a mass of ~ 140 MeV. At the most fundamental level all particles are massless. What we call *mass* is actually the energy of the cloud of quantum fluctuations around the particle interacting with it. For the light quarks, most of the cloud is generated from QCD, whereas for the heavy quark the electroweak interaction is most responsible. The relevant scale is again Λ_{QCD} where the interaction becomes strong, and the quarks that have a substantially lower mass than this scale can be considered as approximately massless. When all fluctuations are included, QCD adds about 300 – 500 MeV to the values in the table, and they are the *constituent quark masses*. Thus, most of the mass of all chemical elements in the periodic table is owed to the dynamical chiral symmetry breaking. Note that neither the current nor the constituent masses can be measured exactly, but are rather resulting from model or lattice calculation.

The low energy regime with its non-perturbative phenomena, among which confinement and chiral symmetry breaking are the most prominent, is even hitherto not entirely understood, and this is what makes QCD so fascinating as research topic even today. The two limits of asymptotic freedom and hadronic physics imply a drastic change of the degrees of freedom. While at high energies, there are weakly interacting light quarks and gluons, at low energies they exist as heavy constituents of color neutral objects, interacting via the exchange of light mesons. It is natural to expect a phase transition somewhere in between the two limits. It is believed that the chiral and the confinement-deconfinement transition are related to each other, but no analytical description for some dynamical link is available yet.

At finite temperature and density we have additional scales in the system. Since the temperature gives rise to a kinetic energy for the particles, it somewhat mimics the physics at high energies. At nonzero densities fermionic states are occupied and therefore quantum fluctuations are suppressed. Thus it is concluded that phase transitions should occur in both these directions. The arguments can be put into a map of the conjectured phase diagram as given in Fig. 1.1. It is an active area of research and a great challenge to understand the nature and properties of the phases and the mechanism behind the transitions, from both the experimental and theoretical side. Indicated are the hadron gas in the low temperature, low density regime, the *quark-gluon-plasma* (QGP) at high temperatures, and the *color superconductivity* at high densities. The precise structure

is far from being known. However, along the T -axis at vanishing densities, convincing evidence has been collected from experimental and theoretical endeavor, that both aforementioned phase transitions exist and approximately coincide [30, 31]. At intermediate densities it was proposed that a new, so-called *quarkyonic phase* may exist, which is confining but chirally symmetric [32–34]. Such a phase is realized in the limit of many colors. The QGP is gas of free quarks and gluons in the infinite temperature limit [35–37], while in the vicinity of the phase transition experiments hint that it behaves like a strongly coupled liquid [38–40]. A finite density is implemented by a chemical potential μ , which actually parametrizes the imbalance between particles and antiparticles. It is believed that the early universe underwent the QCD phase transition from the QGP phase to the hadronic phase by cooling down at about $T_c \approx 160 \text{ MeV} \approx 10^{12} \text{ K}$, at small chemical potentials. This happened within 10^{-6} seconds after the big bang.

Evidently, creating the extreme environment for the experimental study of the QCD phases requires enormous efforts. Nowadays it is realized in ultra-relativistic heavy-ion collisions at RHIC and LHC for small chemical potentials, and in the future FAIR and NICA will investigate the high density regime. When two ions collide with tremendous energies a fireball is created, where for very short lifetime the QGP phase can occur. Such a system can be described by viscous or ideal hydrodynamics, depending on the thermal equilibration [41–45]. For the very early, non-equilibrium stages the so-called *Color Glass Condensate* framework has been developed [46–51]. The next stage is reached when it has cooled down to the hadronic phase. But the particle content is not fixed until the chemical freeze-out, which represents a lower bound for the hadronisation temperature. The final stage is reached when elastic scatterings have ceased at the thermal freeze-out and the momentum distribution is fixed. All information of the fireball have to be reconstructed from this point backwards [52].

Within the hadronic phase lies the liquid-gas phase transition of nuclear matter. At vanishing temperatures it is characterized by a simple onset of the density when the baryon chemical potential is close to the nucleon mass. Aside from the point in the vacuum, this is the only other point in the phase diagram that is empirically certain. At finite temperature there is a gas of baryons, which turns into a liquid of self-bound baryons by increasing the density. The transition is first order and turns into a crossover above $T \approx 15 \text{ MeV}$. The nuclear liquid-gas phase transition is also of particular interest in the context of supernovae evolution [53–55].

The order of phase transition between the hadronic and QGP phase is of course a natural question. The Columbia plot in Fig. 1.2 summarizes the possibilities at vanishing density, dependent on the quark masses. When they are small or vanishing in the chiral limit, then by cooling down system the quark fluctuations set in very suddenly, entailing a first order chiral phase transition [56]. If quarks are heavy, the transition is rendered to a smooth crossover. In between is a critical line for the second order transition, which extends to the limit of a heavy strange quark and massless up and down quarks. The confinement-deconfinement transition is first order if all quarks sufficiently heavy [57], and turns into crossover when they are lighter, again with a critical line in between. The physical point lies in the crossover region for both transitions. The heavy quarks are irrelevant, because when the non-perturbative effects come into play at Λ_{QCD} they are already decoupled. Most of the model calculations show that the phase boundary bends down towards increasing chemical potential along with a steeper becoming crossover. This is rooted in the fact that a finite density suppresses quark fluctuations until the states in momentum space become free at lower temperatures, and since the quarks are still light, intense fluctuations come very suddenly, that at some point the phase transition may become first order. The exact location of the corresponding critical endpoint, if it exists, is of great interest also from the experimental point of view, as the enhanced fluctuations should yield distinct signals [58, 59].

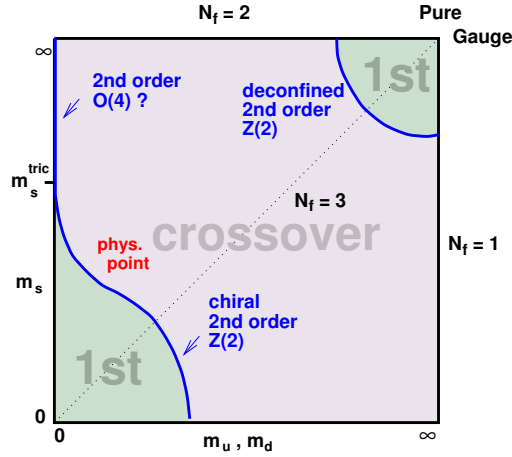


Figure 1.2: The Columbia plot [60].

Cooper pairing in cold, dense quark matter has been mentioned first in 1975 [61] and then further established in [62–64]. It was not until the 1990’s when the relevance of this idea got more attention. In certain diquark channels one-gluon exchange entails an attractive interaction. If the quark density is sufficiently high and the temperature sufficiently low, it necessitates a bound state formation in those channels, which then by virtue of their bosonic nature form a condensate. We can rely on the knowledge from condensed matter physics and also the Higgs mechanism, to deduce that such a state of matter should exhibit a mass gap for some color states of the gluons, by which the interaction is suppressed, and thus the flow of matter is frictionless. Therefore this phenomenon is called *color superconductivity* (CSC). It is unlikely that the temperatures can be small enough in heavy-ion collisions to detect such a state, however in compact stellar objects like neutron stars it might be realized. Their composition and their life cycles crucially depend on the thermodynamic properties and the equation of state of the strongly interacting matter in this region of the phase diagram [65]. At asymptotic densities, i.e. for $\mu \gg \Lambda_{\text{QCD}}$ weak-coupling methods can be successful in analyzing the ground state of the CSC phase [62, 64]. In this limit the strange quark can be considered as degenerate with the lightest quarks, and the ground state is characterized by evenly pairings of combinations with all three quarks flavors. For reviews see [66–71].

The phase structure in the region of intermediate chemical potentials is far from being settled. A two-flavor color superconductor [72–76], spatially inhomogeneous chiral [77–79] or diquark [80–82] condensates leading to crystalline phases, or the quark-hadron continuity between a baryonic superfluid and superconducting quark matter [83, 84], with the disappearance of the phase boundary [66] or new critical endpoints [70, 85], are some of the conjectured scenarios.

The rising coupling constant and the consequential non-perturbative nature of QCD make an exact solution impossible. The closest and most advanced method for calculations from first principles is *Lattice QCD* [86–90]. One has to discretize spacetime within a finite volume and solve the path integral by performing numerical Monte-Carlo simulations on each lattice site. This is possible as the path integral has a statistical interpretation in the Euclidean formulation. The artifacts from the finite size and lattice spacing require a proper extrapolation to the continuum limit. In addition, the implementation of fermions with their anticommuting nature results in difficulties, especially when they are light [91, 92]. The greatest complication is posed by the notorious sign problem [93, 94]. The fermionic determinant takes a complex value at finite μ ,

where then the statistical interpretation does not hold, leading to a breakdown of the Monte-Carlo sampling technique. In regions of $\mu < \pi T$ the sign problem is circumvented by reweighting techniques [95–98], Taylor expansions [99–102], or extrapolations from imaginary chemical potential [103–105]. For further reviews regarding the sign problem see Refs. [106–108]. However, profound information for zero density regime has been obtained from lattice simulations. A steep rise in the pressure and energy density signaling a phase transition was already found in the early stages [23, 109]. Today it is well-established that there is a crossover at $T_c \approx 155$ MeV [110–117]. Also, the mass spectrum of the light hadrons was computed successfully [118].

Recently, the stability of the numerical simulation with the stochastic quantization or the Complex Langevin Equation has been significantly improved [119], which could supersede the Monte-Carlo algorithm in a high-density region where the sign problem is severe. The convergence is well investigated [120] and tested in lower-dimensional models [121, 122] but it is not yet understood why the applicability of this method to real-time problems is limited [123–125]. There are also new developments by means of the mathematical technique in Picard-Lefschetz theory [126, 127], which is still developing but has been successful for several test cases.

Before the establishment of QCD, phenomenological models were already developed. Most prominently are the *linear sigma model* [128] and the *Nambu-Jona Lasinio model* (NJL) [129–131]. Both are based on the chiral symmetry principle, and with ability to describe its breaking, these models still represent the ground work for today’s effective low energy description of QCD. The former is a purely bosonic model of pions and the sigma field, which plays the role of radial mode in the symmetry breaking pattern. At that time the existence of the sigma was prediction, and today it is still not entirely settled which of the observed scalar mesons it should be. The NJL is a purely fermionic model, where it was suggested that the nucleon mass arises through fermionic self-interactions by the same mechanism as the appearance of the energy gap in the theory of superconductivity. Another widely used model is *chiral perturbation theory* [132–134], for which important ingredients were the low energy theorems of the Goldberger-Treiman [135], the PCAC relation [128, 136], the current algebra and the GMOR relation [137]. It allows for a systematic investigation of the low energy structure in terms of a perturbative expansion in the pion momenta and mass. For reviews see [138, 139]. Naturally a pure bosonic model fails to describe the system outside of the hadronic regime. When the bosonization techniques were introduced [140, 141], it soon became possible to connect fermionic and bosonic model with each other and utilize the advantages of both descriptions [142–147].

Typically, effective models are solved within the *mean-field approximation* where fermionic fluctuation are integrated out. However, *functional methods* are continuously getting more attention. Very renowned are *Dyson-Schwinger equations* [148, 149] and the *Functional Renormalization Group* (FRG) [150, 151]. They aim to solve the theory by solving its correlations functions, all that are allowed by the symmetry of the underlying theory. The correlations functions are given in the form of an infinite set of coupled, exact differential or integral equations, taking into account all kinds of fluctuations, which inevitably has to be truncated to a finite set for a practical use. It should be noted that such scheme does not pose a perturbative expansion, as a suitable truncation is still able to capture the important non-perturbative aspects of system. However, a good physical insight to the problem is required for an adequate choice of that approximation, as there is no measure of the quality of the calculation. Nevertheless, a convergence of the results within a systematic improvement of the approximation and the agreement with well-known limiting cases should bestow some certainty. In contrast to Lattice QCD there is no conceptual problem in continuum methods, in particular at finite density. Moreover, the physical mechanism that are at work become visible. Hence, both approaches should be viewed as complementary to each other. At the moment it is actually the best strategy to collect various pieces of insights

from different approaches to construct the most presumable picture of the QCD phase diagram. Mean field approaches [152–160] and Dyson-Schwinger equations [161–169] have provided valuable knowledge about non-perturbative aspects of QCD. In this work we will employ the FRG. It was put forward by Wetterich in 1993 [150] and describes the evolution of a microscopic theory to the macroscopic regime, by successively integrating out quantum and thermal fluctuations in thin momentum shells. With this machinery it is possible to investigate the dynamical change of degrees of freedom in different energy scales. The FRG was successfully employed for the chiral phase transition not only in low energy effective models for QCD, like the quark-meson (QM) models [170–180] but also, with the help of modern bosonization techniques [181–184], recently it became possible to establish a dynamical connection of the high energy quark-gluon sector with the low energy hadronic sector [185, 186]. The formation and dissociation of bound states can now be described with correlation functions emerging directly from QCD, without having a disturbingly large parameter dependence. However, it has turned out that very sophisticated truncations are essential for an accurate description of the non-perturbative phenomena. Furthermore, the confinement mechanism can be incorporated by additionally including the order parameter of the gauge sector, the *Polyakov loop*. The corresponding PQM models have been studied in [187–195]. The pure Yang-Mills part was investigated in [196, 197].

An instructive way to approach the full problem and to shed light on particular aspects, is the investigation of deformations of QCD [198]. Generally, this can be achieved by changing e.g. mass parameters, symmetries or the field content. In this work, we will choose the latter two possibilities and study a theory similar to real QCD, however with two colors, and two quark flavors. An appealing feature within this version of QCD is that, apart from the chirally broken mesonic phase, it allows for the formation and (Bose-Einstein-) condensation of colorless diquarks, i.e. a bosonic baryon state. This results in a rich phase diagram with two dynamically competing order parameters. Since the diquarks are colorless, its condensation does not give rise to color superconductivity, but rather to a baryon superfluid.

Two-color QCD (QC₂D) has attracted strong interest recently and has been studied within mean field theory and the chiral Lagrangian approach [199–207], random matrix models [208, 209] and within the Nambu-Jona-Lasinio model [73, 210–219]. For an even number of quark flavors the $SU(2)$ gauge group provides a positive path integral measure and thus avoids the occurrence of a fermion-sign problem. This facilitates the investigation of the QC₂D phase diagram by lattice simulations [220–232]. In this work we employ an FRG approach to an effective quark-meson-diquark (QMD) model to study the phase diagram of QC₂D. A comprehensible FRG phase diagram for finite temperature and density has previously been established by Strodthoff *et al.* in Refs. [233, 234] by a solution of the FRG evolution equation for the effective potential, which naturally includes the effect of competing fluctuations of the mesonic and baryonic diquark fields. The present work systematically extends the truncation scheme in Ref. [233] by taking into account the scale dependence of the wave function renormalizations and of the Yukawa couplings between the quarks and the order parameter fields. Additional quantitative effects can be accessed systematically by extensions of the truncation scheme within the FRG as has been shown in the non-relativistic analogue of QC₂D, namely the BCS-BEC crossover [235–239]. Here, we can monitor the quantitative corrections that are induced by the additional scale dependent quantities and study their impact on the phase diagram. Due to an alternative expansion scheme for the effective potential we gain direct access to the phenomenon of *pre-condensation*, a regime in the phase diagram where order occurs at intermediate scales but no order is found when all fluctuations are integrated out. In this way, we establish a refined picture of the FRG phase diagram for QC₂D.

In parallel we will construct an effective low energy model for QCD including diquarks and baryons. If the baryon chemical potential is much higher than the temperature, we are still far from any first-principle calculation. It would be thus an urgent task at the present to build a phenomenological model at work. Actually, we would stress that such model studies had played a guiding role in a regime $T \gg \mu$ in early days when the Lattice QCD results were premature. It should be a natural anticipation that, in the same way as the high- T study, some models should guide us to a correct intuition of the dense state of QCD matter. Previous works can be found in Refs. [240–249].

As a matter of fact, the theoretical approach based on the chiral effective theory [249–252] should be a valid description as long as the system is not far from cold nuclear matter. Once the deconfinement happens, we can then investigate the properties of matter entirely out of quarks using the chiral quark models at moderate density and the perturbative QCD calculations [253] at asymptotically high densities. It is a big question how these two descriptions of dense matter in terms of baryons and quarks could be (possibly smoothly [254]) connected in an intermediate density region. In other words, there is no clear picture of quark deconfinement induced by large density effects, while it is a well-studied phenomenon along the temperature axis in Lattice QCD and effective models.

A key ingredient to shed light on a modern picture of deconfinement at high density is, in our belief, the diquark correlation, see Ref. [255] for a comprehensive review. In fact, it is a widely accepted knowledge to introduce a “constituent diquark” to solve a three-body bound state problem, i.e., the Faddeev equation, to make a baryon with constituent quarks [256–258]. The diquark in this formulation is, however, not necessarily a physical object and there are a number of theoretical attempts to seek for a strong and localized correlation of diquarks in hadrons. One of the most well-known examples that suggest the diquark correlation is the inverted mass ordering in the scalar nonet channel [259, 260] and this idea is also supported by the instanton-induced interactions [261], see Ref. [262] for a recent lattice study. It is also said that the exotic XYZ mesons might have a significant overlap with the diquark–anti-diquark state together with the meson molecule, see Ref. [263] for an overview. Evidence for diquark in Lattice QCD can be found in Ref. [264].

There are already some attempts to build an effective model in terms of mesons, quarks, and diquarks. In a conventional model setups as in Ref. [265] for example, it is common to accommodate diquarks as explicit degrees of freedom and generate baryons as bound states of quarks and diquarks. (See also a recent attempt [266] in which diquark dissociation or the Mott transition has been taken into account.) Obviously, however, diquarks should be dynamically generated excitations and we must cope with microscopic structures of diquarks. We will formulate these processes of the formation and the dissociation of diquarks by means of the FRG equations. One could in principle solve the bound state problem by constructing the propagator in the diquark channel and locate the pole position in the complex energy plane as done in Ref. [267].

In this work we will give a theoretical foundation. In the numerical calculation, we will limit ourselves to the simplified the QMD-model and study chiral symmetry breaking and two-flavor superconductivity, not including baryons yet. As we will explicitly see later, this simple framework is already involving and needs much technical developments beyond the similar one in two-color QCD [233]. For instance, as in the FRG framework bosonic fluctuations are included in the first place, we must take the Meissner effect into account by removing the Goldstone modes from the system in color superconducting phase. We would leave a more complete description in terms of baryons as well as quarks, mesons, and diquarks for future works.

Outline of the thesis

This thesis is organized as follows. In the next chapter we will start with the introduction of the QCD action with the field content and gauge symmetry. We will give some brief remarks on the quantization procedure and take a closer look on asymptotic freedom. In the subsequent section we will discuss the underlying symmetries in detail, as well as the breaking patterns and order parameters in QCD. Starting with the center symmetry and confinement, we will go over to the flavor symmetries and the chiral phase transition, through to the diquark condensation within color superconductivity. In the latter we will lay special emphasis on the tensor structure of the diquark in a two-flavor superconductor and in the color-flavor locked phase. The final part of this section will discuss the extended flavor symmetries of two-color QCD and the various breaking patterns. The next section will be about the low-energy degrees of freedom. We will begin with generation of four-fermion interaction from quark-gluon dynamics and the bosonization thereof. Some remarks will be given on the advanced rebosonization techniques, before we turn to an analog baryonization. Based on the symmetries we will then construct an effective four-fermion model for two-color QCD and obtain the bosonized version of it. Thereafter we will generalize this model for QCD and add the baryonic degrees of freedom. At the end of this chapter we will explain, how phase transitions can be computed with an effective potential, and write down an ansatz for it in the form of a 1d as well as a 2d Taylor expansion in the mesonic and diquark fields.

In Chap. 3 we will derive the renormalization group equations for our models. It will be somewhat more technical but also some important physical insights will be given. In the beginning we will give brief introduction of the FRG method with some solution strategies. Then we will derive the propagators that we need for the FRG equations and also discuss the corresponding mass gaps. A numerical result for the mass spectrum will also be shown. As an interlude we will discuss the Silver Blaze property, which is the trivial μ -dependence of the system at vanishing temperature below the first onset, and its realization with the FRG framework. Thereupon we will write down the FRG equation for the effective potential and discuss it in great detail. Particular emphasis will be laid the thermodynamic properties as well as the influence of a baryonic background field. We will be able to anticipate the phase structure by analyzing various limiting cases. Then, after deriving the vertices, we will finally compute the flow of the two-point function, which includes the wave function renormalizations and Yukawa couplings. Their numerical results will be shown as well.

In Chap. 4 the main numerical results of this thesis will be presented, i.e the chiral and diquark condensation. After discussing the relevance of boundary conditions we will first discuss the pre-condensation effect and then show the condensates for our two-color QCD computation and the corresponding map of the phase diagram. We will compare different methods and truncations, in particular with the grid method (as opposed to the Taylor expansion), the linear sigma model as well as lattice computations. In the next section we will look deeper into the effects of our truncation. This includes different orders in the Taylor expansion, the effects of running two-point function and cutoff effects. Here we will also see qualitative differences for different boundary conditions. Finally, we will present our phase diagram for physical QCD with the chirally broken and color superconducting phases. A summary is presented in Chap. 5 and technical details are given in the appendix.

The two-color QCD related part of this work is intended to be publish in Ref. [268]. The physical QCD related part of this work is intended to be publish in Ref. [269].

From Quarks and Gluons to Mesons, Diquarks and Baryons

In this chapter we will begin with a brief introduction of the theory of Quantum Chromodynamics with its properties for different energy regimes. We will state the symmetries of the theory and breaking patterns, and the associated phase transitions. Moreover, the symmetries of the underlying theory are an important ingredient for effective low energy models. We will construct models in order to study the behavior of low energy modes in the form of the lightest mesons and baryons of the theory for physical QCD with three colors as well as for two-color QCD. The latter possesses an extended flavor symmetry which roots in the pseudo reality of the color group generators, and the consequential antiunitarity of the Dirac operator. In consequence there is an extended symmetry in the hadron spectrum linking the mesons and baryons at vanishing chemical potentials [199]. Naturally, in QC₂D the baryons of the theory have the form of color neutral diquarks, which are bosonic states. Hence, the study of QC₂D allows us to play with baryonic degrees of freedom as well as Bose-Einstein condensation in a rather simple manner. Moreover, due to the antiunitarity of the Dirac operator, QC₂D is free of the sign problem, in contrast to physical QCD, allowing lattice simulations at non-vanishing chemical potentials, and therefore a direct comparison of different methods with lattice simulations throughout the phase diagram.

Diquarks will also be considered for the effective description of physical QCD at large chemical potentials. It is assumed that diquarks are intermediate states for the formation of baryons, which consist of three quarks. Also, we will study the condensation of diquarks, which breaks the gauge symmetry and leads to a color superconducting phase. Of course, chiral symmetry breaking and the dynamical generating of the quark mass will be a central theme as well.

2.1 Classical QCD

Field contents QCD is the theory describing the interactions between quarks and gluons [11]. It is based on the coupling of spin-1/2 fermionic particles (quarks), described by the Dirac equation, to a Yang-Mills theory [10] of massless vector bosons (gluons). The latter is based on the *non-Abelian gauge symmetry*, which is the invariance under *local* transformations of the $SU(N_c)$ group, N_c being the number of colors. The coupling is made by demanding that the Dirac equation is also invariant under local gauge transformations of the quark fields, which is realized by promoting the derivative operator to a covariant derivative. The quark fields transform in

the fundamental representation and the gauge fields in the adjoint representation of the gauge group. The N_c colors are quantum numbers of quarks. Furthermore quarks come in different flavors, which simply means that there are quarks with different masses, the number of which is N_f . Hence, the quark fields from N_f fundamental representations of $SU(N_c)$ on a Cartesian product of Dirac spinors. Thus, the classical QCD action reads in Euclidean spacetime

$$S[A, q, \bar{q}] = \int d^4x \left\{ \frac{1}{4} F_{\mu\nu}^a F_{\mu\nu}^a + \bar{q} (i \not{D} + iM) q \right\}, \quad (2.1)$$

where the mass matrix $M = \text{diag}(m_u, m_d, m_s, m_c, m_b, m_t)$ contains the current masses of the $N_f = 6$ different flavors, generated by the Higgs mechanism, given in Tab. 1.1. The field strength tensor and the covariant derivative with the gauge coupling g are given by

$$F_{\mu\nu} = \frac{i}{g} [D_\mu, D_\nu] = \partial_\mu A_\nu - \partial_\nu A_\mu - ig[A_\mu, A_\nu], \quad (2.2)$$

$$\not{D} = \gamma_\mu D_\mu = \gamma_\mu (\partial_\mu + igA_\mu), \quad (2.3)$$

where $A_\mu = A_\mu^a t^a$ are the gauge fields with the $N_c^2 - 1$ group generators t^a , which satisfy the Lie algebra $[t^a, t^b] = if^{abc} t^c$, where f^{abc} are the structure constants. For $N_c = 2$ the generators are given by the Pauli matrices and we have 3 color degrees of freedom in the gauge fields; for $N_c = 3$ the generators are the Gell-Mann matrices with 8 color degrees of freedom. The structure constants and matrices can be found for instance in [270]. The γ_μ are the Dirac matrices given in App. A.4. The greek letters, e.g. $\mu = 1, \dots, 4$, represent Lorentz indices in Euclidean spacetime. The gauge transformations, under which the above action is invariant, are defined as

$$\psi(x) \rightarrow U(x)\psi(x), \quad A_\mu(x) \rightarrow U(x) \left(A_\mu(x) - \frac{i}{g} \partial_\mu \right) U^\dagger(x), \quad (2.4)$$

where $U(x) = e^{-i\alpha^a(x)t^a}$ are the elements of the local $SU(N_c)$ group. The basic processes associated with the classical QCD action are depicted in Fig. 2.1. Note that the pure gauge interactions only appear in non-Abelian gauge theories, where the gauge fields carry charge.

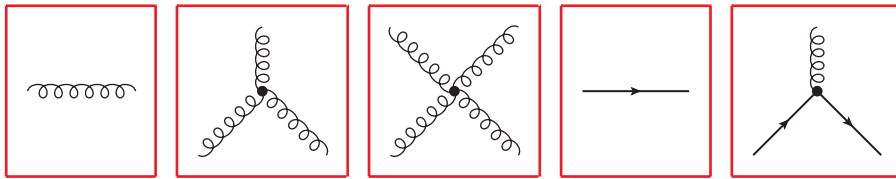


Figure 2.1: These are the building blocks for describing interaction processes in the form of *Feynman diagrams* derived from the classical QCD action (2.1). The curls represent gluons, the straight lines represent quarks, where the arrow marks the direction of the baryon charge flow. The horizontal lines represent *propagators*, and the rest represent interactions, also referred to as *n-point*-, *correlation*- or *vertex functions*. Note that after quantization there are additional building blocks, namely the ghost propagator and a ghost-antighost-gluon vertex.

Remarks on the quantization of gauge fields Since in our model calculations we will consider the gluons to be irrelevant, will not go into details of the quantization of the gauge fields. However, let us briefly outline some of the important concepts.

The quantization of the gauge fields is not straightforward, and it is best done in the path integral formalism [270]. The integration measure respects all possible field configurations, of

which infinitely many are physically equivalent due to the gauge symmetry. To fix this problem, one isolates the part of the functional integral which counts each physical configuration only once by means of the *Faddeev-Popov trick* [271], which amounts to imposing a gauge fixing condition $G(A)$. Applying this method in non-Abelian gauge theories leads to additional degrees of freedom in the theory, the *Faddeev-Popov ghosts*, which are no physical asymptotic particle states but rather a mathematical tool, in fact, canceling the effects of unphysical timelike and longitudinal polarization states of the gauge bosons. Moreover, a free gauge fixing parameter is introduced, of which the observables must be independent.

With the introduction of the ghost fields the Faddeev-Popov action exhibits the so-called *BRST symmetry* [272, 273]. It is a global symmetry of the gauge fixed action, which is well-defined on the perturbative level only. The BRST transformation has an anticommuting nature. The transformation operator distributes the eigenstates of the theory into subspaces with the physical asymptotic states and the unphysical states mentioned above [274].

Finally we, mention that Faddeev-Popov gauge fixing still leaves a redundancy, which is called the *Gribov ambiguity* [275]. A way to resolve this problem is perform the functional integral over a single region, the *Gribov horizon*.

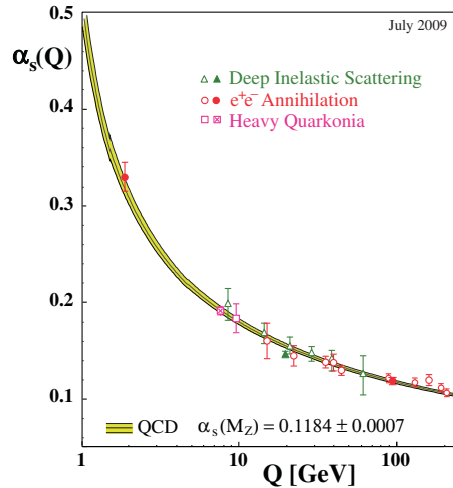


Figure 2.2: Theoretical predictions and experimental measurements of the strong coupling constant α_s as a function of the energy scale Q [15].

Asymptotic Freedom Asymptotic freedom is a general feature of non-abelian gauge theories and crucial for most of the important phenomena in QCD. It states that the interaction becomes weak for large momentum transfers or between small length scales, and therefore it allows perturbative calculations. Coming from the perturbative regime, one solves the *Callan-Symanzik equation* [16–18] for coupling parameter and obtains its dependence from the momentum scale Q . Therefore it also called the *running coupling*. With $\alpha_s = \frac{g^2}{4\pi}$ one finds in leading order

$$\alpha_s(Q) = \frac{2\pi}{\left(\frac{11}{3}N_c - \frac{2}{3}N_f\right) \log\left(\frac{Q}{\Lambda}\right)}, \quad (2.5)$$

where Λ is the intrinsic energy scale, below which a perturbative expansion in α_s of interaction processes breaks down. For QCD, experimental measurements yield $\Lambda_{\text{QCD}} = 200$ MeV. The divergence of Eq. (2.5) at this scale, also known as *Landau pole*, is not a physical pole, but

rather it signals that non-perturbative methods must be applied for the low energy regime, and in particular for the description of bound states or critical phenomena like phase transitions, as was done in e.g. Refs. [185, 186]. Fig. 2.2 shows theoretical predictions beyond leading order and experimental measurements of the strong coupling parameter. At large energies the coupling parameter goes asymptotically to zero, which is also an implication of Eq. (2.5).

Note that in Eq. (2.5) the effects from the fermions ($\propto N_f$) are opposite to the effects from the gauge fields ($\propto N_c$). Whether a theory exhibits asymptotic freedom, depends on the relative number of these degrees of freedom. In quantum electrodynamics (QED) the scale-dependence of the coupling parameter is the other way around, because it is an Abelian gauge theory with uncharged gauge fields. The vacuum in QED acquires a dielectric property due to the virtual electron positron creation, causing the effective electric charge to decrease at large distances. The fermions in QCD produce a similar effect, but it is overcompensated by the gluons, which also produce dipoles in the vacuum but in the opposite direction. Therefore the effective color charge increases at large distances.

The consequences of the rising coupling are related to the breaking of symmetries, which will be discussed in the following.

2.2 Symmetries and Related Phase Transitions

In this section we explore the symmetries of the QCD action (2.1) and the various ways to break them. Symmetries are typically broken in the ground state, which depends on the external circumstances of the system, in particular on temperature T and density, parametrized by the chemical potential μ . As we have shown in the introduction, one can draw diagram in the T - μ plane, where in different regions different symmetries are broken. Important physical properties of the system are associated with the breaking of a symmetry, like the confinement of colored objects, the dynamical generation of the constituent quark mass or color superconductivity. We will discuss each of these phenomena and introduce the corresponding order parameters. Although the confinement-deconfinement phase transition will not be computed in this work, it is important concept upon which the model construction in the next section is based. The somewhat different symmetries and breaking patterns of two-color QCD will be discussed at the end of this section. We remark that all informations given in section are well-known.

2.2.1 Center Symmetry and Confinement

Physical picture Confinement is the phenomenon that color charged objects cannot be isolated, in particular the single particle excitations of the QCD action (2.1) cannot be directly observed. The quarks are held together by the gluons in color neutral states, composed of a quark-antiquark pair (meson) or of three quarks (baryon). These *collective excitations* must be incorporated in a low energy description of QCD. The phenomenon is of course related to the increasing coupling strength at large distances as discussed in the previous section. The common picture is shown in Fig. 2.3(b): If for instance a quark-antiquark pair is pulled apart, the potential energy rises linearly until it surpasses the threshold to create another quark-antiquark pair in the middle, each of which binds together with one of the initial particles, such that we have again colorless mesons. For infinite quark masses the threshold can never be reached, thus it would require an infinite amount of energy to separate the pair. Fig. 2.3(a) shows the potential energy of a static quark-antiquark pair with infinite masses. The potential can be translated into a color-electric field in the form of a narrow flux tube or a string between the charges as shown in

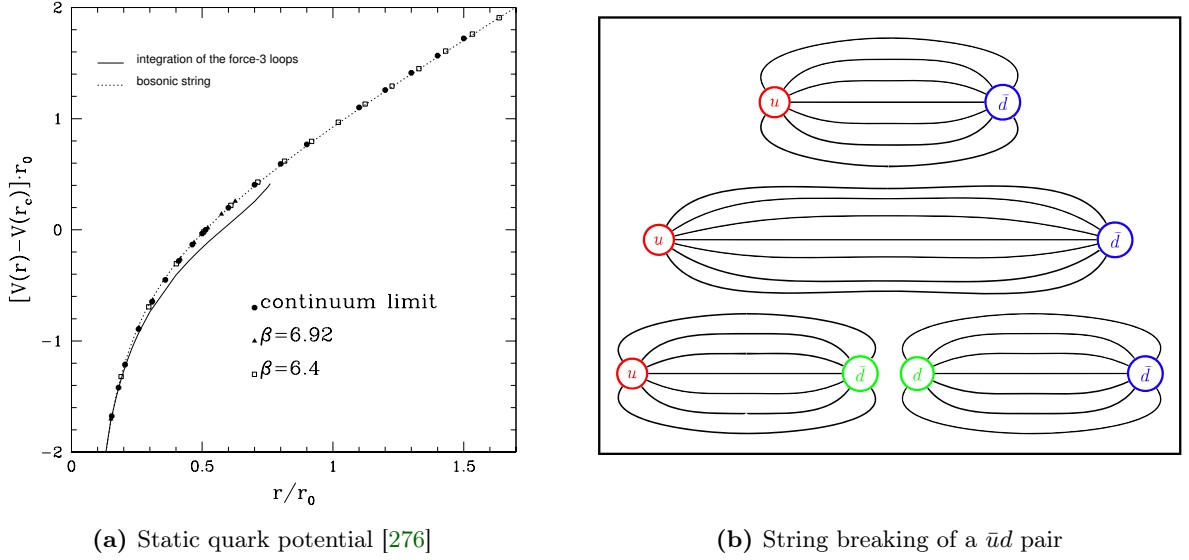


Figure 2.3: In (a) we see the static quark potential from pure $SU(3)_c$ Yang-Mills theory on the lattice with an extrapolation to the continuum limit. Perturbative predictions are shown as well, which are in good agreement for small distances. In (b) the string breaking mechanism for finite quark masses is depicted. Figure taken from [277].

in the upper two of Fig. 2.3(b). At high temperatures the quarks are expected to be deconfined, since a sufficiently high thermal energy does not allow the quarks to be held together.

The Polyakov loop There are many signals for confinement [278]. One that is often used is the *Polyakov loop* [279–281], whose expectation value is related to the free energy F_q of a static test quark [109, 282, 283]. In order to see the relation, we will make a rather heuristic argument: If the quarks are infinitely heavy we can neglect the quark dynamics in the action (2.1) and only consider the interaction term. As we will see in the next subsection, $j_\mu = i\bar{q}\gamma_\mu q$ is the quark number current, which is given by $j_\mu(\vec{x}) = \delta_{4,\mu}\delta(\vec{x} - \vec{y})$ for a single infinitely heavy test quark situated at the position \vec{y} . Now we say that the interaction term is $g\bar{q}\gamma_\mu A_\mu q \sim gj_\mu A_\mu$, and then we evaluate the delta function, which leaves only the Euclidean time integral over the timelike component of the gauge field which is the color-electric potential. Hence, with some more modifications, the partition function of system of gluons in the presence of a static test quark is reads

$$Z_Q = \int \mathcal{D}A L(\vec{x}) e^{-S[A]} \quad \text{with} \quad L(\vec{x}) = \mathcal{P} \text{tr} e^{g \int_0^\beta dx_4 A_4(x)}, \quad (2.6)$$

where the latter is the Polyakov loop with the path ordering operator \mathcal{P} and $S[A]$ is the pure gluon action. The Polyakov loop is a special case of the Wilson line which connects operators in different spacetime point in a gauge invariant way. At finite temperature T the time axis is compactified on a torus with the circumference $\beta = 1/T$, around which bosonic field obey periodic boundary conditions whereas fermionic fields obey anti-periodic boundary conditions [284, 285]. The partition function in Euclidean space is related to the free energy as $Z = e^{-\beta F}$. If we divide Z_Q by partition function Z of the pure gauge theory, we obtain the free energy of the test quark alone, and we see that it relates to expectation value of Polyakov loop as

$$e^{-\beta F_q} = \frac{Z_Q}{Z} = \langle L(\vec{x}) \rangle . \quad (2.7)$$

If we are in the confined phase, the energy required to separate a quark-antiquark pair by an infinite distance diverges, which entails a divergence of F_q and thus a vanishing Polyakov loop. In the deconfined phase on the other hand, only a finite amount of energy is needed for the separation, and then the Polyakov loop is non-vanishing. From the definition of the Polyakov loop (2.6) we can already predict the limiting cases: In the infinite temperature limit $\beta = 0$ the exponent vanishes, from which we can predict a finite expectation value. Whereas in the zero temperature limit the time integration has no boundary and the exponent goes to negative infinity yielding a vanishing Polyakov loop. In fact there is a critical temperature T_c where a phase transition occurs. In summary we have

$$\begin{aligned} \text{Confined phase:} \quad & T < T_c, \quad F_q \rightarrow \infty \quad \Rightarrow \quad \langle L(\vec{x}) \rangle = 0, \\ \text{Deconfined phase:} \quad & T > T_c, \quad F_q < \infty \quad \Rightarrow \quad \langle L(\vec{x}) \rangle \neq 0. \end{aligned} \quad (2.8)$$

The full information is contained in the effective potential $U(\langle L(\vec{x}) \rangle)$, minimizing it yields the ground state value of the Polyakov loop. Since the quarks can be infinitely heavy, confinement is driven purely by the gauge sector, as we have indicated in the previous section.

Center Symmetry The fact that there is a proper phase transition is actually a consequence of a related symmetry that holds on the classical level, but can be broken spontaneously in the ground state, namely the *center symmetry* [286]. The gauge transformations (2.4) must maintain the specific boundary conditions of the fields at finite temperature, which is easily done if the elements of the gauge group $U(x)$ satisfy periodic boundary conditions. However, for a pure gauge theory the necessary condition is more relaxed, namely that the transformations are periodic only up to a constant twist matrix like

$$U(\vec{x}, x_4 + \beta) = z U(\vec{x}, x_4), \quad (2.9)$$

where z are the elements of the center Z_{N_c} of the gauge group $SU(N_c)$ [287, 288]. They are essentially given by the N_c roots of 1 in color space

$$z = e^{2\pi i \frac{n}{N_c}} \mathbb{1}_{N_c} \quad \text{with} \quad n = 0, \dots, N_c, \quad (2.10)$$

and they commute with all group elements. The center symmetry is an additional global symmetry of the pure gauge theory and it can be broken spontaneously in ground state by a non-vanishing Polyakov Loop, as $L \rightarrow zL$. Hence, the Polyakov Loop is true order parameter, and the broken center symmetry signals deconfinement. On the other hand, if there are dynamical quarks in the system, center symmetry is explicitly broken, as the antiperiodic boundary conditions are jeopardized under center transformations. Therefore the phase transition turns into a crossover. Since Z_{N_c} is discrete symmetry there are no Goldstone bosons associated.

2.2.2 Flavor Symmetries and the Chiral Phase Transition

Flavor & chirality First of all, the QCD action (2.1) as it stands, with independent masses for each flavor, is invariant under simple $U(1)$ phase rotations of the quark fields for each flavor. Therefore, each flavor is a conserved charge of the theory. Now, if all masses were equal, there is nothing singling out a flavor, hence we could define a unitary transformation of the complete quark field, which rotates the flavors into each other. In this case only the sum of all flavors is

conserved. Going one step further and saying that all masses are vanishing, we can separate the parts with different Weyl components of the Dirac spinor in the Lagrangian, which are defined via the projection operators (App. A.4) as

$$q_{L,R} = P_{L,R} q, \quad \bar{q}_{R,L} = \bar{q} P_{L,R} = q_{R,L}^\dagger.$$

The *handedness*, also referred to as *helicity* of a particle, defines the orientation of its spin relative to the momentum: If the spin is parallel to the momentum, the particle is called *right-handed* (R), if it is anti-parallel we call it *left-handed* (L). However, the helicity depends on the frame of reference, unless the particle is massless, in which case helicity is the same as *chirality*. A transformation between the two helicities of a field is called *parity*, and the invariance under such a transformation is called *chiral symmetry*.

Chiral symmetry In QCD with degenerate flavors chiral symmetry is part of an extended symmetry, which includes the ones mentioned above. In the massless limit, neglecting the pure gluon part, only the quark kinetic term remains in the Lagrangian

$$\mathcal{L}_{\text{q,kin}} = \bar{q} i \gamma_\mu D_\mu q = q_L^\dagger i \sigma_\mu D_\mu q_L + q_R^\dagger i \sigma_\mu^\dagger D_\mu q_R,$$

where $\sigma_\mu = (i\sigma_j, \mathbb{1})$ with the Pauli matrices. This Lagrangian is invariant under independent unitary transformations of the left- and right-handed spinors in flavor space, i.e. under $U(N_f)_L \times U(N_f)_R$. It means that, if for instance the left-handed flavors are transformed into each other the right-handed ones must not follow the transformation, which leads to the separate conservation of each helicity. It is useful to separate the $U(1)$ part in order to gain more insight, moreover the symmetry group can be defined in terms of vector- and axial transformations:

$$SU(N_f)_L \times SU(N_f)_R \times U(1)_L \times U(1)_R = SU(N_f)_V \times SU(N_f)_A \times U(1)_V \times U(1)_A.$$

The vector transformations correspond to $U_R = U_L$, with $U_{L,R} \in U(N_f)_{L,R}$, hence, $U(N_f)_V = U(N_f)_{L+R}$ is the diagonal subgroup of $U(N_f)_L \times U(N_f)_R$. The axial transformations account for the difference. The $U(1)_V$ can also be interpreted as the baryon number symmetry $U(1)_B$. Each quark carries baryon charge, the total of which is conserved. Let us write down the symmetry transformations

$$\begin{aligned} SU(N_f)_V : \quad q &\rightarrow e^{i\alpha_a^V \tau_a} q, & U(1)_V : \quad q &\rightarrow e^{i\theta^V} q, \\ SU(N_f)_A : \quad q &\rightarrow e^{i\gamma_5 \alpha_a^A \tau_a} q, & U(1)_A : \quad q &\rightarrow e^{i\gamma_5 \theta^A} q, \end{aligned} \quad (2.11)$$

where τ_i are the generators of $SU(N_f)$. The associated conserved currents read

$$\begin{aligned} j_{\mu,a} &= i \bar{q} \gamma_\mu \tau_a q, & j_\mu &= i \bar{q} \gamma_\mu q, \\ j_{\mu,a}^5 &= i \bar{q} \gamma_\mu \gamma_5 \tau_a q, & j_\mu^5 &= i \bar{q} \gamma_\mu \gamma_5 q. \end{aligned}$$

Note that the conserved charge $\int d^3x j_4$ is the quark number. The $U(1)_A$ symmetry only holds on the classical level, it breaks due to quantum fluctuations of the gauge fields. This effect is called axial anomaly and will not be further discussed in this work, for a related FRG studies we refer to [289]. A breaking of $U(1)_A$ does not mean that chiral symmetry broken, but rather the $SU(N_f)_A$ is the actual chiral part of the symmetry. An ordinary Dirac-mass term couples left- and right-handed spinors $\bar{q}q = q_L^\dagger q_R + q_R^\dagger q_L$ and breaks $U(N_f)_A$ explicitly. We remark here that a chemical potential term does not break chiral symmetry.

In reality the masses of the different flavors are neither vanishing nor equal. However, QCD has the intrinsic scale Λ_{QCD} , which defines a lower cutoff for the quark-gluon picture. The masses which are well below this scale can be treated as small perturbations of the chiral symmetry, they must not even be equal. Therefore, typically one considers a model where u , d and s quarks, or at least the both former ones, are treated as degenerate (massless) degrees of freedom. Nevertheless, the invariance under $U(1)_B$ still holds for the combination of all flavors, while each of the heavy flavors are conserved separately. In this work we will implement u and d quark fluctuations with a small and explicit degenerate mass parameter. Hence we have $N_f = 2$ flavors with an approximate $U(2)_A$, and exact $SU(2)_V \times U(1)_B$ symmetry. The generators τ_i are then given by the Pauli matrices.

Flavor	up	down	strange	charm	bottom	top
Constituent mass [MeV]	336	340	486	1550	4730	$177 \cdot 10^3$

Table 2.1: Constituent masses for all flavors taken from [290]. Note that their exact values are model dependent. If we compare to the current masses in Tab. 1.1, we see that the constituent masses of the light quarks is mainly generated by the chiral phase transition.

Dynamical chiral symmetry breaking Now the question is, what happens below Λ_{QCD} , or more precisely, in the QCD vacuum. If the quarks have negligible masses, the vacuum is filled with spontaneous quark-antiquark pair productions. Since the energy cost for such a process is small, we expect that the vacuum contains a whole condensate. Angular momentum conservation forces the pairs to be of opposite helicity, hence the condensate must be of the form

$$\langle \bar{q}q \rangle = \langle 0 | q_L^\dagger q_R + q_R^\dagger q_L | 0 \rangle. \quad (2.12)$$

This is the order parameter of the *chiral phase transition*. All quarks acquire an effective supplement to their masses from this condensate, even though it mainly consist of the light flavors. When quarks travels trough the vacuum, it strongly interacts with condensate via gluon exchange, slowing it down and effectively making it “heavy”. It is a dynamical effect which breaks the chiral symmetry $U(N_f)_A$ *spontaneously*, via a second order phase transition towards the low energy regime for the case two massless quarks flavors [56]. For finite quark masses one observes in lattice calculations that the sharp phase transition turns into a smooth crossover. At high temperatures the ground state is filled with thermally excited fermions blocking quantum fluctuations by the Pauli exclusion principle. Moreover, the temperature sets an energy scale for the system, hence the interaction is weak at high temperatures, and chiral symmetry is restored. Similar is the situation at large chemical potentials.

Lattice simulations indicate that along the temperature axis the confinement and chiral phase transition coincide [291], though there is no analytic description of the linking of these two mechanisms. Nevertheless, the dynamically generated effective mass is referred to as *constituent quark mass*, since these quarks mainly appear as constituents of hadronic bound states. Each flavor receives additional 300-500 MeV to their current masses from the condensate except for the top quark, which receives 5 GeV, see Tab. 2.1. Of course for the light quarks, and also the corresponding hadrons (in particular nucleons), this makes up a very large fraction of their

masses. Note that $SU(N_f)_V$ is also known as *isospin* symmetry linking not only u with d quarks but also pions (isospin triplet) as well as protons with neutrons.

The fact that chiral symmetry can be broken dynamically and the quarks can acquire a much larger effective mass, must be incorporated into an effective low energy description of QCD. How this is done, will be explained in Sec. 2.3.1. Let us mention here that it involves bosonic bound states, of which $N_f^2 - 1$ play the role of the massless Goldstone bosons [20], for $N_f = 2$ they are the aforementioned pions. For the case of an approximate chiral symmetry with small quark current masses, the pions are only *pseudo*-Goldstone bosons with $m_\pi \sim 140$ MeV, which is still small compared to remaining hadronic states. In the IR regime QCD can be reformulated in terms of pion degrees of freedom known as *chiral perturbation theory* [138, 139, 292–294]. In this work however, we want to study the breaking of symmetries for which quark degrees of freedom are crucial.

2.2.3 Color Superconductivity

There are various possibilities for the realization of color superconductivity in QCD [66–71]. The most prominent ones are the two-flavor color superconductivity (2SC) and the color-flavor locking (CFL). The former will be studied explicitly in this work, while the latter will only be mentioned in this subsection for completeness and as a motivation for future improvements of this work.

The Cooper Theorem A system of fermions with an arbitrary weak, attractive interaction, experiences the *Cooper instability* [295] below a critical temperature. This can be better understood in the $T = 0$ limit, starting with non-interacting particles: Fermi-Dirac statistics dictate that all energy states are occupied up to the Fermi sphere given by the momentum $k_F = \mu^2 - m^2$, where μ is the chemical potential and m the mass of the fermions. Now if the attractive interaction is turned on, the Fermi sphere becomes unstable, because the attractive force entails the formation of bound states, the *Cooper pairs*, which are energetically favorable regardless of the weakness of the force, since the mass of the bound state is definitely smaller than masses of two single fermions, due to the negative binding energy. These states are bosonic and hence they obey Bose-Einstein statistics, which in turn dictate that all bosons are in the ground state in the form of a condensate. By the same interaction a fermionic excitation is now coupled to that condensate, which is therefore an energy gap for the excitation, and so the instability is cured. This is the essence of the Bardeen-Cooper-Schrieffer theory [296, 297], originally developed for metallic superconductors.

Even though electrons repel each other on the fundamental level, in a metallic superconductor the attractive forces are mediated by phonon exchange as the photons are screened. Due to the excitation gap, scattering states are blocked, therefore the electrical resistance is exactly zero. Furthermore external magnetic fields are expelled from the superconductor by a current induced by Faraday’s law. This is called the *Meissner effect*. On the elementary level the Meissner effect is analog to the *Higgs mechanism* [21–23]: The condensate breaks the electromagnetic gauge symmetry $U(1)_E$ and the resulting Goldstone boson is absorbed by the photon, which thereby acquires a mass gap. In QCD already the elementary interactions are attractive in certain channels. Therefore it was suggested not long after the discovery of asymptotic freedom, that QCD goes into a state of *color superconductivity* at high densities [61], where pairs of quarks condense into a *diquark condensate*, breaking the color symmetry.

	antisymmetric			symmetric	
Dirac	$C\gamma_5$ (S)	C (P)	$C\gamma_\mu\gamma_5$ (V)	$C\gamma_\mu$ (A)	$C\sigma_{\mu\nu}$ (T)
$SU(2)$	τ_2 singlet			$\mathbb{1}, \tau_1, \tau_3$ triplet	
$SU(3)$	$\lambda_2, \lambda_5, \lambda_7$ antitriplet			$\mathbb{1}, \lambda_1, \lambda_3, \lambda_4, \lambda_6, \lambda_8$ sextet	

Table 2.2: Dirac operators and generators of $U(2)$ and $U(3)$, and their symmetries under transposition [68]. In this table τ_i denote Pauli matrices, and λ_i denote Gell-Mann matrices. $C = \gamma_4\gamma_2$ is the charge conjugation matrix.

Diquark structure The idea of the diquark can be traced back to a classic paper by Gell-Mann [7] and the word “diquark” can be found already in a paper in 1966 [298]. It is a long-standing problem how to characterize diquark degrees of freedom in baryons or in baryonic (nuclear) matter. Because diquarks are colored, we cannot give any gauge invariant definition of diquarks. On the formal level, in any case, whenever there are two quarks, such a system may well be regarded as a diquark. Such a formal argument is inadequate to tell us whether it would behave as a collective mode or not.

Because quarks belong to the color triplet, a system with two quarks can be decomposed to a color anti-triplet and a sextet ($3 \otimes 3 = \bar{3}_a \oplus 6_s$). One gluon exchange suggests an attractive (and repulsive) force in the triple (and sextet, respectively) channel, so that we can discard the sextet pairing. In addition, it is only the $\bar{3}_a$ which can be coupled to a quark in order to give a colorless baryon. Turning to flavor structures, for $N_f = 2$ one has $2 \otimes 2 = 1_a \oplus 3_s$ and for $N_f = 3$, assuming we treat all flavors symmetrically, $3 \otimes 3 = \bar{3}_a \oplus 6_s$. For a given color and flavor representation, the symmetry properties of the spin part is now fixed by the Pauli principle. For a color triplet and flavor triplet, for instance, color and flavor indices are anti-symmetric under exchanging two quarks, and so the spin-orbit part of the diquark wave-function must be anti-symmetric to satisfy the Fermi statistics. Therefore, the spin should be anti-symmetric in the singlet channel, and the allowed quantum numbers are e.g. $J^P = 0^+$. The symmetry properties of various operators under transposition are given in Tab. 2.2.

It is an instanton-induced interaction that favors positive-parity diquarks rather than negative-parity ones. Moreover, it is straightforward to confirm by Fierz transformations [68] that the color-spin and flavor-spin interaction would stabilize the 0^+ diquark more. Thus, the scalar diquark with 0^+ should be the most prominent, and the axial-vector diquark with 1^+ should be the next. It is important to distinguish the diquarks for the phenomenological applications; for example in Ref. [299] the spectrum of high-spin hadrons are nicely parametrized with the scalar and the axial-vector diquarks.

These diquarks play an essential role in QCD matter at asymptotically high density where color superconductivity should be an inevitable consequence from the attractive interaction in the color triplet channel [72, 73]. Among various pairing patterns [300, 301], the 2SC phase and the CFL phase, which are both characterized by condensation of the scalar diquarks, have special importance on the phase diagram of high-density matter. For one-flavor color superconductivity, the flavor sector is symmetric and so only the axial-vector diquark is possible. Then, the rotational symmetry is broken by condensation of axial-vector diquark, leading to a spin-one color superconductivity [302].

Two-flavor color superconductors For the case of an infinitely large strange quark mass, flavor symmetry is given by the $SU(2)$ group. As explained in the previous paragraph, we have a scalar color-antitriplet, flavor-singlet diquark condensate in the 2SC phase, which is given by

$$\langle \Delta_a \rangle = \langle q^T C \gamma_5 \tau_2 \lambda_a q \rangle. \quad (2.13)$$

The three condensates with $a = 2, 5, 7$ form a vector in color space. Without loss of generality we can rotate this vector with a global $SU(3)_c$ transformation to the $a = 2$ direction, such that the condensate reads $\Delta \equiv \langle q^T C \gamma_5 \tau_2 \lambda_2 q \rangle$. In this choice we have a condensate in the ground state given by a totally antisymmetric collective state of red u and green d quarks, like $\sim \langle u_r d_g \rangle$. The blue quark is not a part of it, hence the color symmetry is broken: $SU(3)_c \rightarrow SU(2)_c$. The number of broken generators is $8 - 5 = 3$, which is equally the number of gluons acquiring a mass through the Higgs-mechanism. The would-be Goldstone bosons are eaten by the gauge fields, which actually corresponds to choosing a certain gauge. The corresponding Meissner and Debye masses have been computed in e.g. Ref. [303, 304] with various approaches. Note that if the Goldstone bosons are coupled to a chemical potential, not all of them are massless according to the *Nielsen-Chadha theorem* [305–312]. In the next chapter we will find only three massless modes and two modes with masses proportional to the chemical potential.

The condensate (2.13) is invariant under $SU(2)_V \times SU(2)_A$, thus it leaves chiral symmetry unbroken. Although the condensate carries electric as well as baryonic charge, it neither breaks $U(1)_E$ nor $U(1)_B$, but rather, they survive as modified symmetries that contain additionally a simultaneous color rotation. We denote the modified symmetries as $U(1)_{B+c}$ and $U(1)_{E+c}$. For instance, for the electromagnetic case, this can be seen as follows

$$q \rightarrow e^{i\alpha Q_E} q \quad \Rightarrow \quad \Delta \rightarrow e^{i\alpha/3} \Delta \quad \text{and} \quad q \rightarrow e^{i\alpha' \lambda_8} q \quad \Rightarrow \quad \Delta \rightarrow e^{i2\alpha'/\sqrt{3}} \Delta \quad (2.14)$$

where $Q_E = \text{diag}_f \left(\frac{2}{3}, -\frac{1}{3} \right)$ is the electromagnetic charge operator in flavor space and $\lambda_8 = \frac{1}{\sqrt{3}} \text{diag}_c (1, 1, -2)$, where the first and second entries belong to the red and green color respectively. Now we can define the linear combination $\tilde{Q}_E = Q_E - \frac{1}{2\sqrt{3}} \lambda_8$ under which Δ is neutral. Instead of a massive photon, this leads to rotated one, as a mixture of the original photon and the eighth gluon, whereas the orthogonal state becomes massive. This phenomenon is analogous to the mixing of gauge bosons in electroweak theory, which gives rise to a massive Z-boson and a massless photon. Similar as the electric charge, the modified baryon charge is given by $\tilde{Q}_B = Q_B - \frac{1}{\sqrt{3}} \lambda_8$, with $Q_B = \text{diag}_f \left(\frac{1}{3}, \frac{1}{3} \right)$. In summary, the breaking pattern reads

$$SU(3)_c \times SU(2)_A \times \underbrace{SU(2)_V \times U(1)_B}_{\supset U(1)_E} \quad \rightarrow \quad SU(2)_c \times SU(2)_A \times \underbrace{SU(2)_V \times U(1)_{B+c}}_{\supset U(1)_{E+c}}.$$

The global electromagnetic symmetry happens to be a subgroup of $SU(2)_V \times U(1)_B$, as the electric charge operator in flavor space can be written as a linear combination of the isospin and baryon charge operators. No global symmetries are broken and consequently there are no associated Goldstone bosons. Since the electromagnetic symmetry essentially remains intact the 2SC phase is not an electromagnetic superconductor but an insulator. Moreover, as baryon symmetry is not really broken as well, it is not a superfluid. In Fig. 2.4 the phase structure of QCD for two flavors, including the superconducting phase, is shown.

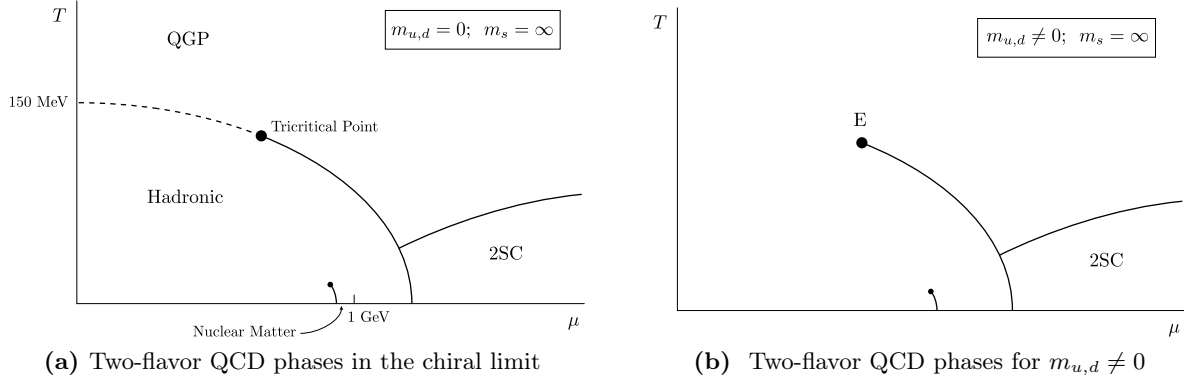


Figure 2.4: In (a) we see the phase diagram for two massless quarks, while in (b) the quark current masses are nonzero. At small μ the transition between the QGP and the hadronic phase is second order in the former figure, and a smooth crossover in the latter. These transitions end in the tricritical endpoint in (a) and critical one in (b) and then become first order. At larger μ and small T is the 2SC regime which has an interface to the hadronic phase along the horizontal axis, if the diquark mass is smaller than twice the quark mass. The structure of the 2SC phase is similar in both diagrams. The transition to nuclear matter will be discussed in Sec. 2.4 (here μ is actually μ_B). Figures taken from [66].

Color-flavor locking If we assume three degenerate quark flavors, i.e. $m_s = m_{u,d}$, we have an $SU(3)$ symmetry in flavor and in color space. Then the diquark condensate can be regarded as a matrix:

$$\langle \Delta_{i,a} \rangle = \langle q^T C \gamma_5 \lambda_i \lambda_a q \rangle, \quad (2.15)$$

where $i, a = 2, 5, 7$, are the indices of the Gell-Mann matrices, now also in flavor space. A Ginzburg-Landau analysis [313, 314] shows that there are two possible non-trivial ground states in such a theory. The first is again a 2SC phase with the condensate $\langle \Delta_{2,2} \rangle \neq 0$ and all other components are vanishing. Such a condensate reduces the three-flavor symmetry down to two flavors, $SU(3)_V \rightarrow SU(2)_V$, hence it has the same properties as discussed above. At higher densities the ground state takes the form of a unit matrix:

$$\Delta = \langle \Delta_{2,2} \rangle = \langle \Delta_{5,5} \rangle = \langle \Delta_{7,7} \rangle \neq 0. \quad (2.16)$$

The off-diagonals are vanishing. Each of these condensates break a different $SU(2)$ subgroups of the flavor and color symmetries, therefore both are broken completely. However, it can be checked that

$$\Delta_{2,2} + \Delta_{5,5} + \Delta_{7,7} \quad \text{is invariant under} \quad q \rightarrow e^{i\alpha_a(\tau_a - \lambda_a^T)} q, \quad (2.17)$$

i.e. simultaneous color and flavor rotations, therefore this is called the *color-flavor locked phase* [315]. The locking is similar to chiral symmetry breaking, where the residual symmetry locks left- and right-handed rotations. Moreover, in ultracold atoms similar pairing and symmetry properties exist in liquid ^3He where the orbital angular momentum of the pair is locked to the spin.

As before we can define a modified electromagnetic charge $\tilde{Q}_E = Q_E - \frac{1}{2}\lambda_3 - \frac{1}{2\sqrt{3}}\lambda_8$, now with $Q_E = \text{diag}_f\left(\frac{2}{3}, -\frac{1}{3}, -\frac{1}{3}\right)$ and $\lambda_3 = \text{diag}_c(1, -1, 0)$, under which all diquark pairs in (2.15) are neutral. On the other hand, we cannot find a modified baryon charge which leaves the ground state unchanged, therefore the CFL phase is a superfluid. We assume that at very high densities the non-superconducting state does not exhibit an axial anomaly, then, for massless quarks, the

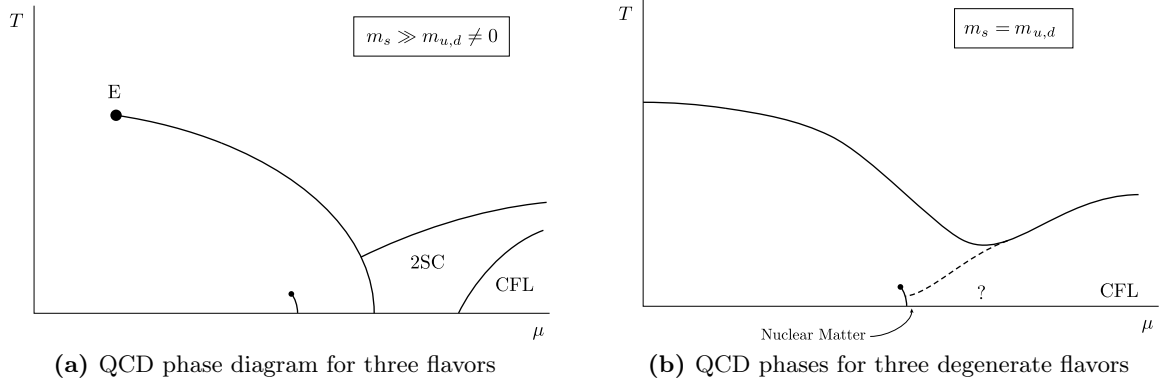


Figure 2.5: In (a) we have the three-flavor QCD phase diagram for quark masses comparable to the ones in nature. The additional strange quark dynamics sharpen the chiral phase transition and shift the critical endpoint to smaller μ in comparison to the two-flavor case. Cold and dense matter is at first in the 2SC phase where u and d quarks form Cooper pairs. When it is even more cold and dense it is in the CFL phase where all three colors and flavors are involved in the pairings. The transition between the 2SC and CFL phases is first order [66]. In (b) we see the phase diagram for three degenerate, light (or massless) quarks. Chiral symmetry is broken below the solid line, which marks the first order transition. Since the strange quark is light, the critical endpoint is shifted away. Below the dashed line we have a superfluid with dibaryon or diquark pairing. Due to the quark-hadron continuity there is no transition between the two kinds of pairing, nevertheless the magnitude of the condensate increases qualitatively in the CFL phase [66]. It is not clear whether in nature the phase diagram looks more like (a) or more like (b). Figures taken from [66]

symmetry breaking pattern in the CFL phase reads

$$SU(3)_c \times \underbrace{SU(3)_V}_{\supset U(1)_E} \times SU(3)_A \times U(1)_B \times U(1)_A \rightarrow \underbrace{SU(3)_{c+V}}_{\supset U(1)_{E+c}}. \quad (2.18)$$

Here the initial global electromagnetic symmetry is a subgroup of the diagonal flavor symmetry. In the CFL phase seven gluons and one gluon-photon mixture acquire a finite Meissner mass by the Higgs mechanism, while another gluon-photon mixture remains massless. Furthermore, there are ten Goldstone bosons, eight from the breaking of $SU(3)_A$ and one each from the breaking of $U(1)_B$ and $U(1)_A$.

Of course in reality the quarks have non-vanishing masses and the strange quark mass is much larger. The QCD phase diagram for this case is depicted in Fig. 2.5(a). The axial symmetries are already broken on the classical level and the flavor symmetry is the isospin $SU(2)_V$. Thus the residual group in the CFL phase is $SU(2)_{c+V}$. The condensates containing strange quarks, $\langle \Delta_{5,5} \rangle$ and $\langle \Delta_{7,7} \rangle$ are expected to be smaller than $\langle \Delta_{2,2} \rangle$, because of the larger mass.

Quark-Hadron Continuity Interestingly, the rotated electromagnetic charges of the quarks \tilde{Q}_E in the CFL phase are integers in units of rotated electron charge, just like in a confining theory. Furthermore, since chiral and baryon number symmetries are broken, the CFL phase for three degenerate flavors has exactly the same symmetries as the dibaryon pairing phase called *hypernuclear matter* [83]. There are good reasons to believe that neutron superfluidity and proton superconductivity occurs in nuclear matter of QCD [316]. It turns out that the quarks, gluons and Goldstone bosons in the CFL phase have a one-to-one correspondence to the baryons, vector mesons and Goldstone bosons in hypernuclear matter [75, 83, 85]. For instance, the quarks in the CFL phase are immersed in a diquark condensate, and so a one-quark excitation can pick up

two quarks from the condensate at will, hence it can continuously go over to “be” a baryon. The massive gauge bosons carrying the forces between the quarks correspond to the vector bosons carrying the forces between the baryons. Similarly the spectrum of all physical excitations are continuously connected [66]. Therefore one is led to believe that both phases are in principle indistinguishable, so that there is no sharp phase boundary. This is called the *Quark-Hadron Continuity*. Accordingly the phase diagram looks like Fig. 2.5(b).

In the spirit of the Quark-Hadron Continuity we cannot exclude a diquark mixture even in ordinary nuclear matter, hence, the hunt for a trace of diquarks in nuclear matter should acquire reality, and the theoretical formulation in this present work should be one important piece of building block toward full theoretical understanding.

2.2.4 Extended Flavor Symmetries for $N_c = 2$

As mentioned before, two-color QCD has a distinct feature compared to the physical case, namely its enlarged flavor symmetry, which is important to understand. It is a direct consequence of pseudo-reality of the $SU(2)_c$ generators in the fundamental representation, which are the Pauli matrices. As a consequence, diquarks, which are incidentally the baryons of the theory, are included in natural way. We will see how the symmetry manifest itself in the classical Lagrangian and how it can be broken by different additional operators or by a nontrivial ground state [199, 200]. Naturally the breaking of symmetries is accompanied by the occurrence of the appropriate number of (pseudo-) Goldstone bosons, which we will quantify.

Kinetic term In order to find the symmetry group of the kinetic term of the quarks, we consider the properties $SU(2)_c$ generators. A representation is pseudoreal if there is a transformation that converts the generators into the negative of its complex conjugate. Hence, by the same transformation we can undo a charge conjugation of the gauge fields. It is easy to see that for the Pauli matrices such a transformation can be performed:

$$-t_a^* = -t_a^T = t_2 t_a t_2. \quad (2.19)$$

Let us define a conjugate field as $\tilde{q}_R = \sigma_2 t_2 q_R^*$. As mentioned before, by the second Pauli matrix charge conjugation is undone, therefore \tilde{q}_R transforms like q_L under Lorentz- as well as gauge transformations. Now let us write the second part of chiral Lagrangian (2.11) in terms of \tilde{q}_R , by transposing the expression and then inserting unities in terms of Pauli matrices

$$\left(q_R^\dagger i \sigma_\mu^\dagger D_\mu q_R \right)^T = -\tilde{q}_R^\dagger i \left(\sigma_2 \sigma_\mu^* \sigma_2 \right) \left(t_2 D_\mu^T t_2 \right) \tilde{q}_R = \tilde{q}_R^\dagger i \sigma_\mu D_\mu \tilde{q}_R.$$

In the first step the minus sign arises from interchanging the anticommuting fields. The derivative term in the Dirac operator is antisymmetric, which can be shown by partial integration, while the gauge interaction term transforms as (2.19), because it is proportional to the generators. Furthermore $\sigma_2 \sigma_\mu^* \sigma_2 = (-i \sigma_2 \sigma_j^* \sigma_2, \mathbb{1}) = \sigma_\mu$, where again the pseudo-reality of the Pauli matrices was used. Now, since both terms of the Lagrangian contain the same matrix in between the fields, we can write all in a single term with an enlarged spinor

$$\mathcal{L}_{q,\text{kin}} = \Psi^\dagger i \sigma_\mu D_\mu \Psi, \quad \Psi = \begin{pmatrix} q_L \\ \tilde{q}_R \end{pmatrix}. \quad (2.20)$$

Since both of the component of this spinor contain N_f flavors component and there is a trivial structure in the $2N_f$ -dimensional flavor space, we now see a manifest $U(2N_f)$ flavour symmetry, also known as *Pauli-Gürsey symmetry* [317, 318], connecting quarks with antiquarks. This unitary group can be decomposed into $SU(2N_f) \times U(1)_A$, where we intentionally separated the axial group, as it breaks on the quantum level. The baryon number symmetry $U(1)_B$ is a subgroup of $SU(2N_f)$.

Quark mass As we have seen in the previous section, a Dirac-mass term for the quarks explicitly breaks the chiral symmetry of the classical Lagrangian, or it can break spontaneously in the ground state by the occurrence of a condensate. Since in two-color QCD the original symmetry is extended, we should write the mass term in terms of the extended spinor in order to see what symmetry is left

$$\bar{q}q = q_L^\dagger \sigma_2 t_2 \tilde{q}_R^* + \tilde{q}_R^T \sigma_2 t_2 q_L = \frac{1}{2} \Psi^T \sigma_2 t_2 \begin{pmatrix} 0 & -\mathbb{1}_{N_f} \\ \mathbb{1}_{N_f} & 0 \end{pmatrix} \Psi + \text{h.c.} \quad (2.21)$$

The matrix has as a dimension of $2N_f \times 2N_f$ in flavor space. The symmetry group which leaves this expression invariant is called the symplectic group $Sp(2N_f)$. In fact, Eq. (2.21) corresponds to the very definition of the elements of this group, namely the matrices $A \in \mathbb{C}^{2n \times 2n}$ with $A^T \Sigma_1 A = \Sigma_1$, where Σ_1 is the matrix in (2.21) with $n = N_f$. The number of the arising (pseudo-) Goldstone bosons is given by the dimension of the coset $SU(2N_f)/Sp(2N_f)$, which is $N_f(2N_f - 1) - 1$.

Baryon chemical potential Next we shall consider a finite baryon chemical potential. As we indicated in Sec. 2.2.2, the quark number is given by the conserved charge associated with baryon number symmetry. A chemical potential is introduced into the action as a Lagrange multiplier along with the quark number [199]. Therefore in the Lagrangian it has the form

$$\bar{q}\gamma_4 q = q_L^\dagger q_L + q_R^\dagger q_R = q_L^\dagger q_L - \tilde{q}_R^\dagger \tilde{q}_R = \Psi^\dagger \begin{pmatrix} \mathbb{1}_{N_f} & 0 \\ 0 & -\mathbb{1}_{N_f} \end{pmatrix} \Psi. \quad (2.22)$$

The physical meaning of the signs is that they are simply the baryon charges of quark and antiquark. This matrix can be used as the generator of $U(1)_B$ transformations. From the block diagonal structure it is obvious that the residual symmetry is given by independent rotations of left- and right-handed components, thus the flavor symmetry of physical QCD $SU(N_f)_V \times SU(N_f)_A \times U(1)_B$, where the axial phase rotations are left out. If there is a quark mass in addition, all axial symmetries are broken.

Let us mention here that the Dirac operator for two-color QCD with finite quark mass and finite chemical potential, which we denote as $\mathcal{D} = \not{D} + m + \mu$, is antiunitary, meaning that there exists a transformation which yields the complex conjugate of the Dirac operator:

$$\gamma_5 C t_2 \mathcal{D} \gamma_5 C t_2 = \mathcal{D}^*, \quad (2.23)$$

where C is the charge conjugation operator. Now, if q is an eigenvector of the Dirac operator with the eigen value λ the above relation implies $\mathcal{D}\tilde{q} = \lambda^* \tilde{q}$, with $\tilde{q} = \gamma_5 C t_2 q$. Thus, all eigenvectors appear in pairs and the determinant $\det \mathcal{D}$ is real. This is the reason why there is no sign problem in lattice calculation for two-color QCD.

Diquark condensate Below a critical temperature T_c we expect a Cooper pairing of the quarks into color neutral bosonic states, and also the Bose-Einstein condensation of these states. In Ref. [199] it is shown that mesonic and diquark-type correlators in two-color QCD are equal at vanishing chemical potential, which is of course directly related to the enlarged flavor symmetry, which allows to rotate quarks into antiquarks. It follows that if there is a condensation, it can be that of a meson or diquark. At $\mu \neq 0$ on the other hand the inequalities of the correlators show that a diquark-type excitation is the lightest one, so the condensation must be that of the diquark. In fact, this is easy to understand, if we start at $\mu = 0$, the masses must be equal due to the degeneracy, while at finite μ the mass of the diquark is immediately reduced, which we will see in our effective model in the next section.

In order to find the residual symmetry in the presence of a diquark condensate, we make a rather heuristic argument, showing it for $N_f = 2$ and then generalizing for arbitrary flavors. A scalar singlet diquark correlator must be antisymmetric in all spaces in which the spinor lives, so simplest choice is

$$q^T \gamma_5 C t_2 \tau_2 q + \text{h.c} = \Psi^T i \sigma_2 t_2 \tau_2 \mathbb{1}_2 \Psi + \text{h.c} = \begin{pmatrix} \Psi_u^T \\ \Psi_d^T \end{pmatrix} i \sigma_2 t_2 \begin{pmatrix} 0 & -i \mathbb{1}_2 \\ i \mathbb{1}_2 & 0 \end{pmatrix} \begin{pmatrix} \Psi_u \\ \Psi_d \end{pmatrix} + \text{h.c}$$

where τ_2 is an antisymmetric matrix in the $N_f = 2$ dimensional flavor space, given by the second Pauli matrix. The unit matrix $\mathbb{1}_2$ acts in the space corresponding to the two components of Ψ as defined in (2.20). By explicitly resolving the flavor structure in the last step we see that this expression is invariant under $Sp(2N_f)$, similar to the mass term (2.21), giving rise to the same number of Goldstone bosons. This is of course not a coincidence, but it is connected to the fact that the diquark and mesonic states are degenerate in two-color QCD.

Note that here the diquark condensate does not break color symmetry as it is a color singlet, hence there is no color superconductivity in QC₂D. However, if QC₂D would exist in a world with electromagnetic interactions, the diquark condensate would give rise to an electromagnetic superconductor, as its electric charge is nonzero. Since the diquark condensate breaks $U(1)_B$ which was a subgroup of $SU(2N_f)$, QC₂D at high densities is baryon number superfluid.

Symmetry breaking patterns Until now we have seen how each operator breaks the enlarged flavor symmetry of two-color QCD. Now let us find the residual symmetries if multiple operators are present in the system. In Fig. 2.6 a summary is shown for $N_f = 2$.

In the presence of a finite chemical potential the symmetry group, which we found for Eq. (2.22), is broken down to $Sp(N_f)_V \times Sp(N_f)_A$ by the diquark condensate with $N_f(N_f - 1) - 1$ Goldstone bosons. The other N_f^2 are pseudo-Goldstone bosons, which must have the limit of vanishing masses for $\mu \rightarrow 0$. For $N_f = 2$ we have $Sp(2) \simeq SU(2)$, so only $U(1)_B$ is broken spontaneously with a single true Goldstone boson, which is given by diquark phase rotations, and 4 pseudo-Goldstone boson, which are the mesons.

If we start with a small explicit quark mass parameter in our theory, the approximate $SU(2N_f)$ breaks down to $Sp(2N_f)$ by a chiral crossover, similar as in the physical QCD case, described in Sec. 2.2.2. The associated $N_f(2N_f - 1) - 1$ pseudo-Goldstone bosons include the diquarks. For additionally $\mu \neq 0$ the starting symmetry is $SU(N_f)_V \times SU(N_f)_A \times U(1)_B$ of which the axial part holds only approximately and is broken by the chiral condensate, with the usual $N_f^2 - 1$ pseudo-Goldstone bosons. An additional diquark condensate leaves only $Sp(N_f)_V$ unbroken, and gives rise to $\frac{N_f(N_f - 1)}{2}$ true Goldstone bosons. As we have mentioned in Sec. 2.2.2, chiral symmetry is expected to be restored in the limit $\mu \rightarrow \infty$, which still holds in QC₂D.

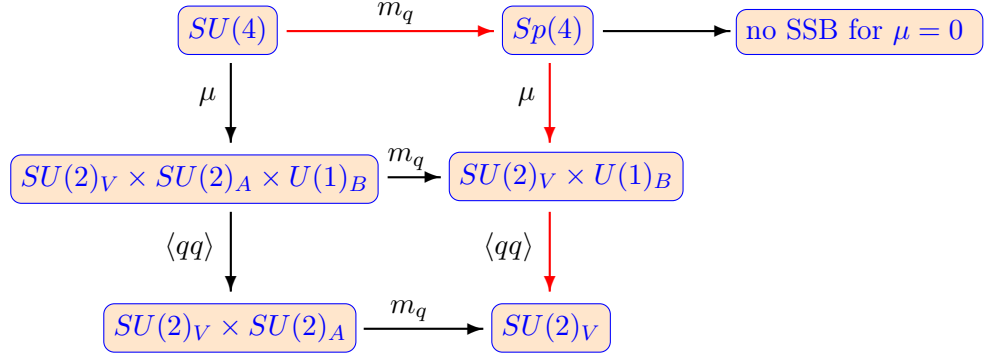


Figure 2.6: Different ways of breaking the enlarged flavor symmetry of QC₂D for $N_f = 2$; only the exact symmetries are shown here. The red arrows mark the way we are going to implement in this work. The $\langle qq \rangle$ denotes the diquark condensate. It is not shown that for $m_q = \mu = 0$ a condensate can break $SU(4) \rightarrow Sp(4)$ spontaneously. In the case of a finite explicit quark mass m_q , the diquarks acquire a small mass from the chiral crossover, similar as the pions. This mass must be reduced to zero by the chemical potential in order for $U(1)_B$ to break spontaneously.

Onset of diquark condensation The onset of the diquark condensation at $T = 0$ is related to the quark current mass, as it is shown in Fig. 2.7, but more directly it is related to the pion mass. For a finite m_q , the pions and the diquarks have finite and degenerate masses at $\mu = 0$ in QC₂D, due to the extended symmetry. This entails that, at $T = 0$ the onset of diquark condensation must be at $\mu_{qq} = m_\pi$, as a consequence of the Silver Blaze property, see Sec. 3.3.3. Furthermore, we know from the GMOR relation [137] that m_q scales quadratically with the pion mass, therefore the onset marked by the continuous line in the $T = 0$ plane is a parabola. In the chiral limit the pion mass is vanishing, therefore the onset is already at vanishing chemical potential. The thick line on the T -axis is a first-order transition in the $\mu_B = 0$ plane which presumably ends in a critical point [233]. Apart from that, the diquark condensation occurs via a second order phase transition as we will see later.

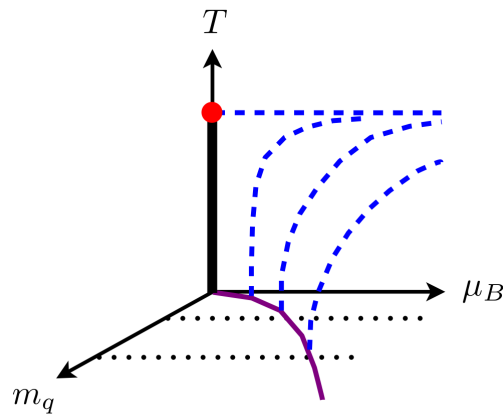


Figure 2.7: Schematic phase diagram for two-color QCD in the parameter space of temperature, baryon (= diquark) chemical potential and quark mass. Below the dashed lines are the regimes with diquark condensation. Figure taken from [233].

2.3 Low Energy Degrees of Freedom

In this section we will derive the low energy models, which effectively describe the isospin symmetric $N_f = 2$ quark matter, and where the gluons are integrated out. The change of the degrees of freedom from quarks and gluons at high energies to hadrons at low energies is well understood within the framework of the functional renormalization group (FRG) that we will introduce in the next chapter in more detail. Here, all we need to know is that the energy-scale dependence of the theory parameters, like couplings and masses, is given by the renormalization group equations (or flow equations, also β -functions), and that all informations of the system at a certain energy k are in principle encoded in the effective action Γ_k , not only for the elementary processes, but also for effective interactions and collective excitations. For our approach, we must deduce the explicit form Γ_k such that it correctly embodies the underlying physics and that it properly describes the phenomena we are interested in.

2.3.1 Hadronization

We have seen in Sec. 2.2.1 that quarks and gluons in QCD are subject to the confinement mechanism, if one looks at the macroscopic length scales of the system. Therefore the effective degrees of freedom at low energies are bound states like mesons and baryons. If one traces the evolution of the system from UV to the IR, dynamically taking into account all important effects, one sees a smooth transition between the quark-gluon phase and the hadronic phase. In the following we would like to sketch how this is done, without going into all details. The diagrams shown in this subsection are only for the motivation of the effective models and will not be computed explicitly.

Four-fermi interactions At large energy scales $k \gg \Lambda_{QCD}$ the effective action is well-described by the quantized and renormalised, classical action of QCD

$$\Gamma_{k \gg \Lambda_{QCD}} = \int_x \left\{ \frac{1}{4} F_{\mu\nu}^a F_{\mu\nu}^a + \bar{q} (i \not{D} + im_q) q + \bar{c} \partial_\mu D_\mu c + \frac{1}{2\xi} (\partial_\mu A_\mu^a)^2 \right\}, \quad (2.24)$$

where, in addition to (2.1), c is the ghost field and ξ is the gauge fixing parameter. Now the first major thing that happens by going to lower scales, is that effective four-fermi interactions $\sim \bar{q}q\bar{q}q$ are generated by a two-gluon exchange in the form of a box diagram, as it is depicted in Fig. 2.8. A lower energy scale means a larger length scale, so that we cannot resolve the structure of the box diagram, which therefore looks to us like a point-like four-fermi interaction. Hence a four-fermi operator must be added to the effective action Γ_k .

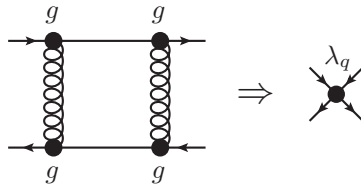


Figure 2.8: Box diagram generating an effective four-fermi coupling $\lambda_q \propto \alpha_s^2 = \frac{g^4}{16\pi^2}$. The FRG relates these two diagrams by an exact equation, and once additional operators are generated, the corresponding four-fermi process with a one-loop are added to the equation, see Fig. 2.9.

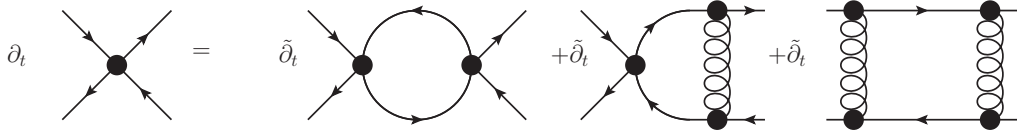


Figure 2.9: Schematic representation for the FRG equation for the four-fermi coupling without bosonization (permutations, signs and diagram multiplicities not shown). Here $t = \ln k$ is the “RG time”, and $\tilde{\partial}_t$ is a formal derivative operator, which will be specified in Sec. 3.6. All we need to know here is that this is a one-loop exact equation, which yields the scale dependence of the four-fermi coupling.

At low energies pure four-fermi models are famous under the name of *Nambu-Jona-Lasinio models* (NJL) [68, 129–131]. The NJL model assumes that gauge degrees of freedom are integrated out and substitutes quark interactions via gauge fields by a point like four-fermion interaction. The model parameter are tuned such that the known limiting cases agree with nature. However, recently the scale-dependence of four-fermi couplings have been solved with the FRG by explicitly integrating out the quark-gluon dynamics starting from the perturbative ultraviolet regime of QCD [185, 186]. The corresponding equation is exemplary shown in Fig. 2.9. In this case, the only input parameters are the gauge coupling and the quark current masses at an ultraviolet scale of $k \approx 20$ GeV.

A peak in the four-fermi coupling means that quark fluctuations are strong, which entails that a lot of quark-antiquark pairs are produced from the vacuum forming a condensate and thus breaking chiral symmetry. The mechanism can be well understood in the present picture: Consider the flow equation for the four-fermi coupling depicted in Fig. 2.9. The gluon box diagram dominates for large momenta as it scales parametrically with $g^4 \ll 1$, and hence λ_q scales with g^4 as well. The back-coupling of the four-fermi vertex leads to the mixed diagrams suppressed with $\sim g^6$, and fermionic self-interaction diagrams going with $\sim g^8$. This suppression is overcome in the non-perturbative regime, where the running coupling grows large. This finally leads to a dominance of the self-interaction diagrams and eventually to a four-fermi resonance. The appearance of a divergent four-fermi coupling can be better understood by looking at the β -function of the dimensionless coupling $\hat{\lambda}_q = \lambda_q/k^2$ [319]. Then one has contributions with opposite signs, such that the β -function can be vanishing and $\hat{\lambda}_q$ remains finite, if the initial value is small. However there is a critical coupling g_{cr} . If $g > g_{cr}$ then the β -function is always negative and $\hat{\lambda}_q$ encounters a pole irrespective of its initial value, see Fig. 2.10.

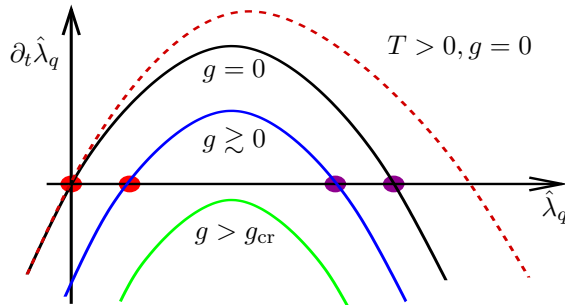


Figure 2.10: Sketch of the β -functions of the dimensionless four-fermi coupling [320]. The red dots are attractive IR fixed points, the violet dots in the UV are repulsive. At finite temperature fermions obtain a thermal mass gap, which entails that the UV fixed point goes further away and eventually prevents the breaking of chiral symmetry.

Partial Bosonization To trace the evolution of the system beyond the chiral symmetry breaking scale into the broken phase, it is convenient to introduce effective composite operators to capture the resonant structures in the four-fermi interactions. Although the composite operators carry the same quantum numbers as mesonic operators they should not be identified with the former but rather be understood as book-keeping devices. They are added to the effective action, but only become relevant below the hadronization scale $k \approx 700$ MeV. The bosonization procedure relies on the fact that in the path integral a four-fermi operator can be rewritten in terms of bosonic operators. It is formally done by introducing auxiliary fields with the *Hubbard-Stratonovich* transformation [321, 322]. For instance, for the scalar four-fermi channel it reads

$$e^{\int d^4x \frac{\lambda_q}{2} (\bar{q}q)^2} = \mathcal{N}_1 \int \mathcal{D}\sigma e^{\int d^4x \left(i h_\phi \sigma \bar{q}q + \frac{1}{2} m_\phi^2 \sigma^2 \right)}, \quad (2.25)$$

where \mathcal{N}_1 is a normalization factor. The exponent on the left-hand side is the scalar four-fermi interaction term of the action, and the exponent on the right-hand side is the bosonized version. Eq. (2.25) is simply proven by completing the square or using the equations of motion for σ with the bosonized action yielding

$$\frac{\delta S[\bar{q}, q, \sigma]}{\delta \sigma} = 0 \quad \Rightarrow \quad \sigma = -\frac{i h_\phi}{m_\phi^2} \bar{q}q. \quad (2.26)$$

The parameters m_ϕ^2 and h_ϕ are arbitrary parameters at our disposal, they will be adjusted to the boundary conditions, the index will be clear in the next subsection. However, the identity $\lambda_q = h_\phi^2/m_\phi^2$ is required for the transformation, where we see that a diverging four-fermi is equivalent to vanishing mass of the auxiliary field. This is exactly what we expect at a phase transition: A vanishing mass amounts an infinite correlation length. Whereas a small λ_q implies a large boson mass, and hence the decoupling of the bosons. In general, λ_q has a non-trivial momentum dependence. Having in mind a bosonic energy dispersion, we generalize the identity to

$$\lambda_q(p^2) = \frac{h_\phi^2}{Z_\phi(p^2)(p^2 + m_\phi^2)} \quad (2.27)$$

which leads to a kinetic term for the auxiliary field along with a *wave function renormalization* Z_ϕ . Eq. (2.27) is defined such that $p_0^2 = m^2$ is the pole, if we make an analytic continuation from the Euclidean space back to Minkowski space. In the next chapter we will see that a running wave function renormalization is important for the rapid decoupling of the bosons towards the UV, which can also be interpreted as the dissociation of the bound states.

The Hubbard-Stratonovich transformation substitutes four-fermi interaction by Yukawa-type interaction with intermediate bosons. The fact that both descriptions are equivalent, is illustrated in Fig. 2.11: A large λ_q implies a high possibility of successive four-fermi interactions to take place, such that it can be regarded as an intermediate bound state, whereas a heavy intermediate bound state cannot travel far in space, rendering the interaction four-fermi like. Thus we add the composite degrees of freedom to the effective action, which serve as a book-keeping device for the inter-quark forces above the symmetry breaking scale, and for the bound states around and below the symmetry breaking scale.

Since the structure of the scalar auxiliary field is $\sigma \sim \bar{q}q$, the expectation value $\langle \sigma \rangle$, which has the form of the chiral condensate (2.12), serves conveniently as the order parameter for chiral symmetry breaking. If the order parameter is nonzero in the ground state, we obtain an explicit quark mass term in our action with the mass $m_q = h \langle \sigma \rangle$. We see that bosonization is a comfortable tool to study chiral symmetry breaking. Moreover, we are free to choose any specific

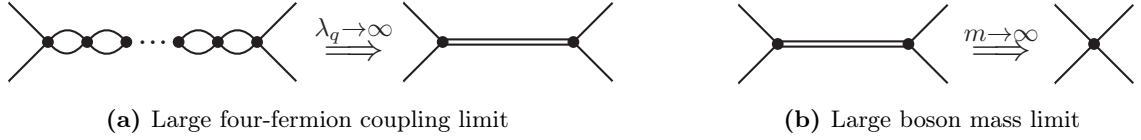


Figure 2.11: Illustration of the limiting cases for λ_q and the boson mass m . They are related to the mass of the bound states through (2.27). Here the double lines emphasize the composite nature of the intermediate state.

channel of four-fermi interactions that we want to bosonize, therefore we will also consider a diquark channel where the intermediate state is of the form qq , that can experience Bose-Einstein condensation. In the next subsections we will introduce all the necessary four-fermi interactions for our models, such that the important phenomena can be captured and the symmetries of the underlying theory are respected; then we apply the Hubbard-Stratonovich transformation on all channels.

Rebosonization Once we have bosonized the four-fermi interaction at some scale k and added the bosonic degrees of freedom to the effective action, the four-fermi interaction is regenerated by the gluon box diagram in Fig. 2.9, even if λ_q was exactly replaced by Eq.(2.27). Moreover, we have similar box diagrams in addition with the newly introduced bosonic degrees of freedom, but these have only a minor quantitative effect since either bosonic or the quark excitations are gapped [185]. It is necessary to bosonize the four-fermi interaction at every RG-scale k . In the framework of the FRG this procedure goes under the name of *rebosonization* or *dynamical hadronisation* [181, 183–185]. It is done by introducing a scale-dependent composite field, like $\sigma_k = a_k \bar{q}q$ for the simplest case. Such an ansatz leads to additional terms in the FRG equations, in particular we get terms in the flow of the four-fermi and Yukawa couplings:

$$\partial_t \lambda_q \rightarrow \partial_t \lambda_q + h \partial_t a_k, \quad \partial_t h \rightarrow \partial_t h - Z(p^2 + m^2) \partial_t a_k, \quad (2.28)$$

where $t = \ln k$. Now, the a_k is an auxiliary function at our disposal, and we choose it such that flow of λ_q vanishes at all scales:

$$\partial_t \lambda_q = 0 \quad \Leftrightarrow \quad \partial_t a_k = -\frac{\partial_t \lambda_q}{h}. \quad (2.29)$$

This way, all information of four-quark correlation is stored in a_k , which in turn is fed to the flow of the Yukawa coupling. Thus, h encodes the four-quark correlations in the quark-gluon phase and the boson-constituent-quark correlations in the hadronic phase, with a dynamical transition between these regimes.

Interestingly, with such an approach within the FRG, it is indeed found that the low energy physics of in terms of bound states can be predicted by the input parameters of QCD, the gauge coupling and the quark current masses, if one starts in the perturbative regime. The low energy parameters are not needed to be fine-tuned at the initial UV scale as long as the scale is high enough. For instance, if initiating the flow between 90 GeV and about 5 GeV with a vanishing Yukawa coupling, one is always attracted to the same trajectory in the IR, which is rather flat below 1 GeV [179, 186, 323]. The initial condition of the Yukawa coupling plays no role. Similarly the initial meson mass simply must be high enough, so that the meson is decoupled in the UV.

The most prominent channel for four-fermi interactions is the scalar-pseudoscalar one, which we will introduce in the coming subsection. In Ref. [186] ten different four-fermi channels of a

Fierz-complete basis were analyzed. It turns out that all channels diverge in the purely fermionic theory at the hadronization scale, unless the scalar-meson channel is rebosonized. Then the remaining channels show only small resonances. This analysis confirmed the heuristic picture of scalar-pseudoscalar channel being the driving channel in the four-fermi system, whereas all other channels are only triggered by this channel.

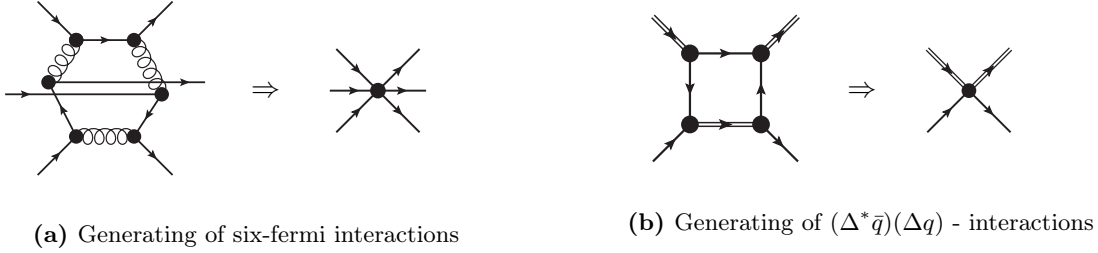


Figure 2.12: Effective baryon correlations. In (a) it is schematically depicted, how $\bar{q}\bar{q}qqqq$ - correlations can be generated from elementary quark-gluon interactions. In (b) a baryonic correlation is generated from 2-quark-2-diquark interaction, which might be the more realistic process.

Baryonization Like the generation of effective four-fermi interactions in Fig. 2.8, also effective six-fermi couplings can be generated from fundamental quark-gluon dynamics, see Fig. 2.12(a). Then we can also perform a transformation like (2.25) of the six-fermi term and introduce the auxiliary field $B \sim qqq$, with the quantum numbers of a nucleon. However, presumably it is rather less likely that three quark meet at one point in phase space, therefore we rather expect that the first step of the baryon formation is an intermediate, color-antitriplet diquark state, which then combines with the third, color-triplet quark to form a color-singlet in the form of a baryon, as shown in Fig. 2.13(a). As we have indicated above, we will bosonize the diquark channel of four-fermi interaction, and thereby obtain a Yukawa type interactions for the diquarks. From this point we can go on and construct the box diagram in Fig. 2.12(b). leading to an effective $(\Delta^* \bar{q})(\Delta q)$ - interaction, which we can baryonize. Here, we already would like to choose the tensor structure such that chiral symmetry is respected

$$\exp \int d^4x \lambda_\mu \Delta^{*a} \Delta^b \bar{q}^a \gamma_\mu q^b = \mathcal{N}_2 \int \mathcal{D}B \mathcal{D}\bar{B} \exp \int d^4x \left[i h_{qdB} (\bar{B} \Delta^a q^a + \bar{q}^a \Delta^{*a} B) + \bar{B} P_\mu \gamma_\mu B \right]. \quad (2.30)$$

The diquark fields are flavor singlets and thus invariant. Naturally, the Lorentz vector $\bar{q}^a \gamma_\mu q^b$ is invariant under chiral transformations as well. The λ_μ is at first an arbitrary vectorial function, which is needed to have a Lorentz scalar, and also contains the coupling strength of the interaction. The equation of motion for the baryon fields yield

$$B = -i h_{qdB} \Delta^a \not{P}^{-1} q^a \quad \text{and} \quad \bar{B} = -i h_{qdB} \bar{q}^a \not{P}^{-1} \Delta^{*a}, \quad (2.31)$$

which requires $\lambda = \frac{h_{qdB}^2}{2} \not{P}^{-1}$ for Eq. (2.30) to hold. With this chiral ansatz the B and \bar{B} respectively transform like \bar{q}^\dagger and q^\dagger under the chiral transformations (2.11). In particular for the axial groups this transformation property is important. Furthermore $\not{P}B$, naturally transforms like a q , and so, all terms on the right-hand side of (2.30) are manifestly chiral invariant. This is in contrast to the conventional baryonization, where a simple scalar structure ($\lambda \rightarrow \lambda \mathbb{1}$) is taken [246, 248], and chiral symmetry in the baryon sector is disregarded. For the baryonic two-point

term we assume a general structure in momentum space of the form

$$P_\mu = \bar{Z}_B(p^2)p_\mu. \quad (2.32)$$

Thus, the box diagram in Fig. 2.12(b) leads to a quark-diquark-baryon interaction and a propagating baryon mode. As for the bosons, the wave function renormalisation for the baryons \bar{Z}_B is important for the decoupling or dissociation in the UV. There will be more details on that matter later.

Aside from that, we need a finite rest mass for the baryons. Since they are made of the quarks which themselves interact via the Yukawa term in (2.25), we assume that constituent quarks within different baryons still do the same. Thereby, an effective Yukawa type interaction for baryons with mesons is generated. In the FRG framework the generating takes place via a triangle diagram with the quark-diquark baryon interactions, introduced by Eq. (2.30), and the quark-meson interactions from Eq. (2.25). The diagrams are shown in Fig. 2.13(b). On microscopic scales this corresponds to an eight-fermi correlation, however the stepwise hadronization procedure is more intuitively accessible. Then, if chiral symmetry is broken, an effective baryon mass term is created with $m_B = h_B \langle \sigma \rangle$. The mass is composed of the triple of the constituent quark mass reduced by the binding energy, thus $h_B \lesssim 3h_\phi$.

Again, as for the bosons, we can perform a *rebaryonization* procedure by introducing a scale dependence in the baryon field as $B_k = b_k \Delta^a \not{p} q^a$, and then remove the regenerated $(\Delta^* \bar{q})(\Delta q)$ -interaction by feeding the box diagram in Fig. 2.12(b) directly into the flow of h_{qdB} .

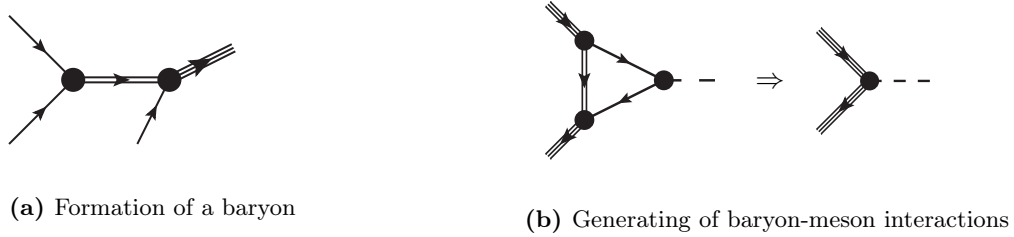


Figure 2.13: It is assumed that a baryon is constructed by the joining of a diquark with quark as shown in (a). A quark state inside a baryon still can emit a meson, thus an effective Yukawa type baryon-meson interaction is generated (b).

2.3.2 The Quark-Meson-Diquark Model for QC₂D

In this subsection we want to construct an effective low energy model for two-color QCD. Our low-energy model for physical QCD will be based on this. Essentially what we are going to do here, is to find a minimal four-fermi model which respects all symmetries of the underlying microscopic theory, in particular the extended flavor symmetry. Then we will bosonize it as shown above. Since the diquarks are the baryons of the theory in QC₂D, we do not consider any higher order correlations.

Following the argument in Ref. [215], we make use of the local group isomorphism $SU(4) \simeq SO(6)$ and define the operator $\Psi^T \sigma_2 t_2 \vec{\Sigma} \Psi$, with the fermionic field as defined in (2.20), and a suitable basis of 4×4 antisymmetric matrices, $\vec{\Sigma} = \{\Sigma_i\}_{i=1}^6$. The basis matrices are unitary and satisfy the orthogonality condition $\Sigma_i \Sigma_j^\dagger + \Sigma_j \Sigma_i^\dagger = 2\delta_{ij}$. They can be chosen to carry the quantum numbers of the four mesons and two diquarks, see [206] for an explicit form of these

matrices. It can be verified with the transformation properties of Ψ and $\vec{\Sigma}$ under $SU(4)$, that the above defined operator transforms as a complex vector of $SO(6)$. We can construct $SO(6)$ invariants simply by taking scalar products with itself or its complex conjugate, and thereby obtain the four-fermi interaction

$$\begin{aligned} \frac{1}{2} |\Psi^T \sigma_2 t_2 \vec{\Sigma} \Psi|^2 + \frac{1}{4} \left[(\Psi^T \sigma_2 t_2 \vec{\Sigma} \Psi)^2 + \text{h.c.} \right] \\ = (\bar{q}q)^2 + (\bar{q}i\gamma_5 \vec{\tau}q)^2 + (\bar{q}i\gamma_5 \tau_2 t_2 C \bar{q}^T)(q^T C i\gamma_5 \tau_2 t_2 q). \end{aligned} \quad (2.33)$$

The hermitian conjugate must be added in order to have real-valued action. Note that while the first term in the upper line is invariant under $U(1)_A$, the second one breaks it. This is fine since it is broken by the quantum anomaly anyway. Inserting explicit expressions for the Σ_i matrices yields the second line with the original Dirac spinors. Now it has become obvious that the channels of interaction we have are the scalar, pseudoscalar and diquark channels. This is essentially the minimal two-flavor NJL model, supplemented with a diquark term. If the symmetry between the mesons and diquarks is broken, the respective channels have independent coupling parameters. If the system has chiral symmetry, then the scalar and pseudoscalar channels keep a common coupling parameter. Note that instead of adding the first and the second term in (2.33) one can subtract them, which leads to the parity partners of the channels we have here. This has been employed in Ref. [215] with a mean-field approach.

If chiral symmetry is broken, according to the Vafa-Witten theorem [324] the scalar condensate must be preferred over the pseudoscalar one, as the ground state does not violate parity conservation. In addition, we want to have a small quark current mass in our model. An explicit Dirac mass term can be included in the Hubbard-Stratonovic transformation (2.25) by shifting $\bar{q}q \rightarrow \bar{q}q + i\frac{m_q}{\lambda_q}$ on both sides of the equation (the constant term is irrelevant). This entails a source term for the scalar field $-\sigma$, with

$$c = \frac{m_\phi^2 m_q}{h}. \quad (2.34)$$

The source term leads to small but non-vanishing expectation value for $\langle \sigma \rangle$, and when quantum fluctuations are integrated out, the condensate can grow much larger. Let us now write down the low energy operators for two-color QCD into an effective action, which we call the *quark-meson-diquark* (QMD) model, with $\Phi = (\vec{\pi}, \sigma, \Delta, \Delta^*, \psi, \bar{\psi})$

$$\begin{aligned} \Gamma_{\text{QMD}}[\Phi] = \int d^4x \left\{ Z_q \bar{q} \left[i\not{\partial} + i\gamma_4 \mu + \sqrt{Z_\phi} i h_\phi (\sigma + i\gamma_5 \vec{\tau} \cdot \vec{\pi}) \right] q \right. \\ + Z_q \sqrt{\frac{Z_\Delta}{2}} h_\Delta \left[\Delta^* q^T C \tau_2 \epsilon \gamma_5 q - \Delta \bar{q} \gamma_5 \epsilon \tau_2 C \bar{q}^T \right] \\ + Z_\Delta \left[(\partial_\nu - \delta_{\nu 4} \mu) \Delta^* \right] \left[(\partial_\nu + \delta_{\nu 4} \mu) \Delta \right] \\ \left. + \frac{Z_\phi}{2} \left[(\partial_\mu \vec{\pi})^2 + (\partial_\mu \sigma)^2 \right] + V(\phi^2, |\Delta|^2) - \sqrt{Z_\phi} c \sigma \right\} \end{aligned} \quad (2.35)$$

Essentially, it is well known *quark-meson* model augmented by the diquark terms. In the first line we have the kinetic term for the quarks and the quark-meson interactions. $\phi = (\vec{\pi}, \sigma)$ gathers the meson fields and transforms like a vector under chiral symmetry transformations as $SU(2)_V \times SU(2)_A \simeq SO(4)$. In the second line are the quark-diquark interactions. The interaction terms are obtained from bosonizing all four-fermi terms in Eq. (2.33) with similar Hubbard-Stratonovic transformations as in (2.25). However, we have rescaled the diquark fields $\Delta \rightarrow \sqrt{2}\Delta$ in order to have the standard convention for a complex scalar field. Also, we have substituted the color matrix by an anti symmetric tensor $t_2 = -i\epsilon$. In the third and forth line we have the kinetic terms for the bosons. As we have discussed in the previous section a momentum dependent four-fermi coupling like (2.27) entails kinetic terms for the bosonized fields. The wave function renormalization is introduced for all fields, including the quarks, as a rescaling factor $\Phi_i \rightarrow \sqrt{Z_{\Phi_i}}\Phi_i$, with no explicit momentum dependence as an approximation. Equivalently, one can parametrize the nontrivial scale dependence of the kinetic terms by the Z 's, and then redefine all the parameters with the appropriate powers of the Z 's. It is clear that if $SU(4)_f$ is not violated, then it must be $Z_\phi = Z_\Delta$ as well as $h_\phi = h_\Delta$.

Furthermore, we have included a baryon chemical potential μ , which is done by means of standard methods [284, 285]. Essentially it is incorporated by a constant shift $c_{\Phi_i}\mu$ in the time derivative, where c_{Φ_i} is the baryon charge of the field Φ_i . Naturally, the diquark transforms under $U(1)_B$ like $\sim qq$ and therefore has twice the baryon charge of a quark. At finite temperature the time axis is compactified on a torus with circumference $\beta = 1/T$. Lorentz invariance, which is simply $O(4)$ in Euclidean spacetime, is broken down to $O(3)$ at finite temperature and density.

In order to study spontaneous symmetry breaking, it is necessary to incorporate an *effective potential* V , which includes the bosonic mass terms arising from the Hubbard-Stratonovic transformations, and at least a quartic interaction term guaranteeing that it is bounded from below. Also, by involving higher bosonic interactions, it acts as a substitute for possible higher quark interaction. We will focus on the effective potential Sec 2.5. Finally we have the source terms, explicitly breaking chiral symmetry. If we consider only a single degenerate mass term in V and solve the equations of motions for all bosonic fields, we can verify that the interactions terms in (2.35) originate from the four-fermi interactions (2.33) with coupling (2.27).

We consider this model to be valid up to the cutoff scale $\Lambda \approx 1$ GeV, below which we assume the gauge degrees of freedom from the high UV action (2.24) to be integrated out, therefore they are no more included in $\Gamma[\Phi]$. With suitable boundary conditions, we expect in the vacuum that this effective action evolves such that at $k \approx \Lambda$ the quark fluctuations with their light masses are the dominating processes, while around $k = 700 - 500$ MeV the bosonic dynamics are expected to take over smoothly, which then remain active down to the mass scale of the lowest excitation, that is $m_\pi \approx 140$ MeV.

2.3.3 The Quark-Meson-Diquark-Baryon Model for QCD

For physical QCD with three colors we can start with Γ_{QMD} and promote the diquark to a color antitriplet of the form (2.13). Accordingly we must replace the antisymmetric Pauli matrix in color space t_2 by the three antisymmetric Gell-Mann matrices $\lambda_2, \lambda_5, \lambda_7$. This amounts to having a totally antisymmetric Levi-Civita-tensor $(\epsilon^a)_{bc} = \epsilon^{abc}$, where the letters represent the three color indices $\{r, g, b\} = \{1, 2, 3\}$. Hence we replace essentially $\Delta \rightarrow \Delta^a$ and $\epsilon \rightarrow \epsilon^a$, with an implied contraction of the indices. Furthermore, we add the baryonic degrees of freedom as discussed at the end of Sec. 2.3.1 and then we obtain a *quark-meson-diquark-baryon* (QMDB) model for QCD, with $\Phi = (\vec{\pi}, \sigma, \Delta, \Delta^*, \psi, \bar{\psi}, \bar{B}, B)$

$$\begin{aligned}
 \Gamma_{\text{QMDB}}[\Phi] = \int d^4x \Big\{ & Z_q \bar{q} \left[i\not{\partial} + i\mu\gamma_4 + \sqrt{Z_\phi} i h_\phi (\sigma + i\gamma_5 \vec{\tau} \cdot \vec{\pi}) \right] q \\
 & + Z_q \sqrt{\frac{Z_\Delta}{2}} h_\Delta \left[\Delta^{*a} q^T C \tau_2 \epsilon^a \gamma_5 q - \Delta^a \bar{q} \gamma_5 \epsilon^a \tau_2 C \bar{q}^T \right] \\
 & + Z_\Delta \left[(\partial_\nu - \delta_{\nu 4} \mu) \Delta^{*a} \right] \left[(\partial_\nu + \delta_{\nu 4} \mu) \Delta^a \right] \\
 & + \frac{Z_\phi}{2} \left[(\partial_\mu \vec{\pi})^2 + (\partial_\mu \sigma)^2 \right] + V(\phi^2, |\Delta|^2) - \sqrt{Z_\phi} c \sigma \\
 & + \sqrt{Z_q Z_\Delta Z_B} i h_{qdB} (\bar{B} \Delta^a q^a + \bar{q}^a \Delta^{*a} B) \\
 & + Z_B \bar{B} \left[z_B (i\not{\partial} + i\gamma_4 \mu_B) + \sqrt{Z_\phi} i h_B (\sigma + i\gamma_5 \vec{\tau} \cdot \vec{\pi}) \right] B \Big\}. \tag{2.36}
 \end{aligned}$$

Except for the color structure in the diquark sector, the first four lines are the same as in Eq. (2.35). The fifth line contains the quark-diquark-baryon interactions, with the rescaled fields. And finally, the last line contains the kinetic term for the baryon with $\mu_B = 3\mu$ and the baryon-meson interaction. since it is essentially a quark inside the baryon that interacts with the meson, the structure is same as for the quark-meson interaction.

As the chiral condensate is melted at high energies, the baryon would become massless. On the other hand a Dirac mass term would break chiral symmetry explicitly. Therefore we introduce a UV - mass gap m_B^{UV} , which is supposed to take care of the decoupling of the baryons at high energies. Hence, we make the following ansatz for the nontrivial momentum dependence introduced in Eq. (2.32),

$$\bar{Z}_B(\tilde{p}^2) = Z_B z_B(\tilde{p}^2) \quad \text{with} \quad z_B(\tilde{p}^2) = \left(1 + \frac{m_B^{\text{UV}}}{|\tilde{p}_\mu|} \right), \tag{2.37}$$

where $\tilde{p}_\mu = (\vec{p}, p_4 + i\mu_B)$. The chemical potential must be included to satisfy the Silver Blaze property, see Sec. 3.3. Also, Lorentz invariance in the vacuum is respected. The Z_B without the argument is momentum independent. We are free to rescale all coupling parameters associated with baryons, such that it corresponds to $B \rightarrow \sqrt{Z_B} B$. In terms of the renormalization group scale k , the UV-mass gap should have the following properties in the vacuum

$$\text{for } k \rightarrow 0: \quad m_B^{\text{UV}} \rightarrow 0, \tag{2.38}$$

$$\text{for } k \rightarrow \Lambda: \quad m_B^{\text{UV}} \gg k. \tag{2.39}$$

Below the chiral symmetry breaking scale $k_\chi \approx 500$ MeV the baryon acquires the known mass by the chiral condensate of $m_B \simeq 939$ MeV, which is much too high to have dynamical impact on the system. With increasing energy scales the excitation gap for all bound states should only grow larger because they dissociate. For the baryons this is ensured by (2.39). Nevertheless, at higher chemical potentials some impact of the baryons can be expected, especially around the critical endpoint. However at $T = 0$ below the onset of the baryon density there cannot be an influence from the baryons on mesonic quantities like the chiral condensate, because of the Silver Blaze property. Above the onset baryonic fluctuations are blocked by the Pauli exclusion principle, as the states are occupied at finite densities. Similar is the case for the diquarks: Their mass is believed to be around twice the quark mass $m_\Delta \approx 600$ MeV after chiral symmetry is broken, otherwise they are much heavier/dissociated. Of course, the diquark condensate will have a significant impact on the phase diagram at high chemical potentials.

2.4 Successive Onsets of Densities

The liquid-gas phase transition of nuclear matter

Our baryon fields introduced in the previous section actually represent the nucleons, i.e. the constituents of atomic nuclei. It can be inferred from the systematics of atomic nuclei, that the binding energy keeping multiple baryons joined, is about 16 MeV, and the baryon density is $n_0 = 0.17 fm^{-3}$ [325], where electromagnetism is neglected. Now, consider the following situation: At sufficiently low, but finite temperature, we have thermally excited baryons in a gaseous state. If the system is compressed, at some point the baryons start joining into droplets. The density of each droplet is n_0 , however on spatial average we have $n_B < n_0$. Eventually the entire volume is filled with droplets and the system goes into a liquid state. Right at the phase transition which is first-order, is the coexisting state. At large temperatures the gas cannot be distinguished from the liquid, so the first-order transition terminates in a critical endpoint, which is around $T = 15$ MeV. At $T = 0$ a finite density can only be achieved, if the chemical potential is not smaller than the minimal energy per baryon. Hence, the transition is at $\mu_B = m_B - 16$ MeV (cf. Fig. 2.4 (a)), which corresponds to a quark chemical potential of $\mu = 308$ MeV. The liquid-gas transition can be computed with phenomenological models for the nuclear interaction, for instance, the Walecka model [241].

The question is where we can expect other degrees of freedom of quarks and diquarks. There are three possibilities in order.

Conventional scenario – quark onset followed by diquarks

A quasi-particle picture gives us an intuition for the onset behavior. If there are any new degrees of freedom in matter coupled to the baryon density, it would appear when the baryon chemical potential exceeds the corresponding mass threshold. If density-induced deconfinement is a smooth phenomenon just like as observed along the temperature axis, confinement would be gradually lost in nuclear matter. Then, the quark onset is located at the (in-medium) constituent quark mass. In the same way, as soon as μ_B gets greater than the (in-medium) constituent diquark mass, the system should accommodate the diquark degrees of freedom. We should note that the diquarks immediately form a condensate because they are bosons, leading to a color superconducting state.

This is actually a conventional scenario. To summarize what is described above, let us introduce some notations; the baryon binding energy is denoted by ΔB (not to be confused with the nuclear binding energy mentioned above), the diquark mass difference by Δd . Then, the baryon mass is $m_B = 3m_q - \Delta B$ and the diquark mass is $m_\Delta = 2m_q - \Delta d$, where $\Delta B > 0$ and $\Delta d < 0$. Then, we have an ordering pattern as $m_B/3 < m_q < m_\Delta/2$.

It is important to note that in this conventional picture $m_\Delta > 2m_q$ by negative Δd and thus the diquark is not a bound state of two quarks. In fact, in a color superconductor, the diquark correlation is seen in not the configuration space but the momentum space only. In the BCS wave-function, two particles having momenta $+\vec{p}$ and $-\vec{p}$ are paired, but such Cooper pairs are not necessarily quasi-particles. This is why $m_\Delta > 2m_q$ in the weak-coupling BCS picture.

BEC-BCS crossover scenario – diquark onset followed by quarks

The BCS picture is possibly changed in the strong-coupling regime. In the strongly correlated systems such as the unitary limit of cold atoms, it is known that the BEC-BCS crossover takes place associated with the formation of bosonic molecular states [326]. It was Leggett [327] who first claimed that superconductivity is nothing but a BEC or superfluid of the Cooper pair. If the attractive force is strong enough, the Cooper pair may be a molecular bound state, and then the chemical potential would turn negative changing its character from a fermionic to a bosonic one [328].

In this case the diquark could be a bound state of two quarks, and then $\Delta d > 0$, so that we have an ordering pattern as $m_B/3 < m_\Delta/2 < m_q$. This means that we have color superconductivity before the onset of quarks. Such a picture is quite consistent with what is expected from the Quark-Hadron Continuity

Quarkyonic scenario – continuous activation

The last and the newest scenario is the picture based on the large- N_c approximation for QCD matter. There may be no particular onset behavior of quarks and diquarks but these degrees of freedom may be gradually developing as the baryon density grows up. In other words, in some sense, nuclear matter is already a sort of quark matter. This is a picture consistent with quarkyonic matter recognized in the large- N_c limit [32]. The baryons interact as strongly as $\sim \mathcal{O}(N_c)$ enhanced by a combinatorial factor due to quark exchanges, while mesons become free particles when the color number N_c is infinitely large. Thus, interestingly, baryon interactions lead to the same N_c counting as quark matter and so quark degrees of freedom should be already there in a form of baryon interactions.

The duality between nuclear matter and quark matter may sound a radical interpretation of the large- N_c observation, but we would emphasize that such a quarkyonic picture is very natural. The baryon interaction is mediated by mesons which are objects of a quark and an anti-quark. So, by the interaction, quarks can hop from one baryon to the other, and this is nothing but our intuitive understanding of deconfinement. The traditional picture in nuclear physics is composed of baryons with meson exchanges, which may well be regarded as partial deconfinement by quark exchanges.

In summary of this section, we would draw the attention to the fact that the onsets of quarks and diquarks are significantly influenced by these different scenarios as discussed above. Although these scenarios are widely prevailing ones, to the best of our knowledge, the crucial difference in the onset properties has been overlooked. For the moment we have no experimental data nor QCD-based calculation in order to let any one of the three scenarios be more likely than others.

2.5 Phase Transitions with the Effective Potential

As we have seen, by the Hubbard-Stratonovich transformation we have terms quadratic in bosonic fields in our action from the four-fermi interactions, which are generated by the box diagrams of quark-gluon interactions. Certainly, one can think of many more, higher order interaction processes, all in terms of quark-gluon interactions, where the external legs correspond to single quarks or to collective excitations. The former can be described effectively by n -fermi and the latter by n -boson interactions. Of course mixed n -fermi- m -boson interactions are possible as well. In general the interactions are momentum dependent. This is why (non-) linear sigma models or chiral perturbation theories are often applied to describe low energy QCD.

Regarding higher order interactions, we will only consider pure bosonic ones in a momentum independent scheme in this work. This leads us to the effective potential which primarily contains all non-derivative terms of the action, thereby it assumes the important role of describing phase transitions and symmetry breaking.

2.5.1 The Ground State and Symmetry Breaking

We know from the analogy of quantum field theories with statistical mechanics, that the minimum of the effective action is the ground state of the system [270]. For a translation-invariant ground state we will find solutions in which the fields are given by constants in spacetime (or momentum). Therefore, the stationary condition of Γ reduces to one for the effective potential U

$$\frac{\delta\Gamma[\Phi]}{\delta\Phi_i(x)} = 0 \quad \Rightarrow \quad \frac{\partial U(\Phi)}{\partial\Phi_i} = 0 \quad (2.40)$$

where Φ is any multi-component field. The functional derivative reduces to a partial derivative and the spacetime integration yielding the euclidian volume Vol_d drops out. The effective action contains averaged field $\Phi = \langle\phi_{\text{quantum}}\rangle$, and there cannot be a nonzero ground state value of fermionic fields due to their anti-commuting nature. Unless there are source terms of the form $\bar{\eta}\psi$ in the exponential of the path integral, we have $\langle\psi\rangle = 0$ since ψe^{-S} is odd in grassmannian fields when the exponential is expanded. Therefore, conventionally the terms containing fermionic fields are not defined as part of the effective potential.

Here we see again the advantage of performing the Hubbard-Stratonovich transformation: In a purely fermionic theory Eq.(2.40) would always have a trivial solution, so the only way to recognize a phase transition, would be to look whether the fermionic interactions are diverging or develop a peak. However, with the introduction of collective excitations in terms of bosonic fields, we have convenient order parameters at hand.

Naturally the shape of the effective potential depends on the system parameters like temperature, chemical potential, and interaction strength. For parameter regions where the minimum is at nonzero fields, we can expand our theory about the minimum with $\Phi = \Phi_0 + \delta\Phi$, where Φ_0 simply acts as a numerical parameter, that is not transformed under the symmetry groups, therefore the theory is no more invariant thereunder. We say that the symmetry is spontaneously broken down to a subgroup. The system chooses spontaneously in which direction to break the symmetry, just like a ball over the tip of a mexican hat chooses spontaneously, where to roll down. Nevertheless, all choices are equivalent since we can rotate the hat before the ball rolls down, and it still looks the same. Thus, we are in principle free to choose the boson fields that are supposed to be the order parameters, while the other bosons associated to the broken symmetry become the massless Goldstone modes.

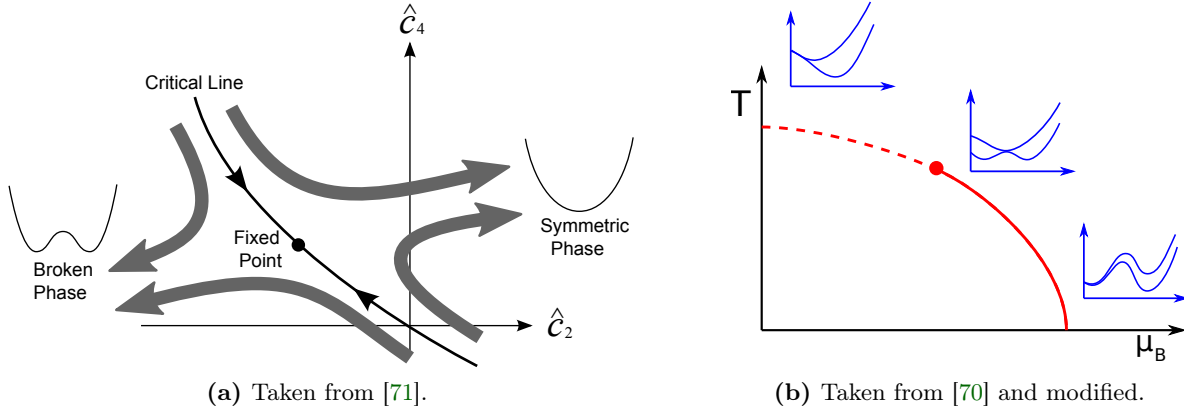


Figure 2.14: Illustration of the shape of the effective potential for different phase transitions.

The transition between the symmetric to the broken regimes is called a phase transition, and the point in the parameter space where it happens, defines the critical parameters. Typically one considers a 1st order phase transition, where the order parameter jumps to a nonzero value, and 2nd order transitions, where it continuously goes away from zero. For the latter case we can distinguish the phases by the following conditions, with the curvature of potential given by the Hessian matrix $H(U) = \partial_{\Phi_i} \partial_{\Phi_j} U$,

$$\begin{aligned} \text{symmetric phase:} & \quad \Phi_0 = 0, \quad \det H(U(\Phi_0)) \neq 0, \\ \text{phase transition:} & \quad \Phi_0 = 0, \quad \det H(U(\Phi_0)) = 0, \\ \text{broken phase:} & \quad \Phi_0 \neq 0, \quad \det H(U(\Phi_0)) = 0. \end{aligned}$$

Φ_0 is also referred to as the condensate. At the phase transition the curvature is vanishing, as the minimum in the center is turning into maximum, see Fig. 2.14(a). At a first order transition $\det H(U(\Phi_0)) = 0$ does not hold, as the initial minimum remains as a local one, see Fig. 2.14(b). Since the Hessian matrix essentially contains the so-called curvature masses of the particles, we see that if the mass of at least one field is vanishing, the symmetry is broken, and that field corresponds to the Goldstone mode. If $\dim \Phi = 1$ then we have a double-well potential in the broken phase, as in Fig. 2.14(a), with no flat direction and thus no massless modes, also $\det H(U(\Phi_0)) \rightarrow U''(\Phi_0) \neq 0$.

Even if the order parameter does never vanish, there are various ways to define a phase boundary. For a transitions along the temperature axis the common definitions are given by

$$\text{Inflection point :} \quad \frac{\partial^2}{\partial T^2} \Phi_0 \Big|_{T_c} = 0, \quad (2.41)$$

$$\text{Half value :} \quad \Phi_0(T_c) = \frac{\Phi_0(T=0)}{2}, \quad (2.42)$$

$$\text{Susceptibility :} \quad \frac{\partial}{\partial T} \chi_{\Phi_0} \Big|_{T_c} = 0. \quad (2.43)$$

Typically we have the situation that if we are far enough from the phase boundary given by T_c , on one side the symmetry is significantly broken, while on the other side it is approximately restored. The transition can be a smooth crossover or a jump between two different nonzero values. This is the case when there is a source term like $-c_i \Phi_i$ breaking the symmetry explicitly

and by which Eq. (2.40) can never be satisfied by vanishing fields. In Ref. [179] it was shown that in the presence of a source term the susceptibility of the order parameter is given by the derivative with respect to the source parameter, which in turn is equal to the inverse mass squared of the mode that carries the condensate, i.e.

$$\chi_{\Phi_0} = \frac{\partial \Phi_0}{\partial c} = \frac{1}{m_{\Phi_0}^2}. \quad (2.44)$$

In Fig. 2.14(a) is a schematic picture of the RG flow in the space of dimensionless system parameters $\{\hat{c}_i\}$ for a second order phase transition. Depending on the initial conditions, the system stays in the symmetric phase, or it goes into the broken phase, where the system spontaneously chooses one of the wells for the ground state in the so called double-well potential. In between is a critical line (or surface in more dimensions), where the system runs into a Wilson-Fischer fixed point [329] right at the phase transition. The three-dimensional extension of the double-well potential has rotational symmetry like a Mexican hat. Then the tangential direction in the well is flat and corresponds to the massless mode. In Fig. 2.14(b) we see the potential shapes for different transitions: In a crossover (left) the minimum goes continuously from smaller to larger values. At the critical point (middle), if it is approached from the crossover region, the potential develops two local minima on both sides of the initial minimum. At a first order transition (right) the global minimum jumps between the two minima. For a basic introduction to critical phenomena see e.g. [330].

2.5.2 Ansatz for the Effective Potential

We will study the chiral and BEC phase transitions in QCD and QC₂D with a 1d and 2d Taylor expansions of the effective potential about the minimum. An expansion about the minimum is expected to be stable [331]. The quality of such an expansion of the order-parameter potential has been studied quantitatively in Ref. [332] at vanishing temperature, and for the proper-time RG at finite temperature in Ref. [175]. A 3d-Taylor expansions was investigated in [333]. As we have just discussed, we write the momentum independent, pure bosonic terms of the effective action into the effective potential

$$U(\rho_\phi, \rho_\Delta, \sigma) = V(\rho_\phi, \rho_\Delta) - 4\mu^2 \rho_\Delta - c\sqrt{Z_\phi} \sigma \quad (2.45)$$

where

$$\rho_\phi = \frac{Z_\phi}{2}(\vec{\pi}^2 + \sigma^2), \quad \rho_\Delta = Z_\Delta \Delta^* \Delta = \frac{Z_\Delta}{2}(\Delta_1^2 + \Delta_2^2) \quad (2.46)$$

are the invariants of the chiral and baryon number symmetry respectively, and ρ_Δ is given in the complex as well as the real representation of the diquarks, which relate to each other by

$$\Delta = \frac{1}{\sqrt{2}}(\Delta_1 + i\Delta_2), \quad \Delta^* = \frac{1}{\sqrt{2}}(\Delta_1 - i\Delta_2). \quad (2.47)$$

The the explicit quark current mass in the form the source term for σ gives rise to a smooth chiral crossover at small densities, whereas a rising chemical potential will lead to a second order phase transition to the BEC phase. As the diquark spontaneously assumes a non-vanishing ground state value, we can always rotate in the complex plane, and choose Δ_1 to carry the condensate.

For two-color QCD we have two diquark degrees of freedom as shown above. Moreover we have the extended flavor symmetry $SU(4) \simeq SO(6)$ at $\mu = 0$ where the effective potential must be a

function of the $SO(6)$ invariant $\rho = \rho_\phi + \rho_\Delta$ with $Z_\phi = Z_\Delta$, aside from the linear source term which simply shifts the minimum; hence $V(\rho_\phi, \rho_\Delta) = V(\rho)$. In this work we are going to study such an ansatz with $Z_\phi \neq Z_\Delta$ at finite chemical potentials as an approximation. Higher order bosonic interactions will be introduced by making a Taylor expansion of V about the minimum $\rho = \kappa$ of U . This will be compared to a two-dimensional expansion in the invariants ρ_ϕ and ρ_Δ .

In physical QCD the diquark is a color anti-triplet, therefore it is implied that the diquark fields in Eqs. (2.46) and (2.47) carry color indices as Δ^a with $a = r, g, b$, which are summed over in the former equation. Then ρ_Δ is also the bosonic invariant with respect to $SU(3)_c$ symmetry. As the symmetry is spontaneously broken, we can make $SU(3)_c$ and $U(1)_B$ rotations such that real part of the blue diquark Δ_1^b carries the condensate. Even if there is no symmetry relating mesons to diquarks, we may use a one-dimensional Taylor expansion in $\rho = \rho_\phi + \gamma\rho_\Delta$ as an approximation, which comprises a constant ratio between the mesonic and diquark sector in the effective potential. The ratio should be given by the mass parameters as $\gamma = m_\Delta^2/m_\phi^2$. Note that this is not well suited for chiral limit calculations with $c = 0$, since a spontaneous breaking of chiral symmetry gives rise to Goldstone bosons with $m_\phi^2 = 0$ leading to either an infinite ratio $\gamma \rightarrow \infty$ or to additional Goldstone bosons in the form of diquarks. Hence, we may infer that even for $c \neq 0$, a 1d-expansion may not be as good as in two-color QCD.

As we mentioned before, we are free to choose the order parameter among the fields associated to a broken symmetry. However, since we have a source term for the σ -field it must be the order parameter of the chiral phase transition. For the diquarks we choose Δ_1 , where the superscript b , denoting blue color in the QCD case, will be suppressed in the remainder of this section. All other fields are vanishing, so for the stationary solution of U we solve the following two equations, with $\vec{\rho} = (\rho_\phi, \rho_\Delta)$ and $\vec{\kappa} = (\kappa_\phi, \kappa_\Delta)$,

$$\left. \frac{\partial U}{\partial \sigma} \right|_{\vec{\rho}=\vec{\kappa}} = \sqrt{2Z_\phi \kappa_\phi} \left(\left. \frac{\partial V}{\partial \rho_\phi} \right|_{\vec{\rho}=\vec{\kappa}} - \frac{c}{\sqrt{2\kappa_\phi}} \right) \stackrel{!}{=} 0, \quad (2.48)$$

$$\left. \frac{\partial U}{\partial \Delta_1} \right|_{\vec{\rho}=\vec{\kappa}} = \sqrt{2Z_\Delta \kappa_\Delta} \left(\left. \frac{\partial V}{\partial \rho_\Delta} \right|_{\vec{\rho}=\vec{\kappa}} - 4\mu^2 \right) \stackrel{!}{=} 0, \quad (2.49)$$

where the chain rule was applied. These equations have to be solved for κ_ϕ and κ_Δ , which are defined to be the minimum of U . In the following we introduce the different Taylor expansions for V and find the specific solutions for the above equations. For convenience we are going to make different parameterizations of the effective potential in the different phases. The regime, where we have no diquark condensate, we will refer to as normal phase, and the regime with $\kappa_\Delta \neq 0$ we refer to as BEC phase.

One-dimensional Taylor expansion

In the normal phase we highlight the mass term in the effective potential by writing

$$V_{nor}(\rho) = m^2 \rho + \sum_{n=2}^N \frac{\lambda_n}{n!} (\rho - \kappa)^n \quad \text{where} \quad \rho = \rho_\phi + \gamma \rho_\Delta, \quad \kappa = \kappa_\phi + \gamma \kappa_\Delta. \quad (2.50)$$

Of course $\gamma = 1$ for QC₂D. Compared to the Taylor formula an irrelevant constant was dropped, which is not necessary for the determination of the ground state. With this ansatz the derivative terms in Eqs. (2.48)-(2.49) reduce to $V'_{nor}(\kappa) = m^2$ and the solution is given by

$$\kappa_\phi = \frac{1}{2} \left(\frac{c}{m^2} \right)^2, \quad \kappa_\Delta = 0. \quad (2.51)$$

It is clear to see, that if there was no quark current mass, i.e. $c = 0$, there would be no chiral condensate unless the mass is zero. For finite c we see that a decrease of the scalar mass parameter leads to an increase of the chiral symmetry breaking accompanied by the occurrence of pseudo Goldstone modes with small masses, rather than massless states. Let us to check the conditions for a minimum. The determinant of the Hessian matrix needs to be larger than zero

$$\det \left(\frac{\partial^2 U}{\partial \varphi_i \partial \varphi_j} \right) \Big|_{\rho=\kappa} = (m^2)^{N_\phi} (\gamma m^2 - 4\mu^2)^{N_\Delta} > 0 \quad (2.52)$$

where φ_i represents all fields contained in the effective potential, and N_ϕ, N_Δ are the number of meson and diquark fields respectively. This is an important result: As long as $\gamma m^2 > 4\mu^2$ we are in the normal regime, while at $\gamma m^2 = 4\mu^2$ the diquark curvature mass vanishes, which indicates a second order phase transition and spontaneous symmetry breaking.

Since m is actually the mass of the pions, for two-color QCD the onset of diquark condensation is exactly when the quark chemical potential reaches half of the pion mass, which by the Silver Blaze property is independent of the chemical potential at $T = 0$, see Sec. 3.3. Hence, if the property is not violated in any way, we can say that in our 1d-Taylor expansion ansatz $\mu_c = m_\pi/2$ holds, fulfilling a well known feature of QC₂D, as it was also discussed in Sec. 2.2.4. In the chiral limit spontaneous symmetry breaking is expected below some critical temperature T_c yielding $m = 0$. In this case we can infer from Eq. (2.52) that, at $\mu = 0$ the condensate has degeneracy of $N_\phi + N_\Delta = 6$ corresponding to the $SO(6)$ symmetry of QC₂D. Now, turning on the chemical potential must entail a rising critical temperature, i.e. $\frac{\partial}{\partial \mu} T_c > 0$, since m must not be vanishing anymore for the Eq. (2.52) to vanish. Moreover, the diquark is the lightest excitation therefore it must be the one that condenses with a reduced degeneracy of $N_\Delta = 2$ corresponding to $U(1) \simeq O(2)$.

For the BEC phase we reparametrize the potential by renaming $m^2 = \lambda_2(\kappa - v)$, thus we exchange m in favor of v . We add another irrelevant constant so that we can write

$$V_{bec}(\rho) = \frac{\lambda_2}{2}(\rho - v)^2 + \sum_{n=3}^N \frac{\lambda_n}{n!}(\rho - \kappa)^n. \quad (2.53)$$

In this parametrization we have $V'_{bec}(\kappa) = \lambda_2(\kappa - v)$, and Eqs. (2.48)-(2.49) yield the following system of linear equations and the solution

$$\begin{aligned} \kappa_\phi + \gamma \kappa_\Delta - v &= \frac{c}{\lambda_2 \sqrt{2\kappa_\phi}}, & \kappa_\phi &= \frac{1}{2} \left(\frac{\gamma c}{4\mu^2} \right)^2, \\ \kappa_\phi + \gamma \kappa_\Delta - v &= \frac{4\mu^2}{\gamma \lambda_2}, & \gamma \kappa_\Delta &= v + \frac{4\mu^2}{\gamma \lambda_2} - \frac{1}{2} \left(\frac{\gamma c}{4\mu^2} \right)^2. \end{aligned} \quad (2.54)$$

It is obvious that we cannot put $v = \kappa$ as usual, in the presence of explicit symmetry breaking terms, because in that case $V'(\kappa) = 0$ leading to $c = \mu = 0$. From the structure of the ground state values, it can already be seen that we are able to reproduce the known behavior of the condensates in QC₂D. For instance the chiral condensate $\sigma_0 = \sqrt{2\kappa_\phi}$ is proportional to μ^{-2} . For the diquark condensate $\Delta_0 = \sqrt{2\kappa_\Delta}$ it becomes more clear if we look at the minimum for $\gamma m^2 < 4\mu^2$ in the normal parametrization (2.50). There it is given by

$$\gamma\kappa_\Delta = \frac{4\mu^2 - \gamma m^2}{\gamma\lambda_2} + \frac{1}{2} \left(\frac{c}{m^2} \right)^2 \left[1 - \left(\frac{\gamma m^2}{4\mu^2} \right)^2 \right], \quad (2.55)$$

while κ_ϕ stays the same. The first term is the typical minimum in a double well potential for single condensate. A rising chemical potential entails that more particles are put into the system, which immediately condense. The second term is the difference of the chiral condensate with respect to its value in the normal phase. Due to the simplified mixing of mesons and diquarks within the 1d potential this difference is added to the diquark. Because there is no melting if temperature effects are not taken into account, the missing condensate has to go somewhere. Hence with rising μ the ground state rotates from the mesonic direction to the diquark direction. Moreover Eqs. (2.54) imply $V'_{bec}(\kappa) = 4\mu^2$ and as we will see this is mass squared of the pions. All these results agree with predictions from leading order chiral perturbation theory [199], which justifies our 1d-ansatz. With the inclusion of fluctuations within the FRG framework we can include effects which go beyond this simple behavior. Above all, we can go to finite temperatures straightforwardly.

Two-dimensional Taylor expansion

In the 2d expansion we have independent mass terms and couplings as well as mixed couplings for the two different sectors,

$$V(\rho_\phi, \rho_\Delta) = m_\phi^2 \rho_\phi + m_\Delta^2 \rho_\Delta + \sum_{\substack{n,m=2 \\ n+m < N}} \frac{\lambda_{n,m}}{n!m!} (\rho_\phi - \kappa_\phi)^n (\rho_\Delta - \kappa_\Delta)^m. \quad (2.56)$$

Now we again have to solve Eqs. (2.48)-(2.49) with this ansatz. The chiral condensate is always given by the same expression in all phases which is basically the same as (2.51)

$$\kappa_\phi = \frac{1}{2} \left(\frac{c}{m_\phi^2} \right)^2. \quad (2.57)$$

In the diquark sector we either have the trivial solution or the parenthesis in (2.49) vanishes when the diquark mass parameter equals twice the chemical potential in the BEC phase. There the mass parameter is kept fixed and thereby is always canceled by the chemical potential, while the condensate takes its place in the parameter space. In summary we have

$$\begin{aligned} \text{Normal regime:} & \quad \kappa_\Delta = 0, \\ \text{BEC regime:} & \quad \kappa_\Delta \neq 0, \quad m_\Delta = 2\mu. \end{aligned} \quad (2.58)$$

With the more general 2d ansatz the behavior cannot be predicted as in the 1d case. Nevertheless we expect qualitatively the same behavior, as it was seen in [233]. However, there is a problem regarding the Silver Blaze property which will be discussed in the next chapter.

Renormalization Group Equations at Finite Temperature and Density

In order to investigate a quantum field theory (QFT) and to compute observable quantities, fluctuations have to be taken into account. For weakly interacting theories, or more generally, weakly interacting regimes of QFTs, observable quantities can be computed directly from the Hamiltonian of the theory within a perturbative expansion in orders of the interaction parameters [270]. Each contribution corresponds to an interaction process described by a Feynman diagram. However, there is the problem with higher order contributions in the form of loop diagrams in such a scheme, namely the corresponding integrals are diverging. The solution of this problem lead to the concept of *Renormalization* where one distinguishes between *bare* quantities, which are the parameters written in the *microscopic* theory, and *renormalized* (also referred to as *full* or *dressed*) quantities, which are the physical and measurable ones. At the perturbative level one expresses the bare parameters of the theory in terms of the physical ones minus *counter terms* which absorb the divergent contributions, while the physical parameters have to be matched with physical observables.

Naturally in a strongly interacting theory a perturbative expansion does not converge. In this case, a way to exactly solve a theory is to discretize it on a lattice and perform numerical simulations. The smaller the lattice spacing is, the closer are the simulations to continuum physics. However lattice computations are numerically expensive and for QCD at finite chemical potential they suffer from the sign problem. Therefore functional methods like Dyson-Schwinger Equations [148, 149] the Renormalization Group are employed in order to study non-perturbative aspects of QFTs. In contrast to a perturbative expansion in the interaction parameters, functional methods are typically based on an expansion of the theory in correlation functions, which are allowed by the symmetry of the underlying theory. The behavior of these functions is governed by equations which are provided by the method.

In the following we will give a brief introduction of the *Functional Renormalization Group* (FRG) put forward by Wetterich in '93 [150]. This method has been proven to be quite successful not only in quantum field theories but also in statistical physics [334]. Afterwards we will derive the necessary tools in order to obtain the specific equations for our model from the FRG, and then discuss them in detail. Different aspects and effects of finite temperatures and chemical potentials will be addressed, in particular the so called *Silver Blaze property*. We will show numerical results for of the T and μ dependence of different parameters of our system, obtained from the renormalization group equations with our best approximation, which we denote as 2d Taylor', see Tab. 4.1.

3.1 The Functional Renormalization Group

We will neither introduce the functional formalism here, nor will we derive the FRG equation, but rather will only state the relevant information. For introduction of the functional formalism see [270]. For reviews and introductions regarding the FRG framework see [183, 335–343].

3.1.1 The Concept

The idea behind the Renormalization Group roots back to Kadanoff’s block spin transformation [344]: Consider a two-dimensional lattice with a spin on each lattice site, which can either have upwards or downwards direction. We are not interested in the orientation of each spin but rather in the collective, macroscopic behavior of the system. To this end we divide the lattice into smaller subsystems and average over the elements in each subsystem. The average values are the relevant information at a larger scale, and they constitute a new system with a reduced number of degrees of freedom. This procedure can be viewed as a *coarse-graining*, which can be repeated until the average behavior of the complete system is known. If the spins interact with each other, it is necessary to perform the averaging in successive steps. Naturally the nearest neighbors interact the strongest, hence it is wise to average in subsystems, which do not contain more than the nearest neighbors of one element. This way the effects of the interaction can be taken into account properly. After averaging once the subsystems are the new elements of the system which interact with each other, hence the interaction length has increased and the strength changes as well. However we can rescale the interaction length in units of the new lattice spacing, such that it coincides with the original interaction length, and then we know how the interaction strength has changed under a change of the scale. This is the essence of the Renormalization Group, namely to see how the system parameters behave if one looks at the system at a larger scale, where the details within the scale are washed out.

This idea of coarse-graining the system successively, was extended by Wilson [345] and Wegner [346] to the continuum. If a QFT is known at some initial scale and one is interested in how the theory looks at a larger length scale, in order to predict observable quantities, one integrates out quantum fluctuations that have the range of the initial scale (corresponding to the nearest neighbor interaction in the spin system). This procedure is iterated until one arrives at macroscopic length scales, and the microscopic degrees of freedom thereby reduced. Note that in QFTs the interactions are typically *local*, meaning that they are point-like. Thus, after an iteration step higher order interaction processes within the initial scale are averaged over, and the result is interpreted as the new point-like interaction by rescaling system, similar as in the block spin transformation. Thereby even new types of interactions can be generated, in fact, all types of processes and collective excitations which are allowed by the symmetries of the initial theory, are generated by the renormalization procedure, which is the fact that we have used in our model construction in the previous chapter. Of course, in practice one takes only a finite number correlations into account, which are considered to be the relevant ones.

Typically the computations are done in momentum space where the coarse-graining procedure corresponds to starting with a theory at some high momentum scale and integrating out fluctuations in thin momentum shells iteratively down to a desired low momentum scale. Based on this idea one can deduce the famous Callan-Symanzik equation [16, 17], which govern the scale dependence of the parameters and physical observables of a theory. In fact, the FRG equation is a variant of the functional form of the Callan-Symanzik equation.

The central object of the FRG framework is the scale dependent *effective average action* Γ_k , where k is the momentum scale, above which fluctuations are integrated out, therefore it also referred to the IR *cutoff*, as it suppress low momentum modes. The scale-dependence is governed by an exact integro-differential equation known as the *flow equation* or *Wetterich equation*, the solution to which interpolates between the classical bare action S of a theory given at a UV cutoff scale Λ and the quantum effective action Γ in the IR, where all fluctuations are integrated out:

$$\Gamma_{k=\Lambda} = S, \quad (3.1)$$

$$\Gamma_{k=0} = \Gamma. \quad (3.2)$$

Thus we conveniently obtain the generating functional of one-particle-irreducible correlation functions allowing to access the macroscopic or thermodynamic properties of the system under consideration. Indeed not only quantum fluctuations are integrated out, but also statistical fluctuations are taken into account in a finite temperature and chemical potential framework of the FRG. Actually, the right-hand side of (3.1) must not be a bare action, but rather it can be any action which describes a system well at the scale Λ which can be obtained by any means, experimentally or theoretically. In any case, the correlation functions obtained from Γ_k contain always the fully dressed and renormalized parameters for momenta $p \gtrsim k$, by construction. Most importantly, we are interested in the ground state of the system, which is given by the minimum of Eq. (3.2) as discussed in Sec. 2.5.1.

3.1.2 The Flow Equation

In order to define a theory where fluctuations are integrated out between Λ and k , we start by defining a scale dependent generating functional of disconnected correlation functions in Euclidean space-time, with an additional term in the exponent that is supposed to suppress the contribution of the modes with momenta $p \lesssim k$:

$$Z_k[J] = e^{W_k[J]} = \int_{\Lambda} \mathcal{D}\phi \, e^{-S[\phi] - \Delta S_k[\phi] + J^T \cdot \phi}, \quad (3.3)$$

where $W_k[J]$ is the scale-dependent Schwinger functional, generator of the connected correlation functions. The scalar product sums up all discrete and continuous indices of the field ϕ and the source J . Discrete indices are for field species and substructures, continuous indices are for position or momentum coordinates. $\Delta S_k[\phi]$ is the regulator term which is usually quadratic in fields, although in principle higher orders are possible as well [183],

$$\Delta S_k[\phi] = \frac{1}{2} \phi^T \cdot R_k \cdot \phi. \quad (3.4)$$

It is meant to act as an IR cutoff by giving an effective mass of the order k for the propagator to the modes with $p \lesssim k$, and no mass to modes with $p \gtrsim k$. Note that the vertices are not explicitly modified. For the average action to behave in the way we explained above, the regulator has to meet the following requirements

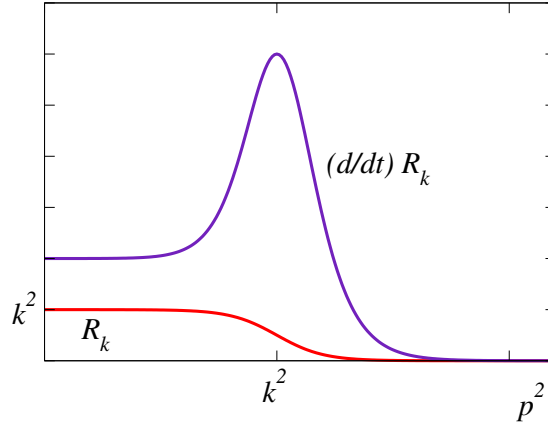


Figure 3.1: Example of a typical regulator function and its scale derivative taken from [342]. The regulator suppresses modes with $p \lesssim k$, while its derivative ensures Wilson's idea of integrating out fluctuations within a momentum shell around $p \simeq k$.

- The propagator should remain finite in the IR, a divergences must be avoided for a massless mode, hence

$$\lim_{p/k \rightarrow 0} R_k(p) > 0 .$$

- If the cutoff is vanishing, we should recover the full quantum theory, $Z_{k \rightarrow 0}[J] = Z[J]$, therefore

$$\lim_{p/k \rightarrow \infty} R_k(p) = 0 .$$

- If the IR cutoff approaches the UV cutoff of the theory, $k \rightarrow \Lambda$, no modes should be integrated out and the theory should remain unchanged in the UV, which is realized by

$$\lim_{k \rightarrow \Lambda} R_k(p) \rightarrow \infty .$$

The choice of the regulator is only restricted by the requirements formulated above, aside from which it is arbitrary. A sketch of a typical regulator that satisfies these three requirements is shown in Fig. 3.1, with the definition of the RG-time

$$t = \ln(k/\Lambda) \quad \Rightarrow \quad \partial_t = k \frac{\partial}{\partial k} . \quad (3.5)$$

Now we turn to the main object, the effective average action. It is defined via a modified Legendre transformation of the scale dependent Schwinger functional

$$\Gamma_k[\Phi] = \sup_J \left(J^T \cdot \Phi - W_k[J] \right) - \Delta S_k[\Phi] , \quad (3.6)$$

where

$$\Phi = \frac{\delta W_k[J]}{\delta J} = \langle \phi \rangle_J \quad (3.7)$$

is the expectation value of the quantum field ϕ at finite source J defined by a functional derivative. It is also called the *classical field*, since it is a weighted average over all possible fluctuations, furthermore it is the variable conjugate to the source. At $k = 0$ the regulator vanishes and Eq. (3.6) approaches the quantum effective action Γ which governs the dynamic of the expectation

value Φ , while the minimum of Γ for vanishing sources defines the ground state of the fully quantized system. Moreover, for a given Φ , there is one $J \equiv J_{sup} = J[\Phi]$ for which $J \cdot \Phi - W[J]$ approaches its supremum, guaranteeing that $\Gamma[\Phi]$ is convex.

Now let us write down the flow equation:

$$\boxed{\partial_t \Gamma_k[\Phi] = \frac{1}{2} \text{STr} (G_k[\Phi] \partial_t R_k)} \quad \text{with} \quad \boxed{G_k[\Phi] = \frac{1}{\Gamma_k^{(2)}[\Phi] + R_k}}. \quad (3.8)$$

The supertrace operation STr is a trace over all continuous and discrete field indices and involves minus signs for Grassmann valued fields like fermions. The regularized propagator G_k is given by the inverse of the two-point function added by the regulator. It is a full propagator containing all possible self interaction processes with momenta above the scale k and it is suppressed (or gapped) by the regulator for momenta smaller than k . The two-point function is given by the second functional derivative of the effective action which will be shown in Sec. 3.2. See Fig. 3.2 for the diagrammatic form of the flow equation.

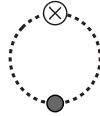
$$\partial_t \Gamma_k[\Phi] = \frac{1}{2} \text{STr} \left(\text{loop} \right)$$


Figure 3.2: Pictorial representation of the exact flow equation. The dotted line represents the complete propagator in field space. The cross denotes cutoff insertions $\partial_t R_k$, the dark circle indicates the fact this is a “dressed” propagator as opposed to a bare one (for simplicity it will be not always shown). The STr operation is implied by the loop structure.

The flow equation is a nonlinear integro-differential equation which relates the change of the effective average action with respect to an infinitesimal change of the RG-scale k to quantum fluctuations in the form of a one-loop process. It is an exact equation and the one-loop structure is a consequence of the regulator term ΔS_k being quadratic in the fields. Since $\partial_t R_k$ is peaked around k and vanishes for large momenta, and G_k is suppressed at low momenta, only a momentum shell around k is picked out in the loop-integration. Hence, both the IR and UV regularizations are guaranteed by the properties of the quantities inside the supertrace.

3.1.3 Solution Methods

Starting with an initial action at the UV scale Λ an RG-step is performed by adding $-\partial_t \Gamma_\Lambda \Delta k$ to Γ_k which defines the effective action at the lowered scale, $\Gamma_{\Lambda-\Delta k}$. Then the subsequent RG-step must be performed with propagator at the lowered scale $G_{\Lambda-\Delta k}$ which is derived from $\Gamma_{\Lambda-\Delta k}$. This procedure is repeated until fluctuations from all scales have been included, yielding the full quantum effective action. Since the field Φ enters the flow equation as a variable, in principle one must solve the flow equation for all field configurations, however this is numerically highly expensive. Therefore one must resort to approximation schemes mostly involving an expansion of Γ_k in terms of a suitable basis.

Vertex expansion A very general scheme is *vertex expansion* [151]

$$\Gamma_k[\Phi] = \sum_{n=0}^{\infty} \frac{1}{n!} \int_{x_1 \dots x_n} \Gamma_k^{(n)}(x_1, \dots, x_n) (\Phi(x_1) - \Phi_0(x_1)) \dots (\Phi(x_n) - \Phi_0(x_n)) , \quad (3.9)$$

where $\Gamma_k^{(n)}$ for $n = 2$ is the full two-point function and for $n > 2$ the correspond the one-particle irreducible vertex function, Φ_0 is a background field. If Φ is a multicomponent field the n -point functions have a tensor structure which is suppressed here. This ansatz turns Eq. (3.8) into a tower of infinitely many coupled differential equations for the expansion coefficients, or equivalently the associated coupling parameters. A suitable expansion scheme should include the relevant degrees of freedom of a given problem at all considered scales and respect the symmetries of the system. Reducing the expansion to a treatable and finite subset of running couplings defines a truncation. It is an important property of the FRG method footing on the exact flow equation that the success of a chosen truncation does not necessarily rely on the existence of a small expansion parameter. It only requires that the neglected operators do not couple too strongly into the flow of the included operators. The quality of a truncation can be tested, by the convergence for systematical extensions of a given truncation scheme, by a study of its regulator dependence (Fig. 3.3) and, of course, by comparison to well-known limiting cases as well as complementary methods.

Derivative expansion Another often used truncation scheme is the *derivative expansion* [151] in the sector of the scalar fields

$$\Gamma_k[\Phi] = \int_x \left\{ U_k(\Phi) + \frac{1}{2} Z_k (\partial_\mu \Phi)^2 + \mathcal{O}(\partial^4) \right\} . \quad (3.10)$$

In lowest order it is also called *local potential approximation* (LPA), where only a scale-dependence of the effective potential U_k is considered. In the next step (LPA') the scale-dependence of the wave function renormalization Z_k is solved. Very accurate critical exponents have computed in in such schemes [347–349]. Further improvement of the truncation include a field-dependent wave function renormalization and higher derivative terms. For the fermionic case a similar scheme is applicable, as well as for mixed correlation functions. Our truncations from the previous chapter correspond to LPA' with additional fermionic degrees of freedom and three-point functions coupling the different sectors. The Taylor expansion of the effective potential actually can be seen as a vertex expansion as well.

Parameter fixing Our work is about low-energy effective models for a theory, which in the classical regime is described by quark-gluon interactions (and ghosts). The initial parameters are the strong coupling constant and the quark current masses, which are known. Since our model ansatz described in the previous section does not contain gluonic degrees of freedom, the question arises how to make the connection to the classical action. We will start the for flow our model at an energy scale far lower than the classical regime of QCD, and there are two possibilities to fix the initial conditions [180]. Firstly, one can solve the QCD-flows in suitable truncation down to the low-energy scale and derive the initial conditions for the model, which corresponds to fixing the microphysics. If QCD-flows are not available, one considers the truncation with the highest number of running couplings in the low-energy model as the one which is closest to the full QCD-flow. Then, by stepwise reducing the number of running couplings, one can test the quality of a truncation. If the resulting differences in $\Gamma_{k=0}$ are relatively small in the

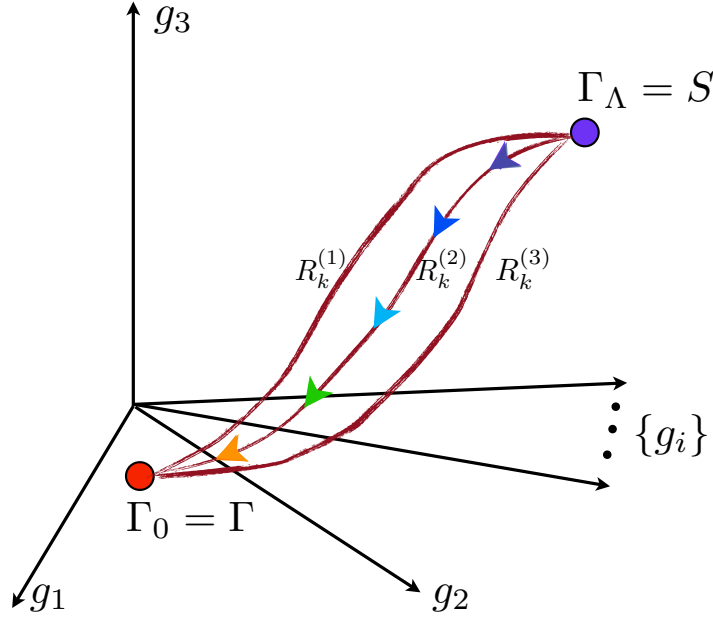


Figure 3.3: Sketch of the RG flow of the effective action in *theory space*, which is spanned by an infinite number of running couplings representing the infinite correlation functions of the effective action for a non-truncated system. The trajectory connects the classical bare action of a theory with its full quantum effective action. Different regulator choices $R_k^{(i)}$ lead to different trajectories with the same endpoints, in principle. In a truncated system a small regulator dependence of Γ_0 indicates the good quality of the truncation. For the optimization of the regularization scheme see [183, 350–352]. Figure taken from [239].

first few steps, the quality of the truncation can be considered to be reliable. On the other hand, if a systematical reduction of the truncation is not done in some specific sector, nothing can be said about the quality of the truncation. If the effects of taking that sector into account are large, it only means that they are important at least. The second possibility is to tune the model parameters such that the known low-energy QCD observables are reproduced within a truncation. Typically this corresponds to fixing the vacuum physics to known mass spectra and decay constants. Of course, if there was no approximation in the low-energy model, the initial conditions from both possibilities coincide.

Many body effects In order to explore the temperature and density effects we are going to solve the flow for a range of the temperature and chemical potential with unchanged UV initial conditions [353]. In this case it is important that the initial conditions are not influenced by many body effects, which can be achieved by starting the flow at a microscopic UV scale Λ that is well above the scale where many body effects come into play, see Fig. 3.4. This way it can be ensured that the temperature and density physics are independent of the UV cutoff, which is necessary to have reliable predictive power. In Fig. 3.4 the initial conditions are fixed in the vacuum therefore the direction of the trajectory is “upwards”. In fact the flow equations can be solved in this direction, if the number of IR conditions agrees with the number of tunable parameters, and if there is no fixed point on the way, where the system loses its memory. On the other hand, if there are more parameters than IR conditions, the UV initial values are not unique. Different sets of values can reproduce the same values for the low-energy constants but lead to different predictions in the finite temperature and chemical potential regime. The differences should be quantified.

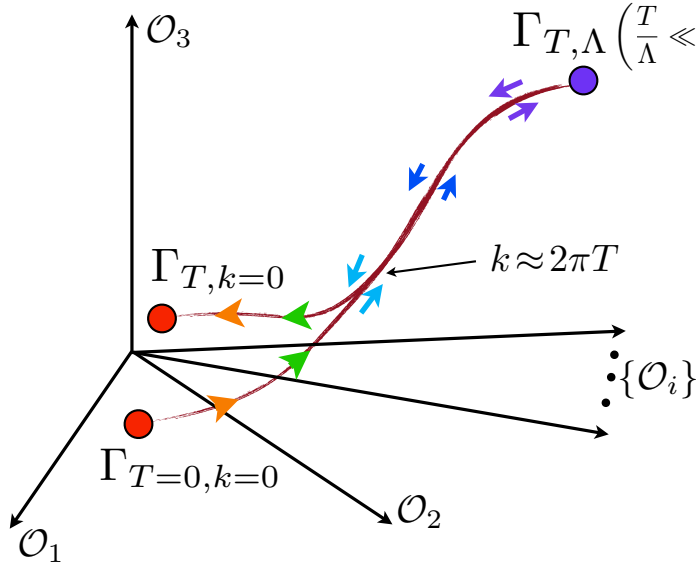


Figure 3.4: Vacuum flow and flow at finite temperature in theory space (The operators O_i can be associated with the couplings g_i). For computations at finite temperature the UV cutoff Λ must be much larger than the T , such that the physical results are independent of the UV cutoff. Many body effects come into play at $k \approx 2\pi T$. Figure taken from [196].

3.2 Propagators and Masses

In order to compute flow equations we first need to find the propagator. Generally, the complete propagator of a theory is given by the inverse curvature matrix of the effective action. Within the FRG framework we find a modified definition for the dressed propagator, where a regulator is added suppressing low momentum modes. At broken Lorentz symmetry a regulator only cutting of the three-momentum and not the frequencies, is a good choice. We are going to solve the flow at the ground state values of the field, hence for the derivation of the flow equations we will use an expansion point which constant in position or momentum space.

Now let us derive the full propagator for general theory, which we will then specify to contain bosonic and fermionic degrees of freedom, before stating the various definitions of the masses, which are extracted from the propagator. Afterwards the specific propagators and masses for our models will be computed. Henceforth we will suppress the index k for the scale dependent quantities for simplicity. Apart from the discussion of the masses, this section is rather technical.

General derivation

Here, we will show a general procedure to find the dressed propagator and from now on and throughout this chapter we are going to use the shorthand notations defined in App. A.3. We mention here that a momentum integration implies a summation over Matsubara frequencies, which will be defined later. In order to find the momentum representation of the curvature matrix/two-point function $\Gamma^{(2)}[\Phi_0]$ at some constant expansion point, we are going to expand the action to second order in the fields and then apply a Fourier transformation. With a general multicomponent field given by the vector Φ , the two-point function in position space is given by

$$\Gamma^{(2)}(x, y) = \frac{\overrightarrow{\delta}}{\delta\Phi^T(x)} \Gamma[\Phi] \frac{\overleftarrow{\delta}}{\delta\Phi(y)} \Big|_{\Phi_0} = \hat{\Gamma}^{(2)} \left(i\overleftarrow{\partial}_x, i\overrightarrow{\partial}_y \right) \delta(x - y) , \quad (3.11)$$

where Φ_0 is expansion point, which can be chosen to be the minimum of the effective action, i.e. the ground state. The spacetime dependences in Eq. (3.11) essentially lies in a Dirac delta function, since all fields are set to the expansion point given by constants in spacetime. In the leading order derivative expansion, other than that there are only spacetime-derivative operators acting on the fields to the left and to the right of $\hat{\Gamma}^{(2)}$, indicated by the arrows over operators. Of course the action is usually written in a way, where all derivatives act on fields to right-hand side, however, when a field derivative with respect to Φ^T in Eq. (3.11) acts in a matrix representation, the expression has to be transposed, which changes the direction of the derivative. Let us write down the second order term of the Taylor expansion of the effective action

$$\frac{1}{2} \int_{x,y} (\Phi(x) - \Phi_0)^T \Gamma^{(2)}(x, y) (\Phi(y) - \Phi_0) . \quad (3.12)$$

Naturally, when we want to find the two-point function, the lower order terms vanish by differentiation while the higher ones vanish by setting Φ to the expansion point Φ_0 . Now we perform a Fourier transformation of the fields

$$\Phi(x) = \int_p e^{-ipx} \Phi(p) . \quad (3.13)$$

Keep in mind, that Φ also contains all antiparticle fields like the complex conjugates. It follows from Eq. (3.13) that after Fourier transformation the antiparticle fields are not exactly the complex conjugates anymore, however, if $\Phi_i(x) = \Phi_j^*(x)$ the relation $\Phi_i(-p) = [\Phi_j(p)]^*$ holds, which can easily be checked by complex conjugating the corresponding components of Eq. (3.13). Such a relation might seem tedious, however, the Fourier transform must be defined in this way, so that Φ keeps being a vector with independent components. Moreover, it is important to designate the representation in field space before performing the Fourier transformation for the same reason. Plugging Eqs. (3.11) and (3.13) into Eq. (3.12), neglecting the constant terms, which will drop out later, yields

$$\begin{aligned} & \frac{1}{2} \int_{x,y} \int_{p,q} \Phi^T(q) e^{-iqx} \hat{\Gamma}^{(2)} \left(i\overleftarrow{\partial}_x, i\overrightarrow{\partial}_y \right) \delta(x - y) \Phi(p) e^{-ipy} \\ &= \frac{1}{2} \int_{p,q} \Phi^T(q) \hat{\Gamma}^{(2)}(q, p) \Phi(p) \underbrace{\int_x e^{-i(p+q)x}}_{\delta(p+q)} \\ &= \frac{1}{2} \int_p \Phi^T(-p) \hat{\Gamma}^{(2)}(-p, p) \Phi(p) . \end{aligned} \quad (3.14)$$

In general, the two-point function contains real entries, as well as complex entries. Real entries are multiplied by pairs of fields which satisfy the relation mentioned below Eq. (3.13), or a combination of them appears such that their sum in Eq. (3.14) is real-valued. Complex entries typically become real by virtue of the integration. Now, the momentum representation of $\Gamma^{(2)}$ can be obtained by taking the second derivative of Eq. (3.14) with respect to the fields in momentum space

$$\begin{aligned}
 \Gamma^{(2)}(-p, q) &= \frac{\overrightarrow{\delta}}{\delta\Phi^T(-p)} \left(\frac{1}{2} \int_{p'} \Phi^T(-p') \hat{\Gamma}^{(2)}(-p', p') \Phi(p') \right) \frac{\overleftarrow{\delta}}{\delta\Phi(q)} \\
 &= \left[\int_{p'} \delta(p - p') \hat{\Gamma}^{(2)}(-p', p') \Phi(p') \right] \frac{\overleftarrow{\delta}}{\delta\Phi(q)} \\
 &= \hat{\Gamma}^{(2)}(-p, p) \delta(p - q)
 \end{aligned} \tag{3.15}$$

The product rule yields twice the same result, since transposing in the expression the parenthesis in the upper line should not change it, as it is a scalar expression. We conclude that we can find the two-point function $\Gamma^{(2)}$ in momentum space at some expansion point in field space by replacing spacetime derivatives by four-momenta with the appropriate signs according to $\hat{\Gamma}^{(2)}(i\overleftarrow{\partial}_x, i\overrightarrow{\partial}_y) \rightarrow \hat{\Gamma}^{(2)}(-p, p)$, then we rename $\Gamma^{(2)}(p) \equiv \hat{\Gamma}^{(2)}(-p, p)$ for convenience. Throughout this chapter, the a dependence on $n-1$ momenta of an n -point function denotes that the functions are evaluated at the expansion point Φ_0 and that the delta functions are excluded. Let us define a sign changing function for interchanging fermionic fields

$$(-1)^{ij} = \begin{cases} 1 & \text{for } i \text{ and } j \text{ fermionic,} \\ -1 & \text{otherwise.} \end{cases} \tag{3.16}$$

With this definition, the off-diagonal elements of the curvature matrix obey the relation

$$\begin{aligned}
 \frac{\overrightarrow{\delta}}{\delta\Phi_i(-p)} \Gamma \frac{\overleftarrow{\delta}}{\delta\Phi_j(q)} &= (-1)^{ij} \frac{\overrightarrow{\delta}}{\delta\Phi_j(-p)} \Gamma \frac{\overleftarrow{\delta}}{\delta\Phi_i(q)} \Big|_{p \leftrightarrow -q} \\
 &= (-1)^{ij} \Gamma_{ji}^{(2)}(p) \delta(p - q) \Big|_{p \leftrightarrow -q} = (-1)^{ij} \Gamma_{ji}^{(2)}(-q) \delta(-q + p),
 \end{aligned}$$

hence

$$\Gamma_{ij}(p) = (-1)^{ij} \Gamma_{ji}(-p). \tag{3.17}$$

An n -point function has n indices in the matrix representation, so the superscript denoting the order of the derivative can be omitted in a representation with matrix indices. The indices denote the fields with respect to which the derivatives were taken as well as the side from which they act. In Eq. (3.17) we can set the argument $-q = -p$ due to the Dirac delta function. For this relation to hold, diagonal terms must be functions of p_4^2 and \vec{p}^2 , since only the space-like $O(3)$ symmetry is always preserved. A similar relation holds for the regulator term, and thereby for the propagator as well. The regulator is R is typically given in the momentum representation, where it has the same structure as the kinetic part of the two-point function. So we can write the propagator from Eq. (3.8) in momentum space at some expansion point as

$$G(p, -q) = G(p) \delta(p - q) = \left(\Gamma^{(2)}(p) + R(p) \right)^{-1} \delta(p - q). \tag{3.18}$$

We emphasize that this form of G is only valid for constant fields.

Bosonic and fermionic components, regulator choice

For our work we write the components of the field and the expansion point as

$$\Phi = \begin{pmatrix} \varphi \\ \Psi \\ \bar{\Psi}^T \end{pmatrix}, \quad \Phi_0 = \begin{pmatrix} \varphi_0 \\ 0 \\ 0 \end{pmatrix},$$

where bosonic species are summarized in φ , while the anti-/fermionic species are summarized in $\bar{\Psi}$ and Ψ . The reason for setting $\Psi = \bar{\Psi} = 0$ for the expansion point is that we want it to be close to or right at the ground state. For the matrix elements we find

$$\Gamma^{(2)}(p) = \begin{pmatrix} \Gamma_{\varphi\varphi} & 0 & 0 \\ 0 & 0 & \Gamma_{\Psi\bar{\Psi}} \\ 0 & \Gamma_{\bar{\Psi}\Psi} & 0 \end{pmatrix}, \quad R(p) = \begin{pmatrix} R_{\varphi} & 0 & 0 \\ 0 & 0 & R_{\Psi\bar{\Psi}} \\ 0 & R_{\bar{\Psi}\Psi} & 0 \end{pmatrix}. \quad (3.19)$$

Apart from the choice of the expansion point, we made the assumption that there cannot be terms proportional to $\varphi\Psi$ or $\varphi\bar{\Psi}$ (or with higher orders in φ), and find a block diagonal structure with a block for each sector. Note that the fermionic sector is purely off-diagonal, again due to the choice of Φ_0 . Each component of $\Gamma^{(2)}$ is to be evaluated with the formula (3.11). Since the kinetic terms are quadratic in fields and without mixing of species, R always has this form. As we allow for a running of the wave function renormalization, the scale derivative of the regulator has two terms

$$\partial_t R \sim \partial_t(Z_{\Phi_i} r_{\Phi_i}) = Z_{\Phi_i} \partial_t r_{\Phi_i} + r_{\Phi_i} \partial_t Z_{\Phi_i} = Z_{\Phi_i} (\dot{r}_{\Phi_i} - \eta_{\Phi_i} r_{\Phi_i}), \quad (3.20)$$

where we have defined the anomalous dimensions for the respective fields as

$$\eta_{\Phi_i} = -Z_{\Phi_i}^{-1} \partial_t Z_{\Phi_i} = -\partial_t \ln Z_{\Phi_i}. \quad (3.21)$$

There is one anomalous dimension for each particle species. More detail are presented in Sec. 3.6. The propagator reads in components

$$G(p) = \begin{pmatrix} (\Gamma_{\varphi\varphi} + R_{\varphi})^{-1} & 0 & 0 \\ 0 & 0 & (\Gamma_{\bar{\Psi}\Psi} + R_{\bar{\Psi}\Psi})^{-1} \\ 0 & (\Gamma_{\Psi\bar{\Psi}} + R_{\Psi\bar{\Psi}})^{-1} & 0 \end{pmatrix} = \begin{pmatrix} G_{\varphi} & 0 & 0 \\ 0 & 0 & G_{\Psi\bar{\Psi}} \\ 0 & G_{\bar{\Psi}\Psi} & 0 \end{pmatrix} \quad (3.22)$$

Note that the indices of off-diagonal components are interchanged because of the inversion. In the following subsections we will treat bosonic and fermionic propagators individually. The addition of R essentially amounts to having regularized momenta, which for the case of a 3d regulator read

$$\vec{p}_r = \begin{cases} \vec{p} \sqrt{1 + r_B(\vec{p}^2/k^2)} & \text{for bosons,} \\ \vec{p} (1 + r_F(\vec{p}^2/k^2)) & \text{for fermions.} \end{cases} \quad (3.23)$$

Obviously a 3d regulator breaks Lorentz invariance at $T = 0$. However, physical quantities are measured in the ground state at $k = 0$, where the regulator is vanishing. Although the frequency modes are not regularized, we will not have any divergent loop integrations. In this work, we employ the optimized regulator shape functions, which is well-suited for finite temperatures [351, 353]

$$r_B(x) = \left(\frac{1}{x} - 1\right) \Theta(1 - x), \quad (3.24)$$

$$r_F(x) = \left(\frac{1}{\sqrt{x}} - 1\right) \Theta(1 - x), \quad (3.25)$$

where $\Theta(1 - x)$ denotes the Heaviside step function. The bosonic propagator is a Galilean invariant quantity at finite temperatures, hence the kinetic terms will turn into

$$\vec{p}_r^2 = \vec{p}^2 + (k^2 - \vec{p}^2)\Theta(k^2 - \vec{p}^2) = \vec{p}^2\Theta(\vec{p}^2 - k^2) + k^2\Theta(k^2 - \vec{p}^2)$$

and our propagator divides into two parts

$$G_\varphi(\vec{p}_r^2) = G_\varphi(\vec{p}^2)\Theta(\vec{p}^2 - k^2) + G_\varphi(k^2)\Theta(k^2 - \vec{p}^2).$$

We see that for $\vec{p}^2 < k^2$ there is no momentum dependence in the propagator other than in the step function. Also, the scale k^2 screens these modes in a mass-like fashion. This will trivialize the integration in the flow equation (3.8), as the regulator insertion $\partial_t R$ acting as a UV cutoff, involves another step function of the form $\Theta(k^2 - \vec{p}^2)$. The fermionic propagator can be split up similarly, however both parts are still explicitly momentum dependent due to the Dirac structure

$$\vec{p}_r = \vec{p} + \left(\frac{\vec{p}}{|\vec{p}|}k - \vec{p}\right)\Theta(k^2 - \vec{p}^2) = \vec{p}\Theta(\vec{p}^2 - k^2) + \frac{\vec{p}}{|\vec{p}|}k\Theta(k^2 - \vec{p}^2),$$

hence

$$G_{\Psi\bar{\Psi}}(\vec{p}_r) = G_{\Psi\bar{\Psi}}(\vec{p})\Theta(\vec{p}^2 - k^2) + G_{\Psi\bar{\Psi}}\left(\frac{\vec{p}}{|\vec{p}|}k\right)\Theta(k^2 - \vec{p}^2). \quad (3.26)$$

Again, the regulator screens the modes for $\vec{p}^2 < k^2$. Since all flow equations are projected in a way, where all momentum structures are contracted ensuring Galilean invariance, the explicit momentum dependence will always drop out in the second term, while the first term will be vanishing again due to the $\partial_t R$ in the flow equation.

Curvature-, pole- and screening masses

As the name suggests, the curvature masses are defined by the curvature of the effective action in the ground state and with vanishing momenta. In general the curvature masses are given by a mass matrix M , which is given by the two-point function without the delta function.

$$M = \Gamma^{(2)}(\vec{p} = 0, p_4 = 0). \quad (3.27)$$

This matrix is in general non-diagonal, even within the blocks of the propagators in Eq. (3.22), in particular if there is a mixing of fields due to finite background fields. Moreover it depends on the representation, hence it is not a physical observable. Nevertheless the curvature masses can give us a feeling for the excitation gaps of the fields.

For the pole masses we have to go to Minkowski space, where we know that for a non-interacting field, the denominator of the propagator has the form $p_\mu p^\mu - m^2$, where the momentum squared is the off-shell energy of the propagating mode. If the off-shell energy coincides with the mass-shell the propagator diverges, as the virtual mode is then identical to the physical mode. In reality, the diverging behavior is turned into a broad resonance, which can be detected in experiments.

Thereby the mass and the decay constant of a particle can be found. Hence the pole mass is the true physical mass gap of the excitation.

Thus, in order to find the pole mass in our theory, we have to look for divergences in the fully dressed propagator where fluctuations are integrated out. The poles are given by the roots of the determinant of the inverse non-regularized propagator, i.e. the two point function. At finite temperature/chemical potential where Lorentz invariance is broken, the propagator can generally have a nontrivial and separate dependence on \vec{p} and p_4 , therefore we can define two kinds of masses either at vanishing momentum or vanishing frequencies, the latter is called *screening mass* [180]. We make an analytic continuation of the non-vanishing components, which yields the same solution as by going to Minkowski space, leading to

$$\det \Gamma^{(2)}(\vec{p}^2 = 0, p_4 = im_{\text{pol}}) = 0, \quad (3.28)$$

$$\det \Gamma^{(2)}(\vec{p}^2 = -m_{\text{scr}}, p_4 = 0) = 0. \quad (3.29)$$

The quantitative difference of all three kinds of masses has been studied in Ref. [180] for a quark-meson model in a fully momentum dependent scheme.

3.2.1 Bosons

Expansion points First we will derive the boson propagator and discuss the masses for the QMD-model of two-color QCD and then we will generalize it for the QMDB-model straightforwardly. We define the six-component boson field and its expansion point for the real and for the complex representation, where we leave the ρ 's as variables

$$\varphi = \begin{pmatrix} \vec{\pi} \\ \sigma \\ \Delta_1 \\ \Delta_2 \end{pmatrix}, \quad \varphi_0 = \begin{pmatrix} \vec{0} \\ \sqrt{2\rho_\phi/Z_\phi} \\ \sqrt{2\rho_\Delta/Z_\Delta} \\ 0 \end{pmatrix} \quad \text{and} \quad \bar{\varphi} = \begin{pmatrix} \vec{\pi} \\ \sigma \\ \Delta \\ \Delta^* \end{pmatrix}, \quad \bar{\varphi}_0 = \begin{pmatrix} \vec{0} \\ \sqrt{2\rho_\phi/Z_\phi} \\ \sqrt{\rho_\Delta/Z_\Delta} \\ \sqrt{\rho_\Delta/Z_\Delta} \end{pmatrix}. \quad (3.30)$$

The flow equation preserves the symmetries of the action, hence we can always rotate to any other choice of φ_0 and $\bar{\varphi}_0$ with the corresponding symmetry group, which, at finite chemical potential, is $O(4) \times O(2)$ for the real representation and $O(4) \times U(1)$ for the complex representation. Indeed, we will see that the flow equations will be functions of the ρ 's without any isolated square roots. Since the observable condensate is defined as $\langle |\Delta| \rangle$, which is always real, we can choose it to be in the real part of the diquark field, and our expansion point accordingly. Consequently there is a ρ_Δ in both diquark fields in the complex representation. The role of the Goldstone mode is then played by phase of the field. The expansion about the minimum then reads

$$\Delta(x) = [\langle |\Delta| \rangle + f(x)] e^{i \frac{\theta(x)}{\langle |\Delta| \rangle}} = \langle |\Delta| \rangle + f(x) + i\theta(x) + \dots, \quad (3.31)$$

where f and θ are real degrees of freedom, which essentially leads back again to real representation. However, since the propagator is diagonal in the complex representation in the normal phase, and moreover, the computation of fermionic self-energy type diagrams is more convenient as well, we will keep all in both representations.

Curvature masses The curvature matrix of the potential around the expansion point φ_0 and $\bar{\varphi}_0$ gives us the mass part of the of the inverse boson propagator

$$M_\varphi = \left. \frac{\partial^2 U(\rho_\phi, \rho_\Delta)}{\partial \varphi_i \partial \varphi_j} \right|_{\varphi_0} = \left. \frac{\partial}{\partial \varphi_i} \left(\frac{\partial \rho_l}{\partial \varphi_j} \frac{\partial U}{\partial \rho_l} \right) \right|_{\varphi_0} = \left. \frac{\partial^2 \rho_l}{\partial \varphi_j \partial \varphi_i} \frac{\partial U}{\partial \rho_l} + \frac{\partial \rho_n}{\partial \varphi_j} \frac{\partial \rho_l}{\partial \varphi_i} \frac{\partial^2 U}{\partial \rho_n \partial \rho_l} \right|_{\varphi_0} \quad (3.32)$$

$$= \begin{pmatrix} Z_\phi V_\phi \mathbb{1}_{3 \times 3} & 0 & 0 & 0 \\ 0 & Z_\phi (V_\phi + 2\rho_\phi V_{\phi\phi}) & 2V_{\phi\Delta} \sqrt{Z_\phi Z_\Delta \rho_\phi \rho_\Delta} & 0 \\ 0 & 2V_{\phi\Delta} \sqrt{Z_\phi Z_\Delta \rho_\phi \rho_\Delta} & Z_\Delta (V_\Delta + 2\rho_\Delta V_{\Delta\Delta} - 4\mu^2) & 0 \\ 0 & 0 & 0 & Z_\Delta (V_\Delta - 4\mu^2) \end{pmatrix},$$

and similarly

$$M_{\bar{\varphi}} = \begin{pmatrix} Z_\phi V_\phi \mathbb{1}_{3 \times 3} & 0 & 0 & 0 \\ 0 & Z_\phi (V_\phi + 2\rho_\phi V_{\phi\phi}) & V_{\phi\Delta} \sqrt{2Z_\phi Z_\Delta \rho_\phi \rho_\Delta} & V_{\phi\Delta} \sqrt{2Z_\phi Z_\Delta \rho_\phi \rho_\Delta} \\ 0 & V_{\phi\Delta} \sqrt{2Z_\phi Z_\Delta \rho_\phi \rho_\Delta} & Z_\Delta \rho_\Delta V_{\Delta\Delta} & Z_\Delta (V_\Delta + \rho_\Delta V_{\Delta\Delta} - 4\mu^2) \\ 0 & V_{\phi\Delta} \sqrt{2Z_\phi Z_\Delta \rho_\phi \rho_\Delta} & Z_\Delta (V_\Delta + \rho_\Delta - 4\mu^2) & Z_\Delta \rho_\Delta V_{\Delta\Delta} \end{pmatrix}.$$

The indices ϕ and Δ of V denote derivatives with respect to ρ_ϕ and ρ_Δ . Actually, one has to take functional derivatives of the potential term in the effective action, which leads to the same result, only with an overall Dirac delta function. To see this, we consider the functional derivative of the effective potential $\frac{\delta U(x)}{\delta \varphi(y)} = \frac{\partial U}{\partial \varphi} \delta(x-y)$. Hence, the first derivative trivializes the overall integral of the effective action, and the second one gives the above mentioned overall delta function. Since the flow equation is evaluated at constant fields, all implicit spacetime dependences are gone, so going to Fourier space will simply transform the delta function to one in momentum space.

Let us take a look at the masses by evaluating M_φ at the vacuum expectation values for the fields. In the normal phase it becomes diagonal with the elements

$$\begin{aligned} m_\pi^2 &= m_\phi^2, \\ m_\sigma^2 &= m_\phi^2 + 2\kappa_\phi \lambda_{2,0}, \\ m_{\Delta, \text{cur}}^2 &= m_\Delta^2 - 4\mu^2. \end{aligned} \quad (3.33)$$

These are all curvature masses of course, however, for the mesons they are identical to the pole masses in a momentum independent approximation. The curvature mass of the diquarks coincides in both representations and is equal for both real and imaginary excitations, as well as for particle and antiparticle excitations. The pions acquire a mass different from the sigma, if chiral symmetry is explicitly broken. In the chiral limit both masses coincide, unless chiral symmetry is broken spontaneously. Then the pions would be massless and the mass of the sigma would be proportional to the condensate. In the case of a 1d-potential where $m_\phi = m_\Delta$, it can be seen that the diquark mass is reduced by the chemical potential compared to the pion mass, with the consequence that if there is an occurrence of a condensate caused by spontaneous symmetry breaking at non-zero chemical potential, it has to be that of the diquark, since it is manifestly the lightest excitation. In any case, according to the Silver Blaze property the mesonic masses must not be affected by the chemical potential below μ_c , therefore the diquark is bound to condense if μ is large enough. In the BEC-regime the mass-matrix M_φ becomes non-diagonal in the σ, Δ -sector due to the mixing of the condensates in (3.32), therefore we should rather look at the poles of the propagator. Nevertheless we can already see at this point that the curvature mass of the imaginary diquark is vanishing $m_{\Delta_2, \text{cur}} = 0$, which can be considered as the true Goldstone mode of the breaking of the $O(2)$ symmetry.

Kinetic part For the kinetic part of the regularized propagator we first define the bosonic regulators in momentum space,

$$R_\varphi = \vec{p}^2 r_B(\vec{p}^2/k^2) \begin{pmatrix} Z_\phi \mathbb{1}_\phi & 0 \\ 0 & Z_\Delta \mathbb{1}_\Delta \end{pmatrix}, \quad R_{\bar{\varphi}} = \vec{p}^2 r_B(\vec{p}^2/k^2) \begin{pmatrix} Z_\phi \mathbb{1}_\phi & 0 \\ 0 & Z_\Delta \sigma_\Delta^1 \end{pmatrix},$$

where $\mathbb{1}_{\phi/\Delta}$ are unit matrices in meson/diquark space, whereas σ_Δ^1 contains ones in off-diagonals and zeros otherwise, like the Pauli matrix. In order to imply these regulators we use the regularized momentum \vec{p}_r as defined in the previous section. Now let us perform a Fourier transformation of the kinetic part of the diquark action for both representations

$$\begin{aligned} \Gamma[\Delta] |_{\text{kin}} &= \int_x Z_\Delta \left[(\partial_\mu \Delta^*)(\partial_\mu \Delta) + 2\mu (\Delta \partial_\tau \Delta^* - \Delta^* \partial_\tau \Delta) \right] \\ &= \int_p Z_\Delta \left[(\vec{p}^2 + p_4^2 + 4i\mu p_4) \Delta^*(-p) \Delta(p) \right] \\ &= \int_x Z_\Delta \left[\frac{(\partial_\mu \Delta_1)^2 + (\partial_\mu \Delta_2)^2}{2} + 2i\mu \left(\Delta_2 \frac{\partial \Delta_1}{\partial \tau} - \Delta_1 \frac{\partial \Delta_2}{\partial \tau} \right) \right] \\ &= \int_p Z_\Delta \left[\frac{\vec{p}^2 + p_4^2}{2} \{ \Delta_1(-p) \Delta_1(p) + \Delta_2(-p) \Delta_2(p) \} + 4\mu p_4 \Delta_2(-p) \Delta_1(p) \right]. \end{aligned} \quad (3.34)$$

The third line is meant to be resulting from the first one using Eq. (2.47). It is important to perform the Fourier transformation after the representation has been specified in order to introduce them as independent degrees of freedom. For the second line to be real-valued it must be $\Delta^*(-p) = [\Delta(p)]^*$, cf. Eq. (3.13) and the paragraph below. The chemical potential term becomes real after integration, since the integral over negative regime of p_4 is the complex conjugate to the integral over the positive regime. In both representations the mixing terms proportional to the chemical potential can be summarized by substituting the integration variable $p \rightarrow -p$. Similarly the kinetic part of the mesonic action reads

$$\Gamma[\phi] |_{\text{kin}} = \int_p \frac{Z_\phi}{2} (\vec{p}^2 + p_4^2) \phi(-p) \phi(p). \quad (3.35)$$

Then the kinetic part of the boson propagator is given by

$$\begin{aligned} P_\varphi &= \begin{pmatrix} Z_\phi (\vec{p}_r^2 + p_4^2) \mathbb{1}_\phi & 0 & 0 \\ 0 & Z_\Delta (\vec{p}_r^2 + p_4^2) & -4Z_\Delta \mu p_4 \\ 0 & 4Z_\Delta \mu p_4 & Z_\Delta (\vec{p}_r^2 + p_4^2) \end{pmatrix} \cong \frac{\vec{\delta}}{\delta \varphi^T(-p)} \Gamma[\varphi] \frac{\overleftarrow{\delta}}{\delta \varphi(q)} \Big|_{\varphi_0^{\text{kin}}} + R_\varphi \\ P_{\bar{\varphi}} &= \begin{pmatrix} Z_\phi (\vec{p}_r^2 + p_4^2) \mathbb{1}_\phi & 0 & 0 \\ 0 & 0 & Z_\Delta (\vec{p}_r^2 + p_4^2 - 4\mu p_4) \\ 0 & Z_\Delta (\vec{p}_r^2 + p_4^2 + 4\mu p_4) & 0 \end{pmatrix} \end{aligned}$$

In the upper line we have indicated the way it is derived, the tilde denotes that that a delta function was dropped. The derivative from the left-hand side determines the row index, while the right-hand side derivative determines the column index. The opposite signs in front of the time-like momentum can be understood from Eq. (3.17). The diagonal terms are doubled, since the derivative hits both fields, even if they have different arguments. We need to invert $G_\varphi^{-1} = P_\varphi + M_\varphi$ to find the propagator, which has the property

$$G_\varphi(p) = G_\varphi^T(-p) \quad \text{and similarly} \quad G_{\bar{\varphi}}(p) = G_{\bar{\varphi}}^T(-p) . \quad (3.36)$$

The explicit components of G_φ and $G_{\bar{\varphi}}$ can be found in App. B.1. The fact that some components of the propagator are proportional to the fields (which are in fact background fields) times the second derivative of the effective action, which in the ground state is a four-point coupling, leads to the interpretation that in Feynman diagrams the propagators are connected to the background field via a four-point vertex. This is illustrated in Fig. 3.5.

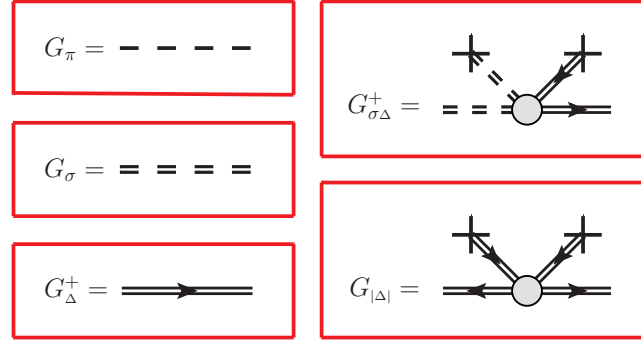


Figure 3.5: Diagrammatic representation of bosonic propagators in the ground state, shown for the complex representation. The sign in the superscript relates to the direction of the arrow, which indicates the flow of the charge. We have propagators representing a mixing of fields via the interaction with the background. The net flow of charge in $G_{|\Delta|}$ from the left to the right of the diagram is vanishing. Since G_σ and G_Δ^\pm receive contributions from the background as well, they can be split up into a disconnected and a connected part with the background. Nevertheless they always go together in flow equations, so we represent both parts with one line.

Finite temperature At finite temperature the time dimension is compactified on a torus with the circumference $1/T$ by making an analogy between statistical mechanics and quantum field theories in a Euclidean formulation [284, 285]. In this framework bosonic fields have to satisfy periodic boundary conditions, with the consequence that the Tr operator implies a summation over the bosonic Matsubara frequencies

$$p_4 \rightarrow \omega_n = 2n\pi T, \quad n \in \mathbb{Z}. \quad (3.37)$$

The temperature enters the bosonic propagator in a mass-like fashion. It follows that if the temperature is much larger than the energy scale, the propagator decouples from the system. In general $G_\varphi \propto T^{-2}$ for $T \gg E_{\varphi_i}$, where we are comparing to the bosonic dispersions. Only the zero mode of the Matsubara frequencies survives this limit, and is the only contribution left. All nonzero modes are gapped by the temperature. This mechanism effectively reduces the dimension of our bosonic system from 4d to 3d, as the p_4 integration breaks down and the only mode in the system has $p_4 = 0$.

Since the boson propagator is quite awkward due to the off diagonal terms, it is not wise to compute analytic expressions for p_4 -summation, if we employ a 3d optimized regulator function. If only a finite number of Matsubara frequencies is taken, the convergence must be checked at low temperatures. At $T = 0$ it is recommended to incorporate a numerical integration with respect to p_4 in the solver. However, it simplifies considerably for $\rho_\Delta \rightarrow 0$, which we can do in the normal phase if we assume unique coupling parameters for the mesonic and diquark sector in the effective potential as in (2.50), see Sec. 3.4.3.

Pole masses Now let us consider the pole masses. They are defined by the solution of $\det G_\varphi^{-1}(\vec{p} = 0, p_4 = im) = 0$ for m , where the propagator diverges. The pole masses are unique, and therefore equal in both representation, which is easy to see with the properties of the determinant and the unitarity of transformations between representations:

$$\det G_\varphi^{-1} = \det U^\dagger G_\varphi^{-1} U = |\det U|^2 \det G_\varphi^{-1} = \det G_\varphi^{-1}. \quad (3.38)$$

As we have mentioned above, the curvature masses of the mesons in Eq. (3.33) are identical to the pole masses in the normal phase. For the diquarks we find $m_{\Delta, \text{pol}, \pm} = m_\Delta \pm 2\mu$. In the BEC phase we have the condition that $m_\Delta = 2\mu$, see (2.58). Thus we find the following pole masses

$$\begin{aligned} m_\pi &= m_\phi, \\ m_{\tilde{\sigma}} &= \sqrt{m_1^2 - m_2^2}, \\ m_{\tilde{\Delta}_1} &= \sqrt{m_1^2 + m_2^2}, \\ m_{\Delta_2} &= 0, \end{aligned} \quad (3.39)$$

with

$$\begin{aligned} m_1^2 &= \frac{m_{\sigma, \text{nor}}^2}{2} + 8\mu^2 + \kappa_\Delta \lambda_{0,2}, \\ m_2^2 &= \sqrt{m_1^4 - 2\kappa_\Delta \left(m_{\sigma, \text{nor}}^2 \lambda_{0,2} - 2\kappa_\phi \lambda_{1,1}^2 \right) - 16m_{\sigma, \text{nor}}^2 \mu^2}, \end{aligned}$$

where $m_{\sigma, \text{nor}}$ is the expression for the sigma mass in the normal phase, given in Eq. (3.33). As indicated the mass eigenstates are different than in the normal phase due to the off-diagonal terms in the propagator. The sigma and one of the diquark states are mixtures of the original states. If the mixing term vanishes ($\lambda_{1,1} = 0$ or $\kappa_\phi = 0$) then the sigma state is the same as in the normal phase, while $m_{\tilde{\Delta}_1}^2 = 4\mu^2 + 2\kappa_\Delta \lambda_{0,2}$. The Δ_2 is immediately identified with Goldstone mode associated with the breaking of $U(1)_B$. In the case of a 1d-potential where $m_\phi = m_\Delta$, we have $V'_{\text{bec}} = 4\mu^2$ and hence a pion mass proportional to the chemical potential, $m_\pi = 2\mu$. This result coincides with leading order chiral perturbation theory [199, 200], and is also in agreement with fact that the pions are pseudo-Goldstone modes associated with the breaking of the enlarged flavor symmetry by a finite chemical potential, as discussed in Sec. 2.2.4. Therefore we can expect that m_ϕ in the 2d-potential ansatz is also proportional to μ in the BEC phase. Within our best truncation we find a proportionality as $m_\pi \approx 2.52\mu$. The difference mainly comes about from the running wave function renormalization.

In Fig. 3.6 we see the temperature and chemical potential dependence of the masses. At $\mu = 0$ the pion and diquark are degenerate. At large temperatures, where chiral symmetry is restored, they join with the sigma mass and all bound states decouple from the system. As the temperature sets a scale in the system, the behavior is very similar as the RG-scale dependence. Along the μ -axis we first see the split of particles and antiparticles. At $\mu = \frac{m_\pi}{2}$ the diquark starts condensing and the behavior of the masses changes accordingly. Due to the coupling to a chemical potential the radial mode does not vanish at the phase transition. At large μ chiral symmetry is restoring and $m_{\tilde{\sigma}} \rightarrow m_\phi$, then the sigma is of course degenerate with the pions. Note the mixing terms between the sigma and diquark are crucial for the connection of mass states between the phases as we have it here. In a simple linear sigma model [233] or NJL analysis [212] the mass of the sigma continues as $m_{\tilde{\Delta}_1}$ in the BEC phase, while the diquark becomes the $m_{\tilde{\sigma}}$.

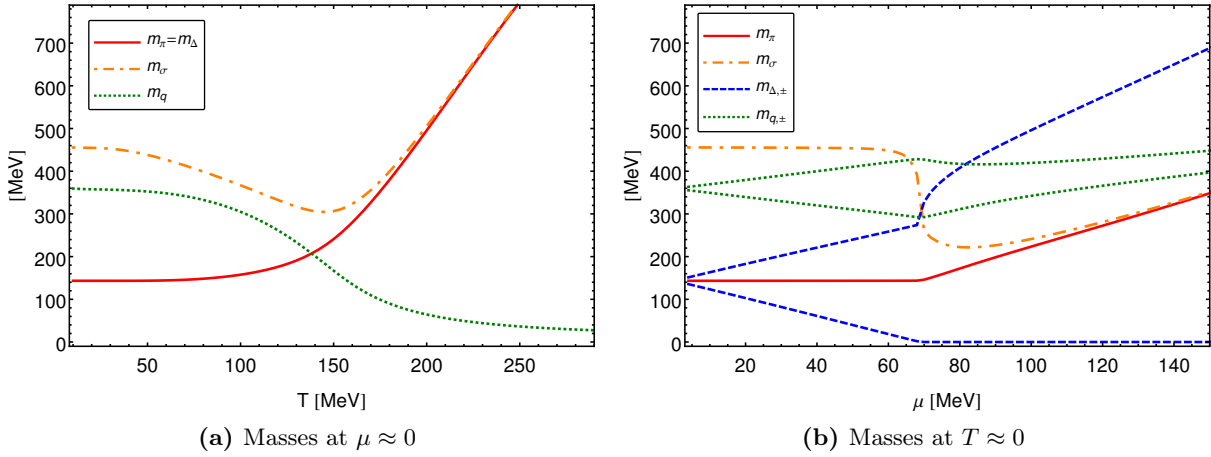


Figure 3.6: Mass spectrum of two-color QCD with the 2d Taylor' truncation, c.f Tab. 4.1. The chiral crossover and the phase transition to the BEC phase are clearly visible from the behavior of the masses. In (a) the quark mass goes from being small to being large with decreasing temperature, while the pions and diquarks become the pseudo-Goldstone modes splitting up from the sigma. Note in particular the minimum of the sigma mass in the middle of the crossover, which justifies the definition of the phase boundary (2.43). In (b) we have a phase transition at $\mu = \frac{m_\pi}{2}$. Note also here that there is a minimum in the sigma mass. Even though chiral symmetry is restored at asymptotic μ , the quarks do not become massless because they are coupled to the diquark condensate.

Extension for the QMDB-model In the QMDB-model the diquark is a color anti-triplet therefore the boson field contains a anti-/diquark pair for each color. In the complex representation it is given by

$$\bar{\varphi} = \left(\vec{\pi}, \sigma, \Delta^b, \Delta^{*b}, \Delta^r, \Delta^{*r}, \Delta^g, \Delta^{*g} \right)^T, \quad (3.40)$$

$$\bar{\varphi}_0 = \left(\bar{\varphi}_{0, QC_2D}, 0, 0, 0, 0 \right)^T. \quad (3.41)$$

The blue diquark basically plays the same role as the diquark in two-color QCD, namely it forms a condensate. This is again an arbitrary choice. Any other choice can be rotated back to this one by performing an $SU(3)_C$ transformation on the diquark color anti-triplet and a $U(1)_B$ transformation between particles and antiparticles. These transformations leave the flow invariant, since flow equations preserve the symmetries of the theory. It follows for the boson propagator that it is given by a part which is equal to the one in QC₂D and the enhancement for the red and green diquarks

$$G_{\bar{\varphi}} = \begin{pmatrix} G_{\bar{\varphi}, QC_2D} & 0 & 0 \\ 0 & G_{\Delta^r} & 0 \\ 0 & 0 & G_{\Delta^g} \end{pmatrix}. \quad (3.42)$$

Since we choose the diquark background field to be blue, the red and green parts are not involved in any mixing and therefore trivial

$$G_{\Delta^r} = G_{\Delta^g} = \frac{1}{Z_\Delta} \begin{pmatrix} 0 & \vec{p}_r^2 + (p_4 - 2\mu)^2 + V_\Delta \\ \vec{p}_r^2 + (p_4 + 2\mu)^2 + V_\Delta & 0 \end{pmatrix}^{-1}. \quad (3.43)$$

The above discussion of the masses in the normal phase applies here accordingly.

2SC phase As we have discussed in Sec. 2.2.3 the Goldstone modes associated with the breaking of color symmetry are absorbed by the gluons via a gauge transformation. For us this means that we simply have to get rid of them. Hence we apply a rotation not only in for the ground state but also for the excitations. Five modes corresponding to the red and green anti-/diquarks and one imaginary part of the blue diquark are gauged away. Note however that the masses of the red and green antidiquarks are not vanishing but rather given by 4μ , they are the type II Goldstone modes according to the Nielsen-Chadha theorem [305] for broken Lorentz symmetry. After the rotation has been carried out, our boson fields are given by

$$\varphi = \left(\vec{\pi}, \sigma, \Delta_1^b \right)^T, \quad (3.44)$$

$$\varphi_0 = \left(\vec{0}, \sqrt{2\rho_\phi/Z_\phi}, \sqrt{2\rho_\Delta/Z_\Delta} \right)^T. \quad (3.45)$$

We could have just as well put zeros for the left out fields. For the QMDB-model in the normal phase we will only use the complex representation, while in the color superconducting phase we use the real representation. The propagator reduces to

$$G_\varphi = \begin{pmatrix} Z_\phi (\vec{p}_r^2 + p_4^2 + V_\phi) \mathbb{1}_{3 \times 3} & 0 & 0 \\ 0 & Z_\phi (\vec{p}_r^2 + p_4^2 + V_\phi + 2\rho_\phi V_{\phi\phi}) & 2V_{\phi\Delta} \sqrt{Z_\phi Z_\Delta \rho_\phi \rho_\Delta} \\ 0 & 2V_{\phi\Delta} \sqrt{Z_\phi Z_\Delta \rho_\phi \rho_\Delta} & Z_\Delta (\vec{p}_r^2 + p_4^2 + V_\Delta + 2\rho_\Delta V_{\Delta\Delta} - 4\mu^2) \end{pmatrix}^{-1} \quad (3.46)$$

The inverted matrix can be found in App. B.1. The mass eigenstates it could be reckoned that on could still take Eqs. (3.39) and drop the Goldstone mode m_{Δ_2} as well as the μ -terms arising from the mixing with Δ_2 . This is almost true, except that the composition of the radial modes is opposite, in the sense that the sign are interchanged:

$$m_\pi = m_\phi, \quad m_{\tilde{\sigma}} = \sqrt{m_1^2 + m_2^2}, \quad m_{\tilde{\Delta}_1} = \sqrt{m_1^2 - m_2^2}, \quad (3.47)$$

now with

$$m_1^2 = \frac{m_{\sigma, \text{nor}}^2}{2} + \kappa_\Delta \lambda_{0,2}, \quad m_2^2 = \sqrt{m_1^4 - 2\kappa_\Delta \left(m_{\sigma, \text{nor}}^2 \lambda_{0,2} - 2\kappa_\phi \lambda_{1,1}^2 \right)}.$$

Indeed, it has turned out that this is the correct interpretation of the modes with the proper limiting cases, as it can be seen in Fig. 3.7. Again, we have the restoration of chiral symmetry at large temperatures and chemical potentials, where the sigma and pions become degenerate, while in the broken phase they are split up. Although the diquark sector is not directly associated with the chiral symmetry breaking at $\mu = 0$, it receives quantitative corrections due to the change of the dynamics in the remaining sectors. At $T = 0$ we have a violation of the Silver Blaze property, which will be discussed later. In consequence the diquark mass parameter does not remain constant and thus $m_{\Delta, \pm}$ is not axisymmetric. When the diquark condensation sets in, the Goldstone modes are removed, two of which would have had a finite mass of 4μ and would have been connected with the upper dashed curve. Instead we only have a radial mode, which behaves in typical way for a second order phase transition, as its mass vanishes at the phase transition. the sigma mass has a nontrivial behavior immediately after the phase transition, which is coming from the coupling $\lambda_{2,0}$.

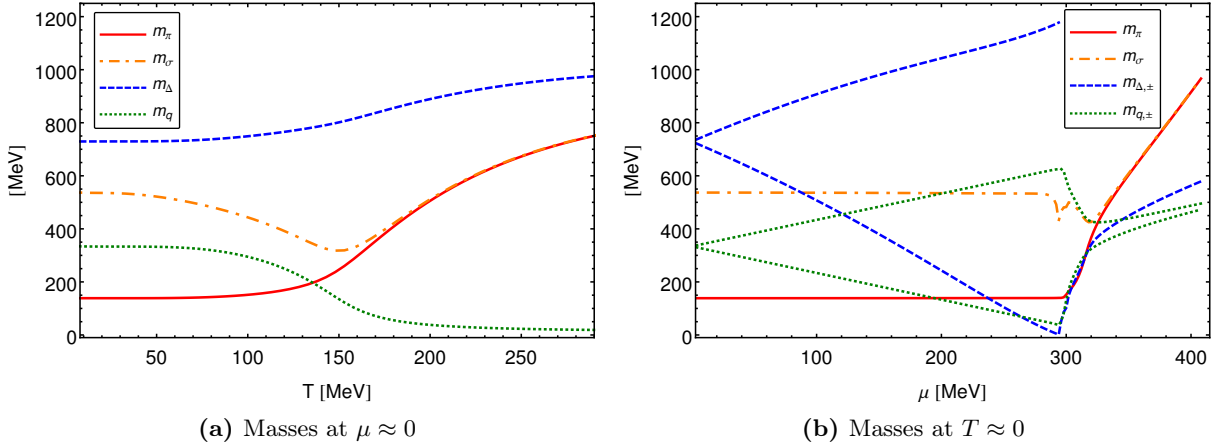


Figure 3.7: Mass spectrum of QCD with the initial conditions from Tab. 4.2.

3.2.2 Fermions

Nambu-Gorkov formalism In a theory with diquarks it is convenient to apply the Nambu-Gorkov formalism, where the quark fields are represented by the bispinors in color space

$$\Psi = \begin{pmatrix} q_r \\ \tau_2 C \bar{q}_g^T \end{pmatrix}, \quad \bar{\Psi} = \begin{pmatrix} \bar{q}_r \\ q_g^T C \tau_2 \end{pmatrix}, \quad (3.48)$$

where the indices r and g denote the color components of the quark spinor. In the convention we apply here, the Nambu-Gorkov space constitutes a color-anticolor space. We rewrite the quark part of the effective action as

$$\Gamma_{\text{quark}} = \int_x \bar{\Psi}(x) S(i\partial) \Psi(x) \quad (3.49)$$

with

$$S(i\partial) = Z_q \begin{pmatrix} i\not{\partial} + i\gamma_4\mu + i\sqrt{Z_\phi}h_\phi(\sigma + i\gamma_5\vec{\tau} \cdot \vec{\pi}) & -\sqrt{2Z_\Delta}h_\Delta\Delta\gamma_5 \\ -\sqrt{2Z_\Delta}h_\Delta\Delta^*\gamma_5 & i\not{\partial} - i\gamma_4\mu + i\sqrt{Z_\phi}h_\phi(\sigma - i\gamma_5\vec{\tau} \cdot \vec{\pi}) \end{pmatrix} \quad (3.50)$$

In App. B.2 it is shown that Eq. (3.49) agrees with the quark part of the QMD action (2.35). Note that S is technically neither two-point function, as it contains only one set of spacetime coordinates (in the arguments of the fields, which is omitted), nor does it correspond to the fermionic part in Eq. (3.19) in a direct way, since S contains fluctuating fields. The cutoff function for fermions has to meet the requirement of being consistent with chiral symmetries, hence it must have the same Lorentz structure as the kinetic term. The 3d fermionic regulator in the Nambu-Gorkov formalism reads

$$R_{\bar{\Psi}\Psi}(\vec{p}) = Z_q \begin{pmatrix} \vec{p} \cdot \vec{r}_F(\vec{p}^2/k^2) & 0 \\ 0 & \vec{p} \cdot \vec{r}_F(\vec{p}^2/k^2) \end{pmatrix}. \quad (3.51)$$

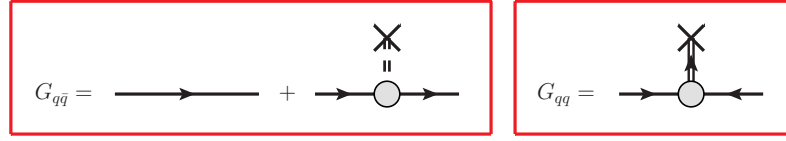


Figure 3.8: Diagrammatic representation of the quark propagators. Due to the substructure in Dirac space, only one of these contributions will be projected out in each part of the flow equations.

The propagator Going to momentum space, the spacetime derivative ∂ in Eq. (3.50) will simply be replaced by the four-momentum $-ip'$ coming from $\Psi(x) = \int_{p'} e^{-ip'x} \Psi(p')$ following that $S(i\partial) \rightarrow S(p')$. For simplicity one can already set the bosonic fields to the expansion points, such that they can be treated as constants. Then, taking the functional derivative with respect to $\bar{\Psi}(-p)$ from the left and with respect to $\Psi(q)$ from the right as in Eq. (3.15), dropping the delta function and adding the regulator $R_{\bar{\Psi}\Psi}$, in fact simply following the prescription described in the beginning of Sec. 3.2, defines our inverse fermion propagator:

$$\begin{aligned} G_{\Psi\bar{\Psi}}^{-1}(p) &= Z_q \begin{pmatrix} \vec{p}_r + \gamma_4(p_4 + i\mu) + i\hat{\sigma} & -\hat{\Delta}\gamma_5 \\ -\hat{\Delta}\gamma_5 & \vec{p}_r + \gamma_4(p_4 - i\mu) + i\hat{\sigma} \end{pmatrix} \equiv Z_q \begin{pmatrix} [G_0^+]^{-1} & \Delta_0 \\ \Delta_0 & [G_0^-]^{-1} \end{pmatrix} \\ &= -[G_{\bar{\Psi}\Psi}^{-1}(-p)]^T. \end{aligned} \quad (3.52)$$

The second line can again be understood from Eq. (3.17), and considering that the fermionic part in the full propagator (3.22) is entirely off-diagonal. Since inverting and transposing a matrix are commuting operations, the above relation holds for the propagator as well, $G_{\Psi\bar{\Psi}}(p) = G_{\bar{\Psi}\Psi}^T(-p)$. Naturally, a similar relation holds for the regulator. For reasons of clarity we have defined

$$\hat{\Delta} = \sqrt{2Z_\Delta} h_\Delta \Delta = \sqrt{Z_\Delta} h_\Delta \Delta_1, \quad \hat{\sigma} = \sqrt{Z_\phi} h_\phi \sigma. \quad (3.53)$$

These are the gaps of fermionic excitations. σ and Δ (Δ_1) correspond to the components of the expansion point $\bar{\varphi}_0$ (φ_0) in Eq. (3.30) and later to the condensates. A finite diquark condensate introduces a mixing of red and green colored quarks. Moreover, like in the bosonic case, the propagator is connected to these background fields. As it is shown in Fig. 3.8, the diagonal entries can be split into a disconnected part and a part connected to the mesonic background field, while the off-diagonal components are entirely proportional to the diquark fields. Although the propagator has linear terms in the bosonic fields, the flow equations will be functions of their squares, such that they can be rewritten in terms of the invariant ρ 's. The definition of the regularized momentum \vec{p}_r is given in Eq. (3.23). Note that if there is no tensor structure regarding a particular space (colour/flavour/spinor space), an identity matrix with respect to that specific space is implied. We choose the diquark condensate to be on the real axis, so we can suppress complex conjugations.

The explicit expression of the fermion propagator can be found in App. B.2. Evidently it is quite awkward if off-diagonal terms are non-zero, which is the case in the BEC phase. It reduces to a much handier form for $\Delta = 0$ as well as for $\mu = 0$. For $\Delta = 0$ the propagator simply becomes block diagonal with G_0^\pm for the blocks, which is given by

$$G_0^\pm = \frac{1}{\vec{p}_r + i\hat{\sigma} + \gamma_4(p_4 \pm i\mu)} = \frac{\vec{p}_r - i\hat{\sigma} + \gamma_4(p_4 \pm i\mu)}{\vec{p}_r^2 + \hat{\sigma}^2 + (p_4 \pm i\mu)^2}. \quad (3.54)$$

Finite temperature Let us make some remarks regarding finite temperature calculations. If a loop contains purely fermionic propagators, the Tr operator implies antiperiodic boundary conditions for the fermions [284, 285], hence a summation over fermionic Matsubara frequencies

$$p_4 \rightarrow \nu_n = (2n + 1) \pi T, \quad n \in \mathbb{Z}. \quad (3.55)$$

On the other hand, if a diagram has external fermionic legs, the external momentum has the above Matsubara frequency for the time-like component, which can be carried on by any propagator, that is connected to the vertex. Typically, in such a case, the leg is connected to a fermionic and bosonic propagator. The loop momentum is unique for both types of propagators, but the fermionic shift of the Matsubara frequency is externally introduced. If the external fermionic Matsubara frequency is then carried on by a boson, we can simply shift the integration variable such that the fermion takes it over. This can always be achieved, hence, we employ the convention in this work, that the functions occurring from the fermionic propagator defined in App. B.2 always carry Eq. (3.55) for the time-like component of the momentum. Similar to the bosonic case, higher modes decouple from the system with increasing temperature. However, the lowest mode is nonzero and still proportional to the temperature, hence in the $T \rightarrow \infty$ limit fermions decouple completely from the system, instead of only being dimensionally reduced.

Pole masses The pole masses for quarks and antiquarks plotted in Fig. 3.6 are given by

$$m_{q,\pm} = \sqrt{(\hat{\sigma} \pm \mu)^2 + \hat{\Delta}^2}. \quad (3.56)$$

They rise from their current mass value to their constituent mass value towards low temperatures or low energy scales. When chiral symmetry is restored at large μ the above expression goes to $\sqrt{\mu^2 + \hat{\Delta}^2}$. However, by looking at the energy dispersions in Sec. 3.4.1 we will see that this is not the minimal energy of quark excitations. In the BSC limit at large chemical potentials $\hat{\Delta}^2$ is the only gap that has to be overcome for thermal quark excitations. The quantum fluctuations are in a different situation, which will be discussed in the same section.

Extension for the QMDB-model In the QMDB-model we choose the same Nambu-Gorkov representation as above, extended by the blue quark and the baryon fields

$$\Psi = \begin{pmatrix} q_r \\ \tau_2 C \bar{q}_g^T \\ q_b \\ B \end{pmatrix}, \quad \bar{\Psi} = \begin{pmatrix} \bar{q}_r \\ q_g^T C \tau_2 \\ \bar{q}_b \\ \bar{B} \end{pmatrix}. \quad (3.57)$$

With this definition all fermionic parts of the action can be rewritten as

$$\Gamma_{\text{fermion}} = \int_x \left(\bar{\Psi} S \Psi + \frac{1}{2} \Delta^{*g} \Psi^T \Sigma \Psi - \frac{1}{2} \Delta^g \bar{\Psi} \Sigma \bar{\Psi}^T \right) \quad (3.58)$$

with

$$S = \begin{pmatrix} S_{rg} & \Delta^{r*} \Xi^T \\ \Delta^{r\Xi} & S_{bB} \end{pmatrix}, \quad \Sigma = \tau_2 C \begin{pmatrix} 0 & -\bar{\Xi} \\ \bar{\Xi} & 0 \end{pmatrix}, \quad (3.59)$$

where we split between the rg -space and the bB -space. Naturally Σ is antisymmetric, as it is situated between two (anti-)particle spinors. There is factor of $1/2$ since all terms emerge twice. Ξ and $\bar{\Xi}$, which are given in App. B.2, contain quark-diquark and qdb -couplings. In the BEC phase where the Goldstone modes are gauged away, Only the first term in (3.58) survives with a block diagonal S . The upper right is $S_{rg} = S_{QC_2D}(\Delta = \Delta^b)$, which is essentially the same as in the QMD-model given by Eq. (3.50), with colorless diquark field replaced by the blue diquark, i.e. the one that condenses. The bB -part is given by

$$S_{bB} = \begin{pmatrix} Z_q i \left[\not{\partial} + \gamma_4 \mu + \sqrt{Z_\phi} h_\phi (\sigma + i\gamma_5 \vec{\tau} \cdot \vec{\pi}) \right] & \sqrt{Z_B Z_\Delta Z_q} i h_{qdB} \Delta^{*b} \\ \sqrt{Z_B Z_\Delta Z_q} i h_{qdB} \Delta^b & Z_B i \left[z_B (\not{\partial} + \gamma_4 \mu_B) + \sqrt{Z_\phi} h_B (\sigma + i\gamma_5 \vec{\tau} \cdot \vec{\pi}) \right] \end{pmatrix}.$$

Note that the convention of the Nambu-Gorkov spinors we are applying here, has the advantage that there is no double counting like in the usual convention. On the other hand, we have disadvantage that we cannot write all terms of the action in one matrix sandwiched by a spinor and anti-spinor, but rather we must write additional terms as we have done in Eq. (3.58), which are important in order to obtain all vertices in this representation.

Extended components of the propagator At the expansion point where $\Delta^r = \Delta^g = 0$, we get a rather simple and block diagonal form for the propagator

$$G_{\Psi\bar{\Psi}} = \begin{pmatrix} G_{rg} & 0 \\ 0 & G_{bB} \end{pmatrix}, \quad (3.60)$$

where the rg -part naturally coincides with two-color QCD case, $G_{rg} = G_{\Psi\bar{\Psi}, QC_2D}$. Now we see the advantage of our choice of the Nambu-Gorkov representation. If we simply doubled the fermion space, we would have obtained a much more complicated substructure in color space. The fermionic regulator (3.51) must simply be extended with two additional dimensions in Nambu-Gorkov space, where the baryonic wave function renormalization must be placed in lower right. We do not take the exact form of the kinetic term for the baryonic regulator, but rather we leave out the z_B for reasons which will become clear below. Furthermore, since we have a 3d-regulator, in order to avoid nontrivial momentum integrations, we replace in momentum space

$$z_B(\tilde{p}^2)\tilde{p}_\mu \rightarrow \left(z_B(\tilde{p}^2)\vec{p}, p_4 + i\mu_B \right) \quad (3.61)$$

The left hand side was introduced in Eq. (2.37). Obviously this breaks Lorentz invariance, but make this approximation for the sake of simplicity nonetheless. Besides, according to Eq. (2.38) the UV-mass gap is supposed to vanish in the ground state of the vacuum, which means $z_B = 1$ and the restoration of Lorentz invariance, at least for this case. At finite temperature and density Lorentz symmetry is broken anyway. Thus, the bB -part of the propagator is given by

$$G_{bB}(p) = \begin{pmatrix} Z_q [\vec{p}_r + \gamma_4(p_4 + i\mu) + i\hat{\sigma}] & \sqrt{Z_B Z_q} i \hat{\Delta}_B \\ \sqrt{Z_B Z_q} i \hat{\Delta}_B & Z_B [\vec{p}_{r,B} + \gamma_4(p_4 + i\mu_B) + i\hat{\sigma}_B] \end{pmatrix}^{-1}, \quad (3.62)$$

with

$$\hat{\sigma}_B = \sqrt{Z_\phi} h_B \sigma, \quad \hat{\Delta}_B = \sqrt{Z_\Delta} h_{qdB} \Delta, \quad \vec{p}_{r,B} = \vec{p}(z_B + r_F). \quad (3.63)$$

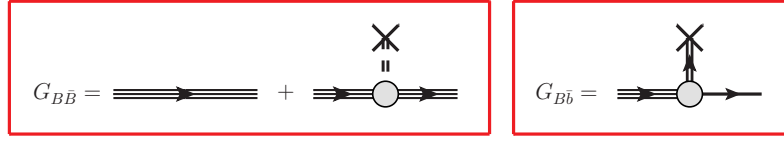


Figure 3.9: Diagrammatic representation of the baryon propagators. Schematically, $G_{b\bar{b}}$ has the same structure as $G_{q\bar{q}}$ in Fig. 3.8, however it is given by a different function, see App. B.2.

This way we find for $\vec{p}^2 < k^2$ that $\vec{p}_{r,B} = z_B(k^2) \frac{\vec{p}}{|\vec{p}|} k$. If the kinetic term was $z_B(\vec{p}^2) \vec{p}_r$, we could obviously not split the propagator as in Eq. (3.26), which would lead to a nontrivial momentum integration in flow equations. Similar is the case without the replacement (3.61). The explicit expression of this propagator can be found in App. B.2. Note that the blue quark as well as the baryon fields have a degeneracy in flavor space, and therefore there is a trivial structure in the propagator with respect to that space. Due to the quark-diquark-baryon interaction we have a mixing of the blue quark with the baryon field leading to a gap. This gap may have perceivable impact on the dynamics in the 2SC phase as compared to models where baryon fields B are neglected and the blue quark is almost gapless, since chiral symmetry is expected to be restored at large chemical potentials. In Fig. 3.9 we see the diagrammatic representation of the baryon propagators. For $\Delta = 0$ all three quarks are degenerate and we have simple and independent propagators like in Eq. (3.54). The baryon field has a similar one where $\hat{\sigma} \rightarrow \hat{\sigma}_B$. The expressions for the pole masses in the BEC phase is rather lengthy; in the normal phase the baryon mass is given by

$$m_{B,\pm} = \sqrt{\hat{\sigma}_B^2 + (m_B^{\text{uv}})^2} \pm \mu_B \quad (3.64)$$

3.3 The Silver Blaze Property

Before we turn to the computation of specific flow equations for our model, let us discuss an important feature of finite density field theories known as the *Silver Blaze property*. It was first derived in [354, 354] for QCD in the presence of a finite baryon/isospin chemical potential, where it was shown that the partition function is independent of respective chemical potential at vanishing temperatures up to a critical μ_c , which is given by the lowest excitation sensitive to the chemical potential. In Ref. [355] the property is shown for the effective action of a complex scalar theory and the corresponding vertex functions. Following this example we will recapitulate the property for the case of arbitrary fields and then consider its implications on our FRG study.

3.3.1 Derivation of the Property

In the presence of a baryon chemical potential, the property is a direct consequence of the baryon number symmetry $U_B(1)$, which can be promoted to a local gauge symmetry in the Euclidean formulation as

$$\Phi \rightarrow e^{i\alpha(\tau)Q}\Phi, \quad \mu \rightarrow \mu - i\partial_\tau\alpha(\tau), \quad (3.65)$$

where Φ is a general multicomponent field and Q is the charge operator. For the case of two color QCD these are given by $\Phi = (\phi, \Delta, \Delta^*, q, \bar{q})$ and $Q = \text{diag}(0, 2, -2, 1, -2)$. Hence the transformations (3.65) leave of effective action (2.35) invariant. At finite temperature periodic

boundary conditions for boson and antiperiodic ones fermions must be retained, therefore the gauge function must be turned into a matrix with bosonic and fermionic parts containing the respective Matsubara frequencies $\alpha(\tau) \rightarrow \alpha\tau = \text{diag}(\omega_n\tau \mathbb{1}_B, \nu_n\tau \mathbb{1}_F)$, and the chemical potential turns into a matrix as well $\mu \rightarrow \mu \text{diag}(\mathbb{1}_B, \mathbb{1}_F)$, such that the symmetry under (3.65) holds true. The frequencies are defined in Sec. 3.2. Adapting the notation of Ref. [355] we now denote the chemical potential dependence of the effective action as an index in order to illustrate the invariance of the effective action by the identity

$$\Gamma_\mu[\Phi] = \Gamma_{\mu-i\alpha}[e^{i\alpha\tau Q}\Phi]. \quad (3.66)$$

For simplicity and in order to respect the finite temperature case, we employed a linear gauge function. Now, let us generalize this for vertex functions by taking an arbitrary number functional derivatives of the above equation and evaluating at an expansion point Φ_0 where all charged fields are vanishing

$$\left. \frac{\delta^n \Gamma_\mu}{\delta \Phi_{i_1}(x_1) \dots \delta \Phi_{i_n}(x_n)} \right|_{\Phi_0} = \left. \frac{\delta^n \Gamma_{\mu-i\alpha}}{\delta \Phi_{i_1}(x_1) \dots \delta \Phi_{i_n}(x_n)} \right|_{\Phi_0} e^{i\alpha(c_{i_1}\tau_1 + \dots + c_{i_n}\tau_n)}, \quad (3.67)$$

where c_{i_n} is the charge of the field Φ_{i_n} . Note that since all charged fields are set to zero there are no remaining exponentials of the gauge function in the vertex function. Now, if the effective action is analytic for $\mu < \mu_c$, we can make a unique analytic continuation from $i\alpha$ to z for $\mu - z < \mu_c$ only at $T = 0$, while the continuation from $i\omega_n$ or $i\nu_n$ is not unique. Then by setting $z = \mu$ in Eq. (3.67) we find

$$\Gamma_\mu^{i_1 \dots i_n}(x_1, \dots, x_n) = \Gamma_0^{i_1 \dots i_n}(x_1, \dots, x_n) e^{\mu(c_{i_1}\tau_1 + \dots + c_{i_n}\tau_n)} \quad (3.68)$$

where the superscripts represent the derivatives in the previous equation. This has the remarkable implication that the μ -dependence of the vertex functions is trivially given by appropriate phase multiplications. Consequently in momentum space we have the following relation

$$\Gamma_\mu^{i_1 \dots i_n}(p_1, \dots, p_n) = \Gamma_0^{i_1 \dots i_n} \left((\vec{p}_1, p_{1,4} + ic_{i_1}\mu), \dots, (\vec{p}_n, p_{n,4} + ic_{i_n}\mu) \right). \quad (3.69)$$

The second index of the momentum is a Lorentz index. We conclude that the vertex functions in momentum space for vanishing baryonic fields at $T = 0$ and $\mu < \mu_c$ can be obtained from the ones at $\mu = 0$ by shifting the frequency modes like $p_4 \rightarrow p_4 + ic_i\mu$ with the respective charges. Of course this holds trivially for the kinetic term in the two-point function, however generically all parameters in the effective action are momentum dependent, we will discuss this in the context of the FRG. Naturally the above relation is valid for the zeroth derivative as well

$$\Gamma_\mu[\Phi_0] = \Gamma_0[\Phi_0], \quad \Phi_0 = (\Phi_{0,\text{neutral}}, \Phi_{0,\text{charged}} = 0) \quad (3.70)$$

meaning that the quantum effective action of the sector which is not charged with respect to the chemical potential, is constant below μ_c . This holds by default for all their pure vertex functions as well. We emphasize that Eq. (3.69) is only valid for the expansion point Φ_0 , as defined here, since it was a necessary condition for the derivation. We remark that, although the vertex functions in Eq. (3.69) become manifestly complex at finite μ , the effective action is remains real-valued by virtue of the p_4 -integration, even if the couplings do not.

3.3.2 Silver Blaze & FRG

Let us consider the previous results in the context of an FRG framework. At first glance it might seem contradicting that the baryonic sector changes with the chemical potential, while the mesonic one does not, since they are coupled to each other. Naturally baryonic loops in the flow equation contribute to the flow in the meson sector, however the contour in of the p_4 -integration can be deformed to $ic_i\mu + \mathbb{R}$ as long as the integrand is analytic, such that the chemical potential drops out, provided that the momentum structure of the baryonic propagators is correctly resolved. Hence Eq. (3.70) is not violated by the flow equation. This can be proven for the n-point functions as well, by differentiating both sides of Eq. (3.69) with respect to the RG-scale and plugging in the respective flow equations. The flow of an n-point function can be found by differentiating the right-hand side of Eq. (3.8) with respect to fields corresponding to the superscripts in Eq. (3.69). We will show it for the example of the two-point function. For the proof we are going to adapt the notation $\tilde{p}_j = (\vec{p}_j, p_{4,j} + ic_{ij}\mu)$ for external momenta and $\tilde{q}_a = (\vec{q}_a, q_{4,a} + ic_a\mu)$ for the loop momenta. The right-hand side is given by

$$\partial_k \Gamma_0^{i_1 i_2}(\tilde{p}_1, \tilde{p}_2) = \frac{1}{2} \int_{q_a \dots q_d} G_0^{ab}(q_a, q_b) \Gamma_0^{b i_1 i_2 c}(q_b, \tilde{p}_1, \tilde{p}_2, q_c) G_0^{cd}(q_c, q_d) \partial_k R^{da}(q_d, q_a) \quad (3.71)$$

where $a \hat{=} \Phi_a(q_a)$ and so on in the superscripts represent the components in field space which are summer over. The trace operation is made explicit in all discrete and continuous indices. For simplicity we are just pointing out a tadpole diagram, however the arguments can be applied to any diagram emerging from the flow equation of any n-point function. Note that the regularized propagator $G = (\Gamma^{(2)} + R)^{-1}$ has the Silver Blaze property only if regulator obeys $R_\mu^{ab}(q_a, q_b) = R_0^{ab}(\tilde{q}_a, \tilde{q}_b)$ like Eq. (3.69). Of course a 3d-regulator is independent of the frequencies and so this relation holds by default. The left-hand side yields

$$\begin{aligned} \partial_k \Gamma_\mu^{i_1 i_2}(p_1, p_2) \Big|_{\substack{\Phi_0 \\ T=0 \\ \mu < \mu_c}} &= \frac{1}{2} \int_{q_a \dots q_d} G_\mu^{ab}(q_a, q_b) \Gamma_\mu^{b i_1 i_2 c}(q_b, p_1, p_2, q_c) G_\mu^{cd}(q_c, q_d) \partial_k R_\mu^{da}(q_d, q_a) \\ &= \frac{1}{2} \int_{q_a \dots q_d} G_0^{ab}(\tilde{q}_a, \tilde{q}_b) \Gamma_0^{b i_1 i_2 c}(\tilde{q}_b, \tilde{p}_1, \tilde{p}_2, \tilde{q}_c) G_0^{cd}(\tilde{q}_c, \tilde{q}_d) \partial_k R_0^{da}(\tilde{q}_d, \tilde{q}_a) \end{aligned} \quad (3.72)$$

where we assumed that Eq. (3.69) holds at the initial RG-scale. The validity of this equation is denoted on the left-hand side. Now we can shift all loop-momenta like $\tilde{q}_i \rightarrow q_i$, provided that the integrands are analytic, and then it is identical to Eq. (3.71). In an ideal situation one starts at some UV scale where the effective action is given by the classical one $\Gamma_{k=\Lambda} = S$, for instance the QCD action, where typically the momentum dependence is only in the kinetic terms in trivial way. Hence Eq. (3.69) holds trivially as well. Thus, we see that solving the scale dependence of an n-point function (including $n = 0$) with FRG does not jeopardize the Silver Blaze property, if it holds at the initial RG-scale, as the flow of both sides of Eq. (3.69) is identical. This remarkable feature is owed to the one-loop structure of the flow equation, because therefore we can easily shift the loop momentum. A vacuum polarization diagram is depicted in Fig. 3.10 illustrating the Silver Blaze property for FRG equations.

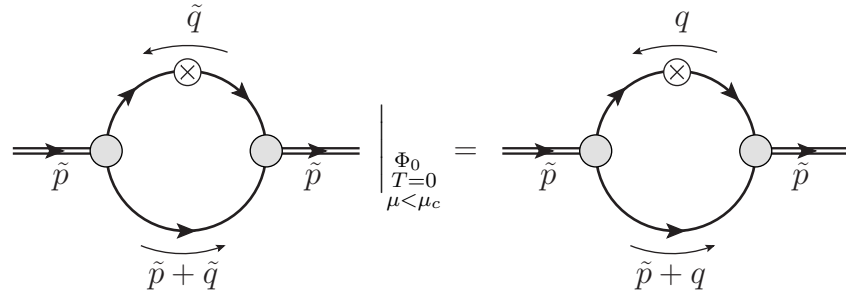


Figure 3.10: Vacuum polarization of the diquark illustrating the Silver Blaze property. The left-hand side is the analog of Eq. (3.72) and the right-hand side the analog of Eq. (3.71). Here we have made use of momentum conservation at vertices. The tilde denotes the μ -enhanced momentum as defined in the main text, there is no other μ . Obviously the “internal” chemical potential can be shifted away, provided there is no pole in the propagator. Of course it is only possible at $T = 0$ and a non-baryonic background. It entails that the flow at finite chemical potential is given by the flow at $\mu=0$ and shifted external momentum $p \rightarrow \tilde{p}$. This is valid for every RG-step hence Eq. (3.69) holds for all scales.

However, resolving the momentum dependence within the FRG framework requires high numerical effort. The only other consistent way would be to impose a vanishing nontrivial momentum dependence on the propagator, thus only having a trivial kinetic term. In order to keep it that way, one would not be allowed to compute the RG-flow of the propagator at vanishing momenta and couple it back to the system, because the μ dependence in its flow, coming from the (trivial) kinetic terms of the contributing propagators, cannot be made to disappear by deforming the contour, since the net baryon number must be nonzero inside the loop. Thus it would be interpreted as a genuine dependence on μ , rather than a simple shift of the momentum. Clearly, according to Eq. (3.69), there cannot be a μ dependence below μ_c if it is assumed that there is no momentum dependence. We emphasize here again that in order to compute the flow of a propagator, the momentum dependence must be correctly resolved for maintaining the Silver Blaze property in a consistent way. On the other hand, if it is indeed observed that the flow of a baryonic propagator is not much affected by a finite chemical potential below μ_c , one might conclude that there is only a mild momentum dependence. In such a case it might be fruitful to consider the flow of a baryonic propagator in a momentum independent scheme and take a small loss of the Silver Blaze property. Then again, even if the violation is large, it is crucial where the effects of μ manifest themselves. If they emerge around or after the critical scale their back coupling to the system might not be large, such that the interesting observables remain less affected.

Note that if one considers an effective potential for complex scalars, like diquarks, in a momentum independent scheme, and observes that the effective potential strongly differs between $\mu = 0$ and μ_c as in [233], it signals that there is a significant momentum dependence in the diquark propagator (since it depends on the curvature of the potential), which should not be disregarded, due to the reasons mentioned above. In particular it is important to improve the scheme, since μ_c depends on the effective potential. On the other hand, it was observed in [180] that incorporating a running wave function renormalization without momentum dependence is in remarkable agreement with the fully momentum dependent scheme at $\mu = 0$. Hence we are tempted to conclude that we might be able to capture the correct physics by the inclusion of running wave function renormalizations.

3.3.3 Pole Mass & μ_c

Now, let us recapitulate the critical chemical potential in the light of the Silver Blaze property. It is obtained by the non-analyticity of the effective action, which is given by the pole of the lowest excitation. Consider the two-point function of a complex scalar field where all nontrivial momentum dependences are stored in the mass function

$$\Gamma_0^{\Delta^* \Delta}(q, p) = \left[p^2 + m^2(p^2) \right] \delta(q + p). \quad (3.73)$$

Due to Lorentz invariance the argument of the mass function must be momentum squared. Now applying the formula (3.69) naturally leads to

$$\Gamma_\mu^{\Delta^* \Delta}(q, p) = \left[\vec{p}^2 + (p_4 + 2i\mu)^2 + m^2(\vec{p}^2 + (p_4 + 2i\mu)^2) \right] \delta(q + p). \quad (3.74)$$

We assumed baryon charge of 2 for the diquark. In the delta function the chemical potential is canceled due to the opposite charges. The pole of the propagator is given by the solution of the implicit equation

$$\Gamma_\mu^{\Delta^* \Delta}(\vec{p} = 0, p_4 = im_{\text{pol}, \mu}) = 0 \quad \Longleftrightarrow \quad m_{\text{pol}, \mu} = m \left(-(m_{\text{pol}, \mu} + 2\mu)^2 \right) - 2\mu. \quad (3.75)$$

The delta function was dropped. The non-analyticity is at vanishing pole mass, from which can deduce the critical chemical potential. By looking at the pole mass at vanishing μ , one sees that $m_{\text{pol}, 0}$ satisfies the same equation, which leads to the identification of the critical chemical potential with pole mass in the vacuum. Let us write down the corresponding equations:

$$m_{\text{pol}, \mu_c} = 0 \quad \Longrightarrow \quad \mu_c = \frac{m(-4\mu_c^2)}{2}, \quad (3.76)$$

$$m_{\text{pol}, 0} = m(-m_{\text{pol}, 0}^2) \quad \Longrightarrow \quad \mu_c = \frac{m_{\text{pol}, 0}}{2}. \quad (3.77)$$

We conclude that the critical chemical potential, after which the Silver Blaze property holds no more and a nontrivial μ -dependence is exhibited, is given by the pole mass at $\mu = 0$ divided by the charge. Thus if the correct momentum structure of the two-point function is known, μ_c can be predicted by analytic continuation, or of course by the experimentally known values of the physical masses in the vacuum. The consequence for two-color QCD is that $\mu = m_\pi/2$, as mentioned in Sec. 2.2.4. A similar computation for fermions leads to the same conclusion. However, there one has to look directly for the pole of the propagator rather than for the zero of the two-point function, since it is non-diagonal. Note that the curvature mass vanishes as well at μ_c

$$m_{\text{cur}, \mu}^2 = \Gamma_\mu^{\Delta^* \Delta}(p = 0) = m^2(-4\mu^2) - 4\mu^2 \quad \Longrightarrow \quad m_{\text{cur}, \mu_c}^2 = 0 \quad (3.78)$$

which follows from Eq. (3.76). The vanishing curvature mass entails a phase transition as discussed in Sec. 2.5. Above μ_c the minimum of the effective potential moves away from the origin giving rise to a Bose-Einstein condensate and a finite density.

In the fermionic case a density onset can definitely be expected at a μ_c due to the Fermi-Dirac distribution, if they do not form Cooper pairs. Other order parameters which depend on fermionic fluctuations, for instance the chiral condensate, will be influenced by the fact that fermionic states are occupied at finite density, which thereby are not available for quantum fluctuations due to the Pauli principle. However, this effect does not necessarily manifest itself at μ_c . The crucial

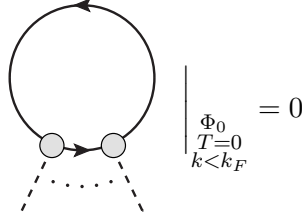


Figure 3.11: Fermionic loop diagram with an arbitrary number of external legs corresponding to fields neutral in the charge associated with the chemical potential. The total charge of such a digram must be vanishing and therefore the of number particles in the loop is equal to the number of antiparticles. Since the particle states below k_F are occupied, a fluctuating pair cannot be produced. Of course $k_F > 0$ only if $\mu > \mu_{c,density}$. We will see this effect explicitly in the FRG equation of the effective potential in the next section. However, this identity is generally true for a neutral background field Φ_0 as in (3.70).

point is whether the occupied states are below or above the energy scale at which the fermionic fluctuations have been integrated out. In an RG framework for instance, if $\mu_c \ll \sqrt{k_\chi^2 + m_{q,k_\chi}^2}$, then the unavailable states are massive ones, not contributing to quantum fluctuations anyway, so there will be no effect on the chiral order parameter. Only if the Fermi energy is close to the chiral symmetry breaking scale, more generally if $k_F = \sqrt{\mu^2 - m_{q,k_F}^2} \gtrsim k_\chi$, there will be an observable effect due to Fig. 3.11 and therefore $\mu_{c,chiral} > \mu_{c,density}$. For heavy fermions like the baryons this means that they cannot influence the chiral condensate at $T = 0$ whatsoever. If they are heavy in the vacuum they remain suppressed below their density onset. And then they are even more suppressed because of Fig. 3.11.

3.4 Flow of the Effective Potential

The RG flow of the effective potential receives contributions from scalar and the fermionic degrees of freedom. We start by evaluating the flow equation (3.8) for constant fields, as we want to minimize the effective action. Naturally the kinetic parts of the effective action drop out. At the constant expansion point $\Phi_0 = (\varphi_0, 0)$, where φ_0 is given in Eq.(3.30) and $\Psi = \bar{\Psi} = 0$, since we want it to be close to or right at the ground state, only the effective potential remains on the left-hand side of the flow equation. Note that the ρ 's are still variables in field space at this point, but constant in position/momentum space. We are free to choose any numerical value for the ρ 's at which we want to evaluate the flow. Ideally one should cover a sufficiently wide range of values, as it has been done in [176, 233]. However we are making a Taylor expansion of the effective potential and we are only interested in minimum, therefore we evaluate the flow at a comoving (running) minimum in this work and check the convergence of the expansion. In contrast in [179] the flow of a quark-meson model is evaluated at non-running points close to the minimum, which leads to a different convergence behavior of the Taylor, which will be discussed in the next chapter. The flow equation yields

$$\begin{aligned} \partial_t \Gamma[\Phi_0] &= \partial_t \int U(\rho_\phi, \rho_\Delta) = Vol_d \partial_t U(\rho_\phi, \rho_\Delta) \\ &= \frac{1}{2} \text{str} \int_{p,q} G(p, -q) \partial_t R(-q, p) = \frac{1}{2} \text{str} \int_p G(p) \partial_t R(p) \underbrace{\delta(0)}_{Vol_d} . \end{aligned}$$

Thus the flow equation of the effective potential reads

$$\partial_t U(\rho_\phi, \rho_\Delta) = \text{tr} \int_p \left(\frac{1}{2} G_\phi \dot{R}_\phi - G_{\Psi\bar{\Psi}} \dot{R}_{\Psi\bar{\Psi}} \right). \quad (3.79)$$

It is easy to see that the second fermionic part $G_{\Psi\bar{\Psi}} \dot{R}_{\Psi\bar{\Psi}}$ yields the same contribution as first one, with Eq. (3.52) and by substituting the integration variable $q \rightarrow -q$ and transposing the expression, which leaves the trace invariant. Hence we can take twice of the contribution from $G_{\Psi\bar{\Psi}}$. The diagrammatic form of Eq. (3.79) is given in Fig. 3.12. If the bosonic fluctuations are neglected by setting $\text{tr} \int_p G_\phi \dot{R}_\phi = 0$, one obtains the standard mean-field theory results for the thermodynamic potential. The remaining quark contribution can then be easily integrated [212]. We will now compute more explicit expressions of the above flow equation for the QMD-model and make a detailed and general analysis of the contributions. Then we will add the additional contributions in QMDB-model.

Figure 3.12: RG flow of the effective potential. Here, the dashed line represents the all bosonic propagators, the continuous line represent the fermionic ones. The blobs denote the fact that we have full propagators, the crosses denote the regulator insertion. The fermionic contribution is doubled since particle and antiparticle contributions coincide. The minus sign is due to the anticommuting nature of fermions.

3.4.1 Flow Equation for the QMD-Model and a General Discussion

Bosonic contribution Let us first turn to the calculation of the bosonic part. The bosonic contribution to the flow of the effective potential is given by

$$\begin{aligned} \frac{1}{2} \text{tr} \int_p G_\phi \dot{R}_\phi &= \frac{1}{2} \int_p \left[3G_\pi(\vec{p}_r^2) \dot{R}_\phi(\vec{p}^2) + G_\sigma(\vec{p}_r^2) \dot{R}_\phi(\vec{p}^2) + 2G_\Delta^+(\vec{p}_r^2) \dot{R}_\Delta(\vec{p}^2) \right] \\ &= \frac{k^5 T}{6\pi^2} \sum_{n \in \mathbb{Z}} \left\{ \left(1 - \frac{\eta_\phi}{5} \right) \left[3G_\pi(k^2) + G_\sigma(k^2) \right] + 2 \left(1 - \frac{\eta_\Delta}{5} \right) G_\Delta^+(k^2) \right\}. \end{aligned} \quad (3.80)$$

The integrals were computed by the use of the formula (C.41). The bosonic contribution contains three degenerate pion, one sigma and two degenerate diquark loops. The propagators can be found in App. B.1 and the scale derivatives of the regulators here are defined as $\dot{R}_{\phi/\Delta}(\vec{p}^2) = \vec{p}^2 [\dot{r}_B(\vec{p}^2/k^2) - \eta_{\phi/\Delta} r_B(\vec{p}^2/k^2)]$, and the Z 's cancel out. The anomalous dimensions stem from Eq. (3.20). The diquark contributions stem from off-diagonal entries of the propagator and can be summarized due to Eq. (3.36) by substituting the integration variable $p \rightarrow -p$, thus the factor of 2. A closed loop without any legs has the interpretation of spontaneous pair production and annihilation of particles. Such a process is given by a propagator which goes back to its starting point. A charged particle propagating back to itself is equivalent to a pair production and annihilation, since time reversal changes the charge of the particle, which is reflected by the fact that $G_\Delta^+(-p_4) = G_\Delta^-(p_4)$. For fermions we have a similar situation. The momentum integration sums up all these processes with all possible momenta, while the regulator puts a constraint on the them, as discussed in Sec. 3.1.2.

Fermionic contribution The fermionic part is given by

$$\begin{aligned}
 \text{tr} \int_p G_{\Psi\bar{\Psi}} \dot{R}_{\Psi\bar{\Psi}} &= \text{tr} \int_p \left(G^+ + G^- \right) \not{p} (\dot{r}_F - \eta_q r_F) \\
 &= 4N_c N_f \int_p \vec{p}_r A_+(\vec{p}_r^2) \cdot \vec{p} (\dot{r}_F - \eta_q r_F) \\
 &= 4N_c N_f \frac{k^5 T}{6\pi^2} \left(1 - \frac{\eta_q}{4} \right) \sum_{n \in \mathbb{Z}} A_+(k^2), \tag{3.81}
 \end{aligned}$$

where the formula (C.42) was employed. The contribution of the lower right part G^- of the fermion propagator in Nambu-Gorkov space, which is given in App. B.2, can be shown to coincide with the contribution from G^+ by substituting the integration variable $p_4 \rightarrow -p_4$, which leaves the integration invariant. Since Nambu-Gorkov space is equivalent to color space in our convention, summarizing yields the factor N_c . In flavor space the propagator has a trivial structure, hence the factor N_f , while in Dirac space only the kinetic term survives due to the tracing properties of the Dirac matrices, where the factor of 4 originates from as well (see App. A.4), accounting for spin up/down and anti-/particle degrees of freedom.

Analytic expressions We see that only the modes where the loop momentum is around the scale, or, in the case of the optimized regulator function, right at $\vec{p}^2 = k^2$, define the change of the effective potential with respect to the scale, as expected. The frequency components of the momentum p_4 are summed over the respective Matsubara frequencies (3.37) and (3.55), which are included in the definition of the propagators in App. B. The analytic expressions of the summation can be found with the residue theorem, but are quite tedious in the sigma and diquark sector due to the mixing structure. Therefore, let us write down the summed expression of the flow of the effective potential in a general form ¹

$$\partial_t U = \frac{k^5}{6\pi^2} \left\{ \sum_{i=1}^6 \left(1 - \frac{\eta_{\varphi_i}}{5} \right) \frac{1}{\hat{E}_{\varphi_i}} \left[\frac{1}{2} + n_B(E_{\varphi_i}) \right] - 2N_c N_f \left(1 - \frac{\eta_q}{4} \right) \sum_{\pm} \frac{1}{\hat{E}_q^{\pm}} \left[\frac{1}{2} - n_F(E_q^{\pm}) \right] \right\} \tag{3.82}$$

where n_B and n_F are the Bose-Einstein and Fermi-Dirac distributions functions, given by

$$n_B(E) = \frac{1}{e^{E/T} - 1}, \quad n_F(E) = \frac{1}{e^{E/T} + 1}.$$

The Bose-Einstein function is not defined for negative energies. In any case, this is avoided by the occurrence of a condensate. The inverse coefficients $\hat{E}_{\varphi_i}(M_\varphi, k, \mu)$ are in general functions of the curvature of the effective potential (3.32), the RG-scale and the chemical potential. The arguments $E_{\varphi_i}(M_\varphi, k, \mu)$ of the distribution functions are given by the roots of the denominators of the propagators in Eq. (3.80), more generally by the roots of the equation $\det G_\varphi^{-1}(\vec{p}_r^2 = k^2, \omega_n^2 = \omega^2) = 0$, which is a polynomial in ω^2 of the order $\dim(\varphi)$, so in our case there are six solutions. Three of the solution are for the pions. The pion and quark energies are given by

¹Note that the bosonic part in Eq. (3.82) is not strictly equal to Eq. (3.80), since in order to write the anomalous dimensions as pre-factors as in (3.82), they must correspond to the diagonal mass eigenstates, which is not the case in (3.80) if there is a mixing of different sectors. Anyway, we are going to implement (3.80) in our numerics, while (3.82) is shown for the sake of discussion.

$$\begin{aligned}
 \hat{E}_\pi &= E_\pi = \sqrt{k^2 + V_\phi}, \\
 \hat{E}_q^\pm &= \sqrt{k^2 + 2h_\phi\rho_\phi + 2h_\Delta\hat{\rho}_\Delta^\pm}, & E_q^\pm &= \sqrt{(\epsilon_q \pm \mu)^2 + 2h_\Delta\rho_\Delta}, \\
 \hat{\rho}_\Delta^\pm &= \rho_\Delta \frac{\epsilon_q^2}{(\epsilon_q \pm \mu)^2}, & \epsilon_q &= \sqrt{k^2 + 2h_\phi\rho_\phi}.
 \end{aligned} \tag{3.83}$$

The implications of the quark energies will be discussed below. For two-color QCD at $\mu = 0$ the effective potential respects the $SO(6)$ symmetry which must be respected by the flow equation as well, therefore Eq. (3.82) must be a function of $SO(6)$ invariant $\rho_\phi + \rho_\Delta$, which easy to see in quark energies. Also the remaining bosonic energies are functions of the invariant. Note that the factors for particle antiparticle degeneracies have turned into distinguishable contributions for finite μ after summation. Let us discuss some general features of the above flow equation. This discussion will not be specific to QC₂D, but also applies to physical QCD as well.

Symmetry breaking & anomalous dimensions First of all, note that due to the opposite sign in the middle, there is a competing effect between fermions and bosons. In the UV we start with symmetric potential, where the minimum is around the origin. Since the fields ρ_ϕ and ρ_Δ act as excitation gaps of the fermions, for small values fermionic contributions are strong. Whereas the bosonic gaps are given by the curvature of U , which is nonzero around the minimum. The magnitudes of the gaps relative to the scale is the crucial quantity. By solving the flow down to the IR, the fermions drive the minimum up and flatten the region more than the outer regions, eventually leading to shift of the minimum to larger fields and breaking the symmetry. On the other hand the flattening reduces the bosonic gaps, in particular for the (pseudo-) Goldstone modes, leading to a counter reaction, until the RG scale is smaller than all gaps in the system, where then the flow freezes out. The interplay of these two effects determines the critical physics.

As can we see, a positive anomalous dimensions reduce the contribution of the respective fields. More details on their behavior can be found in Sec. 3.6. According to our definition of the ρ 's in Eq. (2.46), they depend on the scale k via the wave function renormalizations, therefore the left-hand side of the flow equation can be split up as follows

$$\partial_t U(\rho_\phi, \rho_\Delta) = (\partial_t U)_\rho + \partial_t \rho_\phi \frac{\partial U}{\partial \rho_\phi} + \partial_t \rho_\Delta \frac{\partial U}{\partial \rho_\Delta}. \tag{3.84}$$

The source term will be dealt with in Sec. 3.4.3. Now we solve this for the flow of the effective potential for constant ρ 's and find with the definitions of U (2.45) and the η 's (3.21)

$$(\partial_t U)_\rho = \partial_t U|_{\text{loops}} + \eta_\phi \rho_\phi V_\phi + \eta_\Delta \rho_\Delta (V_\Delta - 4\mu^2) \tag{3.85}$$

where the loops are given by the right-hand side of Eq. (3.82). As before the index of V represents the derivatives, which are shown in Eq. (3.84). For positive anomalous dimensions the additional terms lead to the the following effect: Since the first derivative of U with respect to the ρ 's corresponds to the curvature mass of the (pseudo-) Goldstone modes, at the minimum these additional contributions are always vanishing (small for pseudo Goldstone modes) either by the condensate or by the mass. With increasing ρ 's we have increasing positive contributions driving the potential down towards the IR, more in the outer regions. This entails a flattening of the potential and a faster symmetry breaking. In order to avoid overly breaking the symmetry, a larger curvature must be chosen in the UV, from which we can infer that the bosons decouple much stronger in the UV, by the inclusion of anomalous dimensions.

Thermal contributions There is an obvious split between quantum and thermal contributions. The latter are given by thermal distribution functions, representing the mean occupation numbers for a particular energy state E at temperature T . We can refer to the arguments of distribution functions as *thermal energy dispersion*, while the inverse of the coefficients (denoted with the hats) can be referred to as *quantum energy dispersions*. The reason for a possible discrepancy is that thermal and quantum fluctuations are different processes, however, influencing each other. It will become more clear below. Consider the limiting cases

$$\begin{aligned} n_B &\xrightarrow{E/T \rightarrow \infty} 0, & n_F &\xrightarrow{E/T \rightarrow \infty} 0, \\ n_B &\xrightarrow{E/T \rightarrow 0} \frac{T}{E} - \frac{1}{2}, & n_F &\xrightarrow{E/T \rightarrow 0} \frac{1}{2} - \frac{E}{4T}. \end{aligned} \quad (3.86)$$

Due to the Pauli exclusion principle the occupation number for fermions cannot be larger than one. As a matter of course, the different thermal statistics can be rooted back to the commuting and anti commuting nature of the respective fields. However, as we see in Eq. (3.82), the differences are not limited to the distributions functions, but also the signs of the thermal parts are opposite. Again, this can be traced back to the anticommutativity, but it can also be understood by the Pauli principle in a less abstract way. Before turning to that matter, first note that naturally thermal contributions vanish at $T = 0$ and we are left only with the quantum fluctuations. Now, increasing the temperature entails that the system is coupled to a heat bath from which energy is drawn and particle-antiparticle pairs are created in different energy states according to the respective distributions functions. For the fermions this implies that quantum energy states with the same mode k are no more available for the renormalization group flow, due to the exclusion principle, therefore the thermal part must be subtracted from the flow. In consequence there is no fermionic contribution in the high temperature limit, which was already anticipated from the fermionic Matsubara frequencies. For bosons on the other hand, there is of course no exclusion, but rather the RG-flow takes advantage of the heat bath, such that fluctuations with high energy modes become easier to induce with increasing temperature. This is the manifestation of the only surviving zero mode of bosonic Matsubara frequencies, the contribution of which rises linear with a factor of T from the measure. In summary Eq. (3.82) takes the form

$$\partial_t U|_{E \ll T} = \frac{k^5}{6\pi^2} \left\{ \sum_i \left(1 - \frac{\eta_{\varphi_i}}{5} \right) \frac{1}{\hat{E}_{\varphi_i}} \frac{T}{E_{\varphi_i}} - 2N_c N_f \left(1 - \frac{\eta_q}{4} \right) \sum_{\pm} \frac{1}{\hat{E}_q^{\pm}} \frac{E_q^{\pm}}{4T} \right\} \quad (3.87)$$

in the high temperature limit, where (3.86) was applied. As discussed, fermionic fluctuations decrease with the temperature while bosonic ones increase. Then again, if there was no fermionic flow, bosons retain their high masses, which they had in the UV, hence at large temperatures the effects are small overall, and the system stays in the symmetric regime.

Non-baryonic background & Silver Blaze Next, we shall study the impact of the chemical potential. To that end, we consider the $\rho_{\Delta} \rightarrow 0$ limit, where the all energy dispersions become rather trivial

$$\begin{aligned} \hat{E}_{\sigma} &\rightarrow \sqrt{k^2 + V_{\phi} + 2\rho_{\phi} V_{\phi\phi}}, & E_{\sigma} &\rightarrow \hat{E}_{\sigma}, \\ \hat{E}_{\Delta} &\rightarrow \sqrt{k^2 + V_{\Delta}}, & E_{\Delta}^{\pm} &\rightarrow \hat{E}_{\Delta} \pm 2\mu, \\ \hat{E}_q &\rightarrow e_q, & E_q^{\pm} &\rightarrow e_q \pm \mu. \end{aligned}$$

For the pions it stays the same. In this limit our flow equation has the familiar looking form of a quark-meson model [176] augmented by the diquark contribution, which is given by the generalized flow equation for a complex scalar for vanishing values of the field. The chemical potential, which parametrizes the imbalance of baryonic particles and antiparticles, now only appears in the thermal distribution functions for fermions and diquarks. At vanishing temperature and $E_\Delta^-, E_q^- > 0$ the distribution functions vanish, and so does the imbalance. Hence, it would seem that there is no effect of the chemical potential whatsoever at $T = 0$, but this is not exactly true. Although the effective potential itself does not have a direct impact from the chemical potential at $\rho_\Delta = 0$, its curvature does indeed. Since the flow is affected by a finite μ at $\rho_\Delta \neq 0$ even in the vicinity of the origin, the curvature necessarily changes, as it can be seen directly from the quark energy dispersions in (3.83). Thus, there is an indirect effect on U , and even more from running anomalous dimensions and Yukawa couplings. This is a violation of the Silver Blaze property, according to which non-baryonic quantities, i.e. the meson sector in U , should not change below a threshold, though the violation in this sector is very small as it can be seen in [233]. On the other hand, if we assume an effective potential of the form $U = V(\rho_\phi + \gamma\rho_\Delta) - c\sigma - 4\mu^2\rho_\Delta$ where there is a constant ratio between the meson and diquark sector, we can solve the flow equations for $\rho_\Delta = 0$, and avoid the violation. Furthermore, in a model with real and complex scalar fields in a momentum independent scheme, this is the only way to have an approximation where the curvature mass is by default identical to the pole mass at $\mu = 0$, and where μ_c then coincides with this pole mass as well. Hence the onset condition (3.77) is definitely satisfied, provided that there is no running of any other baryonic quantity like Yukawa couplings and anomalous dimensions. For two-color QCD we have the $SO(6)$ symmetry at $\mu = 0$, hence $\gamma = 1$ might be a good approximation, whereas for physical QCD such a scheme would be rather crude. Of course a momentum resolution of all coupling parameters would ensure the Silver Blaze property altogether.

Interplay of temperature and chemical potential At finite temperature the chemical potential gives rise to an imbalance between thermal particle and antiparticle excitations. It is clear why we referred to the coefficients as quantum energy dispersion, namely because in the presence of a finite μ only the thermal occupation numbers change, while the energy of the modes contributing to the flow remain unchanged (for $\rho_\Delta = 0$). The occupation increases for particles and decreases for antiparticles with μ , while the total number increases for both particle types. The consequence for fermions is again that there are less available states for the RG-flow, while for the bosons there are more. This is the origin of the decreasing of the critical temperature T_c with μ in QCD. In order to emphasize this we write

$$\frac{\partial}{\partial\mu}[n(E^-) + n(E^+)] > 0 \quad \implies \quad \frac{\partial T_c(\mu < \mu_c)}{\partial\mu} < 0. \quad (3.88)$$

The inequality for the distribution functions is valid for fermions as well as for bosons. The reason why it is only valid below the critical chemical potential will be discussed below. Next we shall consider the case $E_q^- < 0$ still at vanishing diquark fields. It implies that the chemical potential is higher than the fermion mass and for $T = 0$ all states with $k^2 < k_F^2 = \mu^2 - m_q^2$ up to the Fermi surface are occupied by external quarks. In terms of the distribution function we have $n_F(E_q^- < 0, T = 0) = 1$. This distribution function instantly cancels both the quark and antiquark part of the flow for $k < k_F$, eventually preventing chiral symmetry breaking at some critical chemical potential μ_c . It can be understood by considering that both quarks and anti quarks are needed for quantum fluctuations contributing to the mesonic effective potential, if one of them is not available the other cannot contribute either. In the flow equation (3.82) this

is reflected by a step function

$$\partial_t U \Big|_{\substack{\rho_\Delta=0 \\ T=0}} = \frac{k^5}{12\pi^2} \left\{ \left(1 - \frac{\eta_\phi}{5}\right) \left[\frac{1}{\hat{E}_\pi} + \frac{1}{\hat{E}_\sigma} \right] + \left(1 - \frac{\eta_\Delta}{5}\right) \frac{2}{\hat{E}_\Delta} - 4N_c N_f \left(1 - \frac{\eta_q}{4}\right) \frac{1}{\epsilon_q} \Theta(\epsilon_q - \mu) \right\} \quad (3.89)$$

Increasing the temperature leads to excitations of particles which are close to the Fermi surface, washing out the step function in the Fermi distribution and giving the opportunity for fermions to break chiral symmetry, until at higher temperature thermal pair production prevents it again. Indeed there is a minimum of $n_F(E_q^-) + n_F(E_q^+)$ in the temperature direction around which chiral symmetry is restored for a small range $\mu_c(T_c = 0) < \mu < \mu_{c,\max}(T_c)$ and we get a back bending of the phase boundary, as it can be seen in [176], hence the constraint in Eq. (3.88). Note that in the phase diagram of two-color QCD this effect cannot be observed, as the Bose-Einstein condensation phase overspreads the region where the bending would occur.

Baryonic background & BEC-BSC crossover Finally we analyze the quark contributions for $\rho_\Delta \neq 0$. Here we have an additional gap in the quark energies suppressing quark excitations. First note that now $E_q^- > 0$ for all μ , thus there cannot be a finite density of quarks at $T = 0$. Since $\rho_\Delta \neq 0$ implies that the condition for fermions condensing into Cooper pairs are met, every two fermions that are added to the system immediately go into condensation. Furthermore, for $m_q < \mu$ (where $m_q = \sqrt{2h_\phi\rho_\phi}$) the minimum of E_q^- arises at a nonzero momentum scale $k_{\min}^2 = k_F^2 = \mu^2 - m_q^2$ (blue lines in Fig. 3.13) meaning that the lowest energy state is given by a BCS-like Cooper pair with finite (and opposite) momenta of the constituents, hence a long range bound state. The momentum of the minimum increases steadily with μ , until at some point the interparticle distance starts falling below the range of the bound states, such that they are overlapping, this is the BCS-limit. Thus $m_q = \mu$ can be used as a rule of thumb for the BEC-BCS crossover [219].

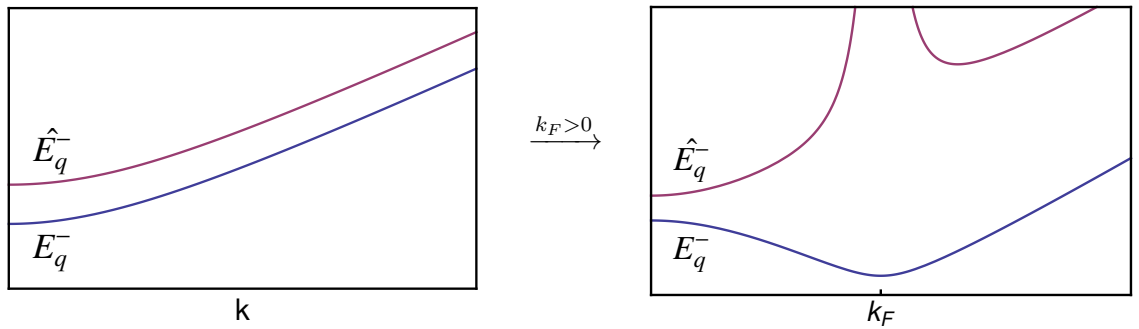


Figure 3.13: On the left-hand side we see the behavior of the quantum and thermal energy dispersions for the case $k_F < 0$. They are both monotonically rising functions with k . On the right-hand side we have the case $k_F > 0$. The thermal dispersion develops a minimum at the Fermi surface, whereas the quantum dispersion diverges. The former effect is related to BSC pairing, while the latter is related to Pauli blocking. See main text for the explanation.

Modified gap & Silver Blaze In Eq. (3.83) we see a modified gap in the quantum energy dispersion, which depends on the ratio of the normal energy of the quarks and the μ -reduced one. Since we are now computing the flow in the presence of a baryonic background, the quantum energy dispersion is no more independent of the chemical potential. Below μ_c the diquark sector of the effective action should change trivially with μ according to Eq. (3.69) for $\rho_\Delta = 0$, which represents the minimum. In a momentum dependent scheme this would automatically be yielding from the flow as was exemplary shown in Eq. (3.72). In our case however, the effective potential around the minimum is directly affected by μ , which entails that the curvature and higher derivatives right at the minimum are affected as well. Thereby a genuine μ dependence of the n-point functions is generated, since our scheme is momentum independent, thus violating the Silver Blaze property. This is a concrete example of the problem we mentioned in Sec 3.3.

Obviously the modified gap is raised for quarks and lowered for antiquarks, due to the baryonic background. In fact this is another remarkable manifestation of the Pauli exclusion principle. Consider the case $m_q < \mu$, where we have shown, that the minimum of the thermal energy dispersion $E_{q,\min}^-$ lies at the Fermi surface. On the other hand, the denominator of the modified gap vanishes at k_F leading to a diverging gap and thus

$$\hat{E}_q^- \xrightarrow{k \rightarrow k_F} \infty, \quad (3.90)$$

see the red lines in Fig. 3.13. This is connected to the fact that the diquark field in the background are Cooper pairs of fermions at the Fermi surface. Therefore quantum fluctuations with the same mode k_F are blocked. This is the Pauli principle at work! Even without the Fermi distribution function. At large scales, or more generally either for $\epsilon_q \rightarrow \infty$ or $\mu \rightarrow 0$, the modified gap goes back to the normal one $\hat{\rho}_\Delta^\pm \rightarrow \rho_\Delta$. All cases are smoothly connected to each other. For vanishing chemical potential the $SO(6)$ symmetry of two color QCD is restored since the Yukawa couplings must coincide as well. The fact that antiparticle quantum fluctuations are favored is in contrast to the thermal excitations, where particles are favored. The reason is that the chemical potential has a different role there. It is just a way of telling the system that there are more thermally excited particles than antiparticles.

3.4.2 Extension for QMDB-Model

For the QMDB-model we must add the contributions from the red and green diquarks as well as the blue quark and the baryons. The additional diquark parts are trivial, while the additional fermionic parts we display without performing the summation over the Matsubara frequencies, since the energy dispersions do not have an overseeable form, but of course it would yield a similar fermionic form like in (3.82) with Fermi-Dirac distribution. We skip the derivation, which is analog to the beginning of Sec. 3.4.1 and write the result as

$$\begin{aligned} \partial_t U = \partial_t U|_{QC_2D} + \frac{k^5}{6\pi^2} \left\{ 2 \left(1 - \frac{\eta_\Delta}{5} \right) \sum_{\pm} \frac{1}{\hat{E}_{\Delta,0}} \left[\frac{1}{2} + n_B \left(\hat{E}_{\Delta,0} \pm 2\mu \right) \right] \right. \\ \left. - 4N_f T \sum_{n \in \mathbb{Z}} \left[\left(1 - \frac{\eta_q}{4} \right) A_b(k^2) + \left(1 - \frac{\eta_B}{4} \right) A_B(k^2) \right] \right\} \quad (3.91) \end{aligned}$$

where $\hat{E}_{\Delta,0} = \sqrt{k^2 + V_\Delta}$ is the diquark energy without a background field. The additional fermionic functions are given in App. B.2. Note that the QC₂D-part is meant literally in the sense that $N_c = 2$, since the blue quark has a separate contribution. For the baryonic contribution

to behave in a physical way, it must decouple from the system at large RG-scale and temperature. Around the critical endpoint of QCD presumably there will some effects of the baryons. In the 2SC phase the five Goldstone modes are gauged away, only the real mode of the blue diquark is left. We can obtain the corresponding flow equations simply by replacing diquark contribution in QC₂D by half of the contribution from the real mode:

$$\partial_t U = \partial_t U \Big|_{2G_{\Delta}^- \rightarrow G_{\Delta_1}} - \frac{k^5}{6\pi^2} 4N_f T \sum_{n \in \mathbb{Z}} \left[\left(1 - \frac{\eta_q}{4}\right) A_b(k^2) + \left(1 - \frac{\eta_B}{4}\right) A_B(k^2) \right]. \quad (3.92)$$

3.4.3 Flow of the Bosonic Parameters

Source term First we want to show that the flow equation does not conduce to a running of linear source terms, such as the explicit chiral symmetry breaking. The right-hand side of (3.82) is a function of integer powers of the ρ 's, hence we have the following discrete symmetry, which implies that there cannot be a linear term on the left-hand side

$$\dot{U}(-\sigma) = \dot{U}(\sigma) \quad \Leftrightarrow \quad \frac{\partial \dot{U}}{\partial \sigma} \Big|_{\sigma=0} = 0. \quad (3.93)$$

By looking at the ansatz of U in (2.45) it follows immediately that

$$\frac{\partial}{\partial t} \left(c \sqrt{Z_\phi} \right) = 0 \quad \Leftrightarrow \quad \partial_t c = \frac{\eta_\phi}{2} c. \quad (3.94)$$

Note that this could have been followed from Eq. (3.85) just as well, by assuming that the effective potential is also a function of the renormalized field $\bar{\sigma} = \sqrt{Z_\phi} \sigma$ like $U(\rho_\phi, \rho_\Delta, \bar{\sigma})$, then we would have the additional term $\frac{\eta_\phi}{2} c \bar{\sigma}$ on the right-hand side. Now, comparing coefficients would finally lead to (3.94). Remarkably the source term does only shift the expectation value of the condensates to non-zero values, but does not affect the RG-flow of integrating out quantum fluctuations at all. This is related to the fact that the propagators which contain the curvature are independent of the linear term

$$\frac{\partial M_\varphi}{\partial c} = 0 \quad \Rightarrow \quad \frac{\partial \dot{U}}{\partial c} = 0. \quad (3.95)$$

However, as we will just discuss, we are going to compute the flow only at the minimum $\rho_\phi = \kappa_\phi$, therefore the source parameter c enters the flow equation via the minimum, but keep in mind that this is nothing but our choice for the expansion point.

Masses, couplings and condensates In the previous discussion we were emphasizing that the curvature/flatness around the minimum changes with the flow, and therefore it is crucial to solve the flow for a sufficient range around the minimum, like it was done in [233]. But we are going to exercise a different approach: Since all we need for the propagators in the flow equation is the curvature at the minimum, we can directly compute its flow by taking ρ -derivatives of Eq. (3.85). Thereby we obtain flow equations which contain higher derivatives of the effective potential corresponding to four-point couplings emerging from the bosonic energy dispersions. This flow equation resembles the one of a two-point function. Now, in order to be more quantitatively accurate, we take ρ -derivatives of (3.85) to the next order, such that we obtain the flow of those four-point couplings, which is then given by even higher derivatives. Of course we also have fermion loop contributions, as the fermion energies also depends on the

ρ 's, where a derivative yields the corresponding Yukawa coupling as a vertex parameter. This iterative method can be done up to arbitrary order until the physical observables, which we are interested in, converge. This is why we made the Taylor expansion ansatz in Eqs. (2.50) and (2.56). Essentially, we are going to solve the flow of the Taylor coefficients up to the order of the expansion, while all higher coefficients are simply set to zero. Effectively this constitutes a vertex expansion approach of the effective action. The convergence of such a scheme has been tested in Refs. [175, 331]. Note, that if the symmetry is broken, we have a non-zero minimum, which depends on the curvature, therefore, instead of solving the flow of the curvature, we solve it directly for the minimum κ , this is why we make the reparametrizations (2.53) and (2.58). Let us write down the ρ -derivatives of Eq. (3.85) for the two-dimensional Taylor expansion ansatz

$$\begin{aligned} \dot{\lambda}_{n,m} = & \lambda_{n+1,m} \dot{\kappa}_\phi + \lambda_{n,m+1} \dot{\kappa}_\Delta + \frac{\partial^n}{\partial \rho_\phi^n} \frac{\partial^m}{\partial \rho_\Delta^m} \dot{U} \Big|_{\substack{\text{loops} \\ \bar{\rho}=\bar{\kappa}}} \\ & + \eta_\phi (n\lambda_{n,m} + \lambda_{n+1,m} \kappa_\phi) + \eta_\Delta (m\lambda_{n,m} - 4\mu^2 \delta_{n0} \delta_{m1} + \lambda_{n,m+1} \kappa_\Delta) . \end{aligned} \quad (3.96)$$

The lowest coefficients represent the mass parameters. In the UV we typically start with small bosonic couplings and large bosonic masses. Hence initially the flow of the couplings is dominated by the fermion loops, while the flow of the masses have self-enhanced contributions from the anomalous dimension terms in the lower line driving them down, as discussed below Eq. (3.85). Since every ρ -derivative of Eq. (3.82) yields an additional minus sign it is expected that the Taylor coefficients will have altering signs. In Fig. 3.14 the flow of the couplings for $T = 0$ at $\mu = 0$ and short before μ_c is plotted for two-color QCD. We see for instance that the $\lambda_{3,0}$ starts off being negative, but around the scale of the chiral phase transition it changes the sign, because the dynamics change from the fermionic sector to the bosonic one. $\lambda_{4,0}$ changes the sign a few times before being negative, whereas $\lambda_{5,0}$ is again positive. Note that the mesonic mass parameter is connected to the expansion point via Eq. (2.57), therefore its flow is simply given by

$$\dot{\lambda}_{1,0} = \frac{\dot{c}}{\sqrt{2\kappa_\phi}} - \frac{c\dot{\kappa}_\phi}{(2\kappa_\phi)^3} . \quad (3.97)$$

This is how Eq. (3.94) enters the system. Now, plugging (3.94) and (3.97) into (3.96) into for the case $(n, m) = (1, 0)$ we can solve for the scale derivative of κ_ϕ and plug it into the other equations. Furthermore, we have the following cases for the different phases

$$\begin{aligned} \text{Normal regime:} & \quad \dot{\kappa}_\Delta = \kappa_\Delta = 0 , \\ \text{BEC regime:} & \quad \dot{\lambda}_{0,1} = 0 , \quad \lambda_{0,1} = (2\mu)^2 . \end{aligned} \quad (3.98)$$

The latter equation actually holds at the critical scale k_c , after which our potential is reparametrized as discussed in Sec. 2.5.2. Hence for $(n, m) = (0, 1)$ we have the scale derivative of κ_Δ , which also can be plugged into the other equations. The expressions for the anomalous dimensions can be plugged in as well. This way we always have a diagonal set of coupled partial differential equations in the sense that there is only one scale derivative per equation for each parameter. This set of equations along with the flow of Yukawa couplings, also given in App. C, will be solved simultaneously for different values of the temperature and chemical potential, by which we can draw a phase diagram.

As mentioned before, in the diquark sector, i.e. for the index $m \neq 0$, there will be a μ -dependence below μ_c at vanishing temperature, despite the fact that we do not consider momentum depen-

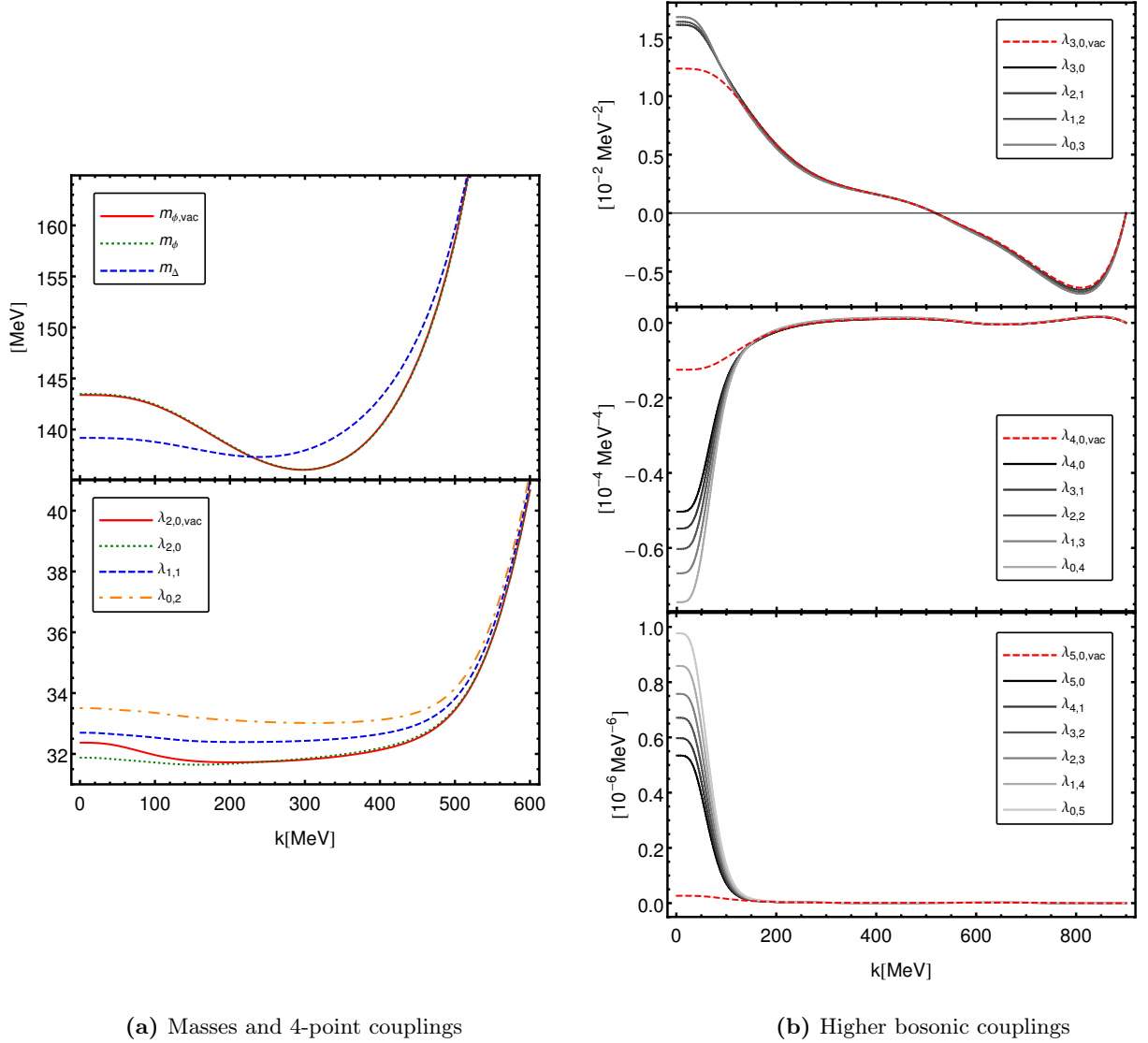


Figure 3.14: Flow of the 2d Taylor coefficients of the effective potential for two-color QCD. The initial conditions are given in Tab 4.1 (2d Taylor). The red lines represent the vacuum flow, i.e. at $T = \mu = 0$, the other lines are at $\mu = 0.4m_\pi$. The initial conditions in the UV are the same. Because in the vacuum we have the $SO(4)$ symmetry between meson and diquarks, all coefficients of a certain order are given by the red line. Since we assume a vanishing momentum dependence, the flow should remain unchanged below $\mu_c = m_\pi/2$, but this not the case.

dences, hence the Silver Blaze property is violated. In Fig. 3.14 we see the extent of the violation. We see a steadily rising violation for rising coefficient. The higher the order of the diquark fields (second index) the sooner the flow starts to separate from the vacuum flow and the higher is the violation. It even couples back to the pure mesonic couplings. It is interesting that $\lambda_{2,0}$ starts to deviate from the vacuum flow at around $k \approx 2\mu$. Nevertheless, even though the higher order terms have a large deviation, they do not couple back very strongly to the physically important quantities: $m_\Delta = \sqrt{\lambda_{0,1}}$ has only a deviation of about 5 MeV, this may very well be the difference of pole and screening mass.

1d Taylor expansion For the one-dimensional Taylor expansion of the effective potential (2.50) we have always $\lambda_{n,m} = \lambda_{n,0}$, so all equations with index $m > 0$ in (3.96) can be dropped out of the set. In the BEC phase we have $\dot{\lambda}_{1,0} = 0$ and $\lambda_{1,0} = 2\mu$ in addition to (3.98), since the mesonic parameters equally represent the diquark ones. In this case the grey lines should coincide with the red lines in Fig. 3.14, except of the violation that is introduced by the anomalous dimensions of baryonic quantities and running Yukawa couplings, which is only minor as we will see in Sec. 3.6. Eq. (3.97) now directly represents the flow of κ_ϕ for the BEC phase (as $\dot{\lambda}_{1,0} = 0$), which is vanishing if $\eta_\phi = 0$, because then c does not flow. So in that case the chiral condensate in the BEC phase is trivially given by Eq. (2.51) simply going like $1/\mu^4$, without any direct influence from the FRG.

Furthermore, in the BEC phase the equation for $(n, m) = (1, 0)$ will be replaced by the one with $(n, m) = (0, 1)$, which gives us the flow of κ_Δ . However, in order to have the onset of the diquark condensation for $T = 0$ at $\mu_c = \frac{m_\pi}{2}$ without violating the Silver Blaze property, the ρ_Δ -derivative of the loop contribution in (3.96) must be replaced by a ρ_ϕ -derivative. The reason is that during the vacuum flow $m_{\pi,vac} = \sqrt{\lambda_{1,0}}$ has a minimum $m_{\pi,vac,k_{min}}$, where it falls below $m_{\pi,vac,k=0}$. This is due to the interplay of fermionic and bosonic fluctuations. Now, if $2\mu > m_{\pi,vac,k_{min}}$ the system has to go into the BEC phase, where we have $m_\pi = 2\mu$ and a finite diquark condensate. Then if $2\mu < m_{\pi,vac,k=0}$ the system goes back to the normal phase, which is quite remarkable. The phenomenon is called *pre-condensation* and will be discussed in the next chapter again for finite temperatures. We have checked that only if the flow of the diquark condensate is projected via a ρ_ϕ -derivative, the points where $\kappa_\Delta = 0$ are exactly where $2\mu = m_{\pi,vac}$ as shown in Fig. 3.15(a) for LPA. After the system goes back to the normal phase m_π goes exactly to its vacuum value. This is only possible when the way of projection is the same in both phases. For LPA', shown in Fig. 3.15(b), we have a slight deviation due to the violation from the baryonic quantities mentioned above.

Actually, in LPA we only have the upper line of Eq. (3.96), and for the 1d Taylor expansion the coefficients of the condensates is simply $\lambda_{2,0}$ whether we project via $(n, m) = (1, 0)$ or $(0, 1)$. However we cannot simply use (1,0) for LPA' because the second line would be different. We have seen that this leads to a decreasing diquark condensate at very large chemical potentials, which is rather unphysical. In conclusion the flow of the diquark condensate is given by the equation

$$0 = \lambda_{2,0} (\dot{\kappa}_\phi + \dot{\kappa}_\Delta + \eta_\phi \kappa_\phi + \eta_\Delta \kappa_\Delta) + \frac{\partial}{\partial \rho_\phi} \dot{U} \Big|_{\substack{\text{loops} \\ \vec{\rho} = \vec{\kappa}}}, \quad (3.99)$$

By comparing the two figures in 3.15 we also see the impact of the anomalous dimension $\eta_\pi = \eta_\phi$. The Eqs. (3.96)-(3.97) can be solved for the flow of the pion mass, then we have a term $\eta_\pi m_\pi$ and the loop contributions. In Fig. 3.15(b) we see that the former part dominates the flow at small scales and still yields significant contributions at larger scales. Therefore it is important to take the anomalous dimensions into account, more details can be found in Sec. 3.6.1.

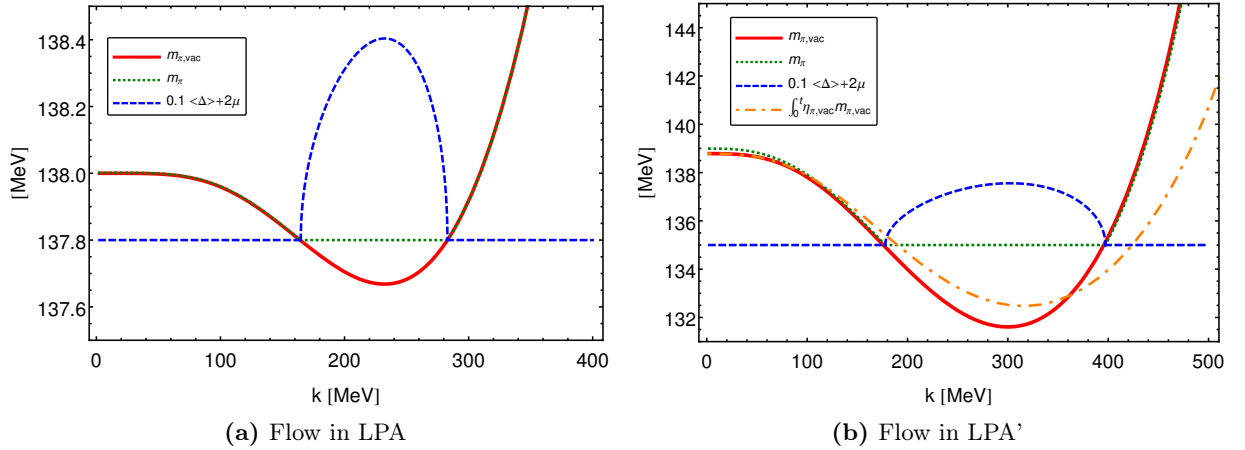


Figure 3.15: Flow of the pion mass and diquark condensate for $T = 0$ at $\mu = 0$ (vac) and $\mu = 0.4m_\pi$ with the different truncations. In the BEC phase the pion mass is given by $m_\pi = 2\mu$ which is the flat part of the dotted line. The behavior shows that the flow in the LPA below μ_c is essentially identical (almost identical in LPA') to the vacuum flow even if there is an intermediate diquark condensate. This only works if the loop contributions to the flow of the diquark condensate is projected out the same way as the flow of the pion mass. In order to put it in the figure we have scaled the diquark condensate and added 2μ . In (b) also the contribution from the anomalous dimension is shown. Note the different scales on the axes.

3.5 Vertices

In order to improve our truncation beyond the local potential approximation, we need to compute Feynman diagrams. Therefore, apart from the propagators, we need vertices as well. Unlike in perturbation theory, we have full vertices and full propagators instead of classical ones, which are determined by differentiating the quantum effective action. In principle all possible higher vertices are generated, which may not be present in the classical action, but preserve its symmetry. We are incorporating them in the bosonic potential up to a certain order by the Taylor expansion, corresponding to a vertex expansion. Moreover, one should introduce momentum as well as field-dependences of the vertices in order to improve the truncation. However, in this work we shall restrict ourselves to a scale dependence of the Yukawa couplings and wave function renormalizations for simplicity, while the running of the bosonic couplings is incorporated in the running of the effective potential. This has been successfully employed in studies of the quark-meson model in Refs. [171, 173, 178].

The flow of the Yukawa couplings and wave function renormalizations can be extracted from the flow of the two-point function, for which in general the three-point- as well four-point vertices are needed. However, we keep the four-fermi interaction bosonized, and the tadpole diagram in the bosonic anomalous dimensions drops out by the momentum derivative for the projection on the wave function renormalizations, since the external momentum does not go into the loop if the four-boson coupling is momentum independent. Thus we only need the three-point vertices. This section is more technical.

3.5.1 Three-Boson Vertex

A three-point function can be seen as a tensor with three indices in field space. We have a three-boson vertex which is proportional to powers of the expansion point. Since the structure of the expansion points (3.30) and (3.41) is very similar in both models, we have the same three-boson vertex for the QMD-model and the QMDB-model in the normal phase. The only difference is that the number of fields is extended in the QMDB-model and therefore the indices can have different maximum numbers $\dim(\varphi)$. We will only apply the three-boson vertex in the real representation of the diquark fields. For this calculation it is more convenient to carry it out in position space and do the Fourier transformation at the end. We essentially differentiate Eq. (3.32) without having the delta functions dropped

$$\begin{aligned} & \frac{\delta^3 \Gamma}{\delta \varphi_k(z) \delta \varphi_j(y) \delta \varphi_i(x)} \\ = & \left(\frac{\partial^2 \rho_l}{\partial \varphi_j \partial \varphi_i} \frac{\partial \rho_n}{\partial \varphi_k} \delta(z-x) + \frac{\partial^2 \rho_n}{\partial \varphi_k \partial \varphi_j} \frac{\partial \rho_l}{\partial \varphi_i} \delta(z-y) + \frac{\partial \rho_n}{\partial \varphi_j} \frac{\partial^2 \rho_l}{\partial \varphi_k \partial \varphi_i} \delta(z-x) \right) \frac{\partial^2 U}{\partial \rho_n \partial \rho_l} \delta(y-x) \\ & + \frac{\partial \rho_m}{\partial \varphi_k} \frac{\partial \rho_n}{\partial \varphi_j} \frac{\partial \rho_l}{\partial \varphi_i} \frac{\partial^3 U}{\partial \rho_m \partial \rho_n \partial \rho_l} \delta(z-x) \delta(y-x). \end{aligned}$$

Now we use that $\delta(z-y)\delta(y-x) = \delta(z-x)\delta(y-x)$ and evaluate the vertex at the expansion point

$$\begin{aligned} \left. \frac{\delta^3 \Gamma}{\delta \varphi_k(z) \delta \varphi_j(y) \delta \varphi_i(x)} \right|_{\varphi_0} &= \left[(Z_\phi \sigma \delta_{k4} + Z_\Delta \Delta \delta_{k5}) (Z_\phi \sigma \delta_{i4} + Z_\Delta \Delta \delta_{i5}) (Z_\phi \sigma \delta_{j4} + Z_\Delta \Delta \delta_{j5}) V_{ijk} \right. \\ & \quad + Z_j \delta_{ji} (Z_\phi \sigma V_{\phi j} \delta_{k4} + Z_\Delta \Delta V_{j\Delta} \delta_{k5}) + Z_k \delta_{kj} (Z_\phi \sigma V_{\phi k} \delta_{i4} + Z_\Delta \Delta V_{k\Delta} \delta_{i5}) \\ & \quad \left. + Z_i \delta_{ik} (Z_\phi \sigma V_{\phi i} \delta_{j4} + Z_\Delta \Delta V_{i\Delta} \delta_{j5}) \right] \delta(z-x) \delta(y-x) \\ &\equiv \Gamma_{\varphi_k \varphi_j \varphi_i} \delta(z-x) \delta(y-x). \end{aligned} \quad (3.100)$$

Note that the fist line corresponds to the last line in the previous equation. Apart from the Kronecker delta, we apply the convention that the index is set to ϕ if it corresponds to a mesonic field, and to Δ if it corresponds to diquark field in φ . Accordingly V_{ijk} , where the indices denote ρ -derivatives, can either have three derivatives with respect to one species or two with respect to one and one with respect to the other. However, in this work this particular part of the vertex will not arise anywhere else. Now it is apparent that extending the model with red and green diquarks only extends the maximum range of the indices and nothing more. The momentum representation of this vertex can be found straightforwardly. With the relation between the field and its Fourier transform $\frac{\delta \varphi_i(x)}{\delta \varphi_j(p)} = e^{ipx} \delta_{ij}$, we find

$$\begin{aligned} \frac{\delta^3 \Gamma}{\delta \varphi_k(p) \delta \varphi_j(p') \delta \varphi_i(q)} &= \int_{x,y,z} e^{i(px+p'y+qz)} \frac{\delta^3 \Gamma}{\delta \varphi_k(z) \delta \varphi_j(y) \delta \varphi_i(x)} \\ &= \Gamma_{\varphi_k \varphi_j \varphi_i} \int_x e^{i(p+p'+q)x} \\ &= \Gamma_{\varphi_k \varphi_j \varphi_i} \delta(p+p'+q). \end{aligned} \quad (3.101)$$

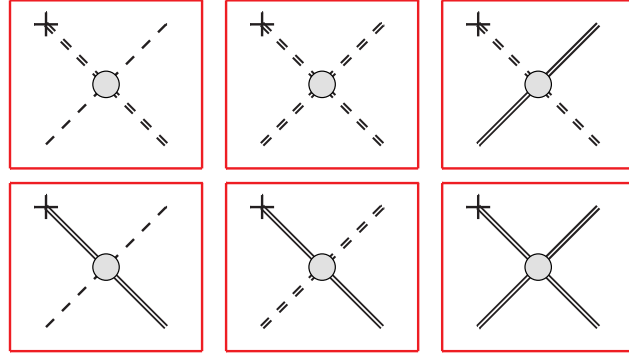


Figure 3.16: These are the three boson vertices that we are going to need. The cross denotes the mesonic and diquark background fields. The diquark line does not have an arrow since in the real representation, as they represent a superposition of both charges.

So essentially only the delta functions were transformed. We see that we can only have a three-boson vertex at finite background fields or condensates, where at least one radial mode must be involved in the interaction. Effectively such a process corresponds to four-point (six-point) interaction, where the forth (fifth and sixth) particle is connected to the background as it is pictorially shown in Fig. 3.16.

3.5.2 Three-Point Vertices with Fermions

Before we compute the three-point vertices of the fermions, we apply the Fourier transformation (3.13) to a three-point interaction term in the effective action

$$\begin{aligned} \int_x \Phi_i(x) \Phi_j(x) \Phi_k(x) &= \int_{p,p',q} \Phi_i(p) \Phi_j(p') \Phi_k(q) \int_x e^{-i(p+p'+q)x} \\ &= \int_{p,p',q} \Phi_i(p) \Phi_j(p') \Phi_k(q) \delta(p+p'+q) \end{aligned}$$

The three-point vertices involving fermions that we have in the QMD-model, are the ones with the Yukawa coupling, which induce interactions between fermions and mesons or diquarks. Differentiating the effective action with respect $\bar{\Psi}(p)$ and $\Psi(p')$ yields the two-point function of which only the interaction terms are

$$\left. \frac{\overrightarrow{\delta}}{\delta \bar{\Psi}(p)} \Gamma \frac{\overleftarrow{\delta}}{\delta \Psi(p')} \right|_{\text{int}} = \int_q \delta(p+q+p') Z_q \begin{pmatrix} i\sqrt{Z_\phi} h_\phi (\sigma + i\gamma_5 \vec{\tau} \cdot \vec{\pi}) & -\sqrt{2Z_\Delta} h_\Delta \Delta \gamma_5 \\ -\sqrt{2Z_\Delta} h_\Delta \Delta^* \gamma_5 & i\sqrt{Z_\phi} h_\phi (\sigma - i\gamma_5 \vec{\tau} \cdot \vec{\pi}) \end{pmatrix} (q) \quad (3.102)$$

The argument to the right of in the matrix indicates that all fields carry the momentum q . Now, differentiating with respect to any bosonic field with the argument q' leaves the corresponding coupling with a tensor structure and a delta function $\delta(p+q'+p')$ ensuring momentum conservation at the vertices. It is irrelevant from which side we let the bosonic derivative act, we will just put the index in between the fermionic ones. The vertices read (delta functions are omitted)

$$\begin{aligned}
 \Gamma_{\bar{\Psi}\sigma\Psi} &= \sqrt{Z_\phi} Z_q i h_\phi \mathbb{1} & \Gamma_{\bar{\Psi}\pi_i\Psi} &= \sqrt{Z_\phi} Z_q h_\phi \begin{pmatrix} -\gamma_5 \tau_i & 0 \\ 0 & \gamma_5 \tau_i \end{pmatrix} \\
 \Gamma_{\bar{\Psi}\Delta\Psi} &= \sqrt{2Z_\Delta} Z_q h_\Delta \begin{pmatrix} 0 & -\gamma_5 \\ 0 & 0 \end{pmatrix} & \Gamma_{\bar{\Psi}\Delta_1\Psi} &= \sqrt{Z_\Delta} Z_q h_\Delta \begin{pmatrix} 0 & -\gamma_5 \\ -\gamma_5 & 0 \end{pmatrix} \\
 \Gamma_{\bar{\Psi}\Delta^*\Psi} &= \sqrt{2Z_\Delta} Z_q h_\Delta \begin{pmatrix} 0 & 0 \\ -\gamma_5 & 0 \end{pmatrix} & \Gamma_{\bar{\Psi}\Delta_2\Psi} &= \sqrt{Z_\Delta} Z_q h_\Delta \begin{pmatrix} 0 & -i\gamma_5 \\ i\gamma_5 & 0 \end{pmatrix}
 \end{aligned} \tag{3.103}$$

The unit matrix $\mathbb{1} = \mathbb{1}_c \times \mathbb{1}_f \times \mathbb{1}_D$ is composed of a tensor product of unit matrices in color, flavor and Dirac space. If there is no tensor structure regarding a particular space, an identity matrix is implied. In the upper line the mesonic vertices are displayed. In the lower left column we see the diquark vertices in the complex representation, while in the right column we see them in the real representation. The factor in the front naturally differs by a $\sqrt{2}$ due to Eq.(2.47), which is compensated by the extra nonzero component in real representation. The fact that mesonic vertices are diagonal in contrast to the diquark vertices, simply reflects the fact that the mesons couples to pairs of quark-antiquark field, while in the quark-diquark interaction there is a directional flow of net baryon number, see Fig. 3.17. Furthermore we can see that a small wave function renormalization leads to a small vertex amplitude, which is quite natural since the corresponding field must be decoupling from the system. These vertices are embedded in the QMDB-model as well, which are shown explicitly in App. B.2. The pictorial representation of the baryon vertices is shown in Fig. 3.17.

Note that if the fermionic indices are the other way around, a minus sign appears, more generally $\Gamma_{\bar{\Psi}\varphi_i\Psi} = -\Gamma_{\Psi\varphi_i\bar{\Psi}}^T$. This is accounted for by transposing the term in the effective action by which a fermionic interchange takes place, before taking the derivative.

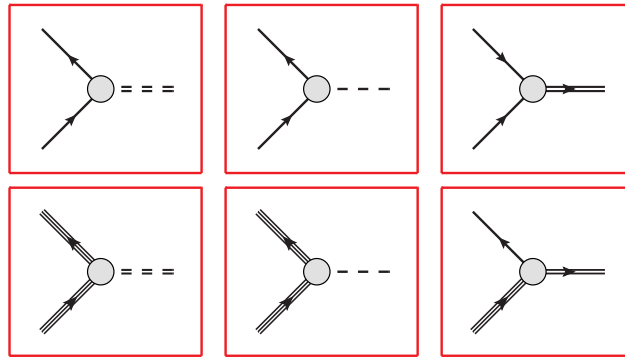


Figure 3.17: In the upper line we have the Yukawa interactions with sigma, pion and diquark fields and in the lower line we see the baryon vertices. The baryon-meson interactions is analog to the quark-meson one. On the right we see the quark-diquark-baryon vertex. Here all lines correspond to the original representation of the fields as they were written in the action (2.35) and (2.36). Note the different arrows indicating the flow of the baryon number.

3.6 Flow of the Two-Point Function

Let us derive a general equation for the flow of a two-point function, starting with

$$\partial_t \Gamma[\Phi] = \frac{1}{2} \text{STr} \frac{1}{\Gamma^{(2)}[\Phi] + R} \partial_t R = \frac{1}{2} \text{STr} \tilde{\partial}_t \ln \left(\Gamma^{(2)}[\Phi] + R \right), \quad (3.104)$$

where Φ is a general multicomponent field, as introduced in the beginning of this chapter. We use the formal scale derivative $\tilde{\partial}_t$ which only acts on R , and rewrite the one-loop form of the flow equation as

$$\begin{aligned} \tilde{\partial}_t \ln \left(\Gamma^{(2)}[\Phi] + R \right) &= \tilde{\partial}_t \ln \left(\Gamma^{(2)}[\Phi_0] + R + \Delta \Gamma^{(2)}[\Phi - \Phi_0] \right) \\ &= \tilde{\partial}_t \ln \left(\Gamma^{(2)}[\Phi_0] + R \right) + \tilde{\partial}_t \ln \left[1 + \left(\Gamma^{(2)}[\Phi_0] + R \right)^{-1} \Delta \Gamma^{(2)}[\Phi - \Phi_0] \right], \end{aligned}$$

where $G^{-1} = \Gamma^{(2)}[\Phi_0] + R$ is independent of the fluctuating fields, so the first term does not survive any projection. For the second part we use $\ln(1+x) = x - \frac{1}{2}x^2 + \mathcal{O}(x^3)$. Only the second order term survives the projection to the flow of a two-point function

$$\frac{\overrightarrow{\delta}}{\delta \Phi_i(-p)} \partial_t \Gamma[\Phi] \frac{\overleftarrow{\delta}}{\delta \Phi_j(p')} = \frac{1}{2} \frac{\overrightarrow{\delta}}{\delta \Phi_i(-p)} \frac{-1}{2} \text{STr} \left[\tilde{\partial}_t \left(G \Delta \Gamma^{(2)} \right)^2 \right] \frac{\overleftarrow{\delta}}{\delta \Phi_j(p')}. \quad (3.105)$$

We can already set p' to zero, p will be set to zero after differentiation for the case of obtaining the flow of the kinetic term. For the derivative of $\Delta \Gamma^{(2)}$ we now introduce the notation $\Gamma_{\Phi_i}^{(3)} \triangleq \Gamma_{\Phi_n \Phi_i \Phi_m}$, which has the dimensions of a matrix. The middle index, which will not be summed over, denotes the external derivative. After differentiation we find two different terms, where the external fields are interchanged with a possible minus sign for the case of fermionic derivatives, defined in Eq. (3.16)

$$\begin{aligned} \dot{\Gamma}_{\Phi_i \Phi_j}(-p, p') \Big|_{\Phi=\Phi_0} &= -\frac{1}{4} \tilde{\partial}_t \text{str} \int_{q,s,t,v} \left[G(q, -s) \Gamma_{\Phi_i}^{(3)}(-s, -p, t) G(t, -v) \Gamma_{\Phi_j}^{(3)}(-v, p', q) \right. \\ &\quad \left. + (-1)^{ij} G(q, -s) \Gamma_{\Phi_j}^{(3)}(-s, p', t) G(t, -v) \Gamma_{\Phi_i}^{(3)}(-v, -p, q) \right] \Big|_{\Phi=\Phi_0}. \end{aligned}$$

The derivative operator always passes through twice the same index, except for the first one on the leftmost or rightmost side. The possible minus signs emerging from those cancel each other, if both derivatives are fermionic or bosonic, which is usually the case. So the only possible minus sign is in the lower line where the derivatives pass each other. We have omitted the four-point interactions, since they will not contribute to the flows of Yukawa couplings and wave function renormalizations. A momentum-independent four-point coupling drops out after differentiation with respect to the momentum. Solving the momentum structure for momentum-independent couplings yields

$$\begin{aligned} &\dot{\Gamma}_{\Phi_i \Phi_j}(p) \delta(p - p') \\ &= -\frac{1}{4} \tilde{\partial}_t \text{str} \int_{q,s,t,v} \left[G(q) \delta(q - s) \Gamma_{\Phi_i}^{(3)} \delta(-s - p + t) G(t) \delta(t - v) \Gamma_{\Phi_j}^{(3)} \delta(-v + p' + q) \right. \\ &\quad \left. + (-1)^{ij} G(q) \delta(q - s) \Gamma_{\Phi_j}^{(3)} \delta(-s + p' + t) G(t) \delta(t - v) \Gamma_{\Phi_i}^{(3)} \delta(-v - p + q) \right] \\ &= -\frac{1}{4} \tilde{\partial}_t \text{str} \int_q G(q) \left[\Gamma_{\Phi_i}^{(3)} G(q + p) \Gamma_{\Phi_j}^{(3)} + (-1)^{ij} \Gamma_{\Phi_j}^{(3)} G(q - p) \Gamma_{\Phi_i}^{(3)} \right] \delta(p - p'). \quad (3.106) \end{aligned}$$

Here the vertex functions are evaluated at the expansion point Φ_0 and the delta functions are excluded, as denoted by the missing arguments. The str operator acts in all spaces except for momentum space. By choosing specific fields, the left-hand side is projected on the scale derivative of the corresponding inverse propagator, while the right hand side represent its β -function. In particular we will apply momentum derivations on the above equation in order to project on the kinetic part and obtain the flow of wave function renormalizations. Furthermore we will use it for obtaining the flow Yukawa couplings, since they appear in the gaps of the fermion propagator. More details will be delivered in the following subsections.

Considering the momentum dependence n-point functions requires high numerical effort, this will not be a subject of this work. For the mesonic two-point function it has been done in [180] for finite temperature, where it was shown that that there is only a mild momentum dependence. For the fermionic two-point and four-point functions it was done in [186], where the RG flow in the vacuum starting from classical QCD was studied without tuning low energy parameters. Furthermore in [179] the effects of a scale and field dependent Yukawa coupling in a low energy quark-meson model for finite temperature and chemical potential were tested, where some quantitative effects were observed. In [185] the same was studied for the vacuum starting from classical QCD. Here, we are going to allow for a simple scale dependence of the two-point functions by running wave function renormalization and running Yukawa coupling without any further dependencies. For the diquark and baryon sector it has not been done before.

In the QMDB-model in the presence of a diquark background field the color symmetry is broken, therefore in principle we must distinguish between the red-green sector and blue sector of quarks and diquarks, meaning that we must introduce separate coupling constants and anomalous dimensions. However we are going to neglect the discrepancy in this work for simplicity and compute only the flow of the red-green parameters and associate them to all colors.

In the following we will turn to the anomalous dimensions. There are two conventional ways of introducing the wave function renormalizations in an RG framework: Either as a non trivial running of the kinetic term or as field strength renormalization of the fluctuating fields. Employing the former way implies that a small wave function renormalizations entails an non-propagating mode. Therefore a decrease of Z with rising k leads to reduction of the flow by the anomalous dimensions as it can be seen in Eq. (3.82). Employing the latter way leads to the interpretation that if the renormalized quantum fields are small, the quantum fluctuations of the associated particles must be small as well. The consequence for Eq. (3.82) is the same. Moreover the vertex functions are reduced as it can be seen in Sec. 3.5. Hence, both descriptions are equivalent which also can be shown by a rescaling of the parameters. The anomalous dimensions do not appear in the thermal distribution functions, since ordinary thermal excitations are not directly affected by the field renormalization. At finite temperature Lorentz symmetry is broken, therefore the time-like part of the kinetic term should be renormalized independently by a wave function renormalization conventionally denoted as Z^\parallel , indicating that it is parallel to the heat bath. However, in the UV and more specifically at $T/k < 1$, the flow is only weakly affected by the heat bath. On the other hand for $T/k \gg 1$ all nonzero Matsubara modes decouple from the system. Hence only in the critical regime Z^\parallel could have a measurable impact, which we are going to neglect here by setting $Z^\parallel = Z$. We mention that in general the anomalous dimensions depend on each other and therefore they constitute a system of linear equations, which should be solved before plugging them into the flow equations. Furthermore, we remark that in our approach the flow of bosonic masses do not need to be computed via the two-point function, since they are part of the effective potential, which has its own flow equation.

3.6.1 Bosonic Anomalous Dimensions

Before turning to the actual flow equation that we will compute, we would like to make some general remarks. The wave function renormalization are in general momentum dependent functions like for the diquark $Z_\Delta(\vec{p}^2 + (p_4 - i\mu_\Delta)^2)$ at $T = 0$, where μ_Δ is diquark chemical potential. Then the projection onto kinetic term looks the following way

$$\frac{\partial}{\partial \vec{p}^2} \dot{Z}_\Delta \left(\vec{p}^2 + (p_4 - i\mu_\Delta)^2 \right) \left(\vec{p}^2 + (p_4 - i\mu_\Delta)^2 \right) \Big|_{p=0} = \dot{Z}_\Delta(-\mu_\Delta^2) - \dot{Z}'_\Delta(-\mu_\Delta^2) \mu_\Delta^2 ,$$

where we assumed that the field derivatives with respect to Δ and Δ^* were already taken. For a nonzero baryon charge we obtain a trivial dependence on the chemical potential on the left-hand side of the flow equation by projecting it onto a vanishing momentum. Even if we do not write a momentum dependence in Z_Δ the right-hand side of the flow equation will yield the corresponding contributions nonetheless. In order to avoid the flow of Z'_Δ it is important to go into the real representation of the diquark field, where μ only couples off-diagonally to Δ_1 and Δ_2 as it can be seen in Eq. (3.34). Thus, taking two derivatives with respect to one of these fields will drop the chemical potential term.

There is a similar problem at finite values of the field as was shown in [179]. In general there must be a field dependence in the wave function renormalizations generated by the RG-flow. Consider the mesonic case: Although the mesons are $O(4)$ symmetric a non-symmetric expansion points leads to different projections

$$\begin{aligned} \frac{\partial^2}{\partial \pi_i^2} \frac{\dot{Z}_\phi(\phi^2)}{2} (\phi^2 - \phi_0^2) \Big|_{\phi^2=\phi_0^2} &= \dot{Z}_\phi(\phi_0^2) \\ \frac{\partial^2}{\partial \sigma} \frac{\dot{Z}_\phi(\phi^2)}{2} (\phi^2 - \phi_0^2) \Big|_{\phi^2=\phi_0^2} &= \dot{Z}_\phi(\phi_0^2) + 4\phi_0^2 \dot{Z}'_\phi(\phi_0^2) \end{aligned} \quad (3.107)$$

where the momentum derivative was already taken. Here the index i is not summed over. We have added an irrelevant term with the constant expansion point $\phi_0 = (\vec{0}, \sigma)$. Thus, we obtain again additional contributions to the right-hand side of flow by projecting onto the radial mode, even if we do not consider a field dependence in the wave function renormalization. The flow of such additional term has been studied in [180]. In order to avoid the flow of Z'_ϕ we must employ a projection by the Goldstone mode. For the diquarks the imaginary part Δ_2 is the Goldstone mode.

From Eq. (3.34) and (3.35) we see that we can make a projection onto the bosonic anomalous dimensions by taking a derivative of the corresponding part in Eq. (3.106) with respect to the space-like momentum, as Lorentz symmetry is broken at finite temperature, in the following way

$$\begin{aligned} \eta_{\varphi_i} &= -\frac{1}{Z_{\varphi_i}} \frac{\partial}{\partial \vec{p}^2} \dot{\Gamma}_{\varphi_i \varphi_i} \Big|_{p=0} \\ &= \frac{1}{4Z_{\varphi_i}} \frac{\partial}{\partial \vec{p}^2} \tilde{\partial}_t \text{str} \int_q G(q) \Gamma_{\varphi_i}^{(3)} [G(q+p) + G(q-p)] \Gamma_{\varphi_i}^{(3)} \Big|_{p=0} \\ &= \frac{1}{2Z_{\varphi_i}} \tilde{\partial}_t \frac{\partial}{\partial \vec{p}^2} \text{str} \int_q G(q) \Gamma_{\varphi_i}^{(3)} G(q+p) \Gamma_{\varphi_i}^{(3)} \Big|_{p=0}, \end{aligned} \quad (3.108)$$

where the definition in Eq. (3.21) was used. In the second term of the second line we have shifted the momentum integration variable $q \rightarrow q + p$ and used the cyclic property of the trace, however this has to be done carefully, as we are dealing with a supertrace, which gives a minus

$$\eta_\phi = \frac{1}{Z_\phi} \tilde{\partial}_t \frac{\partial}{\partial \vec{p}^2} \left[\begin{array}{c} \text{Bosonic diagrams} \\ -\text{tr} \left(\text{Fermionic diagrams} \right) \end{array} \right]_{p=0}$$

Figure 3.18: Diagrammatic equation for the mesonic anomalous dimension after dissolving the str. In the upper line we see the bosonic contributions, and in lower line the fermionic ones. Although they have a negative sign, the contribution is not necessarily negative due to the complex valued and tensor structured quark vertices (3.103). The external momentum p in each loop runs through one of the propagators; which one is irrelevant since the integration variable can be shifted, hence the cancellation of the factor 2 in (3.108). The scale- and momentum derivatives lead to more propagators inside the loop as well as a regulator insertion cutting off the loop integration. At high energies the background fields are typically small or vanishing, so all diagrams with crosses do not contribute, which leaves only one fermion loop. The diagrams with the diquark background fields naturally contribute only in the BEC phase.

sign if the indices, which are summed over by the trace, are fermionic. A cyclic permutation can move the outer fermionic indices away and then have bosonic ones instead. However, for the bosonic anomalous dimension, we do not have any diagrams, where fermionic and bosonic propagators are mixed, therefore, if fermionic indices are moved away, they will only be replaced by other fermionic ones, so the minus sign will still be there. This equations will be solved for the Goldstone modes $\varphi_1 = \pi_1$ and $\varphi_6 = \Delta_2$. The explicit computation can be found in App. C.1. Interestingly, if we set the external time-like component of the momentum to the imaginary chemical potential $p_4 = i\mu$ for $\rho_\Delta = 0$ at vanishing temperature und below μ_c for the diquark anomalous dimension we obtain $\eta_\Delta = \eta_\phi$ for two color QCD. This way, we can ensure the Silver Blaze property For $\mu = 0$ they must coincide anyway due the $SO(6)$ symmetry, even at nonvanishing temperature.

The bosonic anomalous dimension receive contributions from a fermion loop and a bosons loop, which is exemplary shown in Fig. 3.18. Since the bosonic three-point vertex is proportional to the condensates, there are only contributions in the broken phases. As chiral symmetry is explicitly broken, there is always a finite contribution, which is small at large scales and temperatures, due to the decoupling of bosons. In the UV we typically start with small bosonic wave function renormalizations. Here the fermion loop is the main and a powerful drive for its flow. They rise up until the critical scale, which leads to nonzero values of the anomalous dimensions reducing the bosonic contribution in Eq. (3.82), and enhancing the symmetry breaking. This in turn means that the curvature of U flattens out faster and bosonic contribution become stronger. Altogether the flow around the critical region becomes more turbulent. However, in total the fermionic contribution is larger, since the bosons set in only around the critical scale. In order to avoid that the fermions overly flatten the effective potential, its curvature has to be chosen larger in the UV. This leads us to the inference that the bosons decouple much stronger in the UV, by the inclusion of anomalous dimensions, which was also concluded from Eq. (3.85).

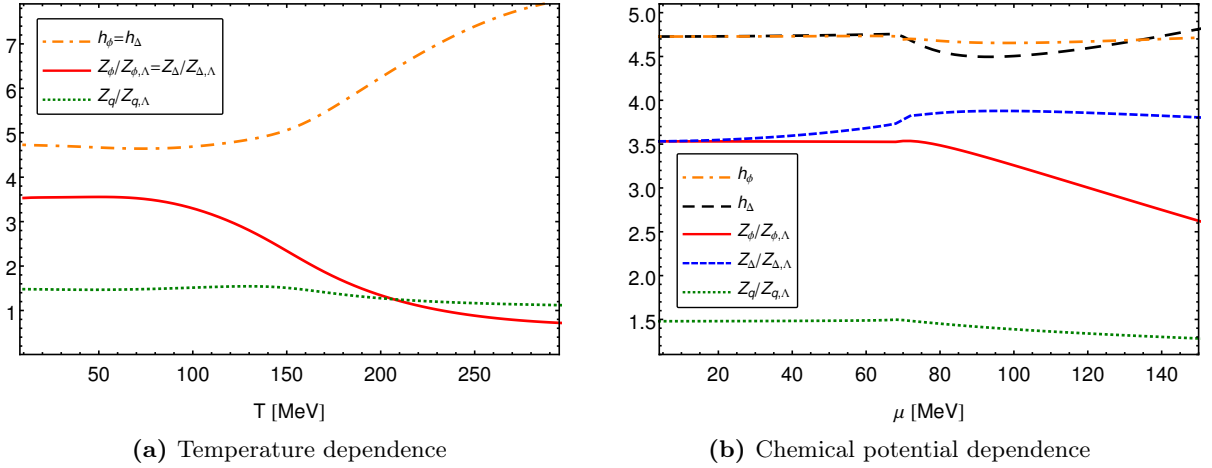


Figure 3.19: The dimensionless parameters in our truncation for two-color QCD with the 2d Taylor' truncation, c.f. Tab. 4.1, for $\mu = 0$ (a) and $T = 0$ (b). The wave function renormalizations are normalized to their initial values in the UV. The explanations of each parameter can be found in the respective subsections.

In Fig 3.19 the temperature/chemical potential dependence of the wave function renormalizations are shown. As fermionic fluctuations are suppressed at high temperatures, the wave function renormalizations stay small and the effects of the anomalous dimensions are suppressed as well. At large chemical potentials only the mesonic one becomes smaller. Regarding the Silver Blaze property, we see visible effects of the chemical potential for the diquark anomalous dimension below $\mu_c = m_\pi/2$. Since it is a baryonic quantity, μ cannot be shifted away in the integral as opposed to the mesonic case. We see in the figure that Z_Δ has the strongest μ dependence, which is due to the fact that it runs with a pure quark loop. However, we have seen in the flow of the mass parameter for the 1d Taylor expansion in Fig. 3.15(b) that there is only a minor back coupling to effective potential.

3.6.2 Fermionic Anomalous Dimensions

Quarks

From Eq. (3.50) it is easy to see that the kinetic part of the Γ_{quark} in momentum space is given by $\int_p' Z_q \bar{\Psi}(-p') \not{p}' \Psi(p')$, so we can project the flow equation onto the quark wave function renormalization by taking derivatives of the flow equation with respect to the quark fields $\bar{\Psi}(-q)$ and $\Psi(p)$ and with respect to the absolute value of the momentum, after multiplying a unit vector in the momentum direction. Then contracting all fermionic indices with a $\vec{\gamma}$, in order to avoid a zero from the trace, leads to the following equation for the QMD-model:

$$4N_f N_c \partial_t Z_q = \Re \frac{\partial}{\partial |\vec{p}|} \text{tr} \left(\hat{\vec{p}} \hat{\Gamma}_{\bar{\Psi}\Psi} \right) \Big|_{p=p_{\min}}, \quad (3.109)$$

where the fermionic part of Eq. (3.106) was taken and $\hat{\vec{p}} = \frac{\vec{p}}{|\vec{p}|}$. Here the trace acts in all fermionic subspaces, i.e. color-space, spinor-space and flavor space, thus the factors N_c and N_f on the left-hand side. The numerical factor originates from the spinor space

$$\frac{\partial}{\partial|\vec{p}|} \text{tr} \hat{\vec{p}} \vec{p} = \frac{\partial}{\partial|\vec{p}|} \frac{p_i p_j}{|\vec{p}|} \text{tr} \gamma_i \gamma_j = \frac{\partial}{\partial|\vec{p}|} \frac{p_i p_j}{|\vec{p}|} 4\delta_{ij} = 4 \frac{\partial}{\partial|\vec{p}|} |\vec{p}| = 4, \quad (3.110)$$

where the index i represents the space-like components $i = 1, 2, 3$ and is summed over. The time-like component is left out, since at finite temperature Lorentz symmetry is broken. The external momentum in Eq. (3.109) is set to the minimum value. If the external legs of a diagram are fermionic, the minimal incoming momentum is $p_{\min} = (\pi T, \vec{0})$ at finite temperature, where the time-like component is given by the lowest fermionic Matsubara frequency. Here the contributing fluctuations are given by a self energy type loop diagram with a bosonic and a fermionic propagator, hence, momentum conservation at the vertex implies that one of the propagators carries on a fermionic Matsubara frequency, depending on which one carries the external momentum. However, by shifting the loop integration of the frequencies by πT , we can always achieve that the fermionic propagator carries on the fermionic Matsubara frequency, which is more convenient.

Similar to the bosonic case, considering the momentum dependence of the wave function renormalization as $Z_q(\vec{p}^2, (p_4 - i\mu)^2)$ leads to an additional term on left-hand side $\propto \dot{Z}'_q \vec{p}^2$ at finite external momentum, whereas at p_{\min} a dependence in Eq. (3.109) remains as $Z_q((\pi T - i\mu)^2)$. Here we see that the fermionic wave function renormalization, and generally the fermionic n-point functions, become manifestly complex at finite temperatures. This is expected by an extrapolation of the Silver Blaze property, where at $T = 0$ we have the same problem for finite external p_4 . Although we do not consider a momentum dependence, the complex parts are generated by the RG-flow nevertheless, therefore it is important to project out the real part of the flow equation in our scheme, in order to keep the action real valued. If indeed one would solve the momentum structure, the action becomes real valued by virtue of the p_4 -integration, even if the couplings are not, similar to the kinetic term. Plugging in the corresponding part of Eq. (3.106) into Eq. (3.109) the quark anomalous dimension is given by

$$\eta_q = \frac{1}{16N_f N_c Z_q} \Re \tilde{\partial}_t \frac{\partial}{\partial|\vec{p}|} \vec{p} \cdot \vec{\gamma}_{\alpha\beta} \text{str} \int_q G(q) \left[\Gamma_{\vec{\Psi}_\beta}^{(3)} G(q+p) \Gamma_{\Psi_\alpha}^{(3)} - \Gamma_{\Psi_\alpha}^{(3)} G(q-p) \Gamma_{\vec{\Psi}_\beta}^{(3)} \right] \Big|_{p=p_{\min}} \quad (3.111)$$

where again the definition (3.21) was applied. The minus sign in the middle is due to the interchange of the external fermionic derivatives. After the supertrace is dissolved, we obtain a matrix in fermion space, due to the external derivatives, which then is contracted with $\vec{\gamma}$. The notation is a bit sloppy, since α and β represent all fermionic subspaces, where it is implied that $\vec{\gamma}$ has a trivial structure in color and flavor space. We cannot summarize the two terms under the integral as for the bosonic case, since we have mixed loops with bosonic and fermionic propagators, and therefore shifting the terms might jeopardize the minus sign of the supertrace. However, after it is dissolved, the terms can be summarized, which is shown in App. C.2 as well as the rest of the computation. It is done in complex representation of the diquark field, for this way mixing terms can be avoided.

As we see in Fig. 3.19 the quark anomalous dimension stays small because its flow is suppressed either by boson masses in the symmetric regime or by the quark mass in the broken regime. Hence only at the critical regime we have some measurable contributions. Therefore we do not see a large violation of the Silver Blaze property either. At large T and μ the meson anomalous dimension is smaller. The flow of Z_q is reduced by η_ϕ (see. Eq.(C.11)), which stays small at large T and μ . Thus, even if the mesons are heavier there is still a running of Z_q and therefore it stays rather flat. Only at the critical temperature, where all masses are more or less light, a slight peak can be seen.

$$\eta_q = \frac{1}{4N_f N_c Z_q} \Re \tilde{\partial}_t \frac{\partial}{\partial |\vec{p}|} \text{tr} \hat{\vec{p}} \left(3 \begin{array}{c} \text{---} \text{---} \text{---} \\ \text{---} \text{---} \text{---} \end{array} + \begin{array}{c} \text{---} \text{---} \text{---} \\ \text{---} \text{---} \text{---} \end{array} + \begin{array}{c} \text{---} \text{---} \text{---} \\ \text{---} \text{---} \text{---} \end{array} \right) \Big|_{p=p_{\min}}$$

Figure 3.20: Diagrammatic equation for the quark anomalous dimension, after dissolving the str. A trace operation in the fermionic space is left, after which the factors of degeneracy cancel out. Moreover, we have a multiplicity of 4 since the external legs can be interchanged and the external momentum can be carried either by the quark or by the boson. Note that only the part of the quark propagator disconnected from the background is projected out, which is $\propto \vec{q}_r$ or $\propto (\vec{q} \pm \vec{p})_r$. Due to a missing factor of 2, the degeneracy of pions and diquarks in QC₂D may not be apparent. The factor is included in the definition of the complex diquark vertices (3.103).

Baryons

It is important to incorporate a running wave function renormalization for the baryons in the QMDB-model in order to have the correct decoupling behavior towards the UV. This will be more clear in the next subsection when we look at the baryon mass. The flow equation is projected out similar to Eq. (3.109) with an additional projection operator extracting the baryonic component in Nambu-Gorkov space

$$4N_f \partial_t Z_B = \Re \frac{\partial}{\partial |\vec{p}|} \text{tr} \left(\hat{\vec{p}} \hat{P}_B \dot{\Gamma}_{\Psi\Psi} \right) \Big|_{p=p_{\min}} \quad \text{with} \quad \hat{P}_B = \begin{pmatrix} 0 & 0 & 0 & 0 \\ 0 & 0 & 0 & 0 \\ 0 & 0 & 0 & 0 \\ 0 & 0 & 0 & 1 \end{pmatrix}. \quad (3.112)$$

Naturally there is no color factor for the baryons. The previous discussion applies here in the same way. In Fig. (3.21) we see the contributions to the corresponding anomalous dimension in diagrammatic form, the explicit equation is given in App. C.2. Since the at least one of the propagators in the loop, always has a large mass gap, our numerical computation did not show a substantial running of Z_B .

$$\eta_B = \frac{1}{4N_f Z_B} \Re \tilde{\partial}_t \frac{\partial}{\partial |\vec{p}|} \text{tr} \hat{\vec{p}} \left(3 \begin{array}{c} \text{---} \text{---} \text{---} \\ \text{---} \text{---} \text{---} \end{array} + \begin{array}{c} \text{---} \text{---} \text{---} \\ \text{---} \text{---} \text{---} \end{array} + N_c \begin{array}{c} \text{---} \text{---} \text{---} \\ \text{---} \text{---} \text{---} \end{array} \right) \Big|_{p=p_{\min}}$$

Figure 3.21: Diagrammatic equation for the baryon anomalous dimension in the normal phase, which is analogous to Fig. 3.20. Here, the trace acts in the baryonic subspace. The quark-diquark contribution has a degeneracy of N_c counting each color.

3.6.3 Baryon UV Mass Gap

Here we are going to see how the baryons of QCD decouple at high energies. We need to compute the flow equation for the UV-mass gap parameter. The projection is done similar as for the baryonic wave function renormalization only without the momentum derivative

$$4N_f \partial_t (Z_B m_B^{\text{UV}}) = \Re \text{tr} \left(\hat{\vec{p}} \hat{P}_B \dot{\Gamma}_{\bar{\Psi}\Psi} \right) \Big|_{p=p_{\min}} \quad (3.113)$$

The factor in the front is the same as before, however it originates from a different way: $\text{tr} \hat{\vec{p}} \hat{\vec{p}} = \frac{p_i p_j}{p^2} 4\delta_{ij} = 4$. On the left-hand side the scale derivative also acts on the wave function renormalization, therefore we obtain two terms by the product rule. Then dividing the equations by Z_B and solving for the flow of the mass gap yields

$$\partial_t m_B^{\text{UV}} = \eta_B m_B^{\text{UV}} + \frac{1}{4N_f Z_B} \Re \text{tr} \left(\hat{\vec{p}} \hat{P}_B \dot{\Gamma}_{\bar{\Psi}\Psi} \right) \Big|_{p=p_{\min}}. \quad (3.114)$$

We have a trivial running of the mass gap with the anomalous dimension, which is very important. If we had a strong running of Z_B implying a large η_B , the first term would be the strongly dominating one, especially because it is self-enhancing, whereas the diagrams are subleading, see Fig 3.22. In fact the loop contributions are negative and should just give a very little inhibition to the flow. The leading term should be responsible for the rise of mass gap towards the UV and thus for the decoupling of the baryons. Then, if the baryons are heavy the loop diagrams cease to contribute, however as long as η_B is finite the self-enhancement stands. Anyway, our model is valid only up the cutoff $\Lambda \approx 1$ GeV, above which gluon dynamics must be included. The explicit flow equation can be found in App. C.3. However, unfortunately η_B always remains small, as we have indicated above, so if m_B^{UV} is large in the UV it remains large. Thus the baryons cannot be included in our FRG framework yet.

$$\partial_t m_B^{\text{UV}} = \eta_B m_B^{\text{UV}} + \frac{1}{4N_f Z_B} \Re \tilde{\partial}_t \text{tr} \hat{\vec{p}} \left(3 \text{ (diagram 1)} + \text{ (diagram 2)} + N_c \text{ (diagram 3)} \right) \Big|_{p=p_{\min}}$$

Figure 3.22: Diagrammatic equation for the baryon UV - mass gap in the normal phase, which is analogous to Fig. 3.21. The trivial running with the anomalous dimension should be the dominating contribution and leads to a strong rise of m_B^{UV} towards the UV.

3.6.4 Yukawa Couplings

Although the Yukawa couplings are associated with three-point interactions, we can compute their flows from self-energy type diagrams. This is also connected to the fact that the Yukawa couplings are part of the gaps in the quark propagator. To that end, we must consider the expansion point φ_0 as a variable such that $\partial_t \varphi_0 = 0$, and set it to the running minimum after the projection procedure, similar as for the flow of the bosonic couplings in Sec. 3.4.3. From Eq. (3.102) we can see how to obtain the projection onto the Yukawa couplings

$$4N_f N_c i\sigma \partial_t \left(Z_q \sqrt{Z_\phi} h_\phi \right) = \Im \operatorname{tr} \left(\dot{\Gamma}_{\bar{\Psi}\Psi} \right) \Big|_{p=p_{\min}}, \quad (3.115)$$

$$4N_f N_c \Delta \partial_t \left(Z_q \sqrt{2Z_\Delta} h_\Delta \right) = \Re \operatorname{tr} \left(\hat{P}_\Delta \dot{\Gamma}_{\bar{\Psi}\Psi} \right) \Big|_{p=p_{\min}} \quad \text{with} \quad \hat{P}_\Delta = \begin{pmatrix} 0 & -\gamma_5 \\ -\gamma_5 & 0 \end{pmatrix}. \quad (3.116)$$

If the bosonic fields would have been set to the running minimum, we could not have pulled them out of the scale derivative. In fact they will cancel on both sides of the equation. It can be checked that these definitions are equivalent to the conventional projection via the third derivatives. The left-hand side of Eq. (3.115) is purely imaginary, therefore we have to take the imaginary part of the flow on the right-hand side, as we want to keep the parameters real. Now we divide the above equations by the wave function renormalizations and solve for the flow of the coupling

$$\partial_t h_\phi = \left(\eta_q + \frac{\eta_\phi}{2} \right) h_\phi + \frac{1}{4N_f N_c} \frac{1}{Z_q \sqrt{Z_\phi} i\sigma} \Im \operatorname{tr} \left(\dot{\Gamma}_{\bar{\Psi}\Psi} \right) \Big|_{p=p_{\min}}, \quad (3.117)$$

$$\partial_t h_\Delta = \left(\eta_q + \frac{\eta_\Delta}{2} \right) h_\Delta + \frac{1}{4N_f N_c} \frac{1}{Z_q \sqrt{2Z_\Delta} \Delta} \Re \operatorname{tr} \left(\hat{P}_\Delta \dot{\Gamma}_{\bar{\Psi}\Psi} \right) \Big|_{p=p_{\min}} \quad (3.118)$$

The matrix inside the trace is essentially given by the same supertrace as in Eq. (3.111). Now a specific expansion point can be chosen for φ_0 ; we will choose the running minimum $(\rho_\phi, \rho_\Delta) = (\kappa_\phi, \kappa_\Delta)$, where the relation between the ρ 's and the φ_0 is given in (3.30). Similar to the quark anomalous dimension the loop diagrams are always gapped either by the fermion mass or the boson mass, however the Yukawa couplings receive the dominating contributions from the anomalous dimension, in particular the bosonic ones. Hence we expect that Yukawa couplings to decrease in IR, even though the diagrammatic contributions to the flow is negative, as it can be seen in App. C.4. Around the critical scale, where all masses are light, there will be a competition of both contributions. For two-color QCD at $\mu = 0$ both Yukawa couplings must coincide at all scales, which is indeed the case and can be seen in the corresponding limits of the flow equations in App. C.4.

Let us make a remark about the flow of the baryon number in Feynman diagrams, see Fig (3.23), as it is a good way to test the correctness of the derivation. In the diagrams corresponding to the flow of the mesonic Yukawa coupling, as well as the quark anomalous dimension, there is an external baryon number flow, which essentially flows in one direction. In the diagrams with the mesonic self energy contribution the baryon number inside the loop is carried by the quark propagator in the direction which coincides with the external one. On the other hand, in the diagrams with the diquark self energy contribution the quark and diquark propagators carry baryon numbers in opposite directions, where the diquark carries it along the external flow, since its baryon number is twice the one of the quarks. Hence the net baryon flow is conserved. This is reflected in the flow equations explicitly by the fact that (anti-) quark propagator is only paired with (anti-) diquark propagator. The reason why they both correspond to (anti-) particle propagators is that in the loop diagram they propagate in opposite directions, hence at a vertex one must be counted as incoming, while the other one as outgoing. Accordingly the flow of the baryon number must be counted oppositely.

Chiral & Diquark Condensation

In this chapter we will show the main numerical results of this thesis. The phase diagram of strongly interacting quark matter is determined by the breaking of symmetries through finite expectation values of certain correlations. If a symmetry is broken, it usually entails a significant change of the dynamics of the system. As throughout this thesis we will focus on chiral & diquark condensation. A chiral condensate leads to large constituent quark mass, while diquark condensate implies baryon superfluidity in two-color QCD or color superconductivity in QCD. With the inclusion of fluctuations by the renormalization group equations derived in the previous chapter, we hope to obtain a higher quantitative accuracy and a better understanding of the physical mechanisms behind. As we have already mentioned, we are able to see a pre-condensation phase, which was never observed in the context of quark matter. We will shed more light on this matter, after discussing the boundary conditions first. Then we will look at the condensates for two-color QCD, which we obtain by solving the FRG equations for a certain range of the temperature and chemical potential, allowing us to map a phase diagram. We will show results for different truncation and compare to previous results in the literature, before going a bit deeper into the effects of different truncations and also boundary conditions. Finally we will show our result for the phase diagram of QCD including the 2SC phase. The baryons are not included at this point. In this chapter the condensates, given by the minimum of the effective potential, are denoted as $\langle \sigma \rangle = \sqrt{2\kappa_\phi}$ and $\langle \Delta \rangle = \sqrt{2\kappa_\Delta}$. Note that compared to the bosonic fields as defined before, a factor of the corresponding \sqrt{Z} is involved in each of these definitions. They are the renormalized order parameters and the actual, physical minimum values.

4.1 Boundary Conditions

In Tab. 4.1 the initial conditions are displayed for our different truncations. The one with highest number of running parameters is denoted as 2d Taylor' with three running wave function renormalizations Z_ϕ , Z_Δ , Z_q , and two running Yukawa couplings h_ϕ , h_Δ . In 1d Taylor' we take only the running of the meson Yukawa coupling and set $h_\Delta = h_\phi$, and similarly all Taylor coefficients of a certain order are given by the pure mesonic one. However, the wave function renormalizations of mesons and diquarks are independent. The Taylor expansion is always to the order of $N = 5$ in the ρ 's. In the UV we always start with an $SO(6)$ symmetric potential, where the Taylor expansion is effectively 1d.

The initial conditions for the first three cases in the table are tuned such that when all fluctuations are integrated out, we obtain an $\sqrt{N_c}$ -scaled pion decay constant of $f_\pi \simeq 76$ MeV in vacuum

	Λ [MeV]	$\langle\sigma\rangle_\Lambda$ [MeV]	$m_{\phi,\Lambda}$ [MeV]	$\lambda_{2,0,\Lambda}$	$h_{\phi,\Lambda}$	m_π [MeV]	$2\mu_c$ [MeV]
2d Taylor'	900	2.28	1135	89.0	6.43	143	138
1d Taylor'	900	2.28	1090	89.0	6.30	139	139
2d Taylor	900	4.50	650	7.0	4.80	158	139
2d T. [233]	900	39.94	247	76.3	4.80	180	143
$f_\pi = 93$ MeV	900	7.55	566	45.8	4.14	138	132
Lattice	1300	72.30	1402	510	4,175	957	700

Table 4.1: Initial conditions for the UV action $\Gamma_{k=\Lambda}$, resulting pion masses m_π in the vacuum and the corresponding critical chemical potential for the onset of diquark condensation at $T = 0$. The prime denotes that running Yukawa couplings and wave function renormalizations are included. In the forth row are the initial conditions used in Ref. [233], where an LPA was solved on a 2d grid, yielding the full effective potential instead of only around the minimum. The resulting m_π and $2\mu_c$ are shown for our 2d Taylor method, and are close to what was found in the reference.

instead of the usual $f_\pi \simeq 93$ MeV, which is identified with the chiral condensate. Further conditions are that the quark mass comes out as $m_q \simeq 360$ MeV in the vacuum, and the onset of the diquark condensation should be at $2\mu_c \simeq 138$ MeV.

At $\mu = 0$ 1d and 2d Taylor' should of course be equivalent. However since in 2d the diquark mass parameter does not stay constant below μ_c , we have to modify the initial conditions, if we want to have the onset at the physical pion mass. Small modifications of the initial mass parameter and the Yukawa couplings are sufficient, and yield a deviation of about 5 MeV between the vacuum mass $m_\pi = m_{\Delta,\mu=0}$ and the onset mass $m_{\Delta,\mu_c} = 2\mu_c$. This can be considered as an estimated difference of the curvature and pole mass of the diquark. Even though, technically, both masses are given by the same expression in our truncation, we know from Ref. [180] that by the inclusion of the wave function renormalizations (LPA') the resulting mass is very close to the pole mass in a fully momentum dependent scheme. As we see in the third and forth row of the table, the deviation of m_π and $2\mu_c$ is much larger in a simple LPA. Note that the 1d truncation that vacuum and onset masses agree by default.

The choice of the initial conditions in [233] is rather unfavorable as they see a deviation of about 40 MeV with an LPA solved on a 2d grid for ρ_ϕ and ρ_Δ . When we solve the LPA with a 2d Taylor ansatz on the comoving minimum we obtain a similar result. However we have found a completely different set of initial values, given in the third row, which yield the same f_π and m_q in the vacuum and also a reduced deviation of about 20 MeV between the vacuum and onset masses. Also note that the $m_{\phi,\Lambda}$ in LPA' is about twice as large as in LPA, which entails a much faster decoupling of the bound states towards the UV.

The set in the fifth row yields $f_\pi \simeq 93$ MeV and $m_q \simeq 340$ MeV in the vacuum. It is interesting that within the same truncation all initial values have to be chosen with a difference of 100%, if in the IR we only want a difference of about 25%. Also the convergence behavior of the Taylor expansion is slightly different as we will see later. Thus, we conclude that the choice of initial conditions is crucial for the behavior of the system throughout the phase diagram. In some regions there might be no visible effect, but in others there usually is.

For our ultimate goal, the confirmation of our understanding of the underlying physical mechanisms by comparing the FRG method to results from first principle QC₂D by lattice simulations, we will compute a tentative phase diagram with large masses, because that is what is possible on the lattice at this point. The corresponding initial conditions are given in the final row. Since the flow of baryonic quantities is much stronger affected at large chemical potential, we have much larger difference between vacuum and onset mass.

4.2 Pre-condensation

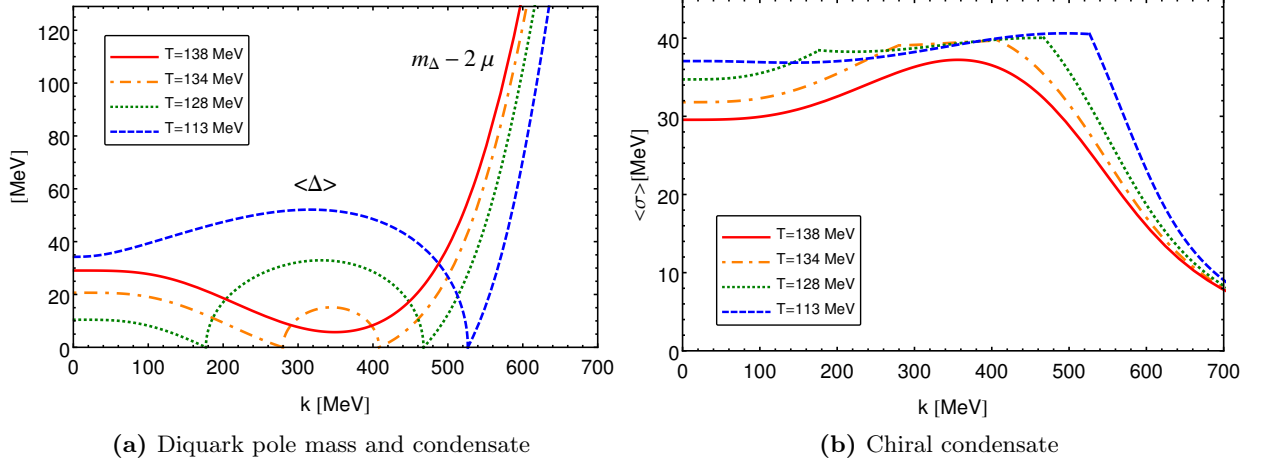


Figure 4.1: Flow of the diquark pole mass and condensate, and the chiral condensate for $\mu = 100$ MeV and different temperatures with the 2d Taylor' truncation. By lowering the temperature the pole mass decreases, and while it is below zero we have intermediate condensation of the diquark. For even smaller temperatures we have a rise of the condensate in the IR. Similarly the chiral condensate increases with decreasing temperature, while the flow is rather flat in the BEC phase.

The pre-condensation effect was already found in our previous work [356] which is unpublished. Here we show the corresponding plots with the improved approximation of the current work and state the explanation for completeness.

As we know, quark fluctuations drive the curvature of the effective potential (or the curvature masses) down. The chiral condensate (2.57) is proportional to the inverse of the meson mass and therefore it rises smoothly. The diquark sector however, experiences a second order phase transition when the pole mass vanishes at some critical scale $k_{\text{cr},1}$. Below that scale the diquark condensate starts rising and is driven up by the quark fluctuations at first, but then it goes back down to zero at some $k_{\text{cr},2}$. The reason is that when the flow starts to feel the temperature at $k \approx 2\pi T$ fermionic fluctuations are suppressed, whereas the bosonic fluctuations are enhanced, as discussed in Sec. 3.4.1. The bosons drive the condensate down to zero, and below $k_{\text{cr},2}$ the diquark mass starts increasing again, as shown by the dash-dotted line in Fig. 4.1(a). If the temperature is lowered the interplay of fermionic and bosonic fluctuations changes, such that the condensate persists for a longer range during the flow (dotted line), until a critical temperature is exceeded, where we find a stable diquark condensate at $k = 0$ (dashed line). In Sec. 3.4.3 we have already seen a similar effect along the μ -direction. Essentially the BEC phase is only maintained if $m_\Delta - 2\mu$ is below zero in the IR.

The corresponding flows of the chiral condensate is shown in Fig. 4.1(b). The solid line is purely in the normal phase and there the flow is smooth. Whereas at the onset of the BEC phase there is a kink. While the system stays there, the flow is rather flat. This is because the condensate goes mainly into the diquark instead of the meson. Also the fact that the pion mass is simply proportional to the chemical potential, as we have seen in Sec. 3.2.1, is in accord with the somewhat flat behavior of the condensate.

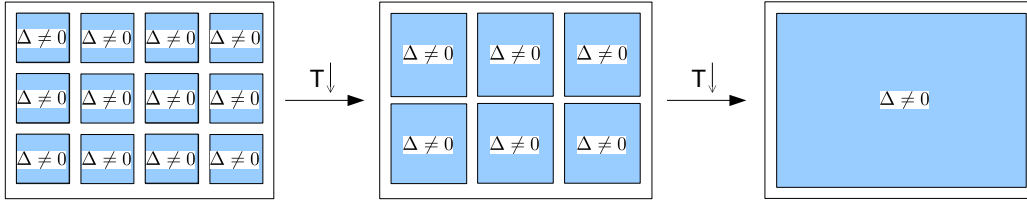


Figure 4.2: Illustration of the pre-condensation effect. Getting close to the T_c leads to local domains of condensation (left and middle figure). Below T_c the whole volume is filled with a condensate.

We can also interpret this effect more visually in position space; this is illustrated in Fig. 4.2. The fact that we have a finite condensate only at intermediate momentum scales, is translated to having small domains of condensation, but with a vanishing average in the whole volume. By reducing the temperature these domains become larger and eventually a single condensate fills out the entire space. This is quite analogous to the magnetic domains in ferromagnetism. If the temperature comes close to the critical value, domains with a finite magnetization are formed but they have different orientations and the average magnetization is zero. Below the critical temperature all magnetic moments are oriented in the same direction. The pre-condensation is in fact a generic effect in second order phase transitions and was also observed in the in ultra cold atoms [239].

4.3 The QC₂D Phase Diagram

In Fig. 4.3 we show the main result of this thesis, namely the phase diagram of two-color QCD with our best truncation. The condensates define the different phases of the system. In the UV we always start with same initial condition, namely a small chiral order parameter and in the normal phase. At small temperatures and small chemical potentials we have large quark fluctuations, by which chiral symmetry is broken and the quarks obtain their constituent mass from the chiral condensate. With increasing temperature we go through a smooth crossover to the approximate chirally symmetric regime, because the quark fluctuations are thermally suppressed. In addition, the bosons in the system wash out some of the quark fluctuations and thereby flatten the crossover.

Along the μ -axis we have the onset of diquark condensation at $\mu = m_\pi/2$ via a second order phase transition breaking the baryon number symmetry. If the diquark chemical potential $\mu_\Delta = 2\mu$ is larger than their excitation gap, i.e. the mass, it means that system is populated with diquarks. The smaller the temperature, the more of them are in the ground state forming the condensate. At larger temperature the condensate is melted because the diquarks are thermally excited. By taking into account fluctuations with the FRG, the running of the diquark mass receives quantitative corrections, which has an important impact on the condensate.

Furthermore the diquark condensate triggers the decay of the chiral condensate. Because the fermions immediately form into bosonic bound states, they cannot contribute to the chiral condensate any more. Due to the small mass of the baryonic bound states compared to in physical QCD, the chiral condensate start decaying smoothly at much smaller chemical potentials. There is no trace of a critical endpoint. Note that obviously there is no inflection point for the chiral condensate along the μ -axis since $\frac{\partial^2}{\partial \mu^2} \langle \sigma \rangle < 0$ except at the BEC phase boundary. However at $T = 0$ the value of the chiral condensate at the BEC phase boundary coincides with the value in vacuum, therefore the inflection point is inappropriate for the chiral phase boundary. It is re-

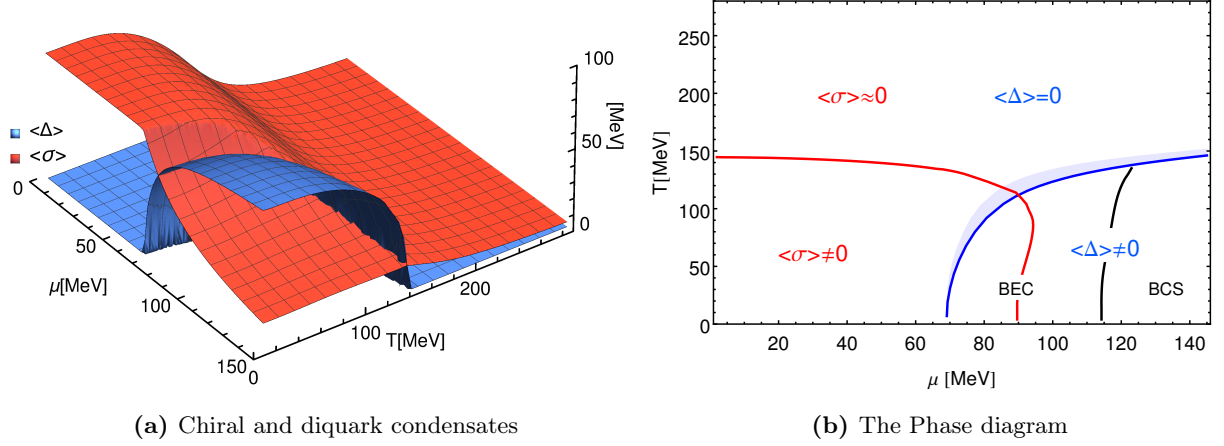


Figure 4.3: Results for two-color QCD with the 2d Taylor' truncation. The red line marking the chiral phase boundary has been computed with by the maximum in chiral susceptibility (2.43). Close to the blue line it is interpolated. The shaded area over the superfluid phase marks the preconcondensation phase. The black line of the BEC-BCS crossover is where $h_\phi \langle \sigma \rangle = \mu$.

markable that the chiral susceptibility is shows a maximum where the condensate has somewhat decayed, even though there is no inflection point. Then again it is of course expected that sigma mass has a minimum between the chirally broken and symmetric regime. We should mention also the at the BEC phase boundary we saw a slight local maximum in the chiral susceptibility, which can also be regarded as an indication for the phase transition.

Since the diquarks are color neutral QC₂D is not a color superconductor, but a baryon superfluid. Furthermore, as we have discussed in Sec. 3.4.1, the minimum of the quark energy dispersion appears at nonzero momenta, if the chemical potential exceeds the mass generated by the chiral condensate. Hence, the quarks are no more closely bound in molecules, but rather there is a long-range BCS pairing of quarks with opposite momenta on the Fermi surface. The BSC state is also characterized by overlapping bound stated. Then this change of behavior is not unexpected, because if the density is increased, at some point the Cooper pairs start overlapping. Note that the BEC-BCS crossover is not a sharp transition, since a finite Fermi surface does not immediately imply BCS pairing, but this is rather a limiting case.

In Fig. 4.4 we show a very tentative phase diagram from the lattice with large masses and our corresponding result. The pion mass is $m_\pi = 700$ MeV, as it can be read off from the onset of the diquark condensation. We have tuned our initial conditions to yield the same onset. The quark mass in our calculation is in the vacuum is $m_q \simeq 380$ MeV, about half of the pion mass plus the binding energy. At large temperatures it settles to a value of $m_{q,T \rightarrow \infty} \simeq 241$ MeV. The crossover line was computed via the inflection point. Remarkably, the blue line agrees with one of the points from the lattice, and the hadronic transition at $\mu = 0$ are close at well. Due to the early transition to the superfluid phase and the related impact on the chiral condensate, the chiral and confinement-deconfinement phase transitions cannot be together at large chemical potential. In a PNJL-model calculation [214] it was found that the phase boundary to QGP phase is a horizontal line along the chiral and superfluid phase boundaries, while in a PQMD-model within the FRG framework [234] it is seen that it bends down into the superfluid phase, which agrees more with the lattice calculations in Fig. 4.4.

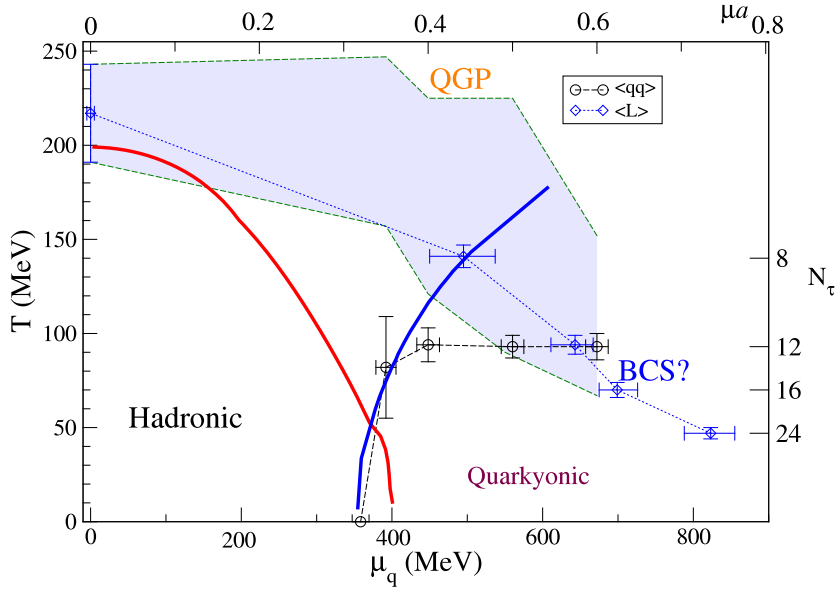


Figure 4.4: Phase diagram of QC₂D from lattice simulations [357]. The dotted line marks the crossover of the Polyakov loop, giving the boundary for the confined and deconfined phases. The shaded area is the width of the crossover. The thick lines are from our 2d Taylor' truncation with large masses, cf. Tab. 4.1.

In Fig. 4.5(a) we see the μ -dependence of the condensates at vanishing temperature, normalized over the vacuum value of the chiral condensate. The μ axis is scaled over the individual pion masses from each calculation. All FRG results are within the LPA and have been computed with the initial conditions from Ref. [233]. Except for the black curves, where the alternative set of initial conditions, with a lower difference of the vacuum and onset masses, were employed. The linear sigma model in fact corresponds to the minimum of our 1d Taylor ansatz (2.54)-(2.55) without the incorporation of fluctuations. In dimensionless form the condensates are [233]

$$\begin{aligned} \frac{\langle \sigma \rangle}{\langle \sigma \rangle_0} &= \begin{cases} 1 & \text{for } \mu < \mu_c \\ \frac{1}{x^2} & \text{for } \mu > \mu_c \end{cases}, & x &= \frac{\mu}{\mu_c} \\ \frac{\langle \Delta \rangle}{\langle \sigma \rangle_0} &= \begin{cases} 0 & \text{for } \mu < \mu_c \\ \sqrt{1 - \frac{1}{x^4} + 2 \frac{x^2 - 1}{y^2 - 1}} & \text{for } \mu > \mu_c \end{cases}, & y &= \frac{m_\sigma}{m_\pi} \end{aligned} \quad (4.1)$$

The masses are for the vacuum, and of course $\mu_c = m_\pi/2$. The more simpler chiral perturbation theory [200] neglects the effects of the sigma mass, meaning that $y \rightarrow \infty$. Then chiral condensate simply rotates into the diquark condensate towards large chemical potentials and the lower equation is always smaller than one. In the LPA the normalized chiral condensate in our 1d truncation exactly coincides with the upper equation, as there is no running of c . For the diquark condensate a difference can come about, if the bosonic mass parameter and the four-point coupling run differently in the BEC phase than in the vacuum. As long as the system is in the normal phase above the critical scale k_c the flow is identical to the vacuum flow because of the Silver Blaze property. And even in the superfluid phase we have seen in Fig. 3.15 that the flow is still in a way identical, at least in the pre-condensation phase for $T = 0$. Therefore we can expect that the behavior of the condensates with our 1d Taylor truncation should be very close to the trivial behavior predicted by the linear sigma model. Surprisingly, even the 2d truncations, solved on a grid or with a Taylor expansion, are very close to Eqs. (4.1), where

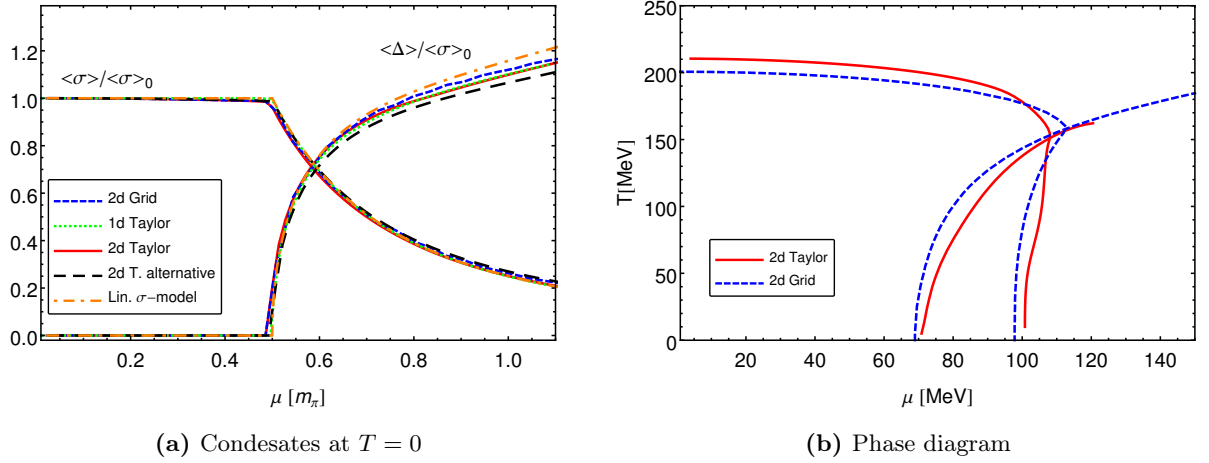


Figure 4.5: In (a) we have the condensates at vanishing temperature with the initial conditions of Ref. [233] and different solving methods. Except for the black lines, which are with the alternative set of initial conditions given in third row of Tab. 4.1. For each curve the μ -axis is scaled over its individual m_{ons} , which is identified with pion pole mass. In (b) are the phase boundaries from the grid method [233] and Taylor method with the same initial conditions.

the pion mass $m_\pi = 138$ MeV and the sigma mass $m_\sigma = 550$ MeV were used. The latter was obtained in the vacuum from the Taylor method.

Note that with the 2d truncations the chiral condensate has a very slight slope below the onset because of the violation of the Silver Blaze property. On the other hand it is surprising that in the superfluid phase the 1d Taylor truncation is almost identical with the 2d one on the scaled μ -axis, although the onset mass in 1d is the same as the vacuum mass by default, and therefore about 40 MeV larger than in 2d. Interestingly, the μ^{-2} behavior of the chiral condensate is maintained in the 2d truncations, even though it is not built in. Also we should mention that with the Taylor method we can start the flow in the normal phase only as long as $\mu < m_{\phi,\Lambda}/2$. Since the initial mass in [233] is very small, we had to initiate the flow in the superfluid phase at large chemical potentials, where the initial value of the diquark condensate is given by Eq. (2.55). However this does not seem to disturb the flow too much, which again reflects the validity of the linear sigma model, if the flow of the two-point function is not taken into account. On the other hand, if we look at the results with the completely different initial conditions (black lines), with the similar vacuum parameters but less difference of vacuum and onset mass, we see that due to the increased amount of fluctuations the curve goes away from the linear sigma model.

In Fig. 4.5(b) we have a comparison of phase diagrams from the Taylor and grid methods. The absolute value of the superfluid onset is shifted about 5 MeV and so are the corresponding lines in the superfluid phase. Furthermore the qualitative behavior is somewhat different towards larger temperatures. The back-bending of the chiral phase boundary appears in all our 2d Taylor results, and seems unnatural, if defined by the half value. Then again, the maximum of the chiral susceptibility in Fig. 4.3 was interpolated in this region. The chiral phase transition at small chemical potentials is shifted about 10 MeV. The reason is that the convergence of the Taylor expansion is not quite satisfactory, as we will see in the next section.

In Fig. 4.6(a) the condensates at vanishing temperature for various methods are shown together with our best truncations in 1d and 2d. The linear sigma model is not shown again, but we

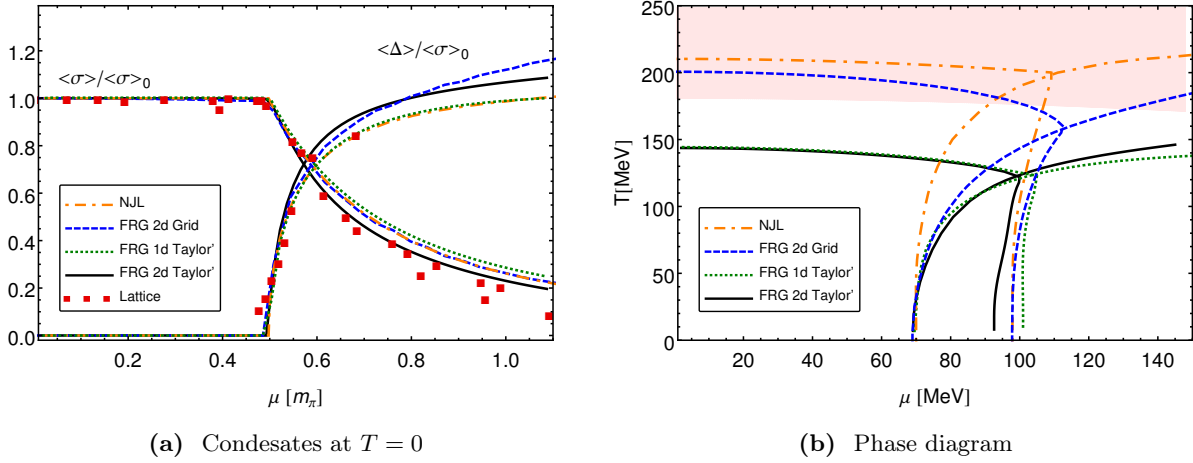


Figure 4.6: Here we have again results from various truncations and methods. The data from the other methods with low energy models is taken from [233], where the NJL calculation is based on [212], and the linear sigma model on [215]. The lattice data from [222]. The chiral phase boundaries are computed via the half value. The red shaded area denotes the region where the effective models are invalid.

can orientate ourselves with grid result. All methods show a general qualitative agreement with lattice results from first principles. By the inclusion of more fluctuations through running wave function renormalizations and Yukawa couplings we see a stronger deviation from the linear sigma model. The diquark condensate from NJL agrees well with lattice, because bosonic fluctuations have been neglected, and on the lattice the bosons are heavy. As we see from Eq. (4.1), a lighter sigma mass entails greater slope of the diquark condensate. Our 1d Taylor' result agrees with that as well, because the anomalous dimensions entail a faster decoupling of the bosons. The chiral condensate has received some corrections. Since Z_ϕ reduces with μ as shown in Fig. 3.19, the source parameter c has to compensate for that, as we have discussed in Sec. 3.4.3, hence the chiral condensate (2.54) has to increase, which it does slightly. The corresponding equation is given below. For the 2d Taylor' the behavior is opposite. If we separate the effects of the wave function renormalisation from the meson mass parameter and say that it then behaves like in the linear sigma model $Z_\phi m_\phi^2 \sim 4\mu^2$ and further use that $\sqrt{Z_\phi}c = c_0$ is constant, then we find with Eq. (2.57) that

$$\begin{aligned}
 \text{2d Taylor':} \quad \frac{\langle\sigma\rangle}{\langle\sigma\rangle_0} &\sim \sqrt{\frac{Z_\phi(\mu)}{Z_\phi(0)}} \frac{\mu_c^2}{\mu^2}, \\
 \text{1d Taylor':} \quad \frac{\langle\sigma\rangle}{\langle\sigma\rangle_0} &= \sqrt{\frac{Z_\phi(0)}{Z_\phi(\mu)}} \frac{\mu_c^2}{\mu^2},
 \end{aligned} \tag{4.2}$$

For the 1d case this result is exact. Thus we see that in the 2d case the chiral condensate is lower than the curve from the linear sigma model, in contrast to the 1d case. Interestingly, the 2d Taylor' truncation is the only one, which exhibit this behavior and thereby is closest to the lattice data. The approximate difference of the chiral condensate between 1d and 2d seem to be added to the diquark condensate. Other than that the shape of the curve is the same. Thus we may conclude that for an accurate description of two-color QCD with effective methods, a two-dimensional ansatz for the effective potential is as mandatory as the running wave function renormalizations.

Finally, in Fig. 4.6(b) we have the corresponding phase diagrams, where the chiral crossover is again defined by the half value. The NJL result has the highest critical temperature for both, the chiral crossover and the superfluid phase transitions, because there are no symmetry-preserving bosons at large T . The LPA with the FRG makes the first step of lowering the phase boundaries, by the inclusion of bosonic fluctuations. Then with LPA' there is another, rather large step further lowering the boundaries. This is because with the anomalous dimensions the initial boson masses in the UV have to be chosen larger, as we discussed in Sec. 3.6.1. But this implies also a smaller chiral condensate in the UV, as they are both connected via Eq. (2.57). In consequence, if the temperature is not small enough, there are not enough quark fluctuations to drive the chiral condensate up to its vacuum value, even though the quarks are lighter. The 1d and 2d truncations are in remarkable agreement in the normal phase, and also the superfluid phase boundary has only minor deviations at small chemical potential. The differences of the chiral crossover lines within the superfluid phase is explained by the extrapolation of Eq. (4.2). Let us mention that there is also phase diagram from mean-field calculations in Ref. [233], which close to the NJL result, however, there is an artifact in the form of a critical endpoint of the superfluid phase boundary at larger chemical potential, after which the second order phase transition turns first order. The red shaded area marks the region where

$$\left| \frac{\dot{\Gamma}_{\Lambda,T,\mu} - \dot{\Gamma}_{\Lambda,0,0}}{\dot{\Gamma}_{\Lambda,0,0}} \right| > 0.1. \quad (4.3)$$

This is the flow of the effective action in-medium and at the initial UV scale Λ , subtracted by the vacuum flow, and then normalized to the vacuum flow. For constant fields the volume cancels out and we can plug in the flow of the effective potential. If this quantity is large, it means that the microscopic action is influenced by in-medium effects, or from a different point of view, the in-medium flow is affected by the cutoff Λ . The cutoff should be large enough, such that the results are independent of it, we will look on this matter more closer in the next section. On the other hand, the initial scale should not be larger as the validity of the model. For our effective low energy models we must remain below the scale where gluon degrees of freedom are relevant. So we have a constraint for Λ from both sides. Since our 2d Taylor' truncation takes into account more fluctuations than any other approach up to date, we evaluated (4.3) the corresponding initial conditions and marked the regime where initial flow deviates more than 10% from the vacuum. Altogether we can say that considering effects beyond pure fermionic fluctuations or LPA is quite important.

4.4 Truncation Effects

In this section, we would like to study to some extent the reliability of our truncation. We start with the convergence behavior of our Taylor expansion. In Fig. 4.7(a) we have the chiral condensate as a function of the temperature for different orders N of the Taylor expansion. At vanishing chemical potential the 1d expansion (2.50) is sufficient for this analysis. All curves are computed with the same UV initial conditions, given in Tab. 4.1, which were tuned such that we obtain the “physical” parameters in the IR for $N = 5$, with $f_\pi = 76$ MeV. The expansion does not converge for the orders we have computed. Up to the fifth order the curves do not differ from each other too much. For the sixth order we had to make some adjustments of the numerical precision in solver in order to make it work. The case $N = 4$ did not work with the initial conditions. This signals some unstable behavior of the truncation. The crossover temperature has been computed with all three definitions introduced in Sec. 2.5.1, which seem to be somewhat

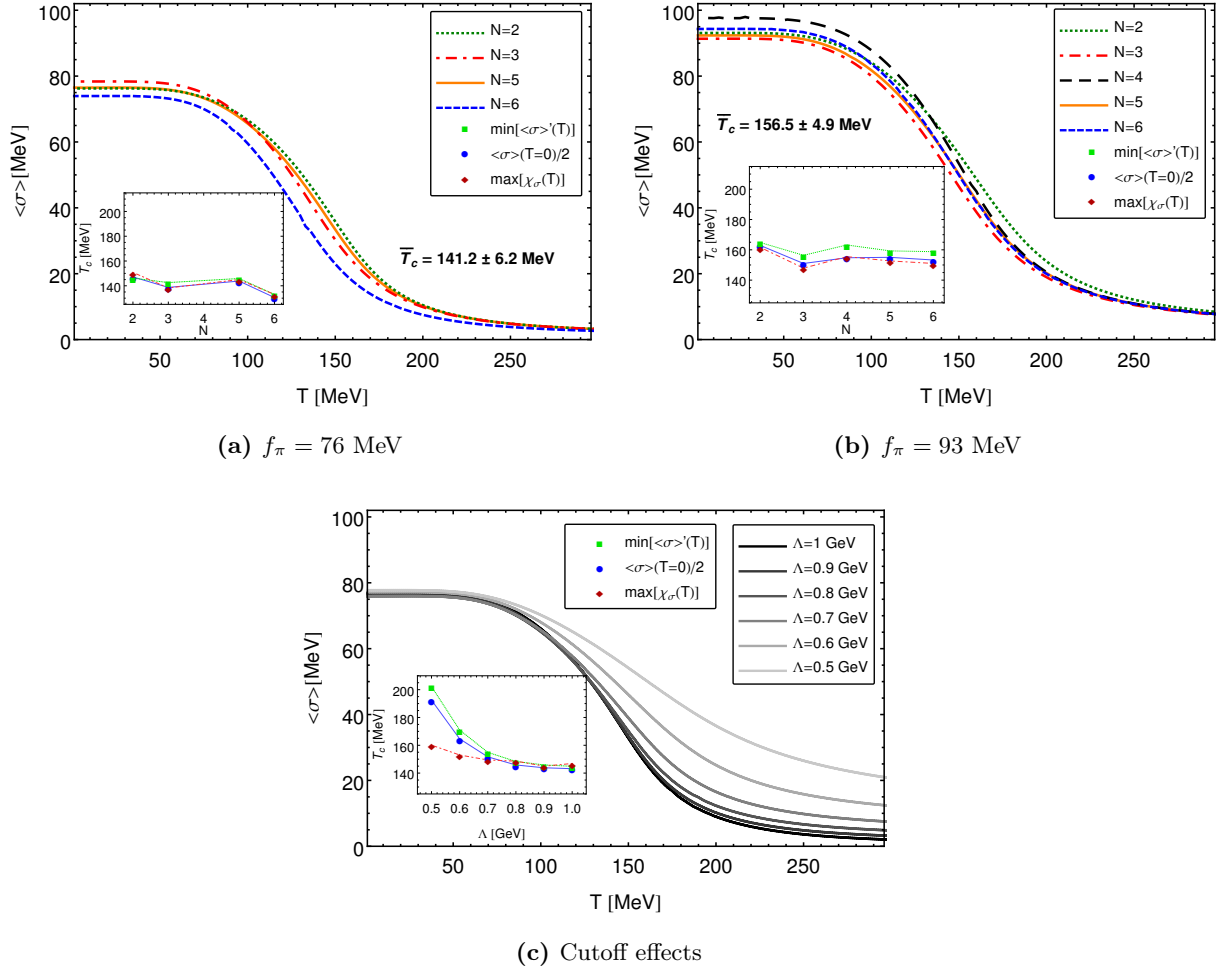


Figure 4.7: Chiral condensate and transition temperatures at $\mu = 0$ for different truncations and parameters. A running Yukawa coupling and wave function renormalizations are always included.

agreeing in the current figure. However as a function of the order N the critical temperature does not converge. Therefore the average \bar{T}_c from all three definitions and from all orders, together with its margin of error, should give a feeling for the error of our phase boundaries. The lack of convergence is the reason for the insufficient agreement with the grid method in Fig. 4.6(b).

Interestingly, we have observed that different initial conditions change the convergence behavior of the Taylor expansion. In Fig. 4.7(b) we are showing the results for the fifth set of initial conditions in Tab. 4.1, which yields $f_\pi = 93$ MeV in the vacuum with $N = 5$. All cases were able to be computed without trouble, however $N = 4$ still seems to be an outlier at small temperatures. Other than that, the expansion seems to be converging quite sufficiently with higher orders, even if at very small temperatures it could be better. In particular a converging behavior for the crossover temperature develops at higher orders. On the other hand the inflection point is a bit apart from the other definitions. Thereby the somewhat large error margin of \bar{T}_c is caused, and not because of a poor convergence. Note that since the condensate is larger in the vacuum, a higher temperature is required in order to melt it.

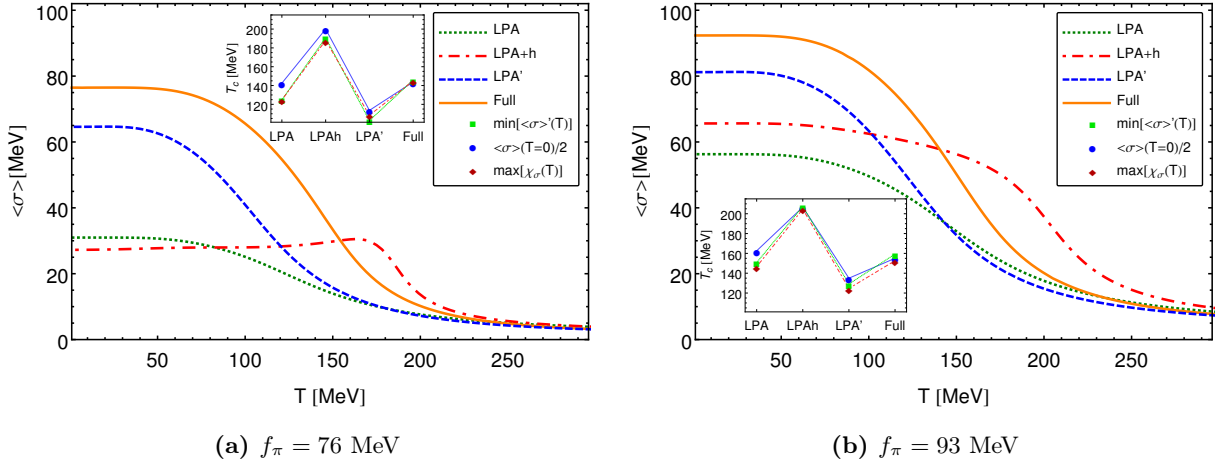


Figure 4.8: Chiral condensate and transition temperatures at $\mu = 0$ for different truncations and parameters. The Taylor expansion is to the order $N = 5$.

In the Ref. [179] a Taylor expansion for the effective potential with a fixed expansion point, rather than a comoving minimum, was employed for a quark-meson model. There, a rapid convergence of the expansion was observed for all temperature regions. A notable difference between both methods is that with the comoving minimum all truncations coincide at the high temperature limit, while with the fixed expansion point the $N = 2$ case goes apart at large temperatures.

In Fig. 4.7(c) we have studied the cutoff dependence. For this study we used the initial conditions in the second row of Tab. 4.1 and solved the flow equations down or up each of the Λ 's in the vacuum. Then each time we used this as the starting point for the finite temperature calculations. However, we always started with a quartic potential in the UV, meaning that the higher order coupling are set to zero at every Λ . This is why we see small deviations at $T = 0$, which can be regarded as subsidiary probe for the convergence of the Taylor expansion. In any case, we clearly see rising deviations at large temperatures with the lowering of the cutoff. As we indicated before, if the microscopic action feels the in-medium effects, it is not really microscopic. In particular the crossover temperature should be independent of the cutoff. In the inset we observe that for cutoffs $\Lambda > 800$ MeV it starts to converge. Also note that for small cutoffs the maximum of the chiral susceptibility is rather far from the other definitions of the crossover.

Finally we will investigate the truncation effects coming from the flow of the two-point function, again for the two sets of initial condition as before. We simply lower the truncation by switching of the corresponding loop contribution. This means that in LPA' the Yukawa coupling still runs with the positive contributions from the anomalous dimensions. In Fig. 4.8(a) we have case with the smaller pion decay constant. We have already mentioned the effects of the anomalous dimensions in the previous section. The difference here is that truncations are not individually tuned, nonetheless the effect is basically the same. Without the anomalous dimension the strong running of the meson mass and thereby also of the chiral condensate, which scales with its inverse, is simply weakened. In the LPA+h the Yukawa increases towards the IR instead decreasing, because the pure diagrammatic contributions are negative. Then it is self-enhanced and it grows over one order of magnitude. In order avoid an instability, we had to reduce the initial value to $h_{\phi,\Lambda} = 5.9$. In the high and low temperature limit this truncation seems to agree with the LPA, because in the former case the Yukawa coupling does not flow, as the fermions are thermally blocked, whereas in the latter case it seems that it plays more the role of contributing to the

fermionic gap $h_\phi\langle\sigma\rangle$ than being a large coupling. At intermediate temperatures probably the exact opposite of this behavior is going on, leading to a bump. We should compare the full truncation to LPA'. The additional diagrammatic contributions to the Yukawa coupling slow down its running, entailing larger fermionic fluctuations at small and intermediate temperatures, and thereby a larger chiral condensate.

In Fig 4.8(b) we see that the effects are not that drastic. Generally, there are less fluctuations with the larger pion decay constant, and hence less truncation effects. The initial value of the chiral condensate is larger and correspondingly the meson mass is smaller, and also the Yukawa coupling is smaller. In consequence the dynamics are more balanced between fermions and bosons. In particular the nontrivial behavior of the LPA+h is not apparent. The effects of the different truncations seem to add up linearly. However both cases have in common that in the LPA+h the crossover temperature is increased, whereas in the LPA' it is decreased. Both effects cancel each other in the full truncation.

4.5 The QCD Phase Diagram

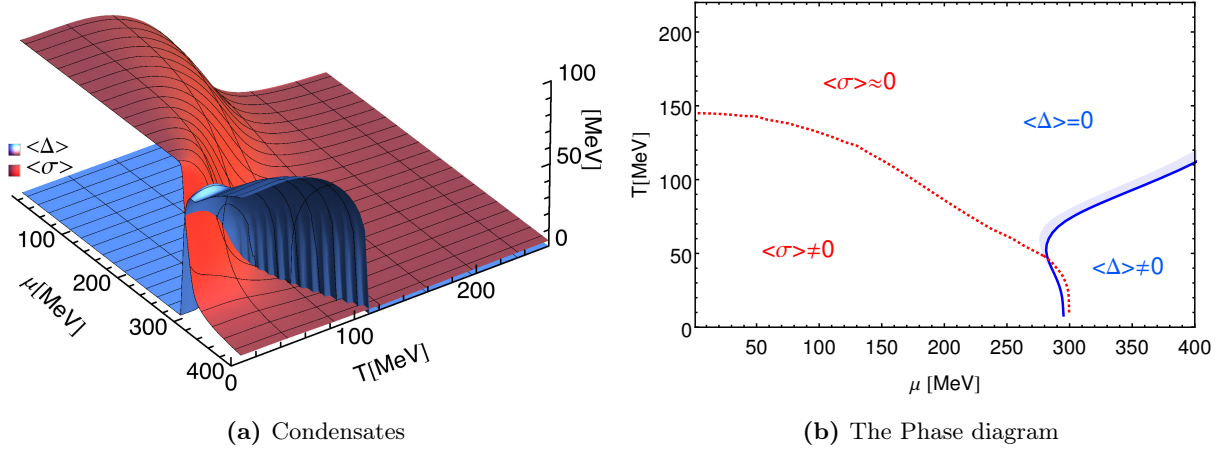


Figure 4.9: Chiral and diquark condensates and the corresponding phase diagram with the QMD-model for QCD. The shaded area again marks the pre-condensation phase.

Lastly, we turn to our results for physical QCD. The baryons are not included at this point. In Tab 4.2 we show the initial conditions. We have applied the 2d Taylor expansion to the order $N = 2$ with an LPA', but kept the Yukawa coupling constant, because for the low energy regime of QCD it was shown in Refs. [185, 186], that it is nearly constant. We see in the table that the violation of the Silver Blaze property is amplified because the onset is at much larger chemical potential, similar as in the case of large masses in QC₂D. The initial conditions are chosen such that the onset of diquark condensation is below the quark mass. In Fig. 4.9 the condensates and the map of on the phase diagram is shown. We have a smooth crossover at about 145 MeV for vanishing density, computed via the inflection point. Entering the 2SC implies a change

of dynamics, actually triggering the restoration of chiral symmetry. This is analogous to the QC_2D case with the difference that the condensates behave much more steeply. Because the chemical potential is much closer to the quark mass the system is more dynamical. However, the chiral phase transition is not first order as there is no jump, which may be an artifact of the truncation. The wiggling behavior of the diquark condensate may also be some unphysical result of our approximation. Since it is also observed in the sigma mass in Fig. 3.7, it must be related to the four-boson coupling. The fact that the diquark condensate rises nearly horizontally at the phase transition even at larger temperatures, is caused by the removing of the Goldstone modes, which thereby cannot counteract to the strong quark fluctuations. Interestingly, the phase boundary of the 2SC phase first bends to the left with increasing temperature, implying that the system favors the chiral condensation at small temperatures, whereas at larger temperatures the diquark condensate is favored before going into the symmetric phase. Also note that we can again see a pre-condensation phase, which is new in the context of color superconductivity.

Λ	$\langle\sigma\rangle_\Lambda$	$m_{\phi,\Lambda}$	γ	$\lambda_{2,0,\Lambda}$	$h_{\phi,\Lambda}$	$h_{\Delta,\Lambda}$	m_Δ	$2\mu_c$
800 MeV	5.9 MeV	680 MeV	0.65	90.0	3.6	2.6	729 MeV	590 MeV

Table 4.2: Initial conditions for the UV action $\Gamma_{k=\Lambda}$, resulting diquark m_π in the vacuum and the corresponding critical chemical potential for the onset of diquark condensation at $T = 0$. There is a difference of about 20 %. The UV potential has the 1d from (2.50), where the diquark sector is distinguished by the factor γ .

Summary, Conclusions & Outlook

For the aim of understanding the high density regime of QCD, we have mainly dedicated this work to the study of a QCD-like theory that is feasible on the lattice. The absence of the fermionic sign problem in the a fictitious theory of QCD with two colors instead of three, has drawn the interest of the lattice community for over a decade. It is very important to test other approaches, which are not from first principles, against lattice results, in order to gain assurance for the validity of the methods, the framework and the models that are applied. Furthermore, both approaches should be seen as complementary, in the sense the physical insights gained from one should be a benefit for the other.

In this work we have applied the framework of the functional renormalization group on an effective, low-energy model for two-color QCD. We have considered the gluon degrees of freedom to be integrated out, and used a description of the theory in terms of quarks and bound states. We have motivated the incorporation of the bound states through a hadronization procedure, where first an effective four-fermi interaction is generated from the quark-gluon dynamics, which is then bosonized by means of standard methods. By examining the underlying symmetries of the microscopic model we have constructed an effective action, with quarks mesons and diquarks, that satisfies those symmetries and also incorporates the various breaking patterns. Due to the properties of the gauge group generators in two-color QCD the flavor symmetry is extended, such that at vanishing chemical potential the diquarks are degenerate with the pions. Moreover, the diquarks are color neutral and therefore the baryons of the theory. Thus we have a playground at hand to study baryonic degrees of freedom in a simplified bosonic description as well as a relativistic BEC-BSC crossover. Because the diquarks must be light in order to satisfy the extended symmetry, an early onset of diquark condensation in the direction of the chemical potential was expected. Moreover previous investigations had already shown that the chiral condensate, which is dominating at small chemical potential, rotates into the diquark after the onset.

The FRG method allows to interpolate between the microscopic and the macroscopic regime of the theory, by integrating out all thermal and quantum fluctuations. All correlations are generated that are allowed by the underlying symmetry, but in practice the system must be truncated. Our microscopic starting point was an effective theory at scale of 900 MeV where the quarks are almost massless and interact through boson exchange in a point-like manner, as the bosons are very heavy at this point. Those interactions lead to the dynamical breaking of symmetries and the associated emergence of light bosons, which all can be described by a scale dependent effective potential. This we have incorporated in the form of a Taylor expansion in the

invariants of the theory, where the order of the expansion relates to the order of the inter-bosonic interactions that are allowed by the approximation. By examining the flow equation of the effective potential, we were able to anticipate the interplay of bosonic and fermionic degrees of freedom for different temperatures and chemical potentials. The ground state of the system is determined by the minimum of the effective potential, i.e. the condensates. We have seen that the chiral condensate goes through a crossover towards large temperatures, where chiral symmetry is restored. The diquark condensate sets in via a second order phase transition, when its pole mass is vanishing at large chemical potentials and small temperatures. By tracing the scale dependence of the diquark condensate, we have observed that before the onset there is a phase of pre-condensation, which is interpreted as having local domains with finite condensates, but a vanishing average over the whole volume. This happens because the temperature effects come into play at a scale where the symmetry is already broken, leading then to its restoration.

We have considered a 1d Taylor expansion of the effective potential in the $O(6)$ invariant containing mesons and diquarks and added the explicit symmetry breaking terms, where some properties of the simple linear sigma model approach are already built in. Concurrently, we have studied a 2d expansion in the $O(4)$ (mesons) and $O(2)$ (diquarks) invariants, as the two sectors should be independent at finite chemical potential. It was seen that at vanishing temperature the condensates from the LPA truncation behave like in the simple linear sigma model, regardless of whether it is solved on a 2d grid or with 1d/2d Taylor expansion. Even all other methods and approximations, including the lattice, show agreeing qualitative behavior and small numerical deviations of about 10 % on scaled axes. But this is not too much surprising, as the minimum more or less moves away from the origin with μ and in addition to the rotation from the chiral to the diquark direction, as predicted from the linear sigma model. However, it should be mentioned that our full truncation is the only one which exhibits the slight decrease of the chiral condensate in the superfluid phase, and thus is closest to the lattice result.

The phase boundaries in the map of the phase diagram from the grid and the Taylor methods deviate about 10 MeV as the convergence of the expansion is insufficient. With our full truncation, including running Yukawa couplings and wave function renormalizations, we have observed significant corrections of the phase boundaries at large temperatures of about 25 %. The main reason is that the running wave function renormalizations entail a faster decoupling of the bound states towards the UV, which goes along with a smaller condensate, and thus a need of more coldness of the system for the condensates to rise. The full 1d and 2d truncations only have minor deviations from each other, except for the chiral crossover at large μ , where it is understandable from the different expressions of the minimum. Since our approximation is to date the most sophisticated, we used the initial conditions to see where cutoff effects come into play in the high temperature region, and thereby invalidated the other effective models. A higher cutoff could resolve this problem, but then gluon dynamics must be taken into account. In any case, we can conclude that solving the nontrivial scale dependence of the propagators is an important ingredient in order to obtain quantitative accuracy. A study of the truncation effects has revealed a dependence from the boundary conditions, in the sense that a larger value of f_π implies less fluctuation in the system and thereby less effects the systematic improvement of the truncation.

The Silver Blaze property was an essential issue of this work. After recapitulating the property for the effective action and n-point functions, we have seen that at vanishing temperature it amounts to a simple shift of the frequencies by the chemical potential with the appropriate charges. We have shown that if this property holds true at the initial scale, it is preserved by the flow equation, owing to its one-loop structure. However, this requires a full momentum resolution of all quantities, which are directly sensitive to the chemical potential. If this is not done, the

μ -dependence is interpreted as a genuine one instead of the simple shift, which is thus unphysical. The diquark sector is much affected by that problem, if its parameters are not identified with the meson sector like in our 1d approximation. Nevertheless, we have seen that the running wave function renormalization somewhat reduces the discrepancy in the two-color case, while for large diquark masses with a late onset, the discrepancy is amplified. Something that should be tried in the near future, is to keep the μ -dependence in the thermal distribution functions, and to remove all others. This may pose a self-consistent approximation, in the sense that momentum dependence is kept away. However, ultimately a momentum resolution should be sought for.

The next natural step to improve our result is to incorporate a phenomenological Polyakov-loop potential to study confinement in two-color QCD, as it was done in [234] with an LPA. Then, following the example of Refs. [185, 186], a dynamical connection of the quark-gluon regime with low-energy effective regime should be established with a dynamical hadronization technique, including running gauge couplings. The effects of a moderate heavy strange mass, would be another interesting matter to study. Coincidentally, on the level of effective theories one can map two-color QCD at finite baryon chemical potential to physical QCD at finite isospin chemical potential [358], where the charged pions play the role of the diquarks. Hence, our truncation should be applied there as well. Also in this case the sign problem is absent [359–361].

The second project in this work was the formulation of an effective theory for QCD at high baryonic densities. We have argued that the diquark is an important ingredient for this matter. Not only can it be an intermediate state in the formation process of the baryon, but also the constituents of the baryons can have diquark type correlations. In addition the condensation of the diquark has significant impact on the phase diagram of QCD. In the scenario where the diquark is lighter than twice the quark mass, the onset of the color superconducting phase is before the chiral symmetry restoration. The consequential change of dynamics then triggers the restoration chiral symmetry, similar as in two-color QCD.

We were able to generalize the quark-meson-quark model for two-color QCD for the physical case, and applied the FRG machinery in order to study the two-flavor color superconductivity. With the explicit inclusion of bosonic fluctuations we took account of the Meissner effect by removing the Goldstone modes in the broken phase. In consequence we have seen a very steep rise of the diquark condensate at the phase transition.

Furthermore, we have added baryonic degrees of freedom to the model, by considering a baryonization procedure in a chirally symmetric way. We have argued that baryonic fluctuations are suppressed at small chemical potentials due to the heavy mass, and when the system is populated with fermions at finite baryon density, fluctuations contributing to the mesonic sector in the effective potential are simply cutoff below the Fermi surface, thus no effect on the chiral condensate should be visible at vanishing temperature. This argument may be extrapolated to finite temperatures.

The dissociation of the baryons at high energies in a simple FRG framework with the effective model remains unsettled. It is not straightforwardly built-in as for boson, where fermionic fluctuations push up the mass gap towards the UV, by which the bosons decouple from the system. Here, too, future improvement should include a momentum resolution as well as the connection to QCD, which may help to establish a dynamical baryonization procedure ensuring the decoupling in the UV. Moreover, including the strange quark leads to many different scenarios at intermediate chemical potentials. Together with the baryons the possibility of the Quark-Hadron Continuity should be explored.

Appendix

Appendix A

Conventions and Notations

A.1 Units

We use natural units throughout this work

$$k_B = c = \hbar = 1 .$$

As a consequence of this convention, the SI units are related to the energy unit as follows:

Unit	Metric value	Derivation
1 eV of length	$1.97 \times 10^{-7} \text{ m}$	$= (1\text{eV}^{-1})\hbar c$
1 eV of time	$1.78 \times 10^{-36} \text{ s}$	$= (1\text{eV}^{-1})c^2$
1 eV of mass	$6.58 \times 10^{-16} \text{ kg}$	$= (1\text{eV}^{-1})\hbar$
1 eV of temperature	$1.16 \times 10^{-4} \text{ K}$	$= (1\text{eV})/k_B$

A.2 Euclidean Space-Time

In Euclidean space-time the metric tensor is given by the Kronecker-Delta

$$g_{\mu\nu}^E = \delta_{\mu\nu} , \tag{A.1}$$

Where $\mu, \nu = 1, \dots, 4$. This convention corresponds to the analytic continuation

$$t \rightarrow -i\tau . \tag{A.2}$$

Hence a four-vector Euclidean space-time is defined as

$$x_\mu^E = (\vec{x}, x_4 = -it) . \quad (\text{A.3})$$

If we use Latin indices in this context, it denotes only the spatial components from 1 to 3. A general dot product changes the sign

$$a^\mu b_\mu = -a_\mu^E b_\mu^E . \quad (\text{A.4})$$

The same holds for the d'Alembertian operator $\partial^\mu \partial_\mu = -\partial_\mu^E \partial_\mu^E$ but not for

$$x^\mu \partial_\mu = x_\mu^E \partial_\mu^E . \quad (\text{A.5})$$

Slashed quantities change as follows

$$\begin{aligned} \not{\partial} &= i\not{\partial}^E \\ \not{p} &= -i\not{p}^E . \end{aligned} \quad (\text{A.6})$$

For Conventions regarding the Dirac matrices we refer to App. A.4. After analytic continuation a time integral turns into

$$\int_{-\infty}^{\infty} dt f(t) = \int_{-\infty}^{\infty} d(-i\tau) f(-i\tau) = -i \int_{-\infty}^{\infty} d\tau f(-i\tau) \quad (\text{A.7})$$

and correspondingly for momentum space. The delta function transforms similarly

$$\delta^{(4)}(x) = \int \frac{d^4 p}{(2\pi)^4} e^{ipx} = -i \int \frac{d^4 p^E}{(2\pi)^4} e^{-ip^E x^E} = -i \delta^{(4)}(x^E) . \quad (\text{A.8})$$

A.3 Abbreviations

Four-vectors we write as $p \equiv p_\mu = (\vec{p}, p_4)^T$, where p_4 is the respective Matsubara frequency.

For integrals and delta functions we use the following abbreviations at finite temperatures:

$$\int_x \equiv \int_0^{1/T} d\tau \int d^3 x , \quad \int_p \equiv T \sum_{n \in \mathbb{Z}} \int \frac{d^3 p}{(2\pi)^3} , \quad \delta(x) \equiv \delta^{(4)}(x) , \quad \delta(p - q) \equiv (2\pi)^3 \delta^{(3)}(p) \delta_{n,m}$$

where n, m are the modes of the Matsubara frequencies for p, q . If there are many variables in index of an integral, an integration with respect to all these variable is implied.

Furthermore we mention that repeated indices are always summed over, unless it is mentioned otherwise.

Within text we use the following abbreviations:

RG	Renormalization Group
RGE	Renormalization Group Equation
FRG	Functional Renormalization Group
IR	Infrared
UV	Ultraviolet
QCD	Quantum Chromodynamics
QC ₂ D	Two Colour QCD
QMD	Quark-Meson-Diquark
QMDB	Quark-Meson-Diquark-Baryon
2SC	Two-Flavor Color Superconductivity
CFL	Color-Flavor Locking
BEC	Bose-Einstein Condensation
BCS	Bardeen-Cooper-Schrieffer
NJL	Nambu Jona-Lasinio

A.4 Dirac Algebra

The Dirac algebra in Euclidean space-time is defined through

$$\begin{aligned}
\{\gamma_\mu, \gamma_\nu\} &= \gamma_\mu \gamma_\nu + \gamma_\nu \gamma_\mu = 2\delta_{\mu\nu} \mathbb{1}_{4 \times 4} , \\
(\gamma_\mu)^\dagger &= \gamma_\mu , \\
\gamma_5 &= \gamma_1 \gamma_2 \gamma_3 \gamma_4 , \\
\{\gamma_\mu, \gamma_5\} &= 0 .
\end{aligned} \tag{A.9}$$

The chiral representation of the γ -matrices is given by

$$\gamma_i = \begin{pmatrix} 0 & -i\sigma_i \\ i\sigma_i & 0 \end{pmatrix}, \quad \gamma_4 = \begin{pmatrix} 0 & \mathbb{1} \\ \mathbb{1} & 0 \end{pmatrix}, \quad \gamma_5 = \begin{pmatrix} \mathbb{1} & 0 \\ 0 & -\mathbb{1} \end{pmatrix}, \tag{A.10}$$

where the σ_i 's are the Pauli matrices

$$\sigma_1 = \begin{pmatrix} 0 & 1 \\ 1 & 0 \end{pmatrix}, \quad \sigma_2 = \begin{pmatrix} 0 & -i \\ i & 0 \end{pmatrix}, \quad \sigma_3 = \begin{pmatrix} 1 & 0 \\ 0 & -1 \end{pmatrix} \tag{A.11}$$

and $\mathbb{1}$ is a 2×2 unit matrix.

The Pauli matrices satisfy the relation

$$\{\sigma_a, \sigma_b\} = 2\delta_{ab} . \quad (\text{A.12})$$

In order to extract the Weyl spinors from a general spinor, we can use the projection operators

$$P_{L,R} = \frac{1}{2} (1 \pm \gamma_5) . \quad (\text{A.13})$$

Furthermore we define the charge conjugation operator

$$C = \gamma_4 \gamma_2 \quad (\text{A.14})$$

with the properties

$$C^{-1} = C^\dagger = C^T = -C , \quad C\gamma_\mu C = \gamma_\mu^T , \quad \{C, \gamma_5\} = 0 . \quad (\text{A.15})$$

The following identities are useful for the computation of flow equations functions

$$\begin{aligned} \text{tr } \gamma_\mu \gamma_\nu &= 4\delta_{\mu\nu} , \\ \text{tr } \gamma_\mu \dots \gamma_\nu &= 0 , \quad \text{for odd } \# \text{ of } \gamma\text{'s} , \\ \text{tr } \gamma_5 &= 0 , \\ \text{tr } \gamma_\mu \gamma_5 &= 0 , \\ \text{tr } \not{p} \not{q} &= p \cdot q , \end{aligned} \quad (\text{A.16})$$

Appendix B

Propagators

The propagator is defined by Eq. (3.18). It is found by taking two functional derivatives of the effective action (2.35) or (2.36) with respect to the fields, adding the regulator and then evaluating at the expansion point, before taking the inverse. For convenience we omit the delta function. Employing a 3d-optimized regulator does nothing but regularizing the space-like momentum like $\vec{p} \rightarrow \vec{p}_r$, with Eq. (3.23). Therefore we will omit the regulator terms in this section, while for the flow equations the momenta can simply be replaced by the regularized ones. The timelike component of the momentum p_4 will be replaced by the respective Matsubara frequencies. The propagator for the QMD-model and the QMDB-model will be covered, as well as the fermionic vertices for the QMDB-model.

B.1 Boson Propagators

Here we will explicitly display the boson Propagator introduced in Sec. 3.2.1. We will show it for the real as well as the complex representation of the diquark fields. Due to nonzero off-diagonal mixing terms at finite mesonic and diquark fields it is rather tedious.

QMD-model of QC₂D

In the real representation the boson propagator is given by

$$\begin{aligned}
 G_\varphi &= \begin{pmatrix} Z_\phi K_\pi \mathbb{1}_{3 \times 3} & 0 & 0 & 0 \\ 0 & Z_\phi K_\sigma & 2V_{\phi\Delta} \sqrt{Z_\phi Z_\Delta \rho_\phi \rho_\Delta} & 0 \\ 0 & 2V_{\phi\Delta} \sqrt{Z_\phi Z_\Delta \rho_\phi \rho_\Delta} & Z_\Delta K_{\Delta_1} & -4Z_\Delta \mu \omega_n \\ 0 & 0 & 4Z_\Delta \mu \omega_n & Z_\Delta K_{\Delta_2} \end{pmatrix}^{-1} \\
 &= \begin{pmatrix} \frac{G_\pi}{Z_\phi} \mathbb{1}_{3 \times 3} & 0 & 0 & 0 \\ 0 & \frac{G_\sigma}{Z_\phi} & -\frac{G_{\sigma\Delta_1}}{\sqrt{Z_\phi Z_\Delta}} & -\frac{G_{\sigma\Delta_2}}{\sqrt{Z_\phi Z_\Delta}} \\ 0 & -\frac{G_{\sigma\Delta_1}}{\sqrt{Z_\phi Z_\Delta}} & \frac{G_{\Delta_1}}{Z_\Delta} & \frac{G_{\Delta_1\Delta_2}}{Z_\Delta} \\ 0 & \frac{G_{\sigma\Delta_2}}{\sqrt{Z_\phi Z_\Delta}} & -\frac{G_{\Delta_1\Delta_2}}{Z_\Delta} & \frac{G_{\Delta_2}}{Z_\Delta} \end{pmatrix}
 \end{aligned}$$

with

$$\begin{aligned}
 G_\pi &= K_\pi^{-1} & K_\pi(\vec{p}^2) &= \vec{p}^2 + \omega_n^2 + V_\phi \\
 G_\sigma &= \left(K_{\Delta_1} K_{\Delta_2} + 16\mu^2 \omega_n^2 \right) / J & K_\sigma(\vec{p}^2) &= \vec{p}^2 + \omega_n^2 + V_\phi + 2\rho_\phi V_{\phi\phi} \\
 G_{\Delta_1} &= K_{\Delta_2} K_\sigma / J & K_{\Delta_1}(\vec{p}^2) &= \vec{p}^2 + \omega_n^2 + V_\Delta + 2\rho_\Delta V_{\Delta\Delta} - 4\mu^2 \\
 G_{\Delta_2} &= \left(K_{\Delta_1} K_\sigma - 4\rho_\phi \rho_\Delta V_{\phi\Delta}^2 \right) / J & K_{\Delta_2}(\vec{p}^2) &= \vec{p}^2 + \omega_n^2 + V_\Delta - 4\mu^2 \\
 G_{\sigma\Delta_1} &= 2V_{\phi\Delta} \sqrt{\rho_\phi \rho_\Delta} K_{\Delta_2} / J \\
 G_{\sigma\Delta_2} &= 8V_{\phi\Delta} \sqrt{\rho_\phi \rho_\Delta} \mu \omega_n / J \\
 G_{\Delta_1\Delta_2} &= 4\mu \omega_n K_\sigma / J
 \end{aligned}$$

where

$$J(\vec{p}^2) = K_\sigma \left(K_{\Delta_1} K_{\Delta_2} + 16\mu^2 \omega_n^2 \right) - 4\rho_\phi \rho_\Delta V_{\phi\Delta}^2 K_{\Delta_2}$$

is the determinant of the $\sigma\Delta$ -part of G_φ without the Z 's. In the left column the momentum dependencies were omitted. For the derivation of flow equations we will need derivatives of each entries of the propagators with respect to the K 's

$$\begin{aligned}
 0 &= \frac{\partial}{\partial K_{\varphi_l}} G_{\varphi,ij} \left(G_\varphi^{-1} \right)_{jk} = \frac{\partial G_{\varphi,ij}}{\partial K_{\varphi_l}} \left(G_\varphi^{-1} \right)_{jk} + G_{\varphi,ij} \underbrace{\frac{\partial \left(G_\varphi^{-1} \right)_{jk}}{\partial K_{\varphi_l}}}_{\delta_{jl} \delta_{ik}} \\
 &\Rightarrow \frac{\partial G_{\varphi,ij}}{\partial K_{\varphi_l}} = -G_{\varphi,il} G_{\varphi,lj} .
 \end{aligned} \tag{B.1}$$

Note that the equal indices do not imply a sum here. Using this relations, one can express momentum derivatives conveniently in terms of the propagators

$$\frac{\partial G_{\varphi,ij}}{\partial \vec{p}^2} = \sum_l \frac{\partial G_{\varphi,ij}}{\partial K_{\varphi_l}} = - \sum_l G_{\varphi,il} G_{\varphi,lj} . \tag{B.2}$$

In the complex representation we have

$$\begin{aligned}
 G_{\bar{\varphi}} &= \begin{pmatrix} Z_\phi K_\pi \mathbb{1}_{3 \times 3} & 0 & 0 & 0 \\ 0 & Z_\phi K_\sigma & V_{\phi\Delta} \sqrt{2Z_\phi Z_\Delta \rho_\phi \rho_\Delta} & V_{\phi\Delta} \sqrt{2Z_\phi Z_\Delta \rho_\phi \rho_\Delta} \\ 0 & V_{\phi\Delta} \sqrt{2Z_\phi Z_\Delta \rho_\phi \rho_\Delta} & Z_\Delta \rho_\Delta V_{\Delta\Delta} & Z_\Delta \left(K_\Delta^- + \rho_\Delta V_{\Delta\Delta} \right) \\ 0 & V_{\phi\Delta} \sqrt{2Z_\phi Z_\Delta \rho_\phi \rho_\Delta} & Z_\Delta \left(K_\Delta^+ + \rho_\Delta V_{\Delta\Delta} \right) & Z_\Delta \rho_\Delta V_{\Delta\Delta} \end{pmatrix}^{-1} \\
 &= \begin{pmatrix} \frac{G_\pi}{Z_\phi} \mathbb{1}_{3 \times 3} & 0 & 0 & 0 \\ 0 & \frac{G_\sigma}{Z_\phi} & \frac{G_{\sigma\Delta}^-}{\sqrt{Z_\phi Z_\Delta}} & \frac{G_{\sigma\Delta}^+}{\sqrt{Z_\phi Z_\Delta}} \\ 0 & \frac{G_{\sigma\Delta}^+}{\sqrt{Z_\phi Z_\Delta}} & \frac{G_{|\Delta|}}{Z_\Delta} & \frac{G_\Delta^+}{Z_\Delta} \\ 0 & \frac{G_{\sigma\Delta}^-}{\sqrt{Z_\phi Z_\Delta}} & \frac{G_\Delta^-}{Z_\Delta} & \frac{G_{|\Delta|}}{Z_\Delta} \end{pmatrix}
 \end{aligned}$$

with

$$\begin{aligned}
 K_{\Delta}^{\pm} &= \bar{p}^2 + (\omega_n \pm 2i\mu)^2 + V_{\Delta} \\
 G_{\Delta}^{\pm} &= \left[(K_{\Delta}^{\mp} + \rho_{\Delta} V_{\Delta\Delta}) K_{\sigma} - 2\rho_{\phi} \rho_{\Delta} V_{\phi\Delta}^2 \right] / J \\
 G_{|\Delta|} &= \left(2\rho_{\phi} V_{\phi\Delta}^2 - V_{\Delta\Delta} K_{\sigma} \right) \rho_{\Delta} / J \\
 G_{\sigma\Delta}^{\pm} &= -\sqrt{2\rho_{\phi} \rho_{\Delta}} V_{\phi\Delta} K_{\Delta}^{\mp} / J \\
 G_{\sigma} &= \left[K_{\Delta}^+ K_{\Delta}^- + \rho_{\Delta} V_{\Delta\Delta} (K_{\Delta}^+ + K_{\Delta}^-) \right] / J \\
 J &= K_{\sigma} \left[K_{\Delta}^+ K_{\Delta}^- + \rho_{\Delta} V_{\Delta\Delta} (K_{\Delta}^+ + K_{\Delta}^-) \right] - 2\rho_{\phi} \rho_{\Delta} V_{\phi\Delta}^2 (K_{\Delta}^+ + K_{\Delta}^-)
 \end{aligned} \tag{B.3}$$

These functions have the following properties, here we explicitly show the ω_n -dependence

$$K_{\Delta}^{\pm}(-\omega_n) = K_{\Delta}^{\mp}(\omega_n), \quad G_{\Delta}^{\pm}(-\omega_n) = G_{\Delta}^{\mp}(\omega_n), \quad G_{\sigma\Delta}^{\pm}(-\omega_n) = G_{\sigma\Delta}^{\mp}(\omega_n), \tag{B.4}$$

also

$$(K_{\Delta}^{\pm})^* = K_{\Delta}^{\mp}, \quad (G_{\Delta}^{\pm})^* = G_{\Delta}^{\mp}, \quad (G_{\sigma\Delta}^{\pm})^* = G_{\sigma\Delta}^{\mp}. \tag{B.5}$$

Since the transformation between representations affects only the diquark space, G_{σ} does not really change. The determinant does not change as well, due to Eq. (3.38). For derivation of flow equations we will require the following derivatives, which were derived similar to Eq. (B.1)

$$\begin{aligned}
 \frac{\partial G_{\sigma}}{\partial K_{\sigma}} &= -G_{\sigma}^2 & \frac{\partial G_{\sigma\Delta}^{\pm}}{\partial K_{\sigma}} &= -G_{\sigma} G_{\sigma\Delta}^{\pm} & \frac{\partial G_{|\Delta|}}{\partial K_{\sigma}} &= -G_{\sigma\Delta}^+ G_{\sigma\Delta}^- \\
 \frac{\partial G_{\Delta}^{\pm}}{\partial K_{\Delta}^{\pm}} &= -\left(G_{\Delta}^{\pm}\right)^2 & \frac{\partial G_{\sigma\Delta}^{\pm}}{\partial K_{\Delta}^{\pm}} &= -G_{\sigma\Delta}^{\pm} G_{\Delta}^{\pm} & \frac{\partial G_{|\Delta|}}{\partial K_{\Delta}^{\pm}} &= -G_{\Delta}^{\pm} G_{|\Delta|} \\
 \frac{\partial G_{\Delta}^{\pm}}{\partial K_{\Delta}^{\mp}} &= -G_{|\Delta|}^2 & \frac{\partial G_{\sigma\Delta}^{\pm}}{\partial K_{\Delta}^{\mp}} &= -G_{\sigma\Delta}^{\mp} G_{|\Delta|} & \frac{\partial G_{\Delta}^{\pm}}{\partial K_{\sigma}} &= \frac{\partial G_{\sigma}}{\partial K_{\Delta}^{\pm}} = -\left(G_{\sigma\Delta}^{\pm}\right)^2
 \end{aligned} \tag{B.6}$$

For $\rho_{\Delta} = 0$ the boson propagator is given by the simple from

$$G_{\bar{\varphi}} = \begin{pmatrix} \frac{1}{Z_{\phi} K_{\pi}} \mathbb{1}_{3 \times 3} & 0 & 0 & 0 \\ 0 & \frac{1}{Z_{\phi} K_{\sigma}} & 0 & 0 \\ 0 & 0 & 0 & \frac{1}{Z_{\Delta} K_{\Delta}^+} \\ 0 & 0 & \frac{1}{Z_{\Delta} K_{\Delta}^-} & 0 \end{pmatrix}. \tag{B.7}$$

Furthermore we have

$$G_{\Delta_2} \rightarrow \frac{K_{\Delta_2}}{K_{\Delta}^+ K_{\Delta}^-} = \frac{K_{\Delta}^+ + K_{\Delta}^-}{2K_{\Delta}^+ K_{\Delta}^-} = \frac{1}{2K_{\Delta}^+} + \frac{1}{2K_{\Delta}^-}. \tag{B.8}$$

The same holds for G_{Δ_1} .

QMDB-model of QCD

The extended parts in the propagator in the normal phase (3.42) of the QMDB-model are given by

$$G_{\Delta^r} = G_{\Delta^g} = \begin{pmatrix} 0 & \frac{1}{Z_{\Delta} K_{\Delta}^+} \\ \frac{1}{Z_{\Delta} K_{\Delta}^-} & 0 \end{pmatrix}. \quad (\text{B.9})$$

For the BEC phase, the inverse of the matrix in Eq. (3.46) is given by

$$G_{\varphi} = \begin{pmatrix} \frac{G_{\pi}}{Z_{\phi}} \mathbb{1}_{3 \times 3} & 0 & 0 \\ 0 & \frac{G_{\sigma}}{Z_{\phi}} & -\frac{G_{\sigma\Delta_1}}{\sqrt{Z_{\phi} Z_{\Delta}}} \\ 0 & -\frac{G_{\sigma\Delta_1}}{\sqrt{Z_{\phi} Z_{\Delta}}} & \frac{G_{\Delta_1}}{Z_{\Delta}} \end{pmatrix} \quad \text{with} \quad \begin{aligned} G_{\sigma} &= K_{\Delta_1}/J \\ G_{\Delta_1} &= K_{\sigma}/J \\ G_{\sigma\Delta_1} &= 2V_{\phi\Delta}\sqrt{\rho_{\phi}\rho_{\Delta}}/J \\ J &= K_{\sigma}K_{\Delta_1} - 4\rho_{\phi}\rho_{\Delta}V_{\phi\Delta}^2 \end{aligned}$$

Most of the flow equations have a G_{Δ}^{\pm} before the formal derivative $\tilde{\partial}_t$ is carried out. The relation between real and the complex representation is

$$G_{\Delta}^{\pm} = \frac{1}{2} (G_{\Delta_1} + G_{\Delta_2}) \mp iG_{\Delta_1\Delta_2} \quad \Rightarrow \quad G_{\Delta}^{\pm} \rightarrow \frac{1}{2} G_{\Delta_1}. \quad (\text{B.10})$$

Since in the BEC $G_{\Delta_2} = G_{\Delta_1\Delta_2} = 0$, we can make this replacement. We emphasize that the replacement should be done before $\tilde{\partial}_t$ is carried out.

B.2 The Nambu-Gorkov Propagator

Here all necessary informations and computations regarding the Nambu-Gorkov representation of fermionic fields will be given, and the propagators for the respective models will be derived. Additionally, the fermionic vertices for the QMDB-model will be shown.

QMD-model of QC₂D

First let us prove Eq. (3.49). After performing the matrix multiplication there are four terms: Two with pure color components and two with mixed ones. The pure red part already has the form of the quark part in the action (2.35). The pure green part can be rewritten to same form as well

$$\begin{aligned} \Gamma_{\text{quark}}|_g &= \int_x Z_q q_g^T C \tau_2 \left[i\phi - i\gamma_4 \mu + i h_{\phi} \sqrt{Z_{\phi}} (\sigma - i\gamma_5 \vec{\tau} \cdot \vec{\pi}) \right] \tau_2 C \bar{q}_g^T \\ &= \int_x Z_q q_g^T \left[i\phi^T - i\gamma_4^T \mu + i h_{\phi} \sqrt{Z_{\phi}} C^2 (\sigma + i\gamma_5 \vec{\tau}^T \cdot \vec{\pi}) \right] \bar{q}_g^T \\ &= \int_x Z_q \bar{q}_g \left[i\phi + i\gamma_4 \mu + i h_{\phi} \sqrt{Z_{\phi}} (\sigma + i\gamma_5 \vec{\tau} \cdot \vec{\pi}) \right] q_g. \end{aligned} \quad (\text{B.11})$$

We have used the properties of the Dirac algebra and Pauli matrices from App. A.4 . It is easy to see that $\tau_2 \vec{\tau} \tau_2 = -\vec{\tau}^T$. In the last step we have transposed the whole expression which gives a minus sign from fermionic interchange and another one in the derivative term, due to partial integration. Now we turn to the off-diagonal terms

$$\begin{aligned}
 \Gamma_{\text{quark}}|_{h_\Delta} &= - \int_x Z_q \sqrt{2Z_\Delta} h_\Delta \left[\Delta \bar{q}_r \gamma_5 \tau_2 C \bar{q}_g^T + \Delta^* q_g^T C \tau_2 \gamma_5 q_r \right] \\
 &= - \int_x Z_q \sqrt{2Z_\Delta} h_\Delta \frac{1}{2} \left[\Delta^* \left(q_g^T C \gamma_5 \tau_2 q_r - q_r^T \gamma_5 C^T \tau_2^T q_g \right) \right. \\
 &\quad \left. + \Delta \left(\bar{q}_r \tau_2 \gamma_5 C \bar{q}_g^T - \bar{q}_g \tau_2^T C^T \gamma_5 \bar{q}_r^T \right) \right] \\
 &= \int_x Z_q \sqrt{\frac{Z_\Delta}{2}} h_\Delta \left[\Delta^* \left(q_r^T C \gamma_5 \tau_2 q_g - q_g^T C \gamma_5 \tau_2 q_r \right) - \Delta \left(\bar{q}_r \tau_2 \gamma_5 C \bar{q}_g^T - \bar{q}_g \tau_2 \gamma_5 C \bar{q}_r^T \right) \right] \\
 &= \int_x Z_q \sqrt{\frac{Z_\Delta}{2}} i h_\Delta \left[\Delta^* q^T C \tau_2 \epsilon \gamma_5 q - \Delta \bar{q} \gamma_5 \epsilon \tau_2 C \bar{q}^T \right] \tag{B.12}
 \end{aligned}$$

In the first step we have added the transposed of the expression and divided all by 2, while in the last step we have summarized the color structure with e.g. $q^T = (q_r^T, q_g^T)$ and the antisymmetric tensor in color space ϵ .

Now we invert Eq. (3.52) to find the Nambu-Gorkov Propagator, see [362]

$$G_{\Psi\bar{\Psi}} = \frac{1}{Z_q} \frac{1}{\begin{pmatrix} [G_0^+]^{-1} & \Delta_0 \\ \Delta_0 & [G_0^-]^{-1} \end{pmatrix}} = \frac{1}{Z_q} \begin{pmatrix} G^+ & \Delta^- \\ \Delta^+ & G^- \end{pmatrix},$$

where

$$G^\pm = \frac{1}{[G_0^\pm]^{-1} - \Delta_0 G_0^\mp \Delta_0} = (\not{p} - i\hat{\sigma}) A_\pm + \gamma_4 B_\pm \tag{B.13}$$

and

$$\Delta^\pm = -G_0^\mp \Delta_0 G^\pm = \gamma_5 \left[\hat{\Delta} A \pm iF(\not{p} + i\hat{\sigma})\gamma_4 \right]. \tag{B.14}$$

The momentum dependencies were omitted here. With

$$\nu_\pm \equiv \nu_n \pm i\mu \tag{B.15}$$

we define the functions as

$$\begin{aligned}
 A &= a(\vec{p}^2)D(\vec{p}^2), & a(\vec{p}^2) &= \vec{p}^2 + \nu_+\nu_- + \hat{\sigma}^2 + \hat{\Delta}^2, \\
 A_{\pm} &= a_{\pm}(\vec{p}^2)D(\vec{p}^2), & a_{\pm}(\vec{p}^2) &= K_q^{\mp}(\vec{p}^2) + \hat{\Delta}^2, \\
 B_{\pm} &= b_{\pm}(\vec{p}^2)D(\vec{p}^2), & b_{\pm}(\vec{p}^2) &= \nu_{\pm}K_q^{\mp}(\vec{p}^2) + \nu_{\mp}\hat{\Delta}^2, \\
 F &= fD(\vec{p}^2), & f &= 2\hat{\Delta}\mu,
 \end{aligned}$$

and

$$K_q^{\pm}(\vec{p}^2) = \vec{p}^2 + \nu_{\pm}^2 + \hat{\sigma}^2, \quad D(\vec{p}^2) = \frac{1}{a_+a_- + f^2}. \quad (\text{B.16})$$

These functions have the following properties, here we explicitly show the ν_n -dependence and omit the \vec{p}^2 -dependence

$$A(-\nu_n) = A(\nu_n), \quad A_{\pm}(-\nu_n) = A_{\mp}(\nu_n), \quad B_{\pm}(-\nu_n) = -B_{\mp}(\nu_n), \quad F(-\nu_n) = F(\nu_n), \quad (\text{B.17})$$

also

$$A^* = A, \quad A_{\pm}^* = A_{\mp}, \quad B_{\pm}^* = B_{\mp}, \quad F^* = F \quad (\text{B.18})$$

For the derivation of flow equations, the following derivatives will be required

$$a' = a'_{\pm} = K_q^{\mp'} = 1, \quad b'_{\pm} = \nu_{\pm}, \quad (D^{-1})' = a_+ + a_- \quad (\text{B.19})$$

hence

$$\begin{aligned}
 A'_{\pm} &= F^2 - A_{\pm}^2, & A' &= D - A(A_+ + A_-), \\
 B'_{\pm} &= \nu_{\pm}D - B_{\pm}(A_+ + A_-), & F' &= -F(A_+ + A_-)
 \end{aligned} \quad (\text{B.20})$$

where primes denote a derivation with respect to the argument of these functions, which is \vec{p}^2 , as defined above. In the $\Delta \rightarrow 0$ limit the off-diagonal parts of $G_{\Psi\bar{\Psi}}$ vanish and the diagonal parts are given by

$$G_0^{\pm} = \frac{1}{\vec{p} + i\hat{\sigma} + \gamma_4\nu_{\pm}} = \frac{\vec{p} - i\hat{\sigma} + \gamma_4\nu_{\pm}}{K_q^{\pm}}, \quad (\text{B.21})$$

hence

$$A_{\pm} \rightarrow \frac{1}{K_q^{\pm}}, \quad B_{\pm} \rightarrow \frac{\nu_{\pm}}{K_q^{\pm}}. \quad (\text{B.22})$$

The elements of the inverse Nambu-Gorkov propagator can be read off from Eq. (3.52). For the derivation of Eq. (B.13), we define $p_{\pm} = (\vec{p}, \nu_{\pm})^T$ and show it for the plus sign

$$\begin{aligned}
 G^+ &= \frac{1}{\not{p}_+ + i\hat{\sigma} - \hat{\Delta}^2 \gamma_5 \frac{\not{p}_- - i\hat{\sigma}}{K_q^-} \gamma_5} \\
 &= \frac{\not{p}_+ + \frac{\hat{\Delta}^2}{K_q^-} \not{p}_- - i\hat{\sigma} \left(1 + \frac{\hat{\Delta}^2}{K_q^-}\right)}{\left(\not{p}_+ + \frac{\hat{\Delta}^2}{K_q^-} \not{p}_-\right)^2 + \hat{\sigma}^2 \left(1 + \frac{\hat{\Delta}^2}{K_q^-}\right)^2} \\
 &= \frac{K_q^- \not{p}_+ + \hat{\Delta}^2 \not{p}_- - i\hat{\sigma} (K_q^- + \hat{\Delta}^2)}{K_q^- (p_+^2 + \hat{\sigma}^2) + \frac{\hat{\Delta}^4}{K_q^-} (p_-^2 + \hat{\sigma}^2) + \hat{\Delta}^2 (\{p_+, p_-\} + 2\hat{\sigma}^2)} \\
 &= \frac{(\not{p} - i\hat{\sigma}) (K_q^- + \hat{\Delta}^2) + \gamma_4 (\nu_+ K_q^- + \nu_- \hat{\Delta}^2)}{K_q^- K_q^+ + \hat{\Delta}^4 + 2\hat{\Delta}^2 (\vec{p}^2 + \nu_+ \nu_- + \hat{\sigma}^2)} \\
 &= \frac{(\not{p} - i\hat{\sigma}) a_+ + \gamma_4 b_+}{K_q^- K_q^+ + \hat{\Delta}^4 + \hat{\Delta}^2 (K_q^- + K_q^+ + 4\mu^2)}. \tag{B.23}
 \end{aligned}$$

Keep in mind, that swapping γ_5 with \not{p}_- yields a minus sign. Furthermore

$$\{\not{p}_-, \not{p}_+\} = p_-^\mu p_+^\nu \{\gamma_\mu, \gamma_\nu\} = 2p_-^\mu p_+^\nu \delta_{\mu\nu} = 2\vec{p}^2 + 2\nu_+ \nu_-.$$

In the last step we used that $\nu_+^2 + \nu_-^2 = 2\nu_n^2 - 2\mu^2$ and $\nu_+ \nu_- = \nu_n^2 + \mu^2$. We see that the denominator agrees with Eq. (B.16), as

$$K_q^- K_q^+ + \hat{\Delta}^4 + \hat{\Delta}^2 (K_q^- + K_q^+ + 4\mu^2) = a_+ a_- + c^2.$$

The derivation of Eq. (B.14) will be shown here

$$\begin{aligned}
 \Delta^\pm &= -\frac{\not{p} - i\hat{\sigma} + \gamma_4 \nu_\pm}{K_q^\mp} (-\hat{\Delta} \gamma_5) \left[(\not{p} - i\hat{\sigma}) A_\pm + \gamma_4 B_\pm \right] \\
 &= \hat{\Delta} \gamma_5 \frac{\not{p} + i\hat{\sigma} + \gamma_4 \nu_\pm}{K_q^\mp} \left[(\not{p} - i\hat{\sigma}) A_\pm + \gamma_4 B_\pm \right] \\
 &= \frac{\hat{\Delta} \gamma_5}{K_q^\mp} \left[(\vec{p}^2 + \hat{\sigma}^2) A_\pm + \nu_\mp B_\pm + (\not{p} + i\hat{\sigma}) \gamma_4 (B_\pm - \nu_\mp A_\pm) \right] \\
 &= \frac{\hat{\Delta} \gamma_5}{K_q^\mp D} \left[(\vec{p}^2 + \hat{\sigma}^2) (K_q^\mp + \hat{\Delta}^2) + \nu_\mp \nu_\pm K_q^\mp (\vec{p}^2) + \nu_\mp^2 \hat{\Delta}^2 \right. \\
 &\quad \left. + (\not{p} + i\hat{\sigma}) \gamma_4 (\nu_\pm K_q^\mp + \nu_\mp \hat{\Delta}^2 - \nu_\mp K_q^\mp (\vec{p}^2) - \nu_\mp \hat{\Delta}^2) \right] \\
 &= \frac{\hat{\Delta} \gamma_5}{K_q^\mp D} \left[K_q^\mp (\vec{p}^2 + \hat{\sigma}^2 + \nu_\mp \nu_\pm) + \hat{\Delta}^2 (\vec{p}^2 + \hat{\sigma}^2 + \nu_\mp^2) \pm (\not{p} + i\hat{\sigma}) \gamma_4 K_q^\mp (\nu_+ - \nu_-) \right] \\
 &= \frac{\hat{\Delta} \gamma_5}{D} \left[a \pm 2i\mu (\not{p} + i\hat{\sigma}) \gamma_4 \right].
 \end{aligned}$$

QMDB-model of QCD

The off-diagonals in Eq. (3.59) are given by

$$\Xi = \sqrt{Z_q Z_\Delta} \begin{pmatrix} 0 & \sqrt{2Z_q} h_\Delta \gamma_5 \\ \sqrt{Z_B} i h_{qdB} & 0 \end{pmatrix}, \quad \bar{\Xi} = \sqrt{Z_q Z_\Delta} \begin{pmatrix} \sqrt{2Z_q} h_\Delta \gamma_5 & 0 \\ 0 & \sqrt{Z_B} i h_{qdB} \end{pmatrix}.$$

Let us briefly discuss the terms in order see that we have constructed them correctly. Naturally Σ is For the case of the qdb -interaction in Σ the matrices in the subspaces cancel with the ones from the g -component of Ψ ($\bar{\Psi}$) yielding a minus sign due to $C^2 = -\mathbb{1}$, which, for the term emerging from the lower left part of Σ in the middle term of (3.58), is canceled by bringing the fermionic fields to the same order as in (2.36). In the upper right of Σ the minus cancels trivially. For the last term the argument goes oppositely (regarding lower right and upper left), since the fields must be opposite order, therefore there is minus sign in the front. It is easy to see that the first term in Eq. (3.58) coincides with the corresponding part in Eq. (2.36). For the kinetic parts and the qdb -interaction it is rather trivial, while for the quark-diquark interaction the minus signs according to the antisymmetric tensor have to be considered. Let us write it down for completeness

$$\Gamma_{\text{fermion}}|_{h_\Delta} = \int_x Z_q \sqrt{2Z_\Delta} h_\Delta \left(\Delta^{*r} q_g^T C \tau_2 \gamma_5 q_b + \Delta^r \bar{q}_b \gamma_5 \tau_2 C \bar{q}_g^T + \Delta^{*g} q_b^T C \tau_2 \gamma_5 q_r - \Delta^g \bar{q}_b \gamma_5 \tau_2 C \bar{q}_r^T \right. \\ \left. - \Delta^{*b} q_g^T C \tau_2 \gamma_5 q_r - \Delta^b \bar{q}_r \gamma_5 \tau_2 C \bar{q}_g^T \right). \quad (\text{B.24})$$

This is how it emerges from Eq. (3.58). We have summarized terms with similar color structure by transposing. We see that every symmetric order of the color indices have a positive sign for Δ^* -terms and a negative sign for the Δ -terms, and vice versa for the antisymmetric orders, just how it is supposed to be according to Eq. (2.36). Now all terms can be duplicated like in Eq. (B.12), then it we have the same form as in (2.36).

The bB -propagator is given by

$$G_{bB} = \begin{pmatrix} \frac{G_b}{Z_q} & \frac{\Delta_{bB}}{\sqrt{Z_B Z_q}} \\ \frac{\Delta_{Bb}}{\sqrt{Z_B Z_q}} & \frac{G_B}{Z_B} \end{pmatrix}. \quad (\text{B.25})$$

The diagonal parts of the this propagator read

$$G_b = \not{p} A_b - i H_b + \gamma_4 B_b, \quad (\text{B.26})$$

$$G_B = \not{p} A_B - i H_B + \gamma_4 B_B \quad (\text{B.27})$$

with

$$\begin{aligned} A_b &= \left[K_B + z_B \hat{\Delta}_B^2 \right] L, & H_b &= \left(\hat{\sigma} K_B + \hat{\sigma}_B \hat{\Delta}_B^2 \right) L, \\ A_B &= \left[z_B K_q^+ + \hat{\Delta}_B^2 \right] L, & H_B &= \left(\hat{\sigma}_B K_q^+ + \hat{\sigma} \hat{\Delta}_B^2 \right) L, \\ K_B &= z_B^2 \vec{p}^2 + \nu_B^2 + \hat{\sigma}_B^2, & B_b &= \left(\nu_+ K_B + \nu_B \hat{\Delta}_B^2 \right) L, \\ L &= \frac{1}{K_q^+ K_B + \hat{\Delta}_B^4 + 2 \hat{\Delta}_B^2 \left[|\vec{p}| (z_B |\vec{p}|) + \nu_+ \nu_B + \hat{\sigma} \hat{\sigma}_B \right]}, & B_B &= \left(\nu_B K_q^+ + \nu_+ \hat{\Delta}_B^2 \right) L, \end{aligned}$$

where $\nu_B = \nu_n + i\mu_B$. The derivation is very similar to the one for G^+ in (B.23) with the difference that $p_- \rightarrow (z_B \vec{p}, \nu_B)^T$ and that there is a h_B in one of the $\hat{\sigma}$. It is clear that within flow equations, z_B always comes together with momentum. Therefore, in the regularized propagator we can make the replacement

$$z_B(\vec{p}^2)|\vec{p}| = |\vec{p}| + m_B^{\text{UV}} \rightarrow |\vec{p}_r| + m_B^{\text{UV}} = z_B(\vec{p}_r^2)|\vec{p}_r|, \quad (\text{B.28})$$

where the $|\vec{p}|$ before the arrow belongs to the trivial momentum dependence of the propagator, which is regularized as usual. So the general way $A(\vec{p}^2) \rightarrow A(\vec{p}_r^2)$ is still correct.

We will need derivatives with respect to the blue quark momentum \vec{p}_b and the baryon momentum \vec{p}_B respectively. Although we have not denoted them distinctively, we can distinguish them simply by the fact that the baryon momentum always comes as $z_B|\vec{p}|$. Therefore we can regard the above functions as $f(|\vec{p}|, z_B|\vec{p}|)$ and apply the somewhat sloppy convention

$$\frac{\partial}{\partial \vec{p}_b^2} f(|\vec{p}|, z_B|\vec{p}|) \equiv \frac{1}{2|\vec{p}|} f^{(1,0)}(|\vec{p}|, z_B|\vec{p}|), \quad (\text{B.29})$$

$$\frac{\partial}{\partial \vec{p}_B^2} f(|\vec{p}|, z_B|\vec{p}|) \equiv \frac{1}{2|\vec{p}|} f^{(0,1)}(|\vec{p}|, z_B|\vec{p}|), \quad (\text{B.30})$$

where the exponents (1,0) and (0,1) denote derivatives with respect to the first and the second argument of the function f respectively. We have used that $\frac{\partial}{\partial |\vec{p}|} z_B|\vec{p}| = 1$. With these rules we find

$$\begin{aligned} \frac{\partial K_b}{\partial \vec{p}_b^2} &= 1, & \frac{\partial L^{-1}}{\partial \vec{p}_b^2} &= K_B + z_B \hat{\Delta}_B^2 = \frac{A_b}{L}, \\ \frac{\partial K_B}{\partial \vec{p}_B^2} &= z_B, & \frac{\partial L^{-1}}{\partial \vec{p}_B^2} &= z_B K_q^+ + \hat{\Delta}_B^2 = \frac{A_B}{L}. \end{aligned}$$

Essentially we will have the above derivative operators acting on $|\vec{p}|A_{b/B}$. In order to correctly distinguish \vec{p}_b and \vec{p}_B , we multiply $|\vec{p}|$ with each term of the numerator of $A_{b/B}$, since it is originally there in the propagators (B.26)-(B.27). Then we have functions of the type $f(|\vec{p}|, |\vec{p}| + m_B)$ and we can apply the rules (B.29)-(B.30):

$$\begin{aligned} \frac{\partial}{\partial \vec{p}_b^2} |\vec{p}| A_b &= |\vec{p}| \left(\frac{K_B L}{2\vec{p}^2} - A_b^2 \right), \\ \frac{\partial}{\partial \vec{p}_B^2} |\vec{p}| A_B &= |\vec{p}| \left(\frac{K_q^+ L}{2\vec{p}^2} - A_B^2 \right), \\ \frac{\partial}{\partial \vec{p}_B^2} |\vec{p}| A_b &= \frac{\partial}{\partial \vec{p}_b^2} |\vec{p}| A_B = |\vec{p}| \left(\left[z_B + \frac{\hat{\Delta}_B^2}{2\vec{p}^2} \right] L - A_B A_b \right). \end{aligned} \quad (\text{B.31})$$

In the $\Delta \rightarrow 0$ limit the off-diagonal parts of the propagator (B.25) vanish and

$$G_b \rightarrow G_0^+, \quad G_B \rightarrow \frac{z_B \vec{p} - i\sigma_B + \gamma_4 \nu_B}{K_B}. \quad (\text{B.32})$$

Hence, the functions turn into

$$L \rightarrow \frac{1}{K_q^+ K_B}, \quad A_b \rightarrow \frac{1}{K_q^+}, \quad A_B \rightarrow \frac{z_B}{K_B}. \quad (\text{B.33})$$

The fermionic vertices are given by

$$\begin{aligned}
 \Gamma_{\bar{\Psi}\sigma\Psi} &= \sqrt{Z_\phi} Z_q i h_\phi \mathbb{1}, & \Gamma_{\bar{\Psi}\pi_i\Psi} &= -\sqrt{Z_\phi} Z_q h_\phi \gamma_5 \tau_i \begin{pmatrix} \sigma_3 & 0 \\ 0 & \mathbb{1} \end{pmatrix}, \\
 \Gamma_{\bar{\Psi}\Delta^r\Psi} &= \begin{pmatrix} 0 & 0 \\ \Xi & 0 \end{pmatrix}, & \Gamma_{\bar{\Psi}\Delta^b\Psi} &= \sqrt{Z_q Z_\Delta} \begin{pmatrix} -\sqrt{2Z_q} h_\Delta \gamma_5 s^T & 0 \\ 0 & \sqrt{Z_B} i h_{qdB} s \end{pmatrix}, \\
 \Gamma_{\bar{\Psi}\Delta^{*r}\Psi} &= \begin{pmatrix} 0 & \Xi^T \\ 0 & 0 \end{pmatrix}, & \Gamma_{\bar{\Psi}\Delta^{*b}\Psi} &= \sqrt{Z_q Z_\Delta} \begin{pmatrix} -\sqrt{2Z_q} h_\Delta \gamma_5 s & 0 \\ 0 & \sqrt{Z_B} i h_{qdB} s^T \end{pmatrix}, \\
 \Gamma_{\Psi\Delta^{*g}\Psi} &= \tau_2 C \begin{pmatrix} 0 & -\bar{\Xi} \\ \bar{\Xi} & 0 \end{pmatrix}, \\
 \Gamma_{\bar{\Psi}\Delta^g\Psi} &= \tau_2 C \begin{pmatrix} 0 & \bar{\Xi} \\ -\bar{\Xi} & 0 \end{pmatrix}
 \end{aligned} \tag{B.34}$$

where $s = \begin{pmatrix} 0 & 0 \\ 1 & 0 \end{pmatrix}$ and σ_3 is a the third Pauli matrix in Nambu-Gorkov space. Note that the σ, π_i, Δ^b vertices in the rg -part coincide with the vertices (3.102) of QC₂D. Furthermore, $\Gamma_{\Psi\varphi_i\Psi} = -\Gamma_{\bar{\Psi}\varphi_i\Psi}^T$ and similarly $\Gamma_{\bar{\Psi}\varphi_i\bar{\Psi}} = -\Gamma_{\bar{\Psi}\varphi_i\bar{\Psi}}^T$.

Flow Equations

In order to keep the equations overseeable we will write the entries of the boson propagator G_φ as functions of the four momentum q (or $q \pm p$) instead of the regularized momentum squared \vec{p}_r^2 . In final equations the bosonic propagators and the functions from the fermionic propagator will be displayed without arguments, which is always meant in the way that all functions of \vec{p}^2 , which are defined in App. B, are evaluated at k^2 .

C.1 Bosonic Anomalous Dimension

Boson Loop

The boson loop contribution to the bosonic anomalous dimensions is given by

$$\eta_{\varphi_i}|_\varphi = \frac{1}{2Z_{\varphi_i}} \tilde{\partial}_t \frac{\partial}{\partial \vec{p}^2} \text{tr} \int_q G_\varphi(q) \Gamma_{\varphi\varphi_i\varphi} G_\varphi(q+p) \Gamma_{\varphi\varphi_i\varphi} \Big|_{p=0}. \quad (\text{C.1})$$

For the mesonic anomalous we basically need two kinds of vertices $\Gamma_{\pi_1\pi_1\sigma} = Z_\phi V_{\phi\phi} \sqrt{2Z_\phi \rho_\phi}$ and $\Gamma_{\pi_1\pi_1\Delta_1} = Z_\phi V_{\phi\Delta} \sqrt{2Z_\Delta \rho_\Delta}$ with permutations of their left and right indices. All other entries of pionic three-point function in the bosonic sector are vanishing, cf. Eq. (3.100). We do not have to take real part of the flow, as its baryon charge is zero, and therefore the loop must be real valued. So, the boson loop for mesonic anomalous is given by

$$\begin{aligned} \eta_\phi|_\varphi &= \frac{1}{Z_\phi} \tilde{\partial}_t \frac{\partial}{\partial \vec{p}^2} \int_q \left[\frac{G_\pi(q)}{Z_\phi} \Gamma_{\pi_1\pi_1\Delta_1} \frac{G_{\Delta_1}(q+p)}{Z_\Delta} \Gamma_{\Delta_1\pi_1\pi_1} + \frac{G_\pi(q)}{Z_\phi} \Gamma_{\pi_1\pi_1\sigma} \frac{G_\sigma(q+p)}{Z_\phi} \Gamma_{\sigma\pi_1\pi_1} \right. \\ &\quad \left. - 2 \frac{G_\pi(q)}{Z_\phi} \Gamma_{\pi_1\pi_1\sigma} \frac{G_{\sigma\Delta_1}(q+p)}{\sqrt{Z_\phi Z_\Delta}} \Gamma_{\Delta_1\pi_1\pi_1} \right] \Big|_{p=0} \\ &= 2\tilde{\partial}_t \frac{\partial}{\partial \vec{p}^2} \int_q G_\pi(q) [\rho_\phi V_{\phi\phi}^2 G_\sigma(q+p) + \rho_\Delta V_{\phi\Delta}^2 G_{\Delta_1}(q+p) - 2\sqrt{\rho_\phi \rho_\Delta} V_{\phi\phi} V_{\phi\Delta} G_{\sigma\Delta_1}(q+p)] \Big|_{p=0}, \end{aligned} \quad (\text{C.2})$$

with the definitions from App. B.1. It is easy to see that all Z 's cancel out when the vertices are inserted. The indices of the propagator matrix are displayed in a sloppy notation, however, a propagator in between two vertices carries the last index of the left vertex and the first index of the right vertex. So the leftmost and rightmost indices of the vertices indicate the way the matrices were multiplied/traced. There were similar terms where the external momentum p is carried by the pion propagator, which yield the same result as the ones displayed above, after

shifting the integration variable $q \rightarrow (q - p)$ and then $p \rightarrow -p$, which leaves the derivative and the point of the evaluation $p = 0$ trivially invariant. hence the cancellation of the factor $\frac{1}{2}$ in the first step. There is a factor of 2 in the last term, as there was another term where the indices $\sigma \leftrightarrow \Delta_1$ are interchanged, which gives the same contribution. The minus sign can be found in the definition of the propagator G_φ . The integrals have the form of Eq. (C.43), thus, with Eq. (C.49) and (B.2) we find for the boson loop in the mesonic anomalous dimension

$$\begin{aligned} \eta_\phi|_\varphi &= 2I_{\eta_B}^{(1)} \left[G_\pi, \rho_\phi V_{\phi\phi}^2 G_\sigma + \rho_\Delta V_{\phi\Delta}^2 G_{\Delta_1} - 2\sqrt{\rho_\phi \rho_\Delta} V_{\phi\phi} V_{\phi\Delta} G_{\sigma\Delta_1} \right] \\ &= \frac{2}{3\pi^2} k^5 T \sum_n G_\pi^2 \left[\rho_\phi V_{\phi\phi}^2 \left(G_\sigma^2 + G_{\sigma\Delta_1}^2 - G_{\sigma\Delta_2}^2 \right) + \rho_\Delta V_{\phi\Delta}^2 \left(G_{\Delta_1}^2 + G_{\sigma\Delta_1}^2 - G_{\Delta_1\Delta_2}^2 \right) \right. \\ &\quad \left. - 2\sqrt{\rho_\phi \rho_\Delta} V_{\phi\phi} V_{\phi\Delta} \left(G_\sigma G_{\sigma\Delta_1} + G_{\sigma\Delta_1} G_{\Delta_1} - G_{\sigma\Delta_2} G_{\Delta_1\Delta_2} \right) \right] \end{aligned}$$

In the $\Delta \rightarrow 0$ limit the contribution reduces to the term with the sigma propagators, which in turn reduces to its simplest version

$$\eta_\phi(\Delta = 0)|_\varphi = 2\rho_\phi V_{\phi\phi}^2 I_{\eta_B}^{(1)} \left[\frac{1}{K_\pi}, \frac{1}{K_\sigma} \right] = \frac{2}{3\pi^2} \rho_\phi V_{\phi\phi}^2 k^5 T \sum_n \frac{1}{K_\pi^2 K_\sigma^2}. \quad (\text{C.3})$$

All functions in previous two equations are evaluated at k^2 .

Similarly, we find for the diquark anomalous dimension, with the vertices $\Gamma_{\Delta_2\Delta_2\sigma} = Z_\Delta V_{\phi\Delta} \sqrt{2Z_\phi \rho_\phi}$ and $\Gamma_{\Delta_2\Delta_2\Delta_1} = Z_\Delta V_{\Delta\Delta} \sqrt{2Z_\Delta \rho_\Delta}$

$$\begin{aligned} \eta_\Delta|_\varphi &= \frac{1}{Z_\Delta} \tilde{\partial}_t \frac{\partial}{\partial \vec{p}^2} \int_q \left[\frac{G_{\Delta_1}(q)}{Z_\Delta} \Gamma_{\Delta_1\Delta_2\Delta_2} \frac{G_{\Delta_2}(q+p)}{Z_\Delta} \Gamma_{\Delta_2\Delta_2\Delta_1} + \frac{G_\sigma(q)}{Z_\phi} \Gamma_{\sigma\Delta_2\Delta_2} \frac{G_{\Delta_2}(q+p)}{Z_\Delta} \Gamma_{\Delta_2\Delta_2\sigma} \right. \\ &\quad + \frac{G_{\Delta_1\Delta_2}(q)}{Z_\Delta} \Gamma_{\Delta_2\Delta_2\Delta_1} \frac{G_{\Delta_1\Delta_2}(q+p)}{Z_\Delta} \Gamma_{\Delta_2\Delta_2\Delta_1} + \frac{G_{\sigma\Delta_2}(q)}{\sqrt{Z_\phi Z_\Delta}} \Gamma_{\Delta_2\Delta_2\sigma} \frac{G_{\sigma\Delta_2}(q+p)}{\sqrt{Z_\phi Z_\Delta}} \Gamma_{\Delta_2\Delta_2\sigma} \\ &\quad \left. - 2 \frac{G_{\sigma\Delta_1}(q)}{\sqrt{Z_\phi Z_\Delta}} \Gamma_{\Delta_1\Delta_2\Delta_2} \frac{G_{\Delta_2}(q+p)}{Z_\Delta} \Gamma_{\Delta_2\Delta_2\sigma} - 2 \frac{G_{\sigma\Delta_2}(q)}{\sqrt{Z_\phi Z_\Delta}} \Gamma_{\Delta_2\Delta_2\Delta_1} \frac{G_{\Delta_1\Delta_2}(q+p)}{Z_\Delta} \Gamma_{\Delta_2\Delta_2\sigma} \right] \Big|_{p=0} \\ &= 2 \tilde{\partial}_t \frac{\partial}{\partial \vec{p}^2} \int_q \left\{ \rho_\Delta V_{\Delta\Delta}^2 [G_{\Delta_1}(q) G_{\Delta_2}(q+p) + G_{\Delta_1\Delta_2}(q) G_{\Delta_1\Delta_2}(q+p)] \right. \\ &\quad + \rho_\phi V_{\phi\Delta}^2 [G_\sigma(q) G_{\Delta_2}(q+p) + G_{\sigma\Delta_2}(q) G_{\sigma\Delta_2}(q+p)] \\ &\quad \left. - 2\sqrt{\rho_\phi \rho_\Delta} V_{\Delta\Delta} V_{\phi\Delta} [G_{\sigma\Delta_1}(q) G_{\Delta_2}(q+p) + G_{\sigma\Delta_2}(q) G_{\Delta_1\Delta_2}(q+p)] \right\} \Big|_{p=0} \end{aligned} \quad (\text{C.4})$$

Again, all contributions appeared twice and can be summarized, which partly can be shown by substituting momentum variables as above and partly by switching indices. Let us discuss the terms in the first equation. In the upper line we have contributions from diagonal elements of the propagator, which also occur in the opposite order. Corresponding to the second line, terms occur where the indices for each matrix element are interchanged, which yields the same result with a $(-1)^2$ from the definition of G_φ . In the last line, the minus is again from the definition of the propagator, the factor of 2 is because of the contributions occur four times, where either the order of the propagators is interchanged or the indices of each matrix element are interchanged and the elements are rearranged. Interchanging indices in the last term gives again a $(-1)^2$. The

integration of the boson loop in the diquark anomalous dimension is then given by

$$\begin{aligned}
 \eta_\Delta|_\varphi &= 2I_{\eta_B}^{(1)} \left[G_{\Delta_2}, \rho_\Delta V_{\Delta\Delta}^2 G_{\Delta_1} + \rho_\phi V_{\phi\Delta}^2 G_\sigma - 2\sqrt{\rho_\phi \rho_\Delta} V_{\Delta\Delta} V_{\phi\Delta} G_{\sigma\Delta_1} \right] + 2\rho_\phi V_{\phi\Delta}^2 I_{\eta_B}^{(1)} [G_{\sigma\Delta_2}, G_{\sigma\Delta_2}] \\
 &\quad + 2\rho_\Delta V_{\Delta\Delta}^2 I_{\eta_B}^{(1)} [G_{\Delta_1\Delta_2}, G_{\Delta_1\Delta_2}] - 4\sqrt{\rho_\phi \rho_\Delta} V_{\Delta\Delta} V_{\phi\Delta} I_{\eta_B}^{(1)} [G_{\sigma\Delta_2}, G_{\Delta_1\Delta_2}] \\
 &= \frac{2}{3\pi^2} k^5 T \sum_n \left\{ G_{\Delta_2} \left[\rho_\Delta V_{\Delta\Delta}^2 (G_{\Delta_1}^2 + G_{\sigma\Delta_1}^2 - G_{\Delta_1\Delta_2}^2) + \rho_\phi V_{\phi\Delta}^2 (G_\sigma^2 + G_{\sigma\Delta_1}^2 - G_{\sigma\Delta_2}^2) \right. \right. \\
 &\quad \left. \left. - 2\sqrt{\rho_\phi \rho_\Delta} V_{\Delta\Delta} V_{\phi\Delta} (G_\sigma G_{\sigma\Delta_1} + G_{\sigma\Delta_1} G_{\Delta_1} - G_{\sigma\Delta_2} G_{\Delta_1\Delta_2}) \right] \right. \\
 &\quad \left. + \left[\sqrt{2\rho_\phi} V_{\phi\Delta} (G_\sigma G_{\sigma\Delta_2} + G_{\sigma\Delta_1} G_{\Delta_1\Delta_2} + G_{\sigma\Delta_2} G_{\Delta_2}) \right. \right. \\
 &\quad \left. \left. - \sqrt{2\rho_\Delta} V_{\Delta\Delta} (G_{\sigma\Delta_1} G_{\sigma\Delta_2} + G_{\Delta_1} G_{\Delta_1\Delta_2} + G_{\Delta_1\Delta_2} G_{\Delta_2}) \right]^2 \right\}
 \end{aligned}$$

Note that although there are square roots of the ρ 's, the square roots will disappear once the definitions of the propagators are inserted from App. B.1, this also reflects the fact that all flow equations must be given in terms of invariants. In the $\Delta \rightarrow 0$ limit the coefficient again reduces to the term with the sigma propagator, while G_{Δ_2} reduces to Eq. (B.8), hence

$$\begin{aligned}
 \eta_\Delta(\Delta=0)|_\varphi &= 2\rho_\phi V_{\phi\Delta}^2 I_{\eta_B}^{(1)} \left[\frac{1}{K_\sigma}, \frac{1}{2K_\Delta^+} + \frac{1}{2K_\Delta^-} \right] = 2\rho_\phi V_{\phi\Delta}^2 I_{\eta_B}^{(1)} \left[\frac{1}{K_\sigma}, \frac{1}{K_\Delta^+} \right] \\
 &= \frac{2}{3\pi^2} \rho_\phi V_{\phi\Delta}^2 k^5 T \sum_n \frac{1}{K_\sigma^2 (K_\Delta^+)^2}.
 \end{aligned} \tag{C.5}$$

We have used the fact that the Matsubara summation yields the same result for the K_Δ^- part as for the K_Δ^+ part. Again, all functions are evaluated at k^2 . At $\mu = 0$ Eq. (C.3) and (C.5) coincide because diquarks and pions are degenerate in two-color QCD and they have the same couplings in the effective potential.

Fermion Loop

As indicated in Eq. (3.108), the quark loop in the bosonic anomalous dimension comes with an overall minus sign, due to the str, so it is given by

$$\begin{aligned}
 \eta_{\varphi_i}|\Psi &= -\frac{1}{2Z_{\varphi_i}} \tilde{\partial}_t \frac{\partial}{\partial p^2} \text{tr} \int_q G_{\Psi\bar{\Psi}}(q) \Gamma_{\bar{\Psi}\varphi_i\Psi} G_{\Psi\bar{\Psi}}(q+p) \Gamma_{\bar{\Psi}\varphi_i\Psi} + G_{\bar{\Psi}\Psi}(q) \Gamma_{\Psi\varphi_i\bar{\Psi}} G_{\bar{\Psi}\Psi}(q+p) \Gamma_{\Psi\varphi_i\bar{\Psi}} \Big|_{p=0} \\
 &= -\frac{1}{Z_{\varphi_i}} \tilde{\partial}_t \frac{\partial}{\partial p^2} \text{tr} \int_q G_{\Psi\bar{\Psi}}(q) \Gamma_{\bar{\Psi}\varphi_i\Psi} G_{\Psi\bar{\Psi}}(q+p) \Gamma_{\bar{\Psi}\varphi_i\Psi} \Big|_{p=0}.
 \end{aligned} \tag{C.6}$$

We can summarize the two expressions in the upper line, as we can write the second term as

$$(-1)^4 \text{tr} \int_q G_{\Psi\bar{\Psi}}^T(-q) \Gamma_{\bar{\Psi}\varphi_i\Psi}^T G_{\Psi\bar{\Psi}}^T(-(q+p)) \Gamma_{\bar{\Psi}\varphi_i\Psi}^T = \text{tr} \int_q \Gamma_{\bar{\Psi}\varphi_i\Psi} G_{\Psi\bar{\Psi}}(-(q+p)) \Gamma_{\bar{\Psi}\varphi_i\Psi} G_{\Psi\bar{\Psi}}(-q).$$

The minus signs are from interchanging fermionic indices and in the next step we have transposed the hole expression. Now one can use the cyclic property of the trace and shift the integration variable $q \rightarrow -q - p$ to see that it is exactly the same expression as the first term in fermionic contribution is obtained.

Now we perform the matrix multiplication of the propagator with the vertex of each boson

$$G_{\Psi\bar{\Psi}}\Gamma_{\bar{\Psi}\pi_1\Psi} = \frac{1}{Z_q} \begin{pmatrix} G^+ & \Delta^- \\ \Delta^+ & G^- \end{pmatrix} \sqrt{Z_\phi} Z_q h_\phi \begin{pmatrix} -\gamma_5 \tau_1 & 0 \\ 0 & \gamma_5 \tau_1 \end{pmatrix} = \sqrt{Z_\phi} h_\phi \begin{pmatrix} -G^+ \gamma_5 \tau_1 & \Delta^- \gamma_5 \tau_1 \\ -\Delta^+ \gamma_5 \tau_1 & G^- \gamma_5 \tau_1 \end{pmatrix},$$

$$G_{\Psi\bar{\Psi}}\Gamma_{\bar{\Psi}\Delta_2\Psi} = \frac{1}{Z_q} \begin{pmatrix} G^+ & \Delta^- \\ \Delta^+ & G^- \end{pmatrix} \sqrt{Z_\Delta} Z_q h_\Delta \begin{pmatrix} 0 & -i\gamma_5 \\ i\gamma_5 & 0 \end{pmatrix} = \sqrt{Z_\Delta} h_\Delta \begin{pmatrix} i\Delta^- \gamma_5 & -iG^+ \gamma_5 \\ iG^- \gamma_5 & -i\Delta^+ \gamma_5 \end{pmatrix}.$$

Thus

$$\begin{aligned} & \int_q \text{tr} [G_{\Psi\bar{\Psi}}(q) \Gamma_{\bar{\Psi}\pi_1\Psi} G_{\Psi\bar{\Psi}}(q+p) \Gamma_{\bar{\Psi}\pi_1\Psi}] \\ &= Z_\phi h_\phi^2 \int_q \text{tr} [G^+(q) \gamma_5 G^+(q+p) \gamma_5 - \Delta^-(q) \gamma_5 \Delta^+(q+p) \gamma_5 \\ & \quad + G^-(q) \gamma_5 G^-(q+p) \gamma_5 - \Delta^+(q) \gamma_5 \Delta^-(q+p) \gamma_5] \\ &= Z_\phi h_\phi^2 N_c \int_q \text{tr} [G^+(q) \gamma_5 G^+(q+p) \gamma_5 - \Delta^+(q) \gamma_5 \Delta^-(q+p) \gamma_5]. \end{aligned}$$

Similarly

$$\begin{aligned} & \int_q \text{tr} [G_{\Psi\bar{\Psi}}(q) \Gamma_{\bar{\Psi}\Delta_2\Psi} G_{\Psi\bar{\Psi}}(q+p) \Gamma_{\bar{\Psi}\Delta_2\Psi}] \\ &= Z_\Delta h_\Delta^2 i^2 \int_q \text{tr} [\Delta^-(q) \gamma_5 \Delta^-(q+p) \gamma_5 - G^+(q) \gamma_5 G^-(q+p) \gamma_5 \\ & \quad + \Delta^+(q) \gamma_5 \Delta^+(q+p) \gamma_5 - G^-(q) \gamma_5 G^+(q+p) \gamma_5] \\ &= Z_\Delta h_\Delta^2 N_c \int_q \text{tr} [G^-(q) \gamma_5 G^+(q+p) \gamma_5 - \Delta^+(q) \gamma_5 \Delta^+(q+p) \gamma_5]. \end{aligned}$$

The matrices in flavor space commute with the propagator, as it has a trivial structure in flavor space. After swapping the flavor matrices they result in a unit matrix, since they are squared, therefore they were omitted. In the last step for each case we have already assumed, that tracing over the Dirac space will yield only terms with same kinds coefficients defined in App. B.2, due to the tracing properties of the Dirac algebra, which are shown in App. A.4. For the G^\pm terms, assuming that $p_4 = 0$ we shift the q_4 -integration like $q_4 \rightarrow -q_4$ and make use of the properties in Eqs. (B.17) in order to make this step. It will become clearer, once it is written down below. The color factor N_c stems from the fact that the Nambu-Gorkov space in our convention is equivalent to color space.

It is apparent now, that the fermion-loop contribution to the mesonic and diquark anomalous dimension are quite similar, except for the signs in front of the chemical potential. After tracing we find with the definitions in App. B.2

$$\begin{aligned} \eta_{\hat{\Delta}}|_{\Psi} = & -4N_c N_f h_{\hat{\Delta}}^2 \tilde{\partial}_t \frac{\partial}{\partial \vec{p}^2} \int_q \left\{ A_{\pm}(\vec{q}_r) A_{+}((\vec{q} + \vec{p})_r) \left[-\vec{q}_r \cdot (\vec{q} + \vec{p})_r + i^2 \hat{\sigma}^2 \right] - B_{\pm}(\vec{q}_r) B_{+}((\vec{q} + \vec{p})_r) \right. \\ & \left. - \hat{\Delta}^2 A(\vec{q}_r) A((\vec{q} + \vec{p})_r) \mp i^2 F(\vec{q}_r) F((\vec{q} + \vec{p})_r) \left[-\vec{q}_r \cdot (\vec{q} + \vec{p})_r + i^2 \hat{\sigma}^2 \right] \right\} \Big|_{p=0} \end{aligned}$$

$$\begin{aligned}
 &= 4N_c N_f h_{\frac{\phi}{\Delta}}^2 \tilde{\partial}_t \frac{\partial}{\partial \vec{p}^2} \int_q \left\{ A_{\pm}(\vec{q}_r) A_{+}((\vec{q} + \vec{p})_r) \left[\vec{q}_r \cdot (\vec{q} + \vec{p})_r + \hat{\sigma}^2 \right] + B_{\pm}(\vec{q}_r) B_{+}((\vec{q} + \vec{p})_r) \right. \\
 &\quad \left. + \hat{\Delta}^2 A(\vec{q}_r) A((\vec{q} + \vec{p})_r) \mp F(\vec{q}_r) F((\vec{q} + \vec{p})_r) \left[\vec{q}_r \cdot (\vec{q} + \vec{p})_r + \hat{\sigma}^2 \right] \right\} \Big|_{p=0}. \quad (\text{C.7})
 \end{aligned}$$

The argument of the functions is the regularized momentum as defined in Sec. 3.2.2. The upper index represents the mesonic anomalous dimension and the lower one represents the diquark one. The upper line in the integral represents the first term (diagonal contribution) of the previous two equations and the lower line represents the second term (off-diagonal contribution). The upper sign in lower line, also representing η_{ϕ} , stems from the relative one in Δ^{\pm} . In the diagonal contribution we receive a minus sign from swapping γ_5 with the γ_i 's, hence the relative minus sign with respect to the mass term. In the off-diagonal contribution the γ_5 's from each vertex cancels with the ones in the off-diagonal parts of the propagator. Then it is left to swap one of the γ_4 with the space-like γ_i 's which gives again relative minus sign with respect to the mass term. Note that the flow equations preserve the symmetries of the action. Hence, as the boson fields only appear as squared, they can be rewritten in terms of the invariant ρ 's.

Now we write the above expression in terms of the loop integrals defined in App. C.5. The integrals have the form of Eq. (C.43) and (C.50), hence, with Eq. (C.49) and (C.60)

$$\eta_{\frac{\phi}{\Delta}}|_{\Psi} = 4N_c N_f h_{\frac{\phi}{\Delta}}^2 \left\{ I_{\eta_B}^{(2)} [A_{\pm}, A_{+}, \hat{\sigma}^2] + I_{\eta_B}^{(1)} [B_{\pm}, B_{+}] + \hat{\Delta}^2 I_{\eta_B}^{(1)} [A, A] \mp I_{\eta_B}^{(2)} [F, F, \hat{\sigma}^2] \right\}$$

The fermion loop the mesonic anomalous dimension is given by

$$\begin{aligned}
 \eta_{\phi}|_{\Psi} = & \frac{4}{3\pi^2} N_c N_f h_{\phi}^2 k^3 T \sum_n \left\{ k^2 \left(k^2 + \hat{\sigma}^2 \right) \left(A_+'^2 - F'^2 \right) + \frac{A_+'}{4} + B_+'^2 + \hat{\Delta}^2 A'^2 \right. \\
 & \left. + (1 - \eta_q) \left[\frac{A_+'}{2} - k^2 (A_+ A_+' - F F') \right] \right\}
 \end{aligned}$$

and for diquarks we have

$$\begin{aligned}
 \eta_{\Delta}|_{\Psi} = & \frac{4}{3\pi^2} N_c N_f h_{\Delta}^2 k^3 T \sum_n \left\{ k^2 \left(k^2 + \hat{\sigma}^2 \right) \left(A_+ A_+' + F'^2 \right) - \frac{D}{4} + B_+ B_+' + \hat{\Delta}^2 A'^2 \right. \\
 & \left. + (1 - \eta_q) D \left(k^2 A_+ - \frac{1}{2} \right) \right\}.
 \end{aligned}$$

The derivatives are given in Eq. (B.20). All functions are evaluated at k^2 after the integration. In the limit of $\Delta \rightarrow 0$ we use Eqs.(B.22), which leads to

$$\begin{aligned}
 \eta_{\frac{\phi}{\Delta}}(\Delta = 0)|_{\Psi} &= 4N_c N_f h_{\frac{\phi}{\Delta}}^2 \left\{ I_{\eta_B}^{(2)} \left[\frac{1}{K_q^{\pm}}, \frac{1}{K_q^{+}}, \hat{\sigma}^2 \right] + I_{\eta_B}^{(1)} \left[\frac{\nu_{\pm}}{K_q^{\pm}}, \frac{\nu_{+}}{K_q^{+}} \right] \right\} \\
 &= 4N_c N_f h_{\frac{\phi}{\Delta}}^2 I_{\eta_B}^{(2)} \left[\frac{1}{K_q^{\pm}}, \frac{1}{K_q^{+}}, \hat{\sigma}^2 + \nu_{\pm} \nu_{+} \right].
 \end{aligned}$$

Hence, for the mesonic case

$$\eta_\phi(\Delta = 0)|_\Psi = \frac{4}{3\pi^2} N_c N_f h_\phi^2 k^3 T \sum_n \frac{1}{(K_q^+)^2} \left[\frac{k^2}{K_q^+} - \frac{1}{4} + (1 - \eta_q) \left(\frac{k^2}{K_q^+} - \frac{1}{2} \right) \right].$$

And for the diquarks

$$\eta_\Delta(\Delta = 0)|_\Psi = \frac{4}{3\pi^2} N_c N_f h_\Delta^2 k^3 T \sum_n \frac{1}{K_q^- K_q^+} \left[\frac{k^2 (k^2 + \hat{\sigma}^2 + \nu_- \nu_+)}{K_q^- K_q^+} - \frac{1}{4} + (1 - \eta_q) \left(\frac{k^2}{K_q^+} - \frac{1}{2} \right) \right].$$

It is easy to see that at $\mu = 0$ the previous two results coincide, since the Yukawa couplings coincide due to the $SU(N_f)$ symmetry in two-color QCD.

C.2 Fermionic Anomalous Dimension

Quarks

We will do the computation in the complex representation of the diquark fields, since it is clearer this way, however it is arbitrary, for we can insert a unit matrix between bosonic indices of the form $\mathbb{1} = U^\dagger U$, which transforms $\varphi \rightarrow \bar{\varphi}$, or vice versa. First we take a look at the supertrace in Eq. (3.111) after shifting the momentum integration in the second term to $q \rightarrow q + p$

$$\begin{aligned} & \text{str} \int_q \left\{ G(q) \Gamma_{\bar{\Psi}\beta}^{(3)} G(q+p) \Gamma_{\Psi\alpha}^{(3)} - G(q+p) \Gamma_{\Psi\alpha}^{(3)} G(q) \tilde{\Gamma}_{\bar{\Psi}\beta}^{(3)} \right\} \\ &= \text{tr} \int_q \left[G_{\bar{\varphi}}(q) \Gamma_{\bar{\varphi}\bar{\Psi}\beta\Psi} G_{\Psi\bar{\Psi}}(q+p) \Gamma_{\bar{\Psi}\Psi\alpha\bar{\varphi}} - G_{\bar{\varphi}}(q+p) \Gamma_{\bar{\varphi}\Psi\alpha\bar{\Psi}} G_{\bar{\Psi}\Psi}(q) \Gamma_{\Psi\bar{\Psi}\beta\bar{\varphi}} \right] \\ & \quad - \text{tr} \int_q \left[G_{\bar{\Psi}\Psi}(q) \Gamma_{\Psi\bar{\Psi}\beta\bar{\varphi}} G_{\bar{\varphi}}(q+p) \Gamma_{\bar{\varphi}\Psi\alpha\bar{\Psi}} - G_{\Psi\bar{\Psi}}(q+p) \Gamma_{\bar{\Psi}\Psi\alpha\bar{\varphi}} G_{\bar{\varphi}}(q) \Gamma_{\bar{\varphi}\bar{\Psi}\beta\Psi} \right] \\ &= 2 \text{tr} \int_q \left[G_{\bar{\varphi}}(q-p) \Gamma_{\bar{\varphi}\bar{\Psi}\beta\Psi} G_{\Psi\bar{\Psi}}(q) \Gamma_{\bar{\Psi}\Psi\alpha\bar{\varphi}} - G_{\bar{\varphi}}(q+p) \Gamma_{\bar{\varphi}\Psi\alpha\bar{\Psi}} G_{\bar{\Psi}\Psi}(q) \Gamma_{\Psi\bar{\Psi}\beta\bar{\varphi}} \right] \quad (\text{C.8}) \\ &= 4 \text{tr} \int_q G_{\bar{\varphi}}(q-p) \Gamma_{\bar{\varphi}\bar{\Psi}\beta\Psi} G_{\Psi\bar{\Psi}}(q) \Gamma_{\bar{\Psi}\Psi\alpha\bar{\varphi}} \quad (\text{C.9}) \end{aligned}$$

In the first step the minus sign in the lower line is due to the str and the ones in the second terms are due to interchange of the fermionic derivatives. In the first term of Eq. (C.8) we have again shifted the integrals to $q \rightarrow q - p$. Note that we can only reorder the terms after the str has been dissolved into separate traces. Furthermore, note that all quantities still have the dimensions of a matrix. In particular the vertex can be viewed as a matrix, which is contracted with others, and the third index is unspecified. To show that both expressions yield the same contribution, we contract the external indices of Eq. (C.8) with the $\vec{\gamma}$ from Eq. (3.111), which can be written as a trace. Then, displaying only the fermionic part from the second term, we find

$$\begin{aligned} \text{tr} \left[\vec{\gamma}^T \Gamma_{\Psi\bar{\varphi}_j\bar{\Psi}} G_{\bar{\Psi}\Psi}(q) \Gamma_{\Psi\bar{\varphi}_i\bar{\Psi}} \right] &= (-1)^3 \text{tr} \left[\vec{\gamma}^T \Gamma_{\bar{\Psi}\bar{\varphi}_j\Psi}^T G_{\bar{\Psi}\Psi}^T(-q) \Gamma_{\bar{\Psi}\bar{\varphi}_i\Psi}^T \right]^T \\ &= -\text{tr} \left[\Gamma_{\bar{\Psi}\bar{\varphi}_i\Psi} G_{\bar{\Psi}\Psi}(-q) \Gamma_{\bar{\Psi}\bar{\varphi}_j\Psi} \vec{\gamma} \right]. \end{aligned}$$

There is no harm in switching a bosonic index with a fermionic one; we did it to denote the external index in this particular expression. Then we switched the fermionic indices, which yields the transposed of the respective matrices with a minus sign for each, and, for the case of the propagator, a change of sign in the argument according to Eq. (3.52). Since the whole expression is a scalar quantity, we can transpose it to find that it is almost what we would get from the first term in Eq. (C.8) contracted with $\vec{\gamma}$. Note that the external bosonic indices were switched in the process, however using the property of the bosonic propagator in Eq. (3.36), we can switch them back by renaming them, with the result that the argument of $G_{\vec{\varphi}}$ switches the sign to $-q - p$. Finally, switching the sign of the integration variable like $q \rightarrow -q$, we see that both terms are identical. Now we shift $q_4 \rightarrow q_4 + p_4$ and define $q_T = (\vec{q}, q_4 + \pi T)$, such that the fermion propagator carries the fermionic Matsubara frequency. Thus, plugging Eq. (C.9) into Eq. (3.111), and rearranging the terms we find

$$\begin{aligned}
 \eta_q &= \frac{1}{4N_f N_c Z_q} \Re \tilde{\partial}_t \frac{\partial}{\partial |\vec{p}|} \hat{p} \cdot \int_q \text{tr} \left[G_{\Psi\Psi}(q_T) \Gamma_{\Psi\vec{\varphi}_i\Psi} \vec{\gamma} \Gamma_{\Psi\vec{\varphi}_j\Psi} \right] G_{\vec{\varphi},ij}(q-p) \Big|_{p=0} \\
 &= -\frac{1}{4N_f N_c Z_q} \Re \tilde{\partial}_t \frac{\partial}{\partial |\vec{p}|} \hat{p} \cdot \int_q \text{tr} \vec{\gamma} \left[Z_q^2 Z_\phi h_\phi^2 \frac{G^+(q_T) + G^-(q_T)}{Z_q} \frac{3G_\pi(q-p) + G_\sigma(q-p)}{Z_\phi} \right. \\
 &\quad \left. + 2Z_q^2 Z_\Delta h_\Delta^2 \frac{G^+(q_T)G_\Delta^+(q-p) + G^-(q_T)G_\Delta^-(q-p)}{Z_q Z_\Delta} \right] \Big|_{p=0} \\
 &= -\frac{1}{4N_f} \Re \tilde{\partial}_t \frac{\partial}{\partial |\vec{p}|} \hat{p} \cdot \int_q \text{tr} \left[\vec{\gamma} G^+(q_T) \right] \left\{ h_\phi^2 [3G_\pi(q-p) + G_\sigma(q-p)] + 2h_\Delta^2 G_\Delta^+(q-p) \right\} \Big|_{p=0} \\
 &= -\Re \tilde{\partial}_t \frac{\partial}{\partial |\vec{p}|} \hat{p} \cdot \int_q \vec{q}_r A_+(\vec{q}_r^2) \left\{ h_\phi^2 [3G_\pi(q-p) + G_\sigma(q-p)] + 2h_\Delta^2 G_\Delta^+(q-p) \right\} \Big|_{p=0} \quad (\text{C.10})
 \end{aligned}$$

Let us explain what we did here. First of all, $\vec{\gamma}$ can be swapped with one of the vertices, which gives the minus sign except for the σ vertex. Then the two vertices can be multiplied with each other for each case, see Eqs. (3.103). The meson vertices are block diagonal and simply yield a unit matrix in fermionic space when they are squared, with the minus sign for the σ case. From the diquark contributions we have combination $\Gamma_{\Psi\Delta\Psi} \Gamma_{\Psi\Delta^*\Psi}$ (and $\Gamma_{\Psi\Delta^*\Psi} \Gamma_{\Psi\Delta\Psi}$), which yields a unit matrix in the upper left (lower right) corner and in Nambu-Gorkov space, and zeros otherwise. It can be checked, that combinations with equal vertices for the diquarks vanish. Terms for the mixing of σ and Δ yield off-diagonals of the quark propagator, that are $\propto \gamma_5$ and vanish after tracing. The factor of 2 in front of the diquark term originates from the diquark vertices in the complex representation from (3.103). The external momentum can be set to zero instead of p_{\min} , since $p_4 = \pi T$ is absorbed in the definition of the fermionic propagator. As we mentioned below Eq. (3.55) fermionic functions like A_+ by convention always carry fermionic Matsubara frequencies. For the third step, make use of the properties in Eqs. (B.5) and (B.18) and the fact that the real part of the expression is taken. Therefore, since the counterparts of the contributions represent the complex conjugated terms, after the trace is carried out, we can summarize the terms in Nambu-Gorkov space which is effectively the color space. Note that here we can not shift the q_4 integration like for the bosonic anomalous dimension, because we would have to do $q_4 \rightarrow -q_4 - 2p_4$, since the lowest Matsubara frequency is not part of the integral. However, doing such a substitution would shift the momentum in the bosonic propagator as well, such that it cannot be summarized. Carrying out the final trace with $\text{tr} \gamma_i \gamma_j = 4\delta_{ij}$, and tracing over the trivial structure in flavor space, we obtain the last line. This integral has the form of Eq. (C.61), hence we apply Eq. (C.64) and find with Eqs. (B.6)

$$\begin{aligned}
 \eta_q &= h_\phi^2 \Re I_{\eta_F} [|\vec{q}_r|A_+, 3G_\pi + G_\sigma] + 2h_\Delta^2 \Re I_{\eta_F} [|\vec{q}_r|A_+, G_\Delta^+] \\
 &= \frac{k^5 T}{3\pi^2} \Re \sum_n A_+ \left\{ \left(1 - \frac{\eta_\phi}{4}\right) \left[h_\phi^2 \{3G_\pi^2 + G_\sigma^2\} + 2h_\Delta^2 (G_{\sigma\Delta}^+)^2 \right] \right. \\
 &\quad \left. + \left(1 - \frac{\eta_\Delta}{4}\right) \left[2h_\Delta^2 \{ (G_\Delta^+)^2 + G_{|\Delta|}^2 \} + h_\phi^2 \{ (G_{\sigma\Delta}^+)^2 + (G_{\sigma\Delta}^-)^2 \} \right] \right\}.
 \end{aligned}$$

The mesonic and diquark contribution cannot be written into one integral representation due to the different anomalous dimensions. In the $\Delta \rightarrow 0$ limit the upper line essentially stays the same, while the explicit expression is given by

$$\eta_q(\Delta = 0) = \frac{k^5 T}{3\pi^2} \Re \sum_n \frac{1}{K_q^+} \left\{ \left(1 - \frac{\eta_\phi}{4}\right) h_\phi^2 \left[\frac{3}{K_\pi^2} + \frac{1}{K_\sigma^2} \right] + \left(1 - \frac{\eta_\Delta}{4}\right) h_\Delta^2 \frac{2}{(K_\Delta^+)^2} \right\}. \quad (\text{C.11})$$

See (B.7) and (B.22) for $\Delta \rightarrow 0$ limits of the propagators. In the BEC phase of the QMDB-model we use (B.10) in order to get rid of the Goldstone modes, and find

$$\begin{aligned}
 \eta_q &= h_\phi^2 \Re I_{\eta_F} [|\vec{q}_r|A_+, 3G_\pi + G_\sigma] + h_\Delta^2 \Re I_{\eta_F} [|\vec{q}_r|A_+, G_{\Delta_1}] \\
 &= \frac{k^5 T}{3\pi^2} \Re \sum_n A_+ \left\{ \left(1 - \frac{\eta_\phi}{4}\right) \left[h_\phi^2 \{3G_\pi^2 + G_\sigma^2\} + h_\Delta^2 G_{\sigma\Delta_1}^2 \right] + \left(1 - \frac{\eta_\Delta}{4}\right) \left[h_\Delta^2 G_{\Delta_1}^2 + h_\phi^2 G_{\sigma\Delta_1}^2 \right] \right\}.
 \end{aligned}$$

All functions are evaluated at k^2 .

Baryons

Now we turn to the baryonic anomalous dimension of the QMDB-model. Similar to Eq. (C.9) we find

$$\begin{aligned}
 &\text{str} \int_q \left\{ G(q) \Gamma_{\bar{\Psi}\beta}^{(3)} G(q+p) \Gamma_{\Psi\alpha}^{(3)} - G(q+p) \Gamma_{\Psi\alpha}^{(3)} G(q) \Gamma_{\bar{\Psi}\beta}^{(3)} \right\} \\
 &= 4 \text{tr} \int_q G_{\bar{\varphi}}(q-p) \Gamma_{\bar{\varphi}\bar{\Psi}\beta\Psi} G_{\Psi\Psi}(q) \Gamma_{\Psi\Psi\alpha\bar{\varphi}} + 4 \text{tr} \int_q G_{\bar{\varphi}}(q-p) \Gamma_{\bar{\varphi}\bar{\Psi}\beta\Psi} G_{\bar{\Psi}\Psi}(q) \Gamma_{\Psi\Psi\alpha\bar{\varphi}}. \quad (\text{C.12})
 \end{aligned}$$

It is completely analogous to show that the four terms with the additional types of vertices are all the same. Let us first perform the matrix multiplications of the diquark vertices given in App. B.2 with the projection operator \hat{P}_B in Nambu-Gorkov space. It can be checked that

$$\begin{aligned}
 \Gamma_{\bar{\Psi}\Delta^{r*}\Psi} \vec{\gamma} \hat{P}_B \Gamma_{\bar{\Psi}\Delta^r\Psi} \vec{\gamma} &= -Z_q Z_\Delta Z_B h_{qdB}^2 \vec{\gamma} \text{diag}(1, 0, 0, 0), \\
 \Gamma_{\bar{\Psi}\Delta^{g*}\Psi} \vec{\gamma} \hat{P}_B \Gamma_{\bar{\Psi}\Delta^g\Psi} \vec{\gamma} &= -Z_q Z_\Delta Z_B h_{qdB}^2 \vec{\gamma}^T \text{diag}(0, 1, 0, 0), \\
 \Gamma_{\bar{\Psi}\Delta^{b*}\Psi} \vec{\gamma} \hat{P}_B \Gamma_{\bar{\Psi}\Delta^b\Psi} \vec{\gamma} &= -Z_q Z_\Delta Z_B h_{qdB}^2 \vec{\gamma} \text{diag}(0, 0, 1, 0).
 \end{aligned}$$

Naturally, the diagonal matrices project out the quark propagator with the same color as the diquark. All other combination of diquark vertices with this projection operator are vanishing, in particular the ones with the reverse order of the vertices in the above expressions, since in Eq. (C.10) all contributions are summarized to the ones where the baryon flow goes in one direction.

Note that the green contribution stems from the second term of Eq. (C.12), where the charge conjugation operators in the vertices transpose the Dirac matrices. The green quark part in the fermion propagator corresponds to an antiquark propagator therefore its contribution is entered via the antifermion propagator with reversed indices. Now we can write down the anomalous dimension similar to Eq. (C.10), but first let us take a closer look at the fermionic part of green contribution

$$\begin{aligned} Z_q \text{tr} \left[G_{\bar{\Psi}\Psi}(q_T) \gamma^T \text{diag}(0, 1, 0, 0) \right] &= \text{tr} \left[- \left(G^-(-q_T) \right)^T \bar{\gamma}^T \right] \\ &= -(-\vec{q}_r) A_- \left(\vec{q}_r^2, -\nu_n \right) = \vec{q}_r A_+ \left(\vec{q}_r^2, \nu_n \right) \end{aligned}$$

where Eq. (3.52) and (B.17) were used. Now it is clear that the green contribution will be identical to the red one. The baryonic anomalous dimension is given by

$$\begin{aligned} \eta_B &= \frac{1}{4N_f Z_B} \Re \tilde{\partial}_t \frac{\partial}{\partial |\vec{p}|} \\ &\quad \times \hat{\vec{p}} \cdot \int_q \text{tr} \left[G_{\Psi\bar{\Psi}}(q_T) \Gamma_{\bar{\Psi}\bar{\varphi}_i\Psi} \bar{\gamma} \hat{P}_B \Gamma_{\bar{\Psi}\bar{\varphi}_j\Psi} + G_{\bar{\Psi}\Psi}(q_T) \Gamma_{\Psi\bar{\varphi}_i\Psi} \bar{\gamma} \hat{P}_B \Gamma_{\bar{\Psi}\bar{\varphi}_j\Psi} \right] G_{\bar{\varphi},ij}(q-p) \Big|_{p=0} \\ &= -\Re \tilde{\partial}_t \frac{\partial}{\partial |\vec{p}|} \hat{\vec{p}} \cdot \int_q \vec{q}_r \\ &\quad \times \left\{ A_B h_B^2 [3G_\pi(q-p) + G_\sigma(q-p)] + h_{qdB}^2 \left[A_b G_\Delta^-(q-p) + \frac{2A_+}{K_\Delta^-(q-p)} \right] \right\} \Big|_{p=0}. \quad (\text{C.13}) \end{aligned}$$

The mesonic contributions are analogous to (C.10), here \hat{P}_B projects out only the baryon propagator. This integral has the form of Eq. (C.61), hence we apply Eq. (C.64) and find with Eqs. (B.6)

$$\begin{aligned} \eta_B &= h_B^2 \Re I_{\eta_F} [|\vec{q}_r| A_B, 3G_\pi + G_\sigma] + h_{qdB}^2 \Re I_{\eta_F} [|\vec{q}_r| A_b, G_\Delta^-] + 2h_{qdB}^2 \Re I_{\eta_F} [|\vec{q}_r| A_+, (K_\Delta^-)^{-1}] \\ &= \frac{k^5 T}{3\pi^2} \Re \sum_n \left\{ \left(1 - \frac{\eta_\phi}{4} \right) \left[h_B^2 A_B \{ 3G_\pi^2 + G_\sigma^2 \} + h_{qdB}^2 A_b (G_{\sigma\Delta}^-)^2 \right] \right. \\ &\quad \left. + \left(1 - \frac{\eta_\Delta}{4} \right) \left[h_{qdB}^2 \left\{ A_b \left[(G_\Delta^-)^2 + G_{|\Delta|}^2 \right] + 2A_+ (K_\Delta^-)^{-2} \right\} + h_B^2 A_B \left\{ (G_{\sigma\Delta}^+)^2 + (G_{\sigma\Delta}^-)^2 \right\} \right] \right\}. \quad (\text{C.14}) \end{aligned}$$

In the $\Delta \rightarrow 0$ limit we have

$$\eta_B(\Delta = 0) = \frac{k^5 T}{3\pi^2} \Re \sum_n \left\{ \left(1 - \frac{\eta_\phi}{4} \right) h_B^2 \frac{z_B}{K_B} \left[\frac{3}{K_\pi^2} + \frac{1}{K_\sigma^2} \right] + \left(1 - \frac{\eta_\Delta}{4} \right) h_{qdB}^2 \frac{3}{K_q^+ (K_\Delta^-)^2} \right\}.$$

The limiting cases of the blue and baryon propagators can be found in (B.33). Without the Goldstone modes we find for the BEC phase with Eq. (B.10)

$$\begin{aligned}
 \eta_B &= h_B^2 \Re I_{\eta_F} [|\vec{q}_r| A_B, 3G_\pi + G_\sigma] + \frac{h_{qdB}^2}{2} \Re I_{\eta_F} [|\vec{q}_r| A_b, G_{\Delta_1}] \\
 &= \frac{k^5 T}{3\pi^2} \Re \sum_n \left\{ \left(1 - \frac{\eta_\phi}{4}\right) \left[h_B^2 A_B \{3G_\pi^2 + G_\sigma^2\} + \frac{h_{qdB}^2}{2} A_b G_{\sigma\Delta_1}^2 \right] \right. \\
 &\quad \left. + \left(1 - \frac{\eta_\Delta}{4}\right) \left[\frac{h_{qdB}^2}{2} A_b G_{\Delta_1}^2 + h_B^2 A_B G_{\sigma\Delta_1}^2 \right] \right\}. \tag{C.15}
 \end{aligned}$$

C.3 Baryon UV Mass Gap

Since the projection onto the flow of the baryon mass (3.114) is quite the same as for the baryonic anomalous dimension (3.112), except for the missing momentum derivative and the minus sign, we can essentially start with a slightly modified Eq. (C.13)

$$\begin{aligned}
 \partial_t m_B^{\text{UV}}|_o &= \Re \tilde{\partial}_t \hat{p} \cdot \int_q \vec{q}_r \left\{ A_B h_B^2 [3G_\pi + G_\sigma] + h_{qdB}^2 \left[A_b G_\Delta^- + A_+ \frac{2}{K_\Delta^-} \right] \right\} \\
 &= -\Re \left\{ h_B^2 I_{m_B} [|\vec{q}_r| A_B, 3G_\pi + G_\sigma] + h_{qdB}^2 I_{m_B} [|\vec{q}_r| A_b, G_\Delta^-] + 2h_{qdB}^2 I_{m_B} \left[|\vec{q}_r| A_+, (K_\Delta^-)^{-1} \right] \right\}.
 \end{aligned}$$

The circle on the left-hand side denotes that we are looking at the (loop-) diagrammatic part of the flow. This integral has the form of Eq. (C.65), hence we apply Eq. (C.67) and find with Eqs. (B.6) and (B.31)

$$\begin{aligned}
 \partial_t m_B^{\text{UV}}|_o &= -\frac{k^6 T}{6\pi^2} \Re \sum_n \left\{ \left(1 - \frac{\eta_\phi}{5}\right) \left[h_B^2 A_B (3G_\pi^2 + G_\sigma^2) + h_{qdB}^2 A_b (G_{\sigma\Delta}^-)^2 \right] \right. \\
 &\quad + \left(1 - \frac{\eta_\Delta}{5}\right) \left[h_{qdB}^2 \left\{ A_b \left[(G_\Delta^-)^2 + G_{|\Delta|}^2 \right] + 2A_+ (K_\Delta^-)^{-2} \right\} + h_B^2 A_B \left\{ (G_{\sigma\Delta}^+)^2 + (G_{\sigma\Delta}^-)^2 \right\} \right] \\
 &\quad + \left(1 - \frac{\eta_B}{4}\right) \left[h_B^2 \left(A_B^2 - \frac{K_q^+ L}{2k^2} \right) (3G_\pi + G_\sigma) + h_{qdB}^2 \left(A_B A_b - \left[z_B + \frac{\hat{\Delta}_B^2}{2k^2} \right] L \right) G_\Delta^- \right] \\
 &\quad + \left(1 - \frac{\eta_q}{4}\right) \left[h_{qdB}^2 \left(A_b^2 - \frac{K_B L}{2k^2} \right) G_\Delta^- + h_B^2 \left(A_B A_b - \left[z_B + \frac{\hat{\Delta}_B^2}{2k^2} \right] L \right) (3G_\pi + G_\sigma) \right. \\
 &\quad \left. + 2h_{qdB}^2 \left(A_+^2 - F^2 - \frac{A_+}{2k^2} \right) (K_\Delta^-)^{-1} \right] \left. \right\}.
 \end{aligned}$$

The first two lines are essentially the same as the flow equation of η_B in Eq. (C.14) except for some different numbers. In the $\Delta \rightarrow 0$ limit we find

$$\begin{aligned} \partial_t m_B^{\text{UV}}(\Delta = 0)|_o = & -\frac{k^6 T}{6\pi^2} \Re \sum_n \left\{ \left(1 - \frac{\eta_\phi}{5}\right) h_B^2 \frac{z_B}{K_B} \left[\frac{3}{K_\pi^2} + \frac{1}{K_\sigma^2} \right] + \left(1 - \frac{\eta_\Delta}{5}\right) h_{qdB}^2 \frac{3}{K_q^+ (K_\Delta^-)^2} \right. \\ & + \left(1 - \frac{\eta_B}{4}\right) h_B^2 \frac{1}{K_B} \left[\frac{z_B^2}{K_B} - \frac{1}{2k^2} \right] \left[\frac{3}{K_\pi} + \frac{1}{K_\sigma} \right] \\ & \left. + \left(1 - \frac{\eta_q}{4}\right) h_{qdB}^2 \frac{1}{K_q^+} \left[\frac{1}{K_q^+} - \frac{1}{2k^2} \right] \frac{3}{K_\Delta^-} \right\}. \end{aligned} \quad (\text{C.16})$$

The limiting cases of the respective functions are given in Eqs. (B.7), (B.22) and (B.33). It is easy to see that the mixed contributions with the blue quark and the baryon propagator vanish. By getting rid of the Goldstone modes with Eq. (B.10) we find for the BEC phase

$$\begin{aligned} \partial_t m_B^{\text{UV}}|_o = & -\frac{k^6 T}{6\pi^2} \Re \sum_n \left\{ \left(1 - \frac{\eta_\phi}{5}\right) \left[h_B^2 A_B (3G_\pi^2 + G_\sigma^2) + \frac{h_{qdB}^2}{2} A_b G_{\sigma\Delta_1}^2 \right] \right. \\ & + \left(1 - \frac{\eta_\Delta}{5}\right) \left[\frac{h_{qdB}^2}{2} A_b G_{\Delta_1}^2 + h_B^2 A_B G_{\sigma\Delta_1}^2 \right] \\ & + \left(1 - \frac{\eta_B}{4}\right) \left[h_B^2 \left(A_B^2 - \frac{K_q^+ L}{2k^2} \right) (3G_\pi + G_\sigma) + \frac{h_{qdB}^2}{2} \left(A_B A_b - \left[z_B + \frac{\hat{\Delta}_B^2}{2k^2} \right] L \right) G_{\Delta_1} \right] \\ & \left. + \left(1 - \frac{\eta_q}{4}\right) \left[\frac{h_{qdB}^2}{2} \left(A_b^2 - \frac{K_B L}{2k^2} \right) G_{\Delta_1} + h_B^2 \left(A_B A_b - \left[z_B + \frac{\hat{\Delta}_B^2}{2k^2} \right] L \right) (3G_\pi + G_\sigma) \right] \right\}. \end{aligned}$$

C.4 Yukawa Couplings

Meson Yukawa coupling

Since the flow matrix in Eqs. (3.117)-(3.118) is the same as in (3.111) with a minus sign, we can use Eq. (C.9) and write the diagrammatic parts of flows of the Yukawa couplings similar to Eq. (C.10) and with the definitions from Eqs. (3.53)

$$\begin{aligned} \partial_t h_\phi|_o &= -\frac{1}{4N_f N_c} \frac{h_\phi}{Z_q i \hat{\sigma}} \Im \tilde{\partial}_t \int_q \text{tr} \left[G_{\Psi\bar{\Psi}}(q_T) \Gamma_{\bar{\Psi}\bar{\varphi}_i\Psi} \Gamma_{\bar{\Psi}\bar{\varphi}_j\Psi} \right] G_{\bar{\varphi},ij}(q) \\ &= h_\phi \Re \tilde{\partial}_t \int_q A_+(\vec{q}_r^2) \left\{ h_\phi^2 [3G_\pi(q) - G_\sigma(q)] + 2h_\Delta^2 G_\Delta^+(q) \right\}. \end{aligned} \quad (\text{C.17})$$

As before, the circle on the left-hand side denotes that we are looking at the (loop-) diagrammatic part of the flow. The steps are similar to the ones in Eq. (C.10). The difference is the missing Dirac matrices, hence the minus sign does not come from any swapping but rather from the trace of G^+ , where also the cancellation of $i\hat{\sigma}$ originates from. Therefore, in this case the sign of the sigma contribution does not match the others. Since we pulled out a factor i from the integral,

in order to cancel it, the projection must be switched to the real part. We can set $p = 0$ from the beginning as there is no derivative. It might be confusing that A_+ is paired with neutral particles as well as with a charged one. This can be understood by recalling, that by turning around the direction of the momentum, particles are turned into antiparticles. This amounts to swapping the external legs of the diagram, by which the net baryon charge and the direction of the flow coincide for all contributions. The integrals have the form of Eq. (C.68); we apply the formula (C.70) and find

$$\begin{aligned} \partial_t h_\phi|_0 &= -h_\phi \Re \left\{ h_\phi^2 I_h [A_+, 3G_\pi(q) - G_\sigma(q)] + 2h_\Delta^2 I_h [A_+, G_\Delta^+] \right\} \\ &= -\frac{k^5 T}{3\pi^2} h_\phi \Re \sum_n \left[\left(1 - \frac{\eta_q}{4}\right) (A_+^2 - F^2) [h_\phi^2 (3G_\pi - G_\sigma) + 2h_\Delta^2 G_\Delta^+] \right. \\ &\quad \left. + A_+ \left\{ \left(1 - \frac{\eta_\phi}{5}\right) \left[h_\phi^2 \{3G_\pi^2 - G_\sigma^2\} + 2h_\Delta^2 (G_{\sigma\Delta}^+)^2 \right] \right. \right. \\ &\quad \left. \left. + \left(1 - \frac{\eta_\Delta}{5}\right) \left[2h_\Delta^2 \{ (G_\Delta^+)^2 + G_{|\Delta|}^2 \} - h_\phi^2 \{ (G_{\sigma\Delta}^+)^2 + (G_{\sigma\Delta}^-)^2 \} \right] \right\} \right] \end{aligned}$$

After the formal scale derivative $\tilde{\partial}_t$ is carried out, the diagrams are somewhat changed. In particular it should be noted that propagators, which are proportional to condensate Δ , carry the baryon charge in/out to/from the condensate. Let us be more precise regarding the last two terms for example: The baryon charge enters the digram from one side of the regulator, passes through the regulator and leaves the diagram from the other side. This can happen in both direction, therefore we have contributions from both charges. In the $\Delta \rightarrow 0$ limit all propagators are given by their simplest form, hence

$$\begin{aligned} \partial_t h_\phi(\Delta = 0)|_0 &= -\frac{k^5 T}{3\pi^2} h_\phi \Re \sum_n \frac{1}{K_q^+} \left\{ \left(1 - \frac{\eta_q}{4}\right) \frac{1}{K_q^+} \left[h_\phi^2 \left(\frac{3}{K_\pi} - \frac{1}{K_\sigma} \right) + h_\Delta^2 \frac{2}{K_\Delta^+} \right] \right. \\ &\quad \left. + \left(1 - \frac{\eta_\phi}{5}\right) h_\phi^2 \left(\frac{3}{K_\pi^2} - \frac{1}{K_\sigma^2} \right) + \left(1 - \frac{\eta_\Delta}{5}\right) h_\Delta^2 \frac{2}{(K_\Delta^+)^2} \right\} \quad (\text{C.18}) \end{aligned}$$

Diquark Yukawa coupling

For the flow of the diquark Yukawa coupling we have the projection operator \hat{P}_Δ which takes the place of the Dirac matrix. Let us first perform the matrix multiplications for the vertices in Nambu-Gorkov space

$$\begin{aligned} \Gamma_{\bar{\Psi}\sigma\Psi} \hat{P}_\Delta \Gamma_{\bar{\Psi}\sigma\Psi} &= \Gamma_{\bar{\Psi}\pi_i\Psi} \hat{P}_\Delta \Gamma_{\bar{\Psi}\pi_i\Psi} = Z_q^2 Z_\phi h_\phi^2 \gamma_5 \begin{pmatrix} 0 & 1 \\ 1 & 0 \end{pmatrix} \\ \Gamma_{\bar{\Psi}\Delta\Psi} \hat{P}_\Delta \Gamma_{\bar{\Psi}\Delta\Psi} &= \left(\Gamma_{\bar{\Psi}\Delta^*\Psi} \hat{P}_\Delta \Gamma_{\bar{\Psi}\Delta^*\Psi} \right)^T = 2Z_q^2 Z_\Delta h_\Delta^2 \gamma_5 \begin{pmatrix} 0 & -1 \\ 0 & 0 \end{pmatrix} \end{aligned} \quad (\text{C.19})$$

$$\begin{aligned}
 \Gamma_{\bar{\Psi}\Delta^*\Psi}\hat{P}_\Delta\Gamma_{\bar{\Psi}\sigma\Psi} &= \Gamma_{\bar{\Psi}\sigma\Psi}\hat{P}_\Delta\Gamma_{\bar{\Psi}\Delta\Psi} = Z_q^2\sqrt{2Z_\phi Z_\Delta}ih_\phi h_\Delta \begin{pmatrix} 0 & 0 \\ 0 & -1 \end{pmatrix} \\
 \Gamma_{\bar{\Psi}\sigma\Psi}\hat{P}_\Delta\Gamma_{\bar{\Psi}\Delta^*\Psi} &= \Gamma_{\bar{\Psi}\Delta\Psi}\hat{P}_\Delta\Gamma_{\bar{\Psi}\sigma\Psi} = Z_q^2\sqrt{2Z_\phi Z_\Delta}ih_\phi h_\Delta \begin{pmatrix} -1 & 0 \\ 0 & 0 \end{pmatrix} \\
 \Gamma_{\bar{\Psi}\Delta\Psi}\hat{P}_\Delta\Gamma_{\bar{\Psi}\Delta^*\Psi} &= \Gamma_{\bar{\Psi}\Delta^*\Psi}\hat{P}_\Delta\Gamma_{\bar{\Psi}\Delta\Psi} = 0.
 \end{aligned}$$

The upper two matrices give rise to off-diagonal contributions from the fermion propagator, while the lower ones lead to diagonal contributions. It is easy to see that the Z 's will cancel out once these vertices are multiplied with the propagators. The diagrammatic part is given by

$$\begin{aligned}
 \partial_t h_\Delta|_o &= -\frac{1}{4N_f N_c} \frac{h_\Delta}{Z_q \hat{\Delta}} \Re \tilde{\partial}_t \int_q \text{tr} \left[G_{\Psi\bar{\Psi}}(q) \Gamma_{\bar{\Psi}\bar{\varphi}_i\Psi} \hat{P} \Gamma_{\bar{\Psi}\bar{\varphi}_j\Psi} \right] G_{\bar{\varphi},ij}(q) \\
 &= -\frac{1}{4N_f N_c} \frac{h_\Delta}{\hat{\Delta}} \Re \tilde{\partial}_t \int_q \text{tr} \left[h_\phi^2 \gamma_5 \left\{ \Delta^+(q_T) + \Delta^-(q_T) \right\} \left\{ 3G_\pi(q) + G_\sigma(q) \right\} \right. \\
 &\quad \left. - 2h_\Delta^2 \gamma_5 \left\{ \Delta^+(q_T) + \Delta^-(q_T) \right\} G_{|\Delta|}(q) - 2\sqrt{2}ih_\phi h_\Delta \left\{ G^+(q_T)G_{\sigma\Delta}^+(q) + G^-(q_T)G_{\sigma\Delta}^-(q) \right\} \right] \\
 &= h_\Delta \Re \tilde{\partial}_t \int_q \left[A(\vec{q}_r^2) \left\{ h_\phi^2 [3G_\pi(q) + G_\sigma(q)] - 2h_\Delta^2 G_{|\Delta|}(q) \right\} - \sqrt{8}h_\phi h_\Delta \frac{\hat{\sigma}}{\hat{\Delta}} A_+(\vec{q}_r^2) G_{\sigma\Delta}^+(q) \right].
 \end{aligned}$$

The reasonings for summarizing the terms is again similar to Eq. (C.10). Let us remark that all loops have zero baryon number, rightly, as was explained above. Note that A represents mixture of quarks and antiquark which are connected to the external diquark condensate, which is canceled out, and similar is the case for $G_{|\Delta|}$ regarding diquarks, where it is not canceled out. In the last term the baryon number flows through the quark propagator and connects to the condensate via the boson propagator, where diquark condensate is canceled out. In any case, the flow equations preserve the symmetries of the action, therefore the bosonic fields only appear as squared and can be rewritten in terms of the invariant ρ 's, as we mentioned before. We mention here again, that fermionic functions like A and A_+ are defined such that they contain fermionic Matsubara frequencies. The integrals have again the form of Eq. (C.68); we apply the formula (C.70) and find

$$\begin{aligned}
 \partial_t h_\Delta|_o &= -h_\Delta \Re \left\{ h_\phi^2 I_h [A, 3G_\pi(q) + G_\sigma(q)] - 2h_\Delta^2 I_h [A, G_{|\Delta|}] - \sqrt{8}h_\phi h_\Delta \frac{\hat{\sigma}}{\hat{\Delta}} I_h [A_+, G_{\sigma\Delta}^+] \right\} \\
 &= -\frac{k^5 T}{3\pi^2} h_\Delta \Re \sum_n \left[\left(1 - \frac{\eta_q}{4} \right) \left\{ [A(A_+ + A_-) - D] [h_\phi^2 (3G_\pi + G_\sigma) - 2h_\Delta^2 G_{|\Delta|}] \right. \right. \\
 &\quad \left. \left. - \sqrt{8}h_\phi h_\Delta \frac{\hat{\sigma}}{\hat{\Delta}} (A_+^2 - F^2) G_{\sigma\Delta}^+ \right\} \right. \\
 &\quad \left. + \left(1 - \frac{\eta_\phi}{5} \right) \left\{ A \left[h_\phi^2 (3G_\pi^2 + G_\sigma^2) - 2h_\Delta^2 G_{\sigma\Delta}^+ G_{\sigma\Delta}^- \right] - \sqrt{8}A_+ h_\phi h_\Delta \frac{\hat{\sigma}}{\hat{\Delta}} G_\sigma G_{\sigma\Delta}^+ \right\} \right. \\
 &\quad \left. + \left(1 - \frac{\eta_\Delta}{5} \right) \left\{ A \left[h_\phi^2 \left((G_{\sigma\Delta}^+)^2 + (G_{\sigma\Delta}^-)^2 \right) - 2h_\Delta^2 G_{|\Delta|} (G_\Delta^+ + G_\Delta^-) \right] \right. \right. \\
 &\quad \left. \left. - \sqrt{8}A_+ h_\phi h_\Delta \frac{\hat{\sigma}}{\hat{\Delta}} (G_{\sigma\Delta}^+ G_\Delta^+ + G_{\sigma\Delta}^- G_{|\Delta|}) \right\} \right].
 \end{aligned}$$

In the limit $\Delta \rightarrow 0$ the flow equation does not resemble the one for the meson Yukawa coupling, this is related to the fact that it must be derived for a non-vanishing diquark field, which is partly canceled out

$$\begin{aligned} & \partial_t h_\Delta(\Delta = 0)|_0 \\ &= -\frac{k^5 T}{3\pi^2} h_\Delta h_\phi^2 \Re \sum_n \frac{1}{K_q^+} \left[\left(1 - \frac{\eta_q}{4}\right) \left\{ \frac{1}{K_q^-} \left[a \left(\frac{1}{K_q^+} + \frac{1}{K_q^-} \right) - 1 \right] \left(\frac{3}{K_\pi} + \frac{1}{K_\sigma} \right) + \frac{4}{K_q^+} \frac{\rho_\phi V_{\phi\Delta}}{K_\sigma K_\Delta^+} \right\} \right. \\ & \quad \left. + \left(1 - \frac{\eta_\phi}{5}\right) \left\{ \frac{a}{K_q^-} \left(\frac{3}{K_\pi^2} + \frac{1}{K_\sigma^2} \right) + \frac{4\rho_\phi V_{\phi\Delta}}{K_\sigma^2 K_\Delta^+} \right\} + \left(1 - \frac{\eta_\Delta}{5}\right) \frac{4\rho_\phi V_{\phi\Delta}}{K_\sigma (K_\Delta^+)^2} \right], \end{aligned}$$

where $a = k^2 + \hat{\sigma}^2 + \nu_- \nu_+$, as in App. B.2 without the diquark term. However, for two-color QCD the extended flavor symmetry $SU(2N_f)$ must be recovered in the $\mu \rightarrow 0$ limit, hence both flow equations must coincide, which is indeed the case. Considering that in this case the effective potential V reduces to a function of one variable $\rho_\phi + \rho_\Delta$, hence $K_\Delta^\pm \rightarrow K_\pi$, as well as $\eta_\Delta \rightarrow \eta_\phi$ and $h_\Delta \rightarrow h_\phi$. Then we see that

$$\frac{1}{K_\sigma} + \frac{4\rho_\phi V''}{K_\sigma K_\pi} = \frac{2}{K_\pi} - \frac{1}{K_\sigma}, \quad \frac{1}{K_\sigma^2} + \frac{4\rho_\phi V''}{K_\sigma^2 K_\pi} + \frac{4\rho_\phi V''}{K_\sigma K_\pi^2} = \frac{2}{K_\pi^2} - \frac{1}{K_\sigma^2}, \quad (\text{C.20})$$

which can easily be checked. Moreover $K_q^\pm \rightarrow K_q$ and $a \rightarrow K_q$, where the missing \pm indicates the vanishing chemical potential. Finally we can write

$$\begin{aligned} & \partial_t h_\Delta(\Delta = 0, \mu = 0)|_0 \\ &= -\frac{k^5 T}{3\pi^2} h_\phi^3 \Re \sum_n \frac{1}{K_q} \left[\left(1 - \frac{\eta_q}{4}\right) \frac{1}{K_q} \left(\frac{5}{K_\pi} - \frac{1}{K_\sigma} \right) + \left(1 - \frac{\eta_\phi}{5}\right) \left(\frac{5}{K_\pi^2} - \frac{1}{K_\sigma^2} \right) \right], \end{aligned}$$

which coincides with Eq. (C.18) if the same limiting cases are applied. We mention here again that all functions are evaluated at k^2 after integration.

C.5 Loop Integrals

Before turning to the Integrals let us make some preparations. We will substitute the momentum integration variable for $x = \vec{q}^2/k^2$. Then the momentum integration will turn into

$$\begin{aligned} \int_q \vec{q}^{2n} y^m &= T \sum_{n \in \mathbb{Z}} \int \frac{d^3 q}{(2\pi)^3} \vec{q}^{2n} y^m \\ &= \frac{1}{(2\pi)^3} T \sum_{n \in \mathbb{Z}} \int_0^\infty dq q^{2n+2} \int_0^{2\pi} d\phi \int_{-1}^1 dy y^m \\ &= \frac{1}{(2\pi)^2} \frac{2}{m+1} k^{2n+3} T \sum_{n \in \mathbb{Z}} \int_0^\infty \frac{dx}{2x^{\frac{1}{2}}} x^{n+1} \\ &= \frac{1}{4\pi^2} \frac{1}{m+1} k^{2n+3} T \sum_{n \in \mathbb{Z}} \int_0^\infty dx x^{n+\frac{1}{2}}. \end{aligned} \quad (\text{C.21})$$

Typically the only effective x -dependence within the integrand will in a Heaviside-function as

$$\int_0^\infty dx x^{n+\frac{1}{2}} \Theta(1-x) = \frac{2}{3+2n} \quad \text{for} \quad n > -\frac{3}{2} \quad (\text{C.22})$$

In this work we will only employ the optimized regulator functions

$$\begin{aligned} r_B(x) &= \left(\frac{1}{x} - 1 \right) \Theta(1-x) \quad \text{for bosons,} \\ r_F(x) &= \left(\frac{1}{\sqrt{x}} - 1 \right) \Theta(1-x) \quad \text{for fermions.} \end{aligned}$$

If the regulator appears in higher orders, there is no harm in setting the order of the Heaviside function to one, as the only way it could make difference is if there is a Dirac delta function in the integral, however, the regulator vanishes then. The derivatives are given by

$$\frac{\partial}{\partial x} r_B(x) = -\frac{1}{x^2} \Theta(1-x) - \left(\frac{1}{x} - 1 \right) \delta(1-x) = -\frac{1}{x^2} \Theta(1-x), \quad (\text{C.23})$$

$$\frac{\partial}{\partial x} r_F(x) = -\frac{1}{2\sqrt{x^3}} \Theta(1-x) - \left(\frac{1}{\sqrt{x}} - 1 \right) \delta(1-x) = -\frac{1}{2\sqrt{x^3}} \Theta(1-x). \quad (\text{C.24})$$

The terms containing Dirac delta functions drop out upon integration. Even if a derivative is applied we have

$$\int dx f(x) \frac{\partial}{\partial x} \left(\frac{1}{x^\alpha} - 1 \right) \delta(1-x) = \int dx \left[\frac{\partial}{\partial x} f(x) \right] \left(\frac{1}{x^\alpha} - 1 \right) \delta(1-x) = 0 \quad (\text{C.25})$$

Furthermore any integrals containing a Dirac delta and Heaviside functions are evaluated to

$$\begin{aligned} \int dx f(x) (\Theta(x))^n \delta(x) &= \int dx f(x) (\Theta(x))^n \frac{d\Theta(x)}{dx} = \int dx f(x) \frac{1}{n+1} \frac{d}{dx} (\Theta(x))^{n+1} \\ &= - \int dx \left(\frac{d}{dx} f(x) \right) \frac{1}{n+1} (\Theta(x))^{n+1} = - \int dx \left(\frac{d}{dx} f(x) \right) \frac{1}{n+1} (\Theta(x)) \\ &= \int dx f(x) \frac{1}{n+1} \frac{d\Theta(x)}{dx} = \int dx f(x) \frac{1}{n+1} \delta(x) \\ &= \frac{1}{n+1} f(0) \end{aligned} \quad (\text{C.26})$$

In the second step of the second line, we can safely set the exponent of the Heaviside function to 1, since there is no delta function present. So any function, which is within an integral in such a way, is still evaluated at the zero of argument of the delta function, therefore the part with the delta function in Eqs. (C.23) and (C.24) always vanishes.

Now we define the regularized dimensionless momentum functions

$$\begin{aligned} P_B(x) &= x(1 + r_B(x)) = x \Theta(x-1) + \Theta(1-x) \\ P_F(x) &= x(1 + r_F(x))^2 = x \left(\Theta(x-1) + \frac{1}{\sqrt{x}} \Theta(1-x) \right)^2 \end{aligned}$$

Both have the simple property $P_{B/F}(x < 1) = 1$. If we are looking at a purely bosonic or purely fermionic integral, we will omit the index. If we make a substitution according to Eq. (C.21),

we will redefine the functions in the integral like

$$\mathcal{G}(P) = G(k^2 P) = G(\vec{q}_r^2). \quad (\text{C.27})$$

where the \vec{q}_r denotes the regularized momentum. Substituting back, we have to put a factor of k^2 for the case of primed quantities, which denotes a derivative, as

$$\mathcal{G}'(P) = \frac{\partial \mathcal{G}(P)}{\partial P} = \frac{\partial G(k^2 P)}{\partial P} = k^2 G'(k^2 P), \quad (\text{C.28})$$

Carrying out the integration, we will often refer to the following properties

$$r_{B/F}(x=1) = 0, \quad P_{B/F}(x \leq 1) = 1, \quad 1 + r_F(x \leq 1) = x^{-\frac{1}{2}}. \quad (\text{C.29})$$

The derivatives the regularized dimensionless momentum functions of are given by

$$\begin{aligned} \frac{\partial}{\partial x} P_B(x) &= 1 + r_B + x \frac{\partial r_B}{\partial x} = \left(\frac{1}{x} - 1 \right) \Theta(1-x) - \frac{1}{x^2} \Theta(1-x) = 1 - \Theta(1-x) \\ &= \Theta(x-1), \end{aligned} \quad (\text{C.30})$$

$$\begin{aligned} \frac{\partial}{\partial x} P_F(x) &= (1 + r_F)^2 + 2x(1 + r_F) \frac{\partial r_F}{\partial x} = (1 + r_F) \left[1 + \left(\frac{1}{\sqrt{x}} - 1 \right) \Theta(1-x) - \frac{1}{\sqrt{x}} \Theta(1-x) \right] \\ &= (1 + r_F) \Theta(x-1) \end{aligned} \quad (\text{C.31})$$

Furthermore we will need

$$\frac{\partial}{\partial r_B} P_B = x, \quad (\text{C.32})$$

$$\frac{\partial}{\partial r_F} P_F = 2x(1 + r_F) = 2x \left(\Theta(x-1) + \frac{1}{\sqrt{x}} \Theta(1-x) \right). \quad (\text{C.33})$$

The formal scale derivative acts only on the regulators, which must yield Eq. (3.20). Since the Z 's are typically canceled out we must define it as

$$\tilde{\partial}_t r_B = \frac{k}{Z_B} \frac{\partial}{\partial k} Z_B r_B \left(\frac{\vec{q}^2}{k^2} \right) = \left[\frac{2}{x} - \eta_B \left(\frac{1}{x} - 1 \right) \right] \Theta(1-x), \quad (\text{C.34})$$

$$\tilde{\partial}_t r_F = \frac{k}{Z_F} \frac{\partial}{\partial k} Z_F r_F \left(\frac{\vec{q}^2}{k^2} \right) = \left[\frac{1}{\sqrt{x}} - \eta_F \left(\frac{1}{\sqrt{x}} - 1 \right) \right] \Theta(1-x). \quad (\text{C.35})$$

It is important to take into account the wave function renormalizations of all species. For instance, if the formal derivative acts on propagator which is involved in a mixing with different species, we must let it act on all kinetic parts separately. We will encounter derivations of functions $\mathcal{H}(P_{B/F})$ of the form

$$\tilde{\partial}_t \mathcal{H}(P_B) = \mathcal{H}' \frac{\partial P_B}{\partial r_B} \tilde{\partial}_t r_B = \mathcal{H}' (2 - \eta_B(1-x)) \Theta(1-x), \quad (\text{C.36})$$

$$\tilde{\partial}_t \mathcal{H}(P_F) = \mathcal{H}' \frac{\partial P_F}{\partial r_F} \tilde{\partial}_t r_F = 2\mathcal{H}'(1 + r_F) [\sqrt{x} - \eta_F(\sqrt{x} - x)] \Theta(1-x), \quad (\text{C.37})$$

as well as

$$\frac{\partial}{\partial x} \tilde{\partial}_t \mathcal{H}(P_{B/F}) = \frac{\partial}{\partial x} \mathcal{H}' \frac{\partial P_{B/F}}{\partial r_{B/F}} \tilde{\partial}_t r_{B/F} = \mathcal{H}' \frac{\partial}{\partial x} \left(\frac{\partial P_{B/F}}{\partial r_{B/F}} \tilde{\partial}_t r_{B/F} \right) + \mathcal{H}'' \frac{\partial P_{B/F}}{\partial x} \frac{\partial P_{B/F}}{\partial r_{B/F}} \tilde{\partial}_t r_{B/F} \quad (\text{C.38})$$

The argument of \mathcal{H} is omitted after the first step. The second term will vanish upon integration, as the x -derivative of the momentum functions contains the opposite Heaviside function as scale derivative of the regulator, cf. Eqs. (C.30) - (C.35). For the bosonic case we find

$$\begin{aligned} \frac{\partial}{\partial x} \tilde{\partial}_t \mathcal{H}(P_B) &= \mathcal{H}' \frac{\partial}{\partial x} (2 - \eta_B(1 - x)) \Theta(1 - x) \\ &= \mathcal{H}' \left[\eta_B \Theta(1 - x) - (2 - \eta_B(1 - x)) \delta(1 - x) \right] \\ &= \mathcal{H}' \left[\eta_B \Theta(1 - x) - 2\delta(1 - x) \right], \end{aligned} \quad (\text{C.39})$$

and for the fermionic one

$$\begin{aligned} \frac{\partial}{\partial x} \tilde{\partial}_t \mathcal{H}(P_F) &= 2\mathcal{H}' \frac{\partial}{\partial x} (1 + r_F) [\sqrt{x} - \eta_F(\sqrt{x} - x)] \Theta(1 - x) \\ &= 2\mathcal{H}' \left\{ -\frac{1}{2\sqrt{x}^3} \Theta(1 - x) [\sqrt{x} - \eta_F(\sqrt{x} - x)] \Theta(1 - x) \right. \\ &\quad \left. + \left(\Theta(x - 1) + \frac{1}{\sqrt{x}} \Theta(1 - x) \right) \left[\frac{1}{2\sqrt{x}} - \eta_F \left(\frac{1}{2\sqrt{x}} - 1 \right) \right] \Theta(1 - x) \right. \\ &\quad \left. - [\sqrt{x} - \eta_F(\sqrt{x} - x)] \delta(1 - x) \right\} \\ &= \mathcal{H}' \left[x^{-\frac{1}{2}} \eta_F \Theta(1 - x) - 2\delta(1 - x) \right], \end{aligned} \quad (\text{C.40})$$

where Eq. (C.24) was used. Again we have used that some terms vanish upon integration, in particular, that $x^\alpha = 1$ for any α in the Dirac delta term, and we have assumed that no more delta functions will be multiplied with the above expressions.

Effective potential

Since in this section all integrals are purely bosonic/fermionic, we will drop the corresponding index. First let us consider bosonic contributions like

$$\begin{aligned} I_U^B[G] &= \int_q G(\vec{q}_r^2) \dot{R}_B = \int_q \vec{q}^2 G(\vec{q}_r^2) \tilde{\partial}_t r_B \\ &= \frac{k^5 T}{4\pi^2} \sum_n \int_0^\infty dx x^{\frac{3}{2}} G(k^2 P) \left[\frac{2}{x} - \eta_B \left(\frac{1}{x} - 1 \right) \right] \Theta(1 - x) \\ &= \frac{k^5 T}{3\pi^2} \left(1 - \frac{\eta_B}{5} \right) \sum_n G(k^2) \end{aligned} \quad (\text{C.41})$$

\dot{R}_B is basically given by Eq. (3.20) multiplied with the momentum squared, therefore it can be written in terms of Eq. (C.34). Next we have applied Eq. (C.21). Finally, in order to carry out the integral, we used Eqs. (C.29). The integration of fermionic contributions is done analogously, with functions of the form $H(\vec{q}_r^2) = |\vec{q}_r| A(\vec{q}_r^2)$, where A represents the fermionic functions from

App. B.2,

$$\begin{aligned}
 I_U^F[H] &= \int_q |\vec{q}| H(\vec{q}_r^2) \tilde{\partial}_t r_F \\
 &= \frac{k^4 T}{4\pi^2} \sum_n \int_0^\infty dx x H(k^2 P) \left[\frac{1}{\sqrt{x}} - \eta_F \left(\frac{1}{\sqrt{x}} - 1 \right) \right] \Theta(1-x) \\
 &= \frac{k^4 T}{6\pi^2} \left(1 - \frac{\eta_F}{4} \right) \sum_n H(k^2)
 \end{aligned} \tag{C.42}$$

Note that we have already inserted the last relation from (C.29) in the first step.

Bosonic anomalous dimensions

In this section all integrals are purely bosonic/fermionic, so again we will drop the corresponding index. In the bosonic anomalous dimension we have integrals, for the fermion as well as boson loop, of the form

$$I_{\eta_B}^{(1)}[G, H] = \tilde{\partial}_t \frac{\partial}{\partial \vec{p}^2} \int_q G(\vec{q}_r^2) H((\vec{q} + \vec{p})_r^2) \Big|_{\vec{p}=0}. \tag{C.43}$$

Let us perform a Taylor expansion of H about $\vec{p} = 0$

$$H((\vec{q} + \vec{p})_r^2) = H(\vec{q}_r^2) + p_i \frac{\partial H(\vec{q}_r^2)}{\partial q_i} + \frac{1}{2} p_i p_j \frac{\partial^2 H(\vec{q}_r^2)}{\partial q_i \partial q_j} + \mathcal{O}(\vec{p}^3). \tag{C.44}$$

The expansion can be written this way, as H is effectively a function of $\vec{q} + \vec{p}$, even if the argument is written differently. Plugging this into Eq. (C.43), the first term drops out by differentiation, the $\mathcal{O}(\vec{p}^3)$ terms vanish after setting $p = 0$ and we find

$$\begin{aligned}
 I_{\eta_B}^{(1)}[G, H] &= \tilde{\partial}_t \frac{\partial}{\partial \vec{p}^2} \int_q G(\vec{q}_r^2) \left[p_i \frac{\partial H(\vec{q}_r^2)}{\partial q_i} + \frac{1}{2} p_i p_j \frac{\partial^2 H(\vec{q}_r^2)}{\partial q_i \partial q_j} \right] \\
 &= \tilde{\partial}_t \frac{\partial}{\partial \vec{p}^2} \int_q \left[2p_i q_i G(\vec{q}_r^2) \frac{\partial H(\vec{q}_r^2)}{\partial \vec{q}^2} - \frac{1}{2} p_i p_j \frac{\partial G(\vec{q}_r^2)}{\partial q_i} \frac{\partial H(\vec{q}_r^2)}{\partial q_j} \right] \\
 &= -2\tilde{\partial}_t \int_q \frac{\partial}{\partial \vec{p}^2} p_i p_j q_i q_j \frac{\partial G(\vec{q}_r^2)}{\partial \vec{q}^2} \frac{\partial H(\vec{q}_r^2)}{\partial \vec{q}^2} \\
 &= -2\tilde{\partial}_t \int_q \vec{q}^2 y^2 \frac{\partial G(\vec{q}_r^2)}{\partial \vec{q}^2} \frac{\partial H(\vec{q}_r^2)}{\partial \vec{q}^2}.
 \end{aligned} \tag{C.45}$$

In the second and the third step we have used

$$\frac{\partial}{\partial q_i} = \frac{\partial \vec{q}^2}{\partial q_i} \frac{\partial}{\partial \vec{q}^2} = 2q_i \frac{\partial}{\partial \vec{q}^2}, \tag{C.46}$$

and in the last one

$$\frac{\partial}{\partial \vec{p}^2} p_i p_j q_i q_j = \frac{\partial}{\partial \vec{p}^2} (\vec{p} \cdot \vec{q})^2 = \frac{\partial}{\partial \vec{p}^2} \vec{p}^2 \vec{q}^2 y^2 = \vec{q}^2 y^2, \tag{C.47}$$

where $y = \cos \theta$ and $\theta = \angle(\vec{p}, \vec{q})$. The first term in second line vanishes upon integration, as the integrand is odd. Now we substitute the momentum integration variable according to Eq. (C.21) and redefine the functions with dimensionless arguments like in Eq. (C.27)

$$\begin{aligned} I_{\eta_B}^{(1)}[G, H] &= -2 \frac{1}{4\pi^2} \frac{1}{3} k^5 T \sum_n \tilde{\partial}_t \int_0^\infty dx x^{\frac{3}{2}} \frac{\partial \mathcal{G}(P)}{k^2 \partial x} \frac{\partial \mathcal{H}(P)}{k^2 \partial x} \\ &= -\frac{1}{3\pi^2} k T \sum_n \int_0^\infty dx x^{\frac{3}{2}} P'(x) \mathcal{G}'(P) \frac{\partial}{\partial x} \tilde{\partial}_t \mathcal{H}(P). \end{aligned} \quad (\text{C.48})$$

$P = P(x)$ represents the fermionic or bosonic momentum function. We will see that the contributions from both terms of chain rule will be the same, therefore we have simply doubled one of the contributions. Looking at Eqs. (C.30)-(C.31) and (C.39)-(C.40), we can see that only the term with the delta function will survive, which still looks same for bosons and fermions

$$\begin{aligned} I_{\eta_B}^{(1)}[G, H] &= \frac{kT}{3\pi^2} \sum_n 2 \int_0^\infty dx x^{\frac{3}{2}} \Theta(x-1) \mathcal{G}'(P) \mathcal{H}'(P) \delta(1-x) \\ &= \frac{k^5 T}{3\pi^2} \sum_n G'(k^2) H'(k^2). \end{aligned} \quad (\text{C.49})$$

We have used that $P(1) = 1$ and we get a factor $1/2$ from integrating over the product of delta and Heaviside functions according to Eq. (C.26), where technically we need to replace first $\Theta(x-1) = 1 - \Theta(1-x)$. The additional factor of k^4 is due to Eq. (C.28).

Next we shall consider fermionic contributions of the form

$$\begin{aligned} I_{\eta_B}^{(3)}[G, H] &= \tilde{\partial}_t \frac{\partial}{\partial \vec{p}^2} \int_q G(\vec{q}_r^2) H((\vec{q} + \vec{p})_r^2) \vec{q}_r \cdot (\vec{q} + \vec{p})_r \Big|_{p=0} \\ &= -\frac{1}{2} \tilde{\partial}_t \int_q \frac{\partial}{\partial \vec{p}^2} p_i p_j \left[\frac{\partial}{\partial q_i} G(\vec{q}_r^2) \vec{q}_r \right] \cdot \left[\frac{\partial}{\partial q_j} H(\vec{q}_r^2) \vec{q}_r \right]. \end{aligned} \quad (\text{C.50})$$

We performed a Taylor expansion for a vector function similar to Eq. (C.44) and did the same steps up to the second line in Eq. (C.45), where we dropped the term with the odd integrand. For the next step we look at the following types of Integrals with $V_l(q) = q_l v(q)$ and $W_l(q) = q_l w(q)$

$$\begin{aligned} \frac{d}{d\vec{p}^2} p_i p_j \int_q \partial_i V_l(q) \partial_j W_l(q) &= \frac{d}{d\vec{p}^2} p_i p_j \int_q (\delta_{il} v + q_l \partial_i v) (\delta_{jl} w + q_l \partial_j w) \\ &= \frac{d}{d\vec{p}^2} p_i p_j \int_q \left(\delta_{ij} v w + q_i v \partial_j w + q_j w \partial_i v + \vec{q}^2 \partial_i v \partial_j w \right) \\ &= \frac{d}{d\vec{p}^2} p_i p_j \int_q \left(\delta_{ij} v w + q_i \partial_j v w + \vec{q}^2 \partial_i v \partial_j w \right) \\ &= \frac{d}{d\vec{p}^2} p_i p_j \int_q \left(\delta_{ij} v w - \delta_{ij} v w + \vec{q}^2 4 q_i q_j \frac{\partial v}{\partial \vec{q}^2} \frac{\partial w}{\partial \vec{q}^2} \right) \\ &= 4 \int_q \vec{q}^4 y^2 \frac{\partial v}{\partial \vec{q}^2} \frac{\partial w}{\partial \vec{q}^2}. \end{aligned} \quad (\text{C.51})$$

For the third step we have renamed the indices and in the one after that we have used Eqs. (C.46)-(C.47). Now we rewrite the integral in terms of dimensionless arguments, according to Eq. (C.21)

$$\begin{aligned}
 I_{\eta_B}^{(3)}[G, H] &= -2\tilde{\partial}_t \int_q \tilde{q}^4 y^2 \left[\frac{\partial}{\partial \tilde{q}^2} (1+r)G \right] \left[\frac{\partial}{\partial \tilde{q}^2} (1+r)H \right] \\
 &= -2\frac{1}{4\pi^2} \frac{1}{3} k^7 T \sum_n \tilde{\partial}_t \int_0^\infty dx x^{\frac{5}{2}} \left[\frac{\partial}{\partial x} (1+r)\mathcal{G}(P) \right] \left[\frac{\partial}{\partial x} (1+r)\mathcal{H}(P) \right] \\
 &= -\frac{1}{6\pi^2} k^3 T \sum_n \int_0^\infty dx x^{\frac{5}{2}} \left\{ \left[\frac{\partial}{\partial x} \tilde{\partial}_t (1+r)\mathcal{G}(P) \right] \left[\frac{\partial}{\partial x} (1+r)\mathcal{H}(P) \right] + \right. \\
 &\quad \left. \left[\frac{\partial}{\partial x} (1+r)\mathcal{G}(P) \right] \left[\frac{\partial}{\partial x} \tilde{\partial}_t (1+r)\mathcal{H}(P) \right] \right\}. \quad (\text{C.52})
 \end{aligned}$$

Let us take a look at the expression in the first parenthesis of the second term

$$\frac{\partial}{\partial x} (1+r)\mathcal{G}(P) = (1+r)\mathcal{G}' \frac{\partial P}{\partial x} + \frac{\partial r}{\partial x} \mathcal{G} = (1+r)^2 \Theta(x-1)\mathcal{G}' - \frac{1}{2\sqrt{x^3}} \Theta(1-x)\mathcal{G}. \quad (\text{C.53})$$

For the next step we will need

$$\begin{aligned}
 \frac{\partial}{\partial x} \tilde{\partial}_t r_F &= \left[-\frac{1}{2\sqrt{x^3}} + \eta_F \frac{1}{2\sqrt{x^3}} \right] \Theta(1-x) - \left[\frac{1}{\sqrt{x}} - \eta_F \left(\frac{1}{\sqrt{x}} - 1 \right) \right] \delta(1-x) \\
 &= -\frac{1}{2\sqrt{x^3}} (1 - \eta_F) \Theta(1-x) - \delta(1-x). \quad (\text{C.54})
 \end{aligned}$$

Now we consider the second parenthesis using Eqs. (C.24), (C.33), (C.35), (C.37), (C.40) and (C.54)

$$\begin{aligned}
 \frac{\partial}{\partial x} \tilde{\partial}_t (1+r)\mathcal{H}(P) &= \frac{\partial}{\partial x} \left[(\tilde{\partial}_t r)\mathcal{H} + (1+r)\tilde{\partial}_t \mathcal{H} \right] \\
 &= \left(\frac{\partial}{\partial x} \tilde{\partial}_t r \right) \mathcal{H} + (\tilde{\partial}_t r) \frac{\partial}{\partial x} \mathcal{H} + \frac{\partial r}{\partial x} \tilde{\partial}_t \mathcal{H} + (1+r) \frac{\partial}{\partial x} \tilde{\partial}_t \mathcal{H} \\
 &= -\left[\frac{1-\eta}{2\sqrt{x^3}} \Theta(1-x) + \delta(1-x) \right] \mathcal{H} + \left[\frac{1}{\sqrt{x}} - \eta \left(\frac{1}{\sqrt{x}} - 1 \right) \right] \Theta(1-x) P' \mathcal{H}' \\
 &\quad - \frac{\Theta(1-x)}{2\sqrt{x^3}} 2x(1+r) \left[\frac{1}{\sqrt{x}} - \eta \left(\frac{1}{\sqrt{x}} - 1 \right) \right] \Theta(1-x) \mathcal{H}' + (1+r) \left[\frac{1}{\sqrt{x}} \eta \Theta(1-x) - 2\delta(1-x) \right] \mathcal{H}' \\
 &= -\left[\frac{1-\eta}{2\sqrt{x^3}} \Theta(1-x) + \delta(1-x) \right] \mathcal{H} - \left[\left(\frac{1-\eta}{\sqrt{x}} + \eta \right) - \eta \right] \Theta(1-x) \frac{1+r}{\sqrt{x}} \mathcal{H}' - 2\delta(1-x)(1+r)\mathcal{H}' \\
 &= -\delta(1-x) [\mathcal{H} + 2(1+r)\mathcal{H}'] - \Theta(1-x) (1-\eta) \left[\frac{\mathcal{H}}{2\sqrt{x^3}} + \frac{(1+r)\mathcal{H}'}{x} \right]. \quad (\text{C.55})
 \end{aligned}$$

The term containing P' vanishes upon integration due to opposite Heaviside functions, see Eq. (C.31). We have set higher orders of Heaviside functions to the order of one, since no delta function will be multiplied with this expression. Integrating the product of the previous two results assuming the properties in Eqs. (C.29) and that $x^\alpha = 1$ for any α in the terms containing a Dirac delta function, yields

$$\begin{aligned}
& \int_0^\infty dx x^{\frac{5}{2}} \left[\frac{\partial}{\partial x} (1+r) \mathcal{G}(P) \right] \left[\frac{\partial}{\partial x} \tilde{\delta}_t (1+r) \mathcal{H}(P) \right] \\
&= -\frac{1}{2} \int_0^\infty dx x^{\frac{5}{2}} \left\{ [2\Theta(1-x)\mathcal{G}' - \Theta(x-1)\mathcal{G}] [\mathcal{H} + 2\mathcal{H}'] \delta(1-x) \right. \\
&\quad \left. - (1-\eta) \frac{\mathcal{G}}{x^3} \left[\frac{\mathcal{H}}{2} + \mathcal{H}' \right] \Theta(1-x) \right\} \\
&= -\frac{1}{4} [2\mathcal{G}'(1) - \mathcal{G}(1)] [\mathcal{H}(1) + 2\mathcal{H}'(1)] - \frac{1-\eta}{2} \mathcal{G}(1) [\mathcal{H}(1) + 2\mathcal{H}'(1)] . \tag{C.56}
\end{aligned}$$

From the x integration we get a factor $1/2$ in the first term by the integration formula in Eq. (C.26) and in second term a factor 2 by ordinary integration. The \mathcal{G}' term in the $1-\eta$ contribution vanishes due to opposite Heaviside functions. All functions are evaluated at $P=1$. Let us expand the first term

$$(2\mathcal{G}' - \mathcal{G})(\mathcal{H} + 2\mathcal{H}') = 4\mathcal{G}'\mathcal{H}' - 2\mathcal{G}\mathcal{H}' + 2\mathcal{G}'\mathcal{H} - \mathcal{G}\mathcal{H} . \tag{C.57}$$

From the first term in Eq. (C.52) we will get the same expression but with interchanged functions $\mathcal{G} \leftrightarrow \mathcal{H}$, therefore the two terms in the middle will be canceled. In general, these functions can be of different particle species, thus we must consider different anomalous dimensions η_H and η_G in the loop. The integral is then given by

$$I_{\eta_B}^{(3)}[G, H] = \frac{k^3 T}{3\pi^2} \sum_n \left[k^4 G' H' - \frac{GH}{4} - \frac{1-\eta_H}{2} G \left(\frac{H}{2} + k^2 H' \right) - \frac{1-\eta_G}{2} H \left(\frac{G}{2} + k^2 G' \right) \right] . \tag{C.58}$$

Here we have turned back to the original functions, which are all evaluated at k^2 . Again, every primed quantity has to be substituted with the original function primed and scaled with k^2 . If the particle species are the same, we know that the coefficient functions G and H only differ potentially by a sign in front of the chemical potential, cf. Eqs. (B.17) and (C.7). Then we can use following steps, explicitly denoting the q_4 dependence,

$$\int dq_4 H(q_4) G'(q_4) = \int dq_4 H(-q_4) G'(-q_4) = (\pm)^2 \int dq_4 G(q_4) H'(q_4) \tag{C.59}$$

and add another term which usually appears in integrals. Defining

$$\begin{aligned}
I_{\eta_B}^{(2)}[G, H, m^2] &= I_{\eta_B}^{(3)}[G, H] + m^2 I_{\eta_B}^{(1)}[G, H] \\
&= \frac{k^3 T}{3\pi^2} \sum_n \left[k^2(k^2 + m^2) G' H' - \frac{GH}{4} - (1-\eta) G \left(\frac{H}{2} + k^2 H' \right) \right] \tag{C.60}
\end{aligned}$$

The m^2 term adds to the first one in Eq. (C.58).

Fermionic anomalous dimensions

In the fermionic anomalous dimension we have mixed integrals, of the form

$$I_{\eta_F}[G_F, H_B] = -\tilde{\partial}_t \frac{\partial}{\partial |\vec{p}|} \vec{p} \cdot \int_q \hat{\vec{q}} G_F(\vec{q}_r^2) H_B((\vec{q} - \vec{p})_r^2) \Big|_{p=0} \quad (\text{C.61})$$

The scalar product of the unit vectors is simply $\hat{\vec{p}} \cdot \hat{\vec{q}} = \cos \theta = y$. The momentum derivative acts only on the bosonic function, of which we performed a Taylor expansion about $\vec{p} = 0$ similar to Eq. (C.44)

$$\frac{\partial}{\partial |\vec{p}|} H_B((\vec{q} - \vec{p})_r^2) \Big|_{p=0} = \frac{\partial}{\partial |\vec{p}|} \left[H_B(\vec{q}_r^2) - 2\vec{p} \cdot \vec{q} \frac{\partial}{\partial \vec{q}^2} H_B(\vec{q}_r^2) + \mathcal{O}(\vec{p}^2) \right] \Big|_{p=0} = -2y |\vec{q}| \frac{\partial}{\partial \vec{q}^2} H_B(\vec{q}_r^2),$$

where we have used Eq. (C.46). Here only the linear term survives. In the last step we used $\frac{\partial}{\partial \vec{p}} \vec{p} = \mathbb{1}$ and Eq. (C.46). After plugging this back in, we substituted the momentum integration according to Eq. (C.21) with $n = \frac{1}{2}$, $m = 2$, and (C.27)

$$\begin{aligned} I_{\eta_F}[G_F, H_B] &= 2\tilde{\partial}_t \int_q y^2 |\vec{q}| G_F(\vec{q}_r^2) \frac{\partial}{\partial \vec{q}^2} H_B(\vec{q}_r^2) \\ &= \frac{1}{12\pi^2} k^4 T \sum_n 2\tilde{\partial}_t \int_0^\infty dx x \mathcal{G}(P_F) \frac{\partial}{k^2 \partial x} \mathcal{H}(P_B) \\ &= \frac{k^2 T}{6\pi^2} \sum_n \int_0^\infty dx x \left[\mathcal{G}(P_F) \frac{\partial}{\partial x} \tilde{\partial}_t \mathcal{H}(P_B) + \mathcal{H}'(P_B) \Theta(x-1) \tilde{\partial}_t \mathcal{G}(P_F) \right] \end{aligned}$$

In the last line Eq. (C.30) was used. The scale derivative in the second term is proportional to the opposite Heaviside function from Eq. (C.35):

$$\tilde{\partial}_t \mathcal{G}(P_F) = \mathcal{G}' \frac{\partial P_F}{\partial r_F} \tilde{\partial}_t r_F \propto \Theta(1-x). \quad (\text{C.62})$$

There are no delta functions in the second term, so it vanishes. In the first term we plug in Eq. (C.39), immediately factoring out -2 , and carry out the integral assuming the properties in Eqs. (C.29)

$$\begin{aligned} I_{\eta_F}[G_F, H_B] &= -\frac{k^2 T}{3\pi^2} \sum_n \int_0^\infty dx x \mathcal{G}(P_F) \mathcal{H}'(P_B) \left[\delta(1-x) - \frac{\eta_B}{2} \Theta(1-x) \right] \\ &= -\frac{k^4 T}{3\pi^2} \left(1 - \frac{\eta_B}{4} \right) \sum_n G_F(k^2) H'_B(k^2) \end{aligned} \quad (\text{C.63})$$

We turned back to the original functions, with a factor k^2 due to Eq. (C.28). We must consider functions $H_B(\vec{q}_{r1}^2, \dots, \vec{q}_{rN}^2)$, which represent mixtures of different bosonic species. Typically the momentum in such functions appears in energy functions like $K_{\varphi_i} = \vec{q}_{r_i}^2 + \dots$, in which case Eq. (C.63) can be generalized straightforwardly

$$I_{\eta_F}[G_F, H_B] = -\frac{k^4 T}{3\pi^2} \sum_n G_F \sum_i \left(1 - \frac{\eta_{\varphi_i}}{4} \right) \frac{\partial H_B}{\partial K_{\varphi_i}}. \quad (\text{C.64})$$

Baryon UV mass gap

In the flow of the baryon UV mass gap we have mixed integrals, of the form

$$\begin{aligned}
I_{m_B}[G_F, H_B] &= -\tilde{\partial}_t \hat{p} \cdot \int_q \hat{q} G_F(\vec{q}_r^2) H_B(\vec{q}_r^2) \Big|_{p=0} = -\tilde{\partial}_t \int_q y G_F(\vec{q}_r^2) H_B(\vec{q}_r^2) \quad (\text{C.65}) \\
&= -\frac{k^3 T}{8\pi^2} \sum_n \tilde{\partial}_t \int_0^\infty dx \sqrt{x} \mathcal{G}(P_F) \mathcal{H}(P_B) \\
&= -\frac{k^3 T}{8\pi^2} \sum_n \int_0^\infty dx \sqrt{x} \left\{ \mathcal{G}(P_F) \tilde{\partial}_t \mathcal{H}(P_B) + \mathcal{H}(P_B) \tilde{\partial}_t \mathcal{G}(P_F) \right\} \\
&= -\frac{k^3 T}{8\pi^2} \sum_n \int_0^\infty dx \sqrt{x} \left\{ \mathcal{G}(P_F) \mathcal{H}'(P_B) (2 - \eta_B(1-x)) + \right. \\
&\quad \left. \mathcal{H}(P_B) 2\mathcal{G}'(P_F)(1+r_F) [\sqrt{x} - \eta_F(\sqrt{x}-x)] \right\} \Theta(1-x) \\
&= -\frac{k^5 T}{6\pi^2} \sum_n \left\{ \left(1 - \frac{\eta_B}{5}\right) H'_B(k^2) G_F(k^2) + \left(1 - \frac{\eta_F}{4}\right) H_B(k^2) G'_F(k^2) \right\}. \quad (\text{C.66})
\end{aligned}$$

In the first line we used the formula (C.21) with $n = 0$ and $m = 1$. In the forth line we used Eq. (C.35)-(C.37) and factored out the common terms. Finally we carry out the integration with (C.29) turn back to the original functions, with a factor k^2 due to Eq. (C.28). We must consider functions $G_F(\vec{q}_{r_1}^2, \dots, \vec{q}_{r_N}^2)$ and $H_B(\vec{q}_{r_1}^2, \dots, \vec{q}_{r_N}^2)$, which represent mixtures of different particle species. The bosonic part is as above,

$$I_{m_B}[G_F, H_B] = -\frac{k^5 T}{6\pi^2} \sum_n \left\{ G_F \sum_i \left(1 - \frac{\eta_{\varphi_i}}{5}\right) \frac{\partial H_B}{\partial K_{\varphi_i}} + H_B \sum_i \left(1 - \frac{\eta_{\Psi_i}}{4}\right) \frac{\partial G_F}{\partial \vec{q}_{r_i}^2} \right\}. \quad (\text{C.67})$$

Yukawa coupling

In the flow of Yukawa couplings we have mixed integrals, of the form

$$\begin{aligned}
I_h[G_F, H_B] &= -\tilde{\partial}_t \int_q G_F(\vec{q}_r^2) H_B(\vec{q}_r^2) \quad (\text{C.68}) \\
&= -\frac{k^3 T}{4\pi^2} \sum_n \int_0^\infty dx \sqrt{x} \left[\mathcal{G}(P_F) \tilde{\partial}_t \mathcal{H}(P_B) + \mathcal{H}(P_B) \tilde{\partial}_t \mathcal{G}(P_F) \right] \\
&= -\frac{k^3 T}{4\pi^2} \sum_n \int_0^\infty dx \sqrt{x} \left\{ \mathcal{G}(P_F) \mathcal{H}'(P_B) (2 - \eta_B(1-x)) \right. \\
&\quad \left. + 2\mathcal{H}(P_B) \mathcal{G}'(P_F)(1+r_F) [\sqrt{x} - \eta_F(\sqrt{x}-x)] \right\} \Theta(1-x) \\
&= -\frac{k^5 T}{3\pi^2} \sum_n \left[\left(1 - \frac{\eta_B}{5}\right) G_F(k^2) H'_B(k^2) + \left(1 - \frac{\eta_F}{4}\right) H_B(k^2) G'_F(k^2) \right]. \quad (\text{C.69})
\end{aligned}$$

This was now a straight forward computation for us. We inserted Eqs. (C.36)-(C.37), carried out the integral assuming the properties in Eqs. (C.29), and turned back to the original functions, with a factor k^2 due to Eq. (C.28). Again we have to consider different species of bosons similar to Eq. (C.64)

$$I_h[G_F, H_B] = -\frac{k^5 T}{3\pi^2} \sum_n \left[G_F \sum_i \left(1 - \frac{\eta_{\varphi_i}}{4} \right) \frac{\partial H_B}{\partial K_{\varphi_i}} + \left(1 - \frac{\eta_F}{4} \right) H_B G'_F \right]. \quad (\text{C.70})$$

Bibliography

- [1] H. Yukawa, “On the Interaction of Elementary Particles I,” *Proc. Phys. Math. Soc. Jap.* **17** (1935) 48–57.
- [2] M. Gell-Mann, “The Eightfold Way: A Theory of strong interaction symmetry,” *California Institute Technology Synchrotron Lab. Report No. CTSL-20* (1961) .
- [3] Y. Ne’eman, “Derivation of strong interactions from a gauge invariance,” *Nucl. Phys.* **26** (1961) 222–229.
- [4] M. Gell-Mann, “Symmetries of baryons and mesons,” *Phys. Rev.* **125** (1962) 1067–1084.
- [5] G. Zweig, “An SU(3) model for strong interaction symmetry and its breaking. Version 1,” *CERN Report No.8182/TH-401* (1964) .
- [6] G. Zweig, “An SU(3) model for strong interaction symmetry and its breaking. Version 2,” *CERN Report No.8419/TH-412* (1964) .
- [7] M. Gell-Mann, “A Schematic Model of Baryons and Mesons,” *Phys. Lett.* **8** (1964) 214–215.
- [8] M. Y. Han and Y. Nambu, “Three Triplet Model with Double SU(3) Symmetry,” *Phys. Rev.* **139** (1965) B1006–B1010.
- [9] O. W. Greenberg, “Spin and Unitary Spin Independence in a Paraquark Model of Baryons and Mesons,” *Phys. Rev. Lett.* **13** (1964) 598–602.
- [10] C.-N. Yang and R. L. Mills, “Conservation of Isotopic Spin and Isotopic Gauge Invariance,” *Phys. Rev.* **96** (1954) 191–195.
- [11] H. Fritzsch, M. Gell-Mann, and H. Leutwyler, “Advantages of the Color Octet Gluon Picture,” *Phys. Lett.* **B47** (1973) 365–368.
- [12] J. S. Poucher *et al.*, “High-Energy Single-Arm Inelastic e - p and e - d Scattering at 6-Degrees and 10-Degrees,” *Phys. Rev. Lett.* **32** (1974) 118.
- [13] **TASSO** Collaboration, R. Brandelik *et al.*, “Evidence for Planar Events in e+ e- Annihilation at High-Energies,” *Phys. Lett.* **B86** (1979) 243.
- [14] **Particle Data Group** Collaboration, K. Nakamura *et al.*, “Review of particle physics,” *J. Phys.* **G37** (2010) 075021.

- [15] S. Bethke, “The 2009 World Average of $\alpha(s)$,” *Eur. Phys. J.* **C64** (2009) 689–703, [arXiv:0908.1135 \[hep-ph\]](#).
- [16] C. G. Callan, Jr., “Broken scale invariance in scalar field theory,” *Phys. Rev.* **D2** (1970) 1541–1547.
- [17] K. Symanzik, “Small distance behavior in field theory and power counting,” *Commun. Math. Phys.* **18** (1970) 227–246.
- [18] D. J. Gross and F. Wilczek, “Ultraviolet Behavior of Nonabelian Gauge Theories,” *Phys. Rev. Lett.* **30** (1973) 1343–1346.
- [19] H. D. Politzer, “Reliable Perturbative Results for Strong Interactions?,” *Phys. Rev. Lett.* **30** (1973) 1346–1349.
- [20] J. Goldstone, “Field Theories with Superconductor Solutions,” *Nuovo Cim.* **19** (1961) 154–164.
- [21] G. S. Guralnik, C. R. Hagen, and T. W. B. Kibble, “Global Conservation Laws and Massless Particles,” *Phys. Rev. Lett.* **13** (1964) 585–587.
- [22] P. W. Higgs, “Broken symmetries, massless particles and gauge fields,” *Phys. Lett.* **12** (1964) 132–133.
- [23] J. Engels, F. Karsch, H. Satz, and I. Montvay, “High Temperature SU(2) Gluon Matter on the Lattice,” *Phys. Lett.* **B101** (1981) 89.
- [24] GSI Darmstadt. www.gsi.de.
- [25] S. Hands, “The Phase diagram of QCD,” *Contemp. Phys.* **42** (2001) 209–225, [arXiv:physics/0105022 \[physics.ed-ph\]](#).
- [26] D. H. Rischke, “The Quark gluon plasma in equilibrium,” *Prog. Part. Nucl. Phys.* **52** (2004) 197–296, [arXiv:nucl-th/0305030 \[nucl-th\]](#).
- [27] P. Braun-Munzinger and J. Wambach, “The Phase Diagram of Strongly-Interacting Matter,” *Rev. Mod. Phys.* **81** (2009) 1031–1050, [arXiv:0801.4256 \[hep-ph\]](#).
- [28] O. Philipsen, “Status of Lattice Studies of the QCD Phase Diagram,” *Prog. Theor. Phys. Suppl.* **174** (2008) 206–213, [arXiv:0808.0672 \[hep-ph\]](#).
- [29] J. M. Pawłowski, “The QCD phase diagram: Results and challenges,” *AIP Conf. Proc.* **1343** (2011) 75–80, [arXiv:1012.5075 \[hep-ph\]](#).
- [30] Y. Aoki, G. Endrodi, Z. Fodor, S. D. Katz, and K. K. Szabo, “The Order of the quantum chromodynamics transition predicted by the standard model of particle physics,” *Nature* **443** (2006) 675–678, [arXiv:hep-lat/0611014 \[hep-lat\]](#).
- [31] P. de Forcrand and O. Philipsen, “The QCD phase diagram for small densities from imaginary chemical potential,” *Nucl. Phys.* **B642** (2002) 290–306, [arXiv:hep-lat/0205016 \[hep-lat\]](#).
- [32] L. McLerran and R. D. Pisarski, “Phases of cold, dense quarks at large $N(c)$,” *Nucl. Phys.* **A796** (2007) 83–100, [arXiv:0706.2191 \[hep-ph\]](#).

-
- [33] A. Andronic *et al.*, “Hadron Production in Ultra-relativistic Nuclear Collisions: Quarkyonic Matter and a Triple Point in the Phase Diagram of QCD,” *Nucl. Phys.* **A837** (2010) 65–86, [arXiv:0911.4806 \[hep-ph\]](#).
 - [34] Y. Hidaka, L. D. McLerran, and R. D. Pisarski, “Baryons and the phase diagram for a large number of colors and flavors,” *Nucl. Phys.* **A808** (2008) 117–123, [arXiv:0803.0279 \[hep-ph\]](#).
 - [35] E. Shuryak, “Physics of Strongly coupled Quark-Gluon Plasma,” *Prog. Part. Nucl. Phys.* **62** (2009) 48–101, [arXiv:0807.3033 \[hep-ph\]](#).
 - [36] T. Schäfer and D. Teaney, “Nearly Perfect Fluidity: From Cold Atomic Gases to Hot Quark Gluon Plasmas,” *Rept. Prog. Phys.* **72** (2009) 126001, [arXiv:0904.3107 \[hep-ph\]](#).
 - [37] A. Adams, L. D. Carr, T. Schäfer, P. Steinberg, and J. E. Thomas, “Strongly Correlated Quantum Fluids: Ultracold Quantum Gases, Quantum Chromodynamic Plasmas, and Holographic Duality,” *New J. Phys.* **14** (2012) 115009, [arXiv:1205.5180 \[hep-th\]](#).
 - [38] **STAR** Collaboration, J. Adams *et al.*, “Experimental and theoretical challenges in the search for the quark gluon plasma: The STAR Collaboration’s critical assessment of the evidence from RHIC collisions,” *Nucl. Phys.* **A757** (2005) 102–183, [arXiv:nuc1-ex/0501009 \[nuc1-ex\]](#).
 - [39] **PHENIX** Collaboration, K. Adcox *et al.*, “Formation of dense partonic matter in relativistic nucleus-nucleus collisions at RHIC: Experimental evaluation by the PHENIX collaboration,” *Nucl. Phys.* **A757** (2005) 184–283, [arXiv:nuc1-ex/0410003 \[nuc1-ex\]](#).
 - [40] **ALICE** Collaboration, K. Aamodt *et al.*, “Elliptic flow of charged particles in Pb-Pb collisions at 2.76 TeV,” *Phys. Rev. Lett.* **105** (2010) 252302, [arXiv:1011.3914 \[nuc1-ex\]](#).
 - [41] D. Teaney, J. Lauret, and E. V. Shuryak, “A Hydrodynamic description of heavy ion collisions at the SPS and RHIC,” [arXiv:nuc1-th/0110037 \[nuc1-th\]](#).
 - [42] D. H. Rischke, S. Bernard, and J. A. Maruhn, “Relativistic hydrodynamics for heavy ion collisions. 1. General aspects and expansion into vacuum,” *Nucl. Phys.* **A595** (1995) 346–382, [arXiv:nuc1-th/9504018 \[nuc1-th\]](#).
 - [43] D. H. Rischke, Y. Pursun, and J. A. Maruhn, “Relativistic hydrodynamics for heavy ion collisions. 2. Compression of nuclear matter and the phase transition to the quark - gluon plasma,” *Nucl. Phys.* **A595** (1995) 383–408, [arXiv:nuc1-th/9504021 \[nuc1-th\]](#). [Erratum: *Nucl. Phys.*A596,717(1996)].
 - [44] P. F. Kolb and U. W. Heinz, “Hydrodynamic description of ultrarelativistic heavy ion collisions,” [arXiv:nuc1-th/0305084 \[nuc1-th\]](#).
 - [45] P. Huovinen and P. V. Ruuskanen, “Hydrodynamic Models for Heavy Ion Collisions,” *Ann. Rev. Nucl. Part. Sci.* **56** (2006) 163–206, [arXiv:nuc1-th/0605008 \[nuc1-th\]](#).
 - [46] F. Gelis, E. Iancu, J. Jalilian-Marian, and R. Venugopalan, “The Color Glass Condensate,” *Ann. Rev. Nucl. Part. Sci.* **60** (2010) 463–489, [arXiv:1002.0333 \[hep-ph\]](#).

- [47] T. Lappi and L. McLerran, “Some features of the glasma,” *Nucl. Phys.* **A772** (2006) 200–212, [arXiv:hep-ph/0602189](#) [hep-ph].
- [48] E. Iancu, A. Leonidov, and L. D. McLerran, “Nonlinear gluon evolution in the color glass condensate. 1,” *Nucl. Phys.* **A692** (2001) 583–645, [arXiv:hep-ph/0011241](#) [hep-ph].
- [49] E. Ferreiro, E. Iancu, A. Leonidov, and L. McLerran, “Nonlinear gluon evolution in the color glass condensate. 2,” *Nucl. Phys.* **A703** (2002) 489–538, [arXiv:hep-ph/0109115](#) [hep-ph].
- [50] J. Berges, K. Boguslavski, S. Schlichting, and R. Venugopalan, “Turbulent thermalization process in heavy-ion collisions at ultrarelativistic energies,” *Phys. Rev.* **D89** no. 7, (2014) 074011, [arXiv:1303.5650](#) [hep-ph].
- [51] J. Berges, K. Boguslavski, S. Schlichting, and R. Venugopalan, “Universal attractor in a highly occupied non-Abelian plasma,” *Phys. Rev.* **D89** no. 11, (2014) 114007, [arXiv:1311.3005](#) [hep-ph].
- [52] P. Braun-Munzinger, K. Redlich, and J. Stachel, “Particle production in heavy ion collisions,” [arXiv:nucl-th/0304013](#) [nucl-th].
- [53] P. J. Siemens, “Liquid–gas phase transition in nuclear matter,” *Nature* **305** (1983) 410–412.
- [54] M. Baldo and L. Ferreira, “Nuclear liquid-gas phase transition,” *Physical Review C* **59** no. 2, (1999) 682–703.
- [55] M. Hempel and J. Schaffner-Bielich, “Statistical Model for a Complete Supernova Equation of State,” *Nucl. Phys.* **A837** (2010) 210–254, [arXiv:0911.4073](#) [nucl-th].
- [56] R. D. Pisarski and F. Wilczek, “Remarks on the Chiral Phase Transition in Chromodynamics,” *Phys. Rev.* **D29** (1984) 338–341.
- [57] M. Fukugita, M. Okawa, and A. Ukawa, “Order of the Deconfining Phase Transition in SU(3) Lattice Gauge Theory,” *Phys. Rev. Lett.* **63** (1989) 1768.
- [58] M. A. Stephanov, K. Rajagopal, and E. V. Shuryak, “Signatures of the tricritical point in QCD,” *Phys. Rev. Lett.* **81** (1998) 4816–4819, [arXiv:hep-ph/9806219](#) [hep-ph].
- [59] M. A. Stephanov, K. Rajagopal, and E. V. Shuryak, “Event-by-event fluctuations in heavy ion collisions and the QCD critical point,” *Phys. Rev.* **D60** (1999) 114028, [arXiv:hep-ph/9903292](#) [hep-ph].
- [60] C. Bonati, P. de Forcrand, M. D’Elia, O. Philipsen, and F. Sanfilippo, “Constraints on the two-flavor QCD phase diagram from imaginary chemical potential,” *PoS LATTICE2011* (2011) 189, [arXiv:1201.2769](#) [hep-lat].
- [61] J. C. Collins and M. J. Perry, “Superdense Matter: Neutrons Or Asymptotically Free Quarks?,” *Phys. Rev. Lett.* **34** (1975) 1353.
- [62] B. C. Barrois, “Superconducting Quark Matter,” *Nucl. Phys.* **B129** (1977) 390.
- [63] S. C. Frautschi, “Asymptotic freedom and color superconductivity in dense quark matter,” in *Erice Hadr.Matter 1978:18*, p. 18. 1978.

-
- [64] D. Bailin and A. Love, “Superfluidity and Superconductivity in Relativistic Fermion Systems,” *Phys. Rept.* **107** (1984) 325.
 - [65] A. Schmitt, “Dense matter in compact stars: A pedagogical introduction,” *Lect. Notes Phys.* **811** (2010) 1–111, [arXiv:1001.3294 \[astro-ph.SR\]](#).
 - [66] K. Rajagopal and F. Wilczek, “The Condensed matter physics of QCD,” [arXiv:hep-ph/0011333 \[hep-ph\]](#).
 - [67] M. G. Alford, “Color superconducting quark matter,” *Ann. Rev. Nucl. Part. Sci.* **51** (2001) 131–160, [arXiv:hep-ph/0102047 \[hep-ph\]](#).
 - [68] M. Buballa, “NJL model analysis of quark matter at large density,” *Phys. Rept.* **407** (2005) 205–376, [arXiv:hep-ph/0402234 \[hep-ph\]](#).
 - [69] M. G. Alford, A. Schmitt, K. Rajagopal, and T. Schäfer, “Color superconductivity in dense quark matter,” *Rev. Mod. Phys.* **80** (2008) 1455–1515, [arXiv:0709.4635 \[hep-ph\]](#).
 - [70] K. Fukushima and T. Hatsuda, “The phase diagram of dense QCD,” *Rept. Prog. Phys.* **74** (2011) 014001, [arXiv:1005.4814 \[hep-ph\]](#).
 - [71] K. Fukushima and C. Sasaki, “The phase diagram of nuclear and quark matter at high baryon density,” *Prog. Part. Nucl. Phys.* **72** (2013) 99–154, [arXiv:1301.6377 \[hep-ph\]](#).
 - [72] M. G. Alford, K. Rajagopal, and F. Wilczek, “QCD at finite baryon density: Nucleon droplets and color superconductivity,” *Phys. Lett. B* **422** (1998) 247–256, [arXiv:hep-ph/9711395 \[hep-ph\]](#).
 - [73] R. Rapp, T. Schäfer, E. V. Shuryak, and M. Velkovsky, “Diquark Bose condensates in high density matter and instantons,” *Phys. Rev. Lett.* **81** (1998) 53–56, [arXiv:hep-ph/9711396 \[hep-ph\]](#).
 - [74] J. Berges and K. Rajagopal, “Color superconductivity and chiral symmetry restoration at nonzero baryon density and temperature,” *Nucl. Phys. B* **538** (1999) 215–232, [arXiv:hep-ph/9804233 \[hep-ph\]](#).
 - [75] M. G. Alford, J. Berges, and K. Rajagopal, “Unlocking color and flavor in superconducting strange quark matter,” *Nucl. Phys. B* **558** (1999) 219–242, [arXiv:hep-ph/9903502 \[hep-ph\]](#).
 - [76] R. D. Pisarski and D. H. Rischke, “Color superconductivity in weak coupling,” *Phys. Rev. D* **61** (2000) 074017, [arXiv:nucl-th/9910056 \[nucl-th\]](#).
 - [77] W. Broniowski, A. Kotlorz, and M. Kutschera, “Quarks with a pion condensate. a new phase of matter,” *Acta Phys. Polon.* **B22** (1991) 145–166.
 - [78] E. Nakano and T. Tatsumi, “Chiral symmetry and density wave in quark matter,” *Phys. Rev. D* **71** (2005) 114006, [arXiv:hep-ph/0411350 \[hep-ph\]](#).
 - [79] S. Carignano, D. Nickel, and M. Buballa, “Influence of vector interaction and Polyakov loop dynamics on inhomogeneous chiral symmetry breaking phases,” *Phys. Rev. D* **82** (2010) 054009, [arXiv:1007.1397 \[hep-ph\]](#).
 - [80] M. G. Alford, J. A. Bowers, and K. Rajagopal, “Crystalline color superconductivity,” *Phys. Rev. D* **63** (2001) 074016, [arXiv:hep-ph/0008208 \[hep-ph\]](#).

- [81] A. K. Leibovich, K. Rajagopal, and E. Shuster, “Opening the crystalline color superconductivity window,” *Phys. Rev.* **D64** (2001) 094005, [arXiv:hep-ph/0104073 \[hep-ph\]](#).
- [82] R. Anglani, R. Casalbuoni, M. Ciminale, N. Ippolito, R. Gatto, M. Mannarelli, and M. Ruggieri, “Crystalline color superconductors,” *Rev. Mod. Phys.* **86** (2014) 509–561, [arXiv:1302.4264 \[hep-ph\]](#).
- [83] T. Schäfer and F. Wilczek, “Continuity of quark and hadron matter,” *Phys. Rev. Lett.* **82** (1999) 3956–3959, [arXiv:hep-ph/9811473 \[hep-ph\]](#).
- [84] T. Schäfer, “Quark hadron continuity in QCD with one flavor,” *Phys. Rev.* **D62** (2000) 094007, [arXiv:hep-ph/0006034 \[hep-ph\]](#).
- [85] T. Hatsuda, M. Tachibana, N. Yamamoto, and G. Baym, “New critical point induced by the axial anomaly in dense QCD,” *Phys. Rev. Lett.* **97** (2006) 122001, [arXiv:hep-ph/0605018 \[hep-ph\]](#).
- [86] K. G. Wilson, “Confinement of Quarks,” *Phys. Rev.* **D10** (1974) 2445–2459.
- [87] J. B. Kogut and L. Susskind, “Hamiltonian Formulation of Wilson’s Lattice Gauge Theories,” *Phys. Rev.* **D11** (1975) 395–408.
- [88] M. Creutz, *Quarks, gluons and lattices*. Cambridge Monographs on Mathematical Physics. Cambridge Univ. Press, Cambridge, UK, 1985.
- [89] I. Montvay and G. Munster, *Quantum fields on a lattice*. Cambridge University Press, 1997.
- [90] C. Gattringer and C. B. Lang, “Quantum chromodynamics on the lattice,” *Lect. Notes Phys.* **788** (2010) 1–343.
- [91] C. Schmidt, “Lattice QCD at finite density,” *PoS LAT2006* (2006) 021, [arXiv:hep-lat/0610116 \[hep-lat\]](#).
- [92] P. de Forcrand, “Simulating QCD at finite density,” *PoS LAT2009* (2009) 010, [arXiv:1005.0539 \[hep-lat\]](#).
- [93] P. Hasenfratz and F. Karsch, “Chemical Potential on the Lattice,” *Phys. Lett.* **B125** (1983) 308.
- [94] J. B. Kogut, H. Matsuoka, M. Stone, H. W. Wyld, S. H. Shenker, J. Shigemitsu, and D. K. Sinclair, “Chiral Symmetry Restoration in Baryon Rich Environments,” *Nucl. Phys.* **B225** (1983) 93.
- [95] A. M. Ferrenberg and R. H. Swendsen, “Optimized Monte Carlo analysis,” *Phys. Rev. Lett.* **63** (1989) 1195–1198.
- [96] I. M. Barbour, S. E. Morrison, E. G. Klepfish, J. B. Kogut, and M.-P. Lombardo, “Results on finite density QCD,” *Nucl. Phys. Proc. Suppl.* **60A** (1998) 220–234, [arXiv:hep-lat/9705042 \[hep-lat\]](#).
- [97] Z. Fodor and S. D. Katz, “Lattice determination of the critical point of QCD at finite T and μ ,” *JHEP* **03** (2002) 014, [arXiv:hep-lat/0106002 \[hep-lat\]](#).

-
- [98] Z. Fodor and S. D. Katz, “Critical point of QCD at finite T and μ , lattice results for physical quark masses,” *JHEP* **04** (2004) 050, [arXiv:hep-lat/0402006 \[hep-lat\]](#).
 - [99] C. R. Allton, S. Ejiri, S. J. Hands, O. Kaczmarek, F. Karsch, E. Laermann, C. Schmidt, and L. Scorzato, “The QCD thermal phase transition in the presence of a small chemical potential,” *Phys. Rev.* **D66** (2002) 074507, [arXiv:hep-lat/0204010 \[hep-lat\]](#).
 - [100] S. Ejiri, C. R. Allton, S. J. Hands, O. Kaczmarek, F. Karsch, E. Laermann, and C. Schmidt, “Study of QCD thermodynamics at finite density by Taylor expansion,” *Prog. Theor. Phys. Suppl.* **153** (2004) 118–126, [arXiv:hep-lat/0312006 \[hep-lat\]](#).
 - [101] R. V. Gavai and S. Gupta, “The Critical end point of QCD,” *Phys. Rev.* **D71** (2005) 114014, [arXiv:hep-lat/0412035 \[hep-lat\]](#).
 - [102] R. V. Gavai and S. Gupta, “QCD at finite chemical potential with six time slices,” *Phys. Rev.* **D78** (2008) 114503, [arXiv:0806.2233 \[hep-lat\]](#).
 - [103] P. de Forcrand and O. Philipsen, “The QCD phase diagram for three degenerate flavors and small baryon density,” *Nucl. Phys.* **B673** (2003) 170–186, [arXiv:hep-lat/0307020 \[hep-lat\]](#).
 - [104] M. D’Elia and F. Sanfilippo, “Thermodynamics of two flavor QCD from imaginary chemical potentials,” *Phys. Rev.* **D80** (2009) 014502, [arXiv:0904.1400 \[hep-lat\]](#).
 - [105] P. de Forcrand and O. Philipsen, “Constraining the QCD phase diagram by tricritical lines at imaginary chemical potential,” *Phys. Rev. Lett.* **105** (2010) 152001, [arXiv:1004.3144 \[hep-lat\]](#).
 - [106] S. Muroya, A. Nakamura, C. Nonaka, and T. Takaishi, “Lattice QCD at finite density: An Introductory review,” *Prog. Theor. Phys.* **110** (2003) 615–668, [arXiv:hep-lat/0306031 \[hep-lat\]](#).
 - [107] **WHOT-QCD** Collaboration, S. Ejiri, K. Kanaya, and T. Umeda, “Ab initio study of QCD thermodynamics on the lattice at zero and finite densities,” *PTEP* **2012** (2012) 01A104, [arXiv:1205.5347 \[hep-lat\]](#).
 - [108] G. Aarts, F. Attanasio, B. Jäger, E. Seiler, D. Sexty, and I.-O. Stamatescu, “QCD at nonzero chemical potential: recent progress on the lattice,” in *Confinement XI St. Petersburg, Russia, September 8-12, 2014*. 2014. [arXiv:1412.0847 \[hep-lat\]](#).
 - [109] L. D. McLerran and B. Svetitsky, “Quark Liberation at High Temperature: A Monte Carlo Study of SU(2) Gauge Theory,” *Phys. Rev.* **D24** (1981) 450.
 - [110] **Wuppertal-Budapest** Collaboration, S. Borsanyi, Z. Fodor, C. Hoelbling, S. D. Katz, S. Krieg, C. Ratti, and K. K. Szabo, “Is there still any T_c mystery in lattice QCD? Results with physical masses in the continuum limit III,” *JHEP* **09** (2010) 073, [arXiv:1005.3508 \[hep-lat\]](#).
 - [111] P. Petreczky, “Lattice QCD at non-zero temperature,” *J. Phys.* **G39** (2012) 093002, [arXiv:1203.5320 \[hep-lat\]](#).
 - [112] M. Cheng *et al.*, “The Transition temperature in QCD,” *Phys. Rev.* **D74** (2006) 054507, [arXiv:hep-lat/0608013 \[hep-lat\]](#).

- [113] Y. Aoki, Z. Fodor, S. D. Katz, and K. K. Szabo, “The QCD transition temperature: Results with physical masses in the continuum limit,” *Phys. Lett.* **B643** (2006) 46–54, [arXiv:hep-lat/0609068 \[hep-lat\]](#).
- [114] Y. Aoki, S. Borsanyi, S. Durr, Z. Fodor, S. D. Katz, S. Krieg, and K. K. Szabo, “The QCD transition temperature: results with physical masses in the continuum limit II.,” *JHEP* **06** (2009) 088, [arXiv:0903.4155 \[hep-lat\]](#).
- [115] A. Bazavov *et al.*, “Equation of state and QCD transition at finite temperature,” *Phys. Rev.* **D80** (2009) 014504, [arXiv:0903.4379 \[hep-lat\]](#).
- [116] S. Borsanyi, G. Endrodi, Z. Fodor, A. Jakovac, S. D. Katz, S. Krieg, C. Ratti, and K. K. Szabo, “The QCD equation of state with dynamical quarks,” *JHEP* **11** (2010) 077, [arXiv:1007.2580 \[hep-lat\]](#).
- [117] A. Bazavov *et al.*, “The chiral and deconfinement aspects of the QCD transition,” *Phys. Rev.* **D85** (2012) 054503, [arXiv:1111.1710 \[hep-lat\]](#).
- [118] S. Durr *et al.*, “Ab-Initio Determination of Light Hadron Masses,” *Science* **322** (2008) 1224–1227, [arXiv:0906.3599 \[hep-lat\]](#).
- [119] G. Aarts, F. Attanasio, B. Jaeger, E. Seiler, D. Sexty, *et al.*, “Exploring the phase diagram of QCD with complex Langevin simulations,” *PoS LATTICE2014* (2014) 200, [arXiv:1411.2632 \[hep-lat\]](#).
- [120] G. Aarts, F. A. James, E. Seiler, and I.-O. Stamatescu, “Complex Langevin: Etiology and Diagnostics of its Main Problem,” *Eur. Phys. J.* **C71** (2011) 1756, [arXiv:1101.3270 \[hep-lat\]](#).
- [121] J. M. Pawłowski and C. Zielinski, “Thirring model at finite density in 0+1 dimensions with stochastic quantization: Crosscheck with an exact solution,” *Phys. Rev.* **D87** no. 9, (2013) 094503, [arXiv:1302.1622 \[hep-lat\]](#).
- [122] J. M. Pawłowski and C. Zielinski, “Thirring model at finite density in 2+1 dimensions with stochastic quantization,” *Phys. Rev.* **D87** no. 9, (2013) 094509, [arXiv:1302.2249 \[hep-lat\]](#).
- [123] J. Berges and I.-O. Stamatescu, “Simulating nonequilibrium quantum fields with stochastic quantization techniques,” *Phys. Rev. Lett.* **95** (2005) 202003, [arXiv:hep-lat/0508030 \[hep-lat\]](#).
- [124] J. Berges and D. Sexty, “Real-time gauge theory simulations from stochastic quantization with optimized updating,” *Nucl. Phys.* **B799** (2008) 306–329, [arXiv:0708.0779 \[hep-lat\]](#).
- [125] R. Anzaki, K. Fukushima, Y. Hidaka, and T. Oka, “Restricted phase-space approximation in real-time stochastic quantization,” *Annals Phys.* **353** (2015) 107–128, [arXiv:1405.3154 \[hep-ph\]](#).
- [126] M. Cristoforetti, F. Di Renzo, A. Mukherjee, and L. Scorzato, “Monte Carlo simulations on the Lefschetz thimble: Taming the sign problem,” *Phys. Rev.* **D88** no. 5, (2013) 051501, [arXiv:1303.7204 \[hep-lat\]](#).

-
- [127] H. Fujii, D. Honda, M. Kato, Y. Kikukawa, S. Komatsu, *et al.*, “Hybrid Monte Carlo on Lefschetz thimbles - A study of the residual sign problem,” *JHEP* **1310** (2013) 147, [arXiv:1309.4371 \[hep-lat\]](#).
- [128] M. Gell-Mann and M. Levy, “The axial vector current in beta decay,” *Nuovo Cim.* **16** (1960) 705.
- [129] Y. Nambu and G. Jona-Lasinio, “Dynamical Model of Elementary Particles Based on an Analogy with Superconductivity. I,” *Phys. Rev.* **122** (1961) 345–358.
- [130] Y. Nambu and G. Jona-Lasinio, “Dynamical Model of Elementary Particles Based on an Analogy with Superconductivity. II,” *Phys. Rev.* **124** (1961) 246–254.
- [131] S. P. Klevansky, “The Nambu-Jona-Lasinio model of quantum chromodynamics,” *Rev. Mod. Phys.* **64** (1992) 649–708.
- [132] S. Weinberg, “Phenomenological Lagrangians,” *Physica* **A96** (1979) 327.
- [133] J. Gasser and H. Leutwyler, “Chiral Perturbation Theory to One Loop,” *Annals Phys.* **158** (1984) 142.
- [134] J. Gasser and H. Leutwyler, “Chiral Perturbation Theory: Expansions in the Mass of the Strange Quark,” *Nucl. Phys.* **B250** (1985) 465.
- [135] M. L. Goldberger and S. B. Treiman, “Decay of the pi meson,” *Phys. Rev.* **110** (1958) 1178–1184.
- [136] Y. Nambu, “Axial vector current conservation in weak interactions,” *Phys. Rev. Lett.* **4** (1960) 380–382.
- [137] M. Gell-Mann, R. J. Oakes, and B. Renner, “Behavior of current divergences under $SU(3) \times SU(3)$,” *Phys. Rev.* **175** (1968) 2195–2199.
- [138] G. Ecker, “Chiral perturbation theory,” *Prog. Part. Nucl. Phys.* **35** (1995) 1–80, [arXiv:hep-ph/9501357 \[hep-ph\]](#).
- [139] S. Scherer, “Introduction to chiral perturbation theory,” *Adv. Nucl. Phys.* **27** (2003) 277, [arXiv:hep-ph/0210398 \[hep-ph\]](#).
- [140] S. R. Coleman, “The Quantum Sine-Gordon Equation as the Massive Thirring Model,” *Phys. Rev.* **D11** (1975) 2088.
- [141] S. Mandelstam, “Soliton Operators for the Quantized Sine-Gordon Equation,” *Phys. Rev.* **D11** (1975) 3026.
- [142] D. Ebert and M. K. Volkov, “Composite Meson Model with Vector Dominance Based on $U(2)$ Invariant Four Quark Interactions,” *Z. Phys.* **C16** (1983) 205.
- [143] M. K. Volkov, “Meson Lagrangians in a Superconductor Quark Model,” *Annals Phys.* **157** (1984) 282–303.
- [144] R. T. Cahill and C. D. Roberts, “Soliton Bag Models of Hadrons from QCD,” *Phys. Rev.* **D32** (1985) 2419.

- [145] C. D. Roberts and R. T. Cahill, “A Bosonization of QCD and Realizations of Chiral Symmetry,” *Austral. J. Phys.* **40** (1987) 499.
- [146] J. Praschifka, C. D. Roberts, and R. T. Cahill, “QCD Bosonization and the Meson Effective Action,” *Phys. Rev.* **D36** (1987) 209.
- [147] M. Wakamatsu and W. Weise, “The Nambu-Jona-Lasinio Model and Low-energy Effective Meson Lagrangians,” *Z. Phys.* **A331** (1988) 173–186.
- [148] F. J. Dyson, “The S matrix in quantum electrodynamics,” *Phys. Rev.* **75** (1949) 1736–1755.
- [149] J. S. Schwinger, “On the Green’s functions of quantized fields. 1.,” *Proc. Nat. Acad. Sci.* **37** (1951) 452–455.
- [150] C. Wetterich, “Exact evolution equation for the effective potential,” *Phys. Lett.* **B301** (1993) 90–94.
- [151] T. R. Morris, “The Exact renormalization group and approximate solutions,” *Int. J. Mod. Phys.* **A9** (1994) 2411–2450, [arXiv:hep-ph/9308265](#) [[hep-ph](#)].
- [152] S. Klimt, M. F. M. Lutz, and W. Weise, “Chiral phase transition in the SU(3) Nambu and Jona-Lasinio model,” *Phys. Lett.* **B249** (1990) 386–390.
- [153] U. Vogl and W. Weise, “The Nambu and Jona Lasinio model: Its implications for hadrons and nuclei,” *Prog. Part. Nucl. Phys.* **27** (1991) 195–272.
- [154] P. Zhuang, J. Hufner, and S. P. Klevansky, “Thermodynamics of a quark - meson plasma in the Nambu-Jona-Lasinio model,” *Nucl. Phys.* **A576** (1994) 525–552.
- [155] T. Hatsuda and T. Kunihiro, “QCD phenomenology based on a chiral effective Lagrangian,” *Phys. Rept.* **247** (1994) 221–367, [arXiv:hep-ph/9401310](#) [[hep-ph](#)].
- [156] O. Scavenius, A. Mocsy, I. N. Mishustin, and D. H. Rischke, “Chiral phase transition within effective models with constituent quarks,” *Phys. Rev.* **C64** (2001) 045202, [arXiv:nucl-th/0007030](#) [[nucl-th](#)].
- [157] K. Fukushima, “Chiral effective model with the Polyakov loop,” *Phys. Lett.* **B591** (2004) 277–284, [arXiv:hep-ph/0310121](#) [[hep-ph](#)].
- [158] C. Ratti, M. A. Thaler, and W. Weise, “Phases of QCD: Lattice thermodynamics and a field theoretical model,” *Phys. Rev.* **D73** (2006) 014019, [arXiv:hep-ph/0506234](#) [[hep-ph](#)].
- [159] S. Roessner, C. Ratti, and W. Weise, “Polyakov loop, diquarks and the two-flavour phase diagram,” *Phys. Rev.* **D75** (2007) 034007, [arXiv:hep-ph/0609281](#) [[hep-ph](#)].
- [160] K. Fukushima, “Phase diagrams in the three-flavor Nambu-Jona-Lasinio model with the Polyakov loop,” *Phys. Rev.* **D77** (2008) 114028, [arXiv:0803.3318](#) [[hep-ph](#)]. [Erratum: *Phys. Rev.* **D78**, 039902(2008)].
- [161] C. D. Roberts and A. G. Williams, “Dyson-Schwinger equations and their application to hadronic physics,” *Prog. Part. Nucl. Phys.* **33** (1994) 477–575, [arXiv:hep-ph/9403224](#) [[hep-ph](#)].

-
- [162] L. von Smekal, R. Alkofer, and A. Hauck, “The Infrared behavior of gluon and ghost propagators in Landau gauge QCD,” *Phys. Rev. Lett.* **79** (1997) 3591–3594, [arXiv:hep-ph/9705242](#) [[hep-ph](#)].
 - [163] L. von Smekal, A. Hauck, and R. Alkofer, “A Solution to Coupled Dyson–Schwinger Equations for Gluons and Ghosts in Landau Gauge,” *Annals Phys.* **267** (1998) 1–60, [arXiv:hep-ph/9707327](#) [[hep-ph](#)]. [Erratum: *Annals Phys.* 269,182(1998)].
 - [164] C. D. Roberts and S. M. Schmidt, “Dyson-Schwinger equations: Density, temperature and continuum strong QCD,” *Prog. Part. Nucl. Phys.* **45** (2000) S1–S103, [arXiv:nucl-th/0005064](#) [[nucl-th](#)].
 - [165] R. Alkofer and L. von Smekal, “The Infrared behavior of QCD Green’s functions: Confinement dynamical symmetry breaking, and hadrons as relativistic bound states,” *Phys. Rept.* **353** (2001) 281, [arXiv:hep-ph/0007355](#) [[hep-ph](#)].
 - [166] C. S. Fischer and R. Alkofer, “Nonperturbative propagators, running coupling and dynamical quark mass of Landau gauge QCD,” *Phys. Rev.* **D67** (2003) 094020, [arXiv:hep-ph/0301094](#) [[hep-ph](#)].
 - [167] C. S. Fischer, “Infrared properties of QCD from Dyson-Schwinger equations,” *J. Phys.* **G32** (2006) R253–R291, [arXiv:hep-ph/0605173](#) [[hep-ph](#)].
 - [168] C. S. Fischer, A. Maas, and J. M. Pawłowski, “On the infrared behavior of Landau gauge Yang-Mills theory,” *Annals Phys.* **324** (2009) 2408–2437, [arXiv:0810.1987](#) [[hep-ph](#)].
 - [169] R. Alkofer, C. S. Fischer, F. J. Llanes-Estrada, and K. Schwenzer, “The Quark-gluon vertex in Landau gauge QCD: Its role in dynamical chiral symmetry breaking and quark confinement,” *Annals Phys.* **324** (2009) 106–172, [arXiv:0804.3042](#) [[hep-ph](#)].
 - [170] U. Ellwanger and C. Wetterich, “Evolution equations for the quark - meson transition,” *Nucl. Phys.* **B423** (1994) 137–170, [arXiv:hep-ph/9402221](#) [[hep-ph](#)].
 - [171] D. U. Jungnickel and C. Wetterich, “Effective action for the chiral quark-meson model,” *Phys. Rev.* **D53** (1996) 5142–5175, [arXiv:hep-ph/9505267](#) [[hep-ph](#)].
 - [172] D. U. Jungnickel and C. Wetterich, “Nonperturbative flow equations, low-energy QCD and the chiral phase transition,” 1997. [arXiv:hep-ph/9710397](#) [[hep-ph](#)].
 - [173] J. Berges, D. U. Jungnickel, and C. Wetterich, “Two flavor chiral phase transition from nonperturbative flow equations,” *Phys. Rev.* **D59** (1999) 034010, [arXiv:hep-ph/9705474](#) [[hep-ph](#)].
 - [174] J. Berges, D.-U. Jungnickel, and C. Wetterich, “The Chiral phase transition at high baryon density from nonperturbative flow equations,” *Eur. Phys. J.* **C13** (2000) 323–329, [arXiv:hep-ph/9811347](#) [[hep-ph](#)].
 - [175] G. Papp, B. J. Schaefer, H. J. Pirner, and J. Wambach, “On the convergence of the expansion of renormalization group flow equation,” *Phys. Rev.* **D61** (2000) 096002, [arXiv:hep-ph/9909246](#) [[hep-ph](#)].
 - [176] B.-J. Schaefer and J. Wambach, “The Phase diagram of the quark meson model,” *Nucl. Phys.* **A757** (2005) 479–492, [arXiv:nucl-th/0403039](#) [[nucl-th](#)].

- [177] B.-J. Schaefer and J. Wambach, “Renormalization group approach towards the QCD phase diagram,” *Phys. Part. Nucl.* **39** (2008) 1025–1032, [arXiv:hep-ph/0611191 \[hep-ph\]](#).
- [178] J. Braun, “Thermodynamics of QCD low-energy models and the derivative expansion of the effective action,” *Phys. Rev.* **D81** (2010) 016008, [arXiv:0908.1543 \[hep-ph\]](#).
- [179] J. M. Pawłowski and F. Rennecke, “Higher order quark-mesonic scattering processes and the phase structure of QCD,” *Phys. Rev.* **D90** no. 7, (2014) 076002, [arXiv:1403.1179 \[hep-ph\]](#).
- [180] A. J. Helmboldt, J. M. Pawłowski, and N. Strodthoff, “Towards quantitative precision in the chiral crossover: masses and fluctuation scales,” *Phys. Rev.* **D91** no. 5, (2015) 054010, [arXiv:1409.8414 \[hep-ph\]](#).
- [181] H. Gies and C. Wetterich, “Renormalization flow of bound states,” *Phys. Rev.* **D65** (2002) 065001, [arXiv:hep-th/0107221 \[hep-th\]](#).
- [182] H. Gies and C. Wetterich, “Universality of spontaneous chiral symmetry breaking in gauge theories,” *Phys. Rev.* **D69** (2004) 025001, [arXiv:hep-th/0209183 \[hep-th\]](#).
- [183] J. M. Pawłowski, “Aspects of the functional renormalisation group,” *Annals Phys.* **322** (2007) 2831–2915, [arXiv:hep-th/0512261 \[hep-th\]](#).
- [184] S. Floerchinger and C. Wetterich, “Exact flow equation for composite operators,” *Phys. Lett.* **B680** (2009) 371–376, [arXiv:0905.0915 \[hep-th\]](#).
- [185] J. Braun, L. Fister, J. M. Pawłowski, and F. Rennecke, “From Quarks and Gluons to Hadrons: Chiral Symmetry Breaking in Dynamical QCD,” [arXiv:1412.1045 \[hep-ph\]](#).
- [186] M. Mitter, J. M. Pawłowski, and N. Strodthoff, “Chiral symmetry breaking in continuum QCD,” *Phys. Rev.* **D91** (2015) 054035, [arXiv:1411.7978 \[hep-ph\]](#).
- [187] B.-J. Schaefer, J. M. Pawłowski, and J. Wambach, “The Phase Structure of the Polyakov–Quark–Meson Model,” *Phys. Rev.* **D76** (2007) 074023, [arXiv:0704.3234 \[hep-ph\]](#).
- [188] B.-J. Schaefer, M. Wagner, and J. Wambach, “Thermodynamics of (2+1)-flavor QCD: Confronting Models with Lattice Studies,” *Phys. Rev.* **D81** (2010) 074013, [arXiv:0910.5628 \[hep-ph\]](#).
- [189] B.-J. Schaefer, M. Wagner, and J. Wambach, “QCD thermodynamics with effective models,” *PoS CPOD2009* (2009) 017, [arXiv:0909.0289 \[hep-ph\]](#).
- [190] J. Braun, L. M. Haas, F. Marhauser, and J. M. Pawłowski, “Phase Structure of Two-Flavor QCD at Finite Chemical Potential,” *Phys. Rev. Lett.* **106** (2011) 022002, [arXiv:0908.0008 \[hep-ph\]](#).
- [191] T. K. Herbst, J. M. Pawłowski, and B.-J. Schaefer, “The phase structure of the Polyakov–quark–meson model beyond mean field,” *Phys. Lett.* **B696** (2011) 58–67, [arXiv:1008.0081 \[hep-ph\]](#).
- [192] F. Karsch, B.-J. Schaefer, M. Wagner, and J. Wambach, “Towards finite density QCD with Taylor expansions,” *PoS LATTICE2011* (2011) 219, [arXiv:1110.6038 \[hep-lat\]](#).

-
- [193] L. M. Haas, R. Stiele, J. Braun, J. M. Pawłowski, and J. Schaffner-Bielich, “Improved Polyakov-loop potential for effective models from functional calculations,” *Phys. Rev. D* **87** no. 7, (2013) 076004, [arXiv:1302.1993 \[hep-ph\]](#).
 - [194] T. K. Herbst, J. M. Pawłowski, and B.-J. Schaefer, “Phase structure and thermodynamics of QCD,” *Phys. Rev. D* **88** no. 1, (2013) 014007, [arXiv:1302.1426 \[hep-ph\]](#).
 - [195] T. K. Herbst, M. Mitter, J. M. Pawłowski, B.-J. Schaefer, and R. Stiele, “Thermodynamics of QCD at vanishing density,” *Phys. Lett. B* **731** (2014) 248–256, [arXiv:1308.3621 \[hep-ph\]](#).
 - [196] L. Fister and J. M. Pawłowski, “Yang-Mills correlation functions at finite temperature,” [arXiv:1112.5440 \[hep-ph\]](#).
 - [197] L. Fister and J. M. Pawłowski, “Confinement from Correlation Functions,” *Phys. Rev. D* **88** (2013) 045010, [arXiv:1301.4163 \[hep-ph\]](#).
 - [198] L. von Smekal, “Universal Aspects of QCD-like Theories,” *Nucl.Phys.Proc.Suppl.* **228** (2012) 179–220, [arXiv:1205.4205 \[hep-ph\]](#).
 - [199] J. Kogut, M. A. Stephanov, and D. Toublan, “On two color QCD with baryon chemical potential,” *Phys.Lett. B* **464** (1999) 183–191, [arXiv:hep-ph/9906346 \[hep-ph\]](#).
 - [200] J. Kogut, M. A. Stephanov, D. Toublan, J. Verbaarschot, and A. Zhitnitsky, “QCD - like theories at finite baryon density,” *Nucl.Phys. B* **582** (2000) 477–513, [arXiv:hep-ph/0001171 \[hep-ph\]](#).
 - [201] K. Splittorff, D. Son, and M. A. Stephanov, “QCD - like theories at finite baryon and isospin density,” *Phys.Rev. D* **64** (2001) 016003, [arXiv:hep-ph/0012274 \[hep-ph\]](#).
 - [202] K. Splittorff, D. Toublan, and J. Verbaarschot, “Diquark condensate in QCD with two colors at next-to-leading order,” *Nucl.Phys. B* **620** (2002) 290–314, [arXiv:hep-ph/0108040 \[hep-ph\]](#).
 - [203] K. Splittorff, D. Toublan, and J. Verbaarschot, “Thermodynamics of chiral symmetry at low densities,” *Nucl.Phys. B* **639** (2002) 524–548, [arXiv:hep-ph/0204076 \[hep-ph\]](#).
 - [204] G. V. Dunne and S. M. Nishigaki, “Two color QCD in 3-D at finite baryon density,” *Nucl.Phys. B* **654** (2003) 445–465, [arXiv:hep-ph/0210219 \[hep-ph\]](#).
 - [205] G. V. Dunne and S. M. Nishigaki, “3-D two color QCD at finite temperature and baryon density,” *Nucl.Phys. B* **670** (2003) 307–328, [arXiv:hep-ph/0306220 \[hep-ph\]](#).
 - [206] T. Brauner, “On the chiral perturbation theory for two-flavor two-color QCD at finite chemical potential,” *Mod.Phys.Lett. A* **21** (2006) 559–570, [arXiv:hep-ph/0601010 \[hep-ph\]](#).
 - [207] T. Kanazawa, T. Wettig, and N. Yamamoto, “Chiral Lagrangian and spectral sum rules for dense two-color QCD,” *JHEP* **0908** (2009) 003, [arXiv:0906.3579 \[hep-ph\]](#).
 - [208] T. Kanazawa, T. Wettig, and N. Yamamoto, “Chiral random matrix theory for two-color QCD at high density,” *Phys.Rev. D* **81** (2010) 081701, [arXiv:0912.4999 \[hep-ph\]](#).
 - [209] T. Kanazawa, T. Wettig, and N. Yamamoto, “Singular values of the Dirac operator in dense QCD-like theories,” *JHEP* **1112** (2011) 007, [arXiv:1110.5858 \[hep-ph\]](#).

- [210] L. Kondratyuk, M. Giannini, and M. Krivoruchenko, “The SU(2) color superconductivity,” *Phys.Lett.* **B269** (1991) 139–143.
- [211] L. Kondratyuk and M. Krivoruchenko, “Superconducting quark matter in SU(2) color group,” *Z.Phys.* **A344** (1992) 99–115.
- [212] C. Ratti and W. Weise, “Thermodynamics of two-colour QCD and the Nambu Jona-Lasinio model,” *Phys.Rev.* **D70** (2004) 054013, [arXiv:hep-ph/0406159](#) [[hep-ph](#)].
- [213] G.-f. Sun, L. He, and P. Zhuang, “BEC-BCS crossover in the Nambu-Jona-Lasinio model of QCD,” *Phys.Rev.* **D75** (2007) 096004, [arXiv:hep-ph/0703159](#) [[hep-ph](#)].
- [214] T. Brauner, K. Fukushima, and Y. Hidaka, “Two-color quark matter: U(1)(A) restoration, superfluidity, and quarkyonic phase,” *Phys.Rev.* **D80** (2009) 074035, [arXiv:0907.4905](#) [[hep-ph](#)].
- [215] J. O. Andersen and T. Brauner, “Phase diagram of two-color quark matter at nonzero baryon and isospin density,” *Phys.Rev.* **D81** (2010) 096004, [arXiv:1001.5168](#) [[hep-ph](#)].
- [216] M. Harada, C. Nonaka, and T. Yamaoka, “Masses of vector bosons in two-color dense QCD based on the hidden local symmetry,” *Phys.Rev.* **D81** (2010) 096003, [arXiv:1002.4705](#) [[hep-ph](#)].
- [217] T. Zhang, T. Brauner, and D. H. Rischke, “QCD-like theories at nonzero temperature and density,” *JHEP* **1006** (2010) 064, [arXiv:1005.2928](#) [[hep-ph](#)].
- [218] S. Imai, H. Toki, and W. Weise, “Quark-Hadron Matter at Finite Temperature and Density in a Two-Color PNJL model,” [arXiv:1210.1307](#) [[nucl-th](#)].
- [219] L. He, “Nambu-Jona-Lasinio model description of weakly interacting Bose condensate and BEC-BCS crossover in dense QCD-like theories,” *Phys.Rev.* **D82** (2010) 096003, [arXiv:1007.1920](#) [[hep-ph](#)].
- [220] A. Nakamura, “Quarks and gluons at finite temperature and density,” *Phys.Lett.* **B149** (1984) 391.
- [221] S. Hands, J. B. Kogut, M.-P. Lombardo, and S. E. Morrison, “Symmetries and spectrum of SU(2) lattice gauge theory at finite chemical potential,” *Nucl.Phys.* **B558** (1999) 327–346, [arXiv:hep-lat/9902034](#) [[hep-lat](#)].
- [222] S. Hands, I. Montvay, S. Morrison, M. Oevers, L. Scorzato, *et al.*, “Numerical study of dense adjoint matter in two color QCD,” *Eur.Phys.J.* **C17** (2000) 285–302, [arXiv:hep-lat/0006018](#) [[hep-lat](#)].
- [223] S. Hands, I. Montvay, L. Scorzato, and J. Skullerud, “Diquark condensation in dense adjoint matter,” *Eur.Phys.J.* **C22** (2001) 451–461, [arXiv:hep-lat/0109029](#) [[hep-lat](#)].
- [224] S. Muroya, A. Nakamura, and C. Nonaka, “Study of the finite density state based on SU(2) lattice QCD,” *Nucl.Phys.Proc.Suppl.* **119** (2003) 544–546, [arXiv:hep-lat/0208006](#) [[hep-lat](#)].
- [225] S. Chandrasekharan and F.-J. Jiang, “Phase-diagram of two-color lattice QCD in the chiral limit,” *Phys.Rev.* **D74** (2006) 014506, [arXiv:hep-lat/0602031](#) [[hep-lat](#)].

-
- [226] S. Hands, S. Kim, and J.-I. Skullerud, “Deconfinement in dense 2-color QCD,” *Eur. Phys. J.* **C48** (2006) 193, [arXiv:hep-lat/0604004](#).
 - [227] S. Hands, S. Kim, and J.-I. Skullerud, “A Quarkyonic Phase in Dense Two Color Matter?,” *Phys.Rev.* **D81** (2010) 091502, [arXiv:1001.1682 \[hep-lat\]](#).
 - [228] S. Hands, P. Kenny, S. Kim, and J.-I. Skullerud, “Lattice Study of Dense Matter with Two Colors and Four Flavors,” *Eur. Phys. J.* **A47** (2011) 60, [arXiv:1101.4961 \[hep-lat\]](#).
 - [229] S. Cotter, P. Giudice, S. Hands, and J.-I. Skullerud, “Towards the phase diagram of dense two-color matter,” *Phys.Rev.* **D87** (2013) 034507, [arXiv:1210.4496 \[hep-lat\]](#).
 - [230] S. Hands, S. Kim, and J.-I. Skullerud, “Non-relativistic spectrum of two-color QCD at non-zero baryon density,” *Phys.Lett.* **B711** (2012) 199–204, [arXiv:1202.4353 \[hep-lat\]](#).
 - [231] T. Boz, S. Cotter, L. Fister, D. Mehta, and J.-I. Skullerud, “Phase transitions and gluodynamics in 2-colour matter at high density,” [arXiv:1303.3223 \[hep-lat\]](#).
 - [232] P. Scior and L. von Smekal, “Baryonic Matter Onset in Two-Color QCD with Heavy Quarks,” [arXiv:1508.00431 \[hep-lat\]](#).
 - [233] N. Strodthoff, B.-J. Schaefer, and L. von Smekal, “Quark-meson-diquark model for two-color QCD,” *Phys.Rev.* **D85** (2012) 074007, [arXiv:1112.5401 \[hep-ph\]](#).
 - [234] N. Strodthoff and L. von Smekal, “Polyakov-Quark-Meson-Diquark Model for two-color QCD,” *Phys. Lett.* **B731** (2014) 350–357, [arXiv:1306.2897 \[hep-ph\]](#).
 - [235] S. Diehl, S. Floerchinger, H. Gies, J. Pawłowski, and C. Wetterich, “Functional renormalization group approach to the BCS-BEC crossover,” *Annalen Phys.* **522** (2010) 615–656, [arXiv:0907.2193 \[cond-mat.quant-gas\]](#).
 - [236] S. Floerchinger, M. Scherer, S. Diehl, and C. Wetterich, “Particle-hole fluctuations in the BCS-BEC Crossover,” *Phys.Rev.* **B78** (2008) 174528, [arXiv:0808.0150 \[cond-mat.supr-con\]](#).
 - [237] S. Floerchinger, M. Scherer, and C. Wetterich, “Modified Fermi-sphere, pairing gap and critical temperature for the BCS-BEC crossover,” *Phys.Rev.* **A81** (2010) 063619, [arXiv:0912.4050 \[cond-mat.quant-gas\]](#).
 - [238] M. M. Scherer, S. Floerchinger, and H. Gies, “Functional renormalization for the BCS-BEC crossover,” [arXiv:1010.2890 \[cond-mat.quant-gas\]](#).
 - [239] I. Boettcher, J. M. Pawłowski, and S. Diehl, “Ultracold atoms and the Functional Renormalization Group,” *Nucl.Phys.Proc.Suppl.* **228** (2012) 63–135, [arXiv:1204.4394 \[cond-mat.quant-gas\]](#).
 - [240] F. E. Serr and J. D. Walecka, “A Relativistic Quantum Field Theory of Finite Nuclei,” *Phys. Lett.* **B79** (1978) 10. [Erratum: *Phys. Lett.* 84B,529(1979)].
 - [241] B. D. Serot and J. D. Walecka, “The Relativistic Nuclear Many Body Problem,” *Adv. Nucl. Phys.* **16** (1986) 1–327.

- [242] B. D. Serot and J. D. Walecka, “Recent progress in quantum hadrodynamics,” *Int. J. Mod. Phys. E* **6** (1997) 515–631, [arXiv:nuc1-th/9701058 \[nuc1-th\]](#).
- [243] J. Berges, D. U. Jungnickel, and C. Wetterich, “Quark and nuclear matter in the linear chiral meson model,” *Int. J. Mod. Phys. A* **18** (2003) 3189–3220, [arXiv:hep-ph/9811387 \[hep-ph\]](#).
- [244] S. Pepin, M. C. Birse, J. A. McGovern, and N. R. Walet, “Nucleons or diquarks? Competition between clustering and color superconductivity in quark matter,” *Phys. Rev. C* **61** (2000) 055209, [arXiv:hep-ph/9912475 \[hep-ph\]](#).
- [245] W. Bentz and A. W. Thomas, “The Stability of nuclear matter in the Nambu-Jona-Lasinio model,” *Nucl. Phys. A* **696** (2001) 138–172, [arXiv:nuc1-th/0105022 \[nuc1-th\]](#).
- [246] L. J. Abu-Raddad, A. Hosaka, D. Ebert, and H. Toki, “Path integral hadronization for the nucleon and its interactions,” *Phys. Rev. C* **66** (2002) 025206, [arXiv:nuc1-th/0206002 \[nuc1-th\]](#).
- [247] A. H. Rezaeian, N. R. Walet, and M. C. Birse, “Baryon structure in a quark-confining non-local NJL model,” *Phys. Rev. C* **70** (2004) 065203, [arXiv:hep-ph/0408233 \[hep-ph\]](#).
- [248] J.-c. Wang, Q. Wang, and D. H. Rischke, “Baryon formation and dissociation in dense hadronic and quark matter,” *Phys. Lett. B* **704** (2011) 347–353, [arXiv:1008.4029 \[nuc1-th\]](#).
- [249] M. Drews, T. Hell, B. Klein, and W. Weise, “Thermodynamic phases and mesonic fluctuations in a chiral nucleon-meson model,” *Phys. Rev. D* **88** no. 9, (2013) 096011, [arXiv:1308.5596 \[hep-ph\]](#).
- [250] K. Hebeler, J. Lattimer, C. Pethick, and A. Schwenk, “Equation of state and neutron star properties constrained by nuclear physics and observation,” *Astrophys. J.* **773** (2013) 11, [arXiv:1303.4662 \[astro-ph.SR\]](#).
- [251] S. Floerchinger and C. Wetterich, “Chemical freeze-out in heavy ion collisions at large baryon densities,” *Nucl. Phys. A* **890-891** (2012) 11–24, [arXiv:1202.1671 \[nuc1-th\]](#).
- [252] K. Fukushima, “Hadron resonance gas and mean-field nuclear matter for baryon number fluctuations,” [arXiv:1409.0698 \[hep-ph\]](#).
- [253] A. Kurkela, P. Romatschke, and A. Vuorinen, “Cold Quark Matter,” *Phys. Rev. D* **81** (2010) 105021, [arXiv:0912.1856 \[hep-ph\]](#).
- [254] T. Kojo, P. D. Powell, Y. Song, and G. Baym, “Phenomenological QCD equation of state for massive neutron stars,” *Phys. Rev. D* **91** no. 4, (2015) 045003, [arXiv:1412.1108 \[hep-ph\]](#).
- [255] M. Anselmino, E. Predazzi, S. Ekelin, S. Fredriksson, and D. Lichtenberg, “Diquarks,” *Rev. Mod. Phys.* **65** (1993) 1199–1234.
- [256] N. Ishii, W. Bentz, and K. Yazaki, “Faddeev approach to the nucleon in the Nambu-Jona-Lasinio (NJL) model,” *Phys. Lett. B* **301** (1993) 165–169.

-
- [257] N. Ishii, W. Bentz, and K. Yazaki, “Solution of the relativistic three quark Faddeev equation in the Nambu-Jona-Lasinio (NJL) model,” *Phys. Lett.* **B318** (1993) 26–31.
 - [258] N. Ishii, W. Bentz, and K. Yazaki, “Baryons in the NJL model as solutions of the relativistic Faddeev equation,” *Nucl. Phys.* **A587** (1995) 617–656.
 - [259] R. L. Jaffe, “Multi-Quark Hadrons. 1. The Phenomenology of (2 Quark 2 anti-Quark) Mesons,” *Phys. Rev.* **D15** (1977) 267.
 - [260] R. L. Jaffe, “Multi-Quark Hadrons. 2. Methods,” *Phys. Rev.* **D15** (1977) 281.
 - [261] G. ’t Hooft, G. Isidori, L. Maiani, A. D. Polosa, and V. Riquer, “A Theory of Scalar Mesons,” *Phys. Lett.* **B662** (2008) 424–430, [arXiv:0801.2288 \[hep-ph\]](#).
 - [262] M. Wakayama, T. Kunihiro, S. Muroya, A. Nakamura, C. Nonaka, M. Sekiguchi, and H. Wada, “Lattice QCD study of four-quark components of the isosinglet scalar mesons: Significance of disconnected diagrams,” *Phys. Rev.* **D91** no. 9, (2015) 094508, [arXiv:1412.3909 \[hep-lat\]](#).
 - [263] W. Chen, W.-Z. Deng, J. He, N. Li, X. Liu, Z.-G. Luo, Z.-F. Sun, and S.-L. Zhu, “XYZ States,” *PoS Hadron2013* (2013) 005, [arXiv:1311.3763 \[hep-ph\]](#).
 - [264] C. Alexandrou, P. de Forcrand, and B. Lucini, “Evidence for diquarks in lattice QCD,” *Phys. Rev. Lett.* **97** (2006) 222002, [arXiv:hep-lat/0609004 \[hep-lat\]](#).
 - [265] W. Bentz, H. Mineo, A. W. Thomas, and K. Yazaki, “Properties of nucleons and nuclear matter in the quark diquark model and extension to finite density,” *Int. J. Mod. Phys.* **A18** (2003) 1409–1412.
 - [266] D. Blaschke, A. Dubinin, and M. Buballa, “Polyakov-loop suppression of colored states in a quark-meson-diquark plasma,” [arXiv:1412.1040 \[hep-ph\]](#).
 - [267] M. Kitazawa, D. H. Rischke, and I. A. Shovkovy, “Bound diquarks and their Bose-Einstein condensation in strongly coupled quark matter,” *Phys. Lett.* **B663** (2008) 228–233, [arXiv:0709.2235 \[hep-ph\]](#).
 - [268] N. Khan, J. M. Pawłowski, F. Rennecke, and M. Scherer *In preparation*.
 - [269] K. Fukushima, N. Khan, J. M. Pawłowski, and N. Strodthoff *In preparation*.
 - [270] M. E. Peskin and D. V. Schroeder, *An Introduction to quantum field theory*. 1995.
 - [271] L. D. Faddeev and V. N. Popov, “Feynman Diagrams for the Yang-Mills Field,” *Phys. Lett.* **B25** (1967) 29–30.
 - [272] C. Becchi, A. Rouet, and R. Stora, “Renormalization of Gauge Theories,” *Annals Phys.* **98** (1976) 287–321.
 - [273] I. V. Tyutin, “Gauge Invariance in Field Theory and Statistical Physics in Operator Formalism,” [arXiv:0812.0580 \[hep-th\]](#).
 - [274] T. Kugo and I. Ojima, “Local Covariant Operator Formalism of Nonabelian Gauge Theories and Quark Confinement Problem,” *Prog. Theor. Phys. Suppl.* **66** (1979) 1–130.
 - [275] V. N. Gribov, “Quantization of Nonabelian Gauge Theories,” *Nucl. Phys.* **B139** (1978) 1.

- [276] S. Necco and R. Sommer, “The $N(f) = 0$ heavy quark potential from short to intermediate distances,” *Nucl. Phys.* **B622** (2002) 328–346, [arXiv:hep-lat/0108008 \[hep-lat\]](#).
- [277] P. Tanedo. <http://www.quantumdiaries.org/2010/10/22/qcd-and-confinement/>.
- [278] J. Greensite, “The Confinement problem in lattice gauge theory,” *Prog. Part. Nucl. Phys.* **51** (2003) 1, [arXiv:hep-lat/0301023 \[hep-lat\]](#).
- [279] A. M. Polyakov, “Thermal Properties of Gauge Fields and Quark Liberation,” *Phys. Lett.* **B72** (1978) 477–480.
- [280] L. Susskind, “Lattice Models of Quark Confinement at High Temperature,” *Phys. Rev.* **D20** (1979) 2610–2618.
- [281] R. D. Pisarski, “Quark gluon plasma as a condensate of $SU(3)$ Wilson lines,” *Phys. Rev.* **D62** (2000) 111501, [arXiv:hep-ph/0006205 \[hep-ph\]](#).
- [282] S. Nadkarni, “Nonabelian Debye Screening. 1. The Color Averaged Potential,” *Phys. Rev.* **D33** (1986) 3738.
- [283] S. Nadkarni, “Nonabelian Debye Screening. 2. The Singlet Potential,” *Phys. Rev.* **D34** (1986) 3904.
- [284] J. I. Kapusta and C. Gale, *Finite-temperature field theory: Principles and applications*. Cambridge University Press, 2011.
- [285] M. L. Bellac, *Thermal Field Theory*. Cambridge University Press, 2011.
- [286] K. Holland and U.-J. Wiese, “The Center symmetry and its spontaneous breakdown at high temperatures,” [arXiv:hep-ph/0011193 \[hep-ph\]](#).
- [287] B. Svetitsky and L. G. Yaffe, “Critical Behavior at Finite Temperature Confinement Transitions,” *Nucl. Phys.* **B210** (1982) 423.
- [288] B. Svetitsky, “Symmetry Aspects of Finite Temperature Confinement Transitions,” *Phys. Rept.* **132** (1986) 1–53.
- [289] M. Mitter and B.-J. Schaefer, “Fluctuations and the axial anomaly with three quark flavors,” *Phys. Rev.* **D89** no. 5, (2014) 054027, [arXiv:1308.3176 \[hep-ph\]](#).
- [290] D. Griffiths, *Introduction to elementary particles*. 2008.
- [291] F. Karsch, “Deconfinement and chiral symmetry restoration,” in *Strong and electroweak matter ’98. Proceedings, Conference, SEWM’98, Copenhagen, Denmark, December 2-5, 1998*. 1998. [arXiv:hep-lat/9903031 \[hep-lat\]](#).
- [292] H. Leutwyler, “On the foundations of chiral perturbation theory,” *Annals Phys.* **235** (1994) 165–203, [arXiv:hep-ph/9311274 \[hep-ph\]](#).
- [293] A. V. Manohar, “Effective field theories,” *Lect. Notes Phys.* **479** (1997) 311–362, [arXiv:hep-ph/9606222 \[hep-ph\]](#).
- [294] H. Leutwyler, “Principles of Chiral Perturbation Theory,” *Proc. Int. Sch. Phys. Fermi* **130** (1996) 1–50.

-
- [295] L. N. Cooper, “Bound electron pairs in a degenerate Fermi gas,” *Phys. Rev.* **104** (1956) 1189–1190.
 - [296] J. Bardeen, L. N. Cooper, and J. R. Schrieffer, “Microscopic theory of superconductivity,” *Phys. Rev.* **106** (1957) 162.
 - [297] J. Bardeen, L. N. Cooper, and J. R. Schrieffer, “Theory of superconductivity,” *Phys. Rev.* **108** (1957) 1175–1204.
 - [298] M. Ida and R. Kobayashi, “Baryon resonances in a quark model,” *Prog. Theor. Phys.* **36** (1966) 846.
 - [299] A. Selem and F. Wilczek, “Hadron systematics and emergent diquarks,” in *New trends in HERA physics. Proceedings, Ringberg Workshop, Tegernsee, Germany, October 2-7, 2005*, pp. 337–356. 2006. [arXiv:hep-ph/0602128](#) [[hep-ph](#)].
 - [300] K. Iida, T. Matsuura, M. Tachibana, and T. Hatsuda, “Melting pattern of diquark condensates in quark matter,” *Phys. Rev. Lett.* **93** (2004) 132001, [arXiv:hep-ph/0312363](#) [[hep-ph](#)].
 - [301] K. Fukushima, C. Kouvaris, and K. Rajagopal, “Heating (gapless) color-flavor locked quark matter,” *Phys. Rev.* **D71** (2005) 034002, [arXiv:hep-ph/0408322](#) [[hep-ph](#)].
 - [302] A. Schmitt, Q. Wang, and D. H. Rischke, “Electromagnetic Meissner effect in spin one color superconductors,” *Phys. Rev. Lett.* **91** (2003) 242301, [arXiv:nucl-th/0301090](#) [[nucl-th](#)].
 - [303] D. H. Rischke, “Debye screening and Meissner effect in a two flavor color superconductor,” *Phys. Rev.* **D62** (2000) 034007, [arXiv:nucl-th/0001040](#) [[nucl-th](#)].
 - [304] G. W. Carter and D. Diakonov, “The Nonperturbative color Meissner effect in a two flavor color superconductor,” *Nucl. Phys.* **B582** (2000) 571–590, [arXiv:hep-ph/0001318](#) [[hep-ph](#)].
 - [305] H. B. Nielsen and S. Chadha, “On How to Count Goldstone Bosons,” *Nucl. Phys.* **B105** (1976) 445.
 - [306] V. A. Miransky and I. A. Shovkovy, “Spontaneous symmetry breaking with abnormal number of Nambu-Goldstone bosons and kaon condensate,” *Phys. Rev. Lett.* **88** (2002) 111601, [arXiv:hep-ph/0108178](#) [[hep-ph](#)].
 - [307] D. Blaschke, D. Ebert, K. G. Klimenko, M. K. Volkov, and V. L. Yudichev, “Abnormal number of Nambu-Goldstone bosons in the color asymmetric 2SC phase of an NJL type model,” *Phys. Rev.* **D70** (2004) 014006, [arXiv:hep-ph/0403151](#) [[hep-ph](#)].
 - [308] T. Brauner, “Goldstone boson counting in linear sigma models with chemical potential,” *Phys. Rev.* **D72** (2005) 076002, [arXiv:hep-ph/0508011](#) [[hep-ph](#)].
 - [309] L. He, M. Jin, and P. Zhuang, “Superfluidity in a three-flavor Fermi gas with SU(3) symmetry,” *Phys. Rev.* **A74** (2006) 033604, [arXiv:cond-mat/0604580](#) [[cond-mat](#)].
 - [310] H. Watanabe and T. Brauner, “On the number of Nambu-Goldstone bosons and its relation to charge densities,” *Phys. Rev.* **D84** (2011) 125013, [arXiv:1109.6327](#) [[hep-ph](#)].

- [311] H. Watanabe and H. Murayama, “Unified Description of Nambu-Goldstone Bosons without Lorentz Invariance,” *Phys. Rev. Lett.* **108** (2012) 251602, [arXiv:1203.0609 \[hep-th\]](#).
- [312] H. Watanabe, T. Brauner, and H. Murayama, “Massive Nambu-Goldstone Bosons,” *Phys. Rev. Lett.* **111** no. 2, (2013) 021601, [arXiv:1303.1527 \[hep-th\]](#).
- [313] R. D. Pisarski and D. H. Rischke, “A First order transition to, and then parity violation in, a color superconductor,” *Phys. Rev. Lett.* **83** (1999) 37–40, [arXiv:nucl-th/9811104 \[nucl-th\]](#).
- [314] T. Schäfer, “Patterns of symmetry breaking in QCD at high baryon density,” *Nucl. Phys.* **B575** (2000) 269–284, [arXiv:hep-ph/9909574 \[hep-ph\]](#).
- [315] M. G. Alford, K. Rajagopal, and F. Wilczek, “Color flavor locking and chiral symmetry breaking in high density QCD,” *Nucl. Phys.* **B537** (1999) 443–458, [arXiv:hep-ph/9804403 \[hep-ph\]](#).
- [316] R. L. Jaffe, “Perhaps a Stable Dihyperon,” *Phys. Rev. Lett.* **38** (1977) 195–198. [Erratum: *Phys. Rev. Lett.* 38,617(1977)].
- [317] W. Pauli, “On the conservation of the lepton charge,” *Il Nuovo Cimento (1955-1965)* **6** no. 1, (1957) 204–215.
- [318] F. Gürsey, “Relation of charge independence and baryon conservation to pauli’s transformation,” *Il Nuovo Cimento (1955-1965)* **7** no. 3, (1958) 411–415.
- [319] J. Braun, “Fermion Interactions and Universal Behavior in Strongly Interacting Theories,” *J. Phys.* **G39** (2012) 033001, [arXiv:1108.4449 \[hep-ph\]](#).
- [320] J. Braun and H. Gies, “Running coupling at finite temperature and chiral symmetry restoration in QCD,” *Phys. Lett.* **B645** (2007) 53–58, [arXiv:hep-ph/0512085 \[hep-ph\]](#).
- [321] J. Hubbard, “Calculation of partition functions,” *Phys. Rev. Lett.* **3** (1959) 77–80.
- [322] R. Stratonovich, “On a method of calculating quantum distribution functions,” in *Soviet Physics Doklady*, vol. 2, p. 416. 1957.
- [323] F. Rennecke, “The Vacuum Structure of Vector Mesons in QCD,” [arXiv:1504.03585 \[hep-ph\]](#).
- [324] C. Vafa and E. Witten, “Parity Conservation in QCD,” *Phys. Rev. Lett.* **53** (1984) 535.
- [325] R. Brockmann and R. Machleidt, “Relativistic nuclear structure. 1: Nuclear matter,” *Phys. Rev.* **C42** (1990) 1965–1980.
- [326] Y. Ohashi and A. Griffin, “BCS-BEC crossover in a gas of Fermi atoms with a Feshbach resonance,” *Phys. Rev. Lett.* **89** (2002) 130402.
- [327] A. J. Leggett, “A theoretical description of the new phases of liquid He-3,” *Rev.Mod.Phys.* **47** (1975) 331–414.
- [328] Y. Nishida and H. Abuki, “BCS-BEC crossover in a relativistic superfluid and its significance to quark matter,” *Phys. Rev.* **D72** (2005) 096004, [arXiv:hep-ph/0504083 \[hep-ph\]](#).

-
- [329] K. G. Wilson and M. E. Fisher, “Critical exponents in 3.99 dimensions,” *Phys. Rev. Lett.* **28** (1972) 240–243.
 - [330] J. Zinn-Justin, “Quantum field theory and critical phenomena,” *Int. Ser. Monogr. Phys.* **113** (2002) 1–1054.
 - [331] K.-I. Aoki, K. Morikawa, W. Souma, J.-I. Sumi, and H. Terao, “Rapidly converging truncation scheme of the exact renormalization group,” *Prog. Theor. Phys.* **99** (1998) 451–466, [arXiv:hep-th/9803056 \[hep-th\]](#).
 - [332] N. Tetradis and C. Wetterich, “Critical exponents from effective average action,” *Nucl. Phys. B* **422** (1994) 541–592, [arXiv:hep-ph/9308214 \[hep-ph\]](#).
 - [333] A. Eichhorn, D. Mesterházy, and M. M. Scherer, “Stability of fixed points and generalized critical behavior in multifield models,” *Phys. Rev.* **E90** no. 5, (2014) 052129, [arXiv:1407.7442 \[cond-mat.stat-mech\]](#).
 - [334] J. Berges, N. Tetradis, and C. Wetterich, “Nonperturbative renormalization flow in quantum field theory and statistical physics,” *Phys. Rept.* **363** (2002) 223–386, [arXiv:hep-ph/0005122 \[hep-ph\]](#).
 - [335] M. Reuter, “Effective average actions and nonperturbative evolution equations,” in *5th Hellenic School and Workshops on Elementary Particle Physics (CORFU 1995) Corfu, Greece, September 3-24, 1995*. 1996. [arXiv:hep-th/9602012 \[hep-th\]](#).
 - [336] M. E. Fisher, “Renormalization group theory: Its basis and formulation in statistical physics,” *Rev. Mod. Phys.* **70** (1998) 653–681.
 - [337] D. F. Litim and J. M. Pawłowski, “On gauge invariant Wilsonian flows,” in *The exact renormalization group. Proceedings, Workshop, Faro, Portugal, September 10-12, 1998*, pp. 168–185. 1998. [arXiv:hep-th/9901063 \[hep-th\]](#).
<http://alice.cern.ch/format/showfull?sysnb=0302190>.
 - [338] K. Aoki, “Introduction to the nonperturbative renormalization group and its recent applications,” *Int.J.Mod.Phys.* **B14** (2000) 1249–1326.
 - [339] C. Bagnuls and C. Bervillier, “Exact renormalization group equations. An Introductory review,” *Phys.Rept.* **348** (2001) 91, [arXiv:hep-th/0002034 \[hep-th\]](#).
 - [340] J. Polonyi, “Lectures on the functional renormalization group method,” *Central Eur.J.Phys.* **1** (2003) 1–71, [arXiv:hep-th/0110026 \[hep-th\]](#).
 - [341] M. Salmhofer and C. Honerkamp, “Fermionic renormalization group flows: Technique and theory,” *Prog.Theor.Phys.* **105** (2001) 1–35.
 - [342] H. Gies, “Introduction to the functional RG and applications to gauge theories,” *Lect. Notes Phys.* **852** (2012) 287–348, [arXiv:hep-ph/0611146 \[hep-ph\]](#).
 - [343] B. Delamotte, “An Introduction to the nonperturbative renormalization group,” *Lect. Notes Phys.* **852** (2012) 49–132, [arXiv:cond-mat/0702365 \[cond-mat.stat-mech\]](#).
 - [344] L. P. Kadanoff, “Scaling laws for Ising models near $T(c)$,” *Physics* **2** (1966) 263–272.
 - [345] K. G. Wilson, “Renormalization group and critical phenomena. 1. Renormalization group and the Kadanoff scaling picture,” *Phys. Rev.* **B4** (1971) 3174–3183.

- [346] F. J. Wegner and A. Houghton, “Renormalization group equation for critical phenomena,” *Phys. Rev.* **A8** (1973) 401–412.
- [347] D. F. Litim, “Critical exponents from optimized renormalization group flows,” *Nucl. Phys.* **B631** (2002) 128–158, [arXiv:hep-th/0203006 \[hep-th\]](#).
- [348] L. Canet, B. Delamotte, D. Mouhanna, and J. Vidal, “Nonperturbative renormalization group approach to the Ising model: A Derivative expansion at order partial**4,” *Phys. Rev.* **B68** (2003) 064421, [arXiv:hep-th/0302227 \[hep-th\]](#).
- [349] D. F. Litim and D. Zappala, “Ising exponents from the functional renormalisation group,” *Phys. Rev.* **D83** (2011) 085009, [arXiv:1009.1948 \[hep-th\]](#).
- [350] S.-B. Liao, J. Polonyi, and M. Strickland, “Optimization of renormalization group flow,” *Nucl. Phys.* **B567** (2000) 493–514, [arXiv:hep-th/9905206 \[hep-th\]](#).
- [351] D. F. Litim, “Optimization of the exact renormalization group,” *Phys. Lett.* **B486** (2000) 92–99, [arXiv:hep-th/0005245 \[hep-th\]](#).
- [352] D. F. Litim, “Optimized renormalization group flows,” *Phys. Rev.* **D64** (2001) 105007, [arXiv:hep-th/0103195 \[hep-th\]](#).
- [353] D. F. Litim and J. M. Pawłowski, “Non-perturbative thermal flows and resummations,” *JHEP* **11** (2006) 026, [arXiv:hep-th/0609122 \[hep-th\]](#).
- [354] T. D. . Cohen, “Functional integrals for QCD at nonzero chemical potential and zero density,” *Phys. Rev. Lett.* **91** (2003) 222001, [arXiv:hep-ph/0307089 \[hep-ph\]](#).
- [355] G. Markó, U. Reinosa, and Z. Szép, “Bose-Einstein condensation and Silver Blaze property from the two-loop Φ -derivable approximation,” *Phys. Rev.* **D90** no. 12, (2014) 125021, [arXiv:1410.6998 \[hep-ph\]](#).
- [356] N. Khan, “The phase diagram of two-color qcd with the functional renormalization group,”.
- [357] T. Boz, S. Cotter, L. Fister, and J.-I. Skullerud, “Phase transitions in dense 2-colour QCD,” *PoS LATTICE2013* (2014) 189, [arXiv:1311.1367 \[hep-lat\]](#).
- [358] K. Kamikado, N. Strodthoff, L. von Smekal, and J. Wambach, “Fluctuations in the quark-meson model for QCD with isospin chemical potential,” *Phys. Lett.* **B718** (2013) 1044–1053, [arXiv:1207.0400 \[hep-ph\]](#).
- [359] J. B. Kogut and D. K. Sinclair, “The Finite temperature transition for 2-flavor lattice QCD at finite isospin density,” *Phys. Rev.* **D70** (2004) 094501, [arXiv:hep-lat/0407027 \[hep-lat\]](#).
- [360] D. K. Sinclair and J. B. Kogut, “Searching for the elusive critical endpoint at finite temperature and isospin density,” *PoS LAT2006* (2006) 147, [arXiv:hep-lat/0609041 \[hep-lat\]](#).
- [361] P. de Forcrand, M. A. Stephanov, and U. Wenger, “On the phase diagram of QCD at finite isospin density,” *PoS LAT2007* (2007) 237, [arXiv:0711.0023 \[hep-lat\]](#).
- [362] Z. G. Wang, S. L. Wan, and W. M. Yang, “A New approach for calculating the Nambu-Gorkov propagator in color superconductivity theory,” [arXiv:hep-ph/0508302 \[hep-ph\]](#).

Danksagung

An erster Stelle gilt ganz besonderer Dank an meinem Doktorvater Prof. Dr. Jan M. Pawlowski, in dessen Arbeitsgruppe ich über solch ein interessantes Gebiet der Physik promovieren durfte. Seine Betreuung ist geprägt von viel Geduld, Ermutigung und Unterstützung. Er hat sich stets Zeit für mich genommen, um jegliche Punkte zu klären, durch aufschlussreiche und inspirierende Diskussionen. Er erzeugt eine angenehme Atmosphäre, sodass die Arbeit eine Freude bereitet. Weiterhin bedanke ich mich sehr für die finanzielle Unterstützung der Promotion und ebenso für das Ermöglichen der Teilnahme an zahlreichen Konferenzen und Schulen. Der Dank hierfür geht auch an die HGS-HIRE, die HGSP und das ITP Heidelberg.

Ich bin Prof. Dr. Jürgen Berges sehr dankbar für das Interesse an meiner Forschung und für die freundliche Übernahme der Zweitbegutachtung der Dissertation.

Kenji Fukushima danke sehr für die wertvolle Zusammenarbeit und für eine sehr sorgsame und freundliche Betreuung während meines Forschungsaufenthalts an der Keio Universität in Yokohama.

Für eine angenehme und produktive Zusammenarbeit bedanke ich mich ebenfalls bei Michael Scherer, Nils Strodthoff und Fabian Rennecke.

Auch allen weiteren Mitgliedern des Instituts danke ich für die vielen, erkenntnisreichen und unterhaltsamen Diskussionen und für eine wunderbare Zeit. Insbesondere gehören dazu Igor Böttcher, Nicolai Christiansen, Youness Ayaita, Andreas Samberg, Leonard Fister, Lisa Haas, Tina Herbst, Mario Mitter, Sebastian Wetzel, Sören Lammers, Laura Classen, Anton Cyrol und Felix Ziegler.

Schließlich gebührt meiner Familie großer Dank für die unermüdliche Unterstützung in allen Lebenslagen.